University of Nottingham
Faculty of Medicine and Health Sciences
School of Medicine
Division of Cancer and Stem Cells
Cancer Biology Unit
Cancer Genetics & Stem Cell Group

Studying Colon Cancer Using Intestinal Organoid Models for Anticancer Drug and Gene Functional Analysis

Seyed Mohammad Hossein Kashfi

Thesis submitted to the University of Nottingham in fulfilment for the degree of Doctor of Philosophy

March 2020

Declaration

Except where acknowledged in the text, I declare that this thesis is my own work and is based on research that was undertaken by me in Cancer Genetics & Stem Cell Group, under the supervision of Dr. Abdolrahman Shams Nateri at the School of medicine, University of Nottingham, UK.

Seyed Mohammad Hossein Kashfi

ID: 4265509

Date: 30/03/2020

Abstract

Colorectal tumours demonstrate broad genetic and phenotypic heterogeneity in comparison to their matched normal tissue. To shed light into this diversity in depth, an advanced *in-vitro* 3D model capable of self-renewal, self-organisation and exhibit organ functionality is required. Self-renewal of the small intestine and colonic epithelium is mediated by the proliferation of stem cells and their progenitors in the crypt base. Recently, a long-term and stable 3D culture system maintaining basic crypt physiology known as organoid became available from both normal and matched-tumour tissues of the intestine. Organoids faithfully reproduce functional genetic, pharmacological and morphological alterations exist in their parental tissue. Patient-derived organoids (PDO) can be generated and expanded indefinitely *in-vitro* from a small biopsy sample of CRC patients (from both tumour and adjacent normal tissue), providing a promising platform for personalised medicine, drug discovery and targeted gene editing research studies. Therefore, in this study, we have initially adapted patient-derived organoids culture from 17 CRC patients in our laboratory and further investigated the phenotypical alteration of both tumour, and normal adjacent derived organoids. Based on our findings, tumour organoids displayed different phenotypical traits from one patient to another, highlighting their distinct molecular subtyping. The growth and morphological alterations of tumour organoids also significantly differed from normal derived organoids in culture.

We further evaluated the effect of Noggin, a BMP antagonist on PDO and colon cancer cell lines. Our findings demonstrate that despite the significant role of

Noggin in the homeostasis of normal colonic derived organoids, the administration of Noggin does not influence colon cancer cells and PDOs behaviour in culture.

Furthermore, organoids have opened a new window toward drug discovery and personalised medicine. To address this, the anticancer therapeutic value of Rifabutin antibiotic, recently screened on our laboratory were also assessed in PDO and colon cancer cell lines. Rifabutin drastically hindered the growth of PDOs and colon cancer cell lines in culture and impeded Wnt/β-catenin signalling mediated cancer cell growth.

With CRISPR/Cas9 induced-accurate mutations and 3D organoids cultures, it is now possible to model how individual genes may function in multiple tissue types and without the cost and ethical considerations of *in-vivo* alternatives. Hence, we aimed to combine the organoid system with genome editing technology, CRISPR/Cas9, to generate knockout organoids for rapid identification of genes with unknown biological function in the intestinal epithelium. Here, we evaluated the role of F-box genes as substrate recognition subunit of Skp, Cullin, F-box containing complex (SCF) E3-ligases in intestinal organoids. Knockout F-box intestinal organoids demonstrated differential phenotypical alterations that were associated with aberrant proliferation and differentiation and led the identification of different F-box genes including Fbxl5, Fbxo31, Fbxl18, Fbxo17 and Fbxl17. In conclusion, we have shown that organoids are invaluable and flexible tools to investigate multiple aspects of cellular events for homeostasis and disease condition and they may represent a significant step forward in reducing and replacing the use of animal models in research.

List of publications

Resulted from this study

1. Hossein Kashfi, Nicholas Jinks and Abdolrahman S. Nateri. "A method for using Cas9-overexpressing Murine Intestinal Organoids for Genetic Screening". Methods in molecular biology (Intestinal Stem Cells: Springer; 2020. p. 257-69).

2. Hossein Kashfi, Sheema Almozyan, Nicholas Jinks, Bon-Kyoung Koo and Abdolrahman S. Nateri. "Morphological alterations of cultured human colorectal matched tumour and normal organoids". Oncotarget 9 (12), 10572.

3. Hossein Kashfi and Abdolrahman S. Nateri. "Secreted Noggin, has no Tumour-induction or Suppressive Effects on Cultured Human Colon Cancer Cells and Tumour Derived Organoids". (Manuscript in submission).

In collaboration with others

1. Mehreen Ahmed, Nicholas Jinks, Roya Babaei Jadidi, **Hossein Kashfi,** Marcus Castellanos-Uribe and Abdolrahman S. Nateri. "Repurposing Antibacterial AM404 as a Potential Anticancer Drug for Targeting Colorectal Cancer Stem-Like Cells". Cancers 12 (1), 106.

2. Belal A Muhammad, Sheema Almozyan, Roya Babaei-Jadidi, Emenike K Onyido, Anas Saadeddin, **Hossein Kashfi**, Bradley Spencer-Dene, Mohammad Ilyas, Anbarasu Lourdusamy, Axel Behrens, Abdolrahman S Nateri. "FLYWCH1, a novel suppressor of nuclear β-catenin, regulates migration and morphology in colorectal cancer". Molecular Cancer Research 16 (12), 1977-1990.

Acknowledgement

I would like to take the opportunity to express my fathomless gratitude to my supervisor Dr. Abdolrahman S. Nateri for his invaluable guidance and supports through the work and I am particularly grateful for his unending patience, generosity and valuable comments during my PhD time and in the writing of my thesis.

I would like to extend my gratitude to all of my colleagues in Cancer Genetics and Stem Cell group, especially Dr. Roya Babaei-Jadidi (my laboratory advisor), and Dr. Federica Lorenzi (my second laboratory advisor) for their collaboration, sharing knowledge and technical experience with me during my PhD.

I would specially take this opportunity to thank my sponsor, Dr. Hassan Jalaeikhoo who generously raised this funding for me during my PhD and without his support and encouragement, I would not achieve this accomplishment.

My sincerest gratitude goes to my family especially my father and my mother, whose moral support, encouragements and patience over this time has been greatly appreciated.

List of Figures

Figure 1-1. Generation of organoids from various human organs……11

Figure 1-2. Multiple application of organoids in disease modelling and cancer study…….. 12

Figure 1-3. Generation of organoids from both human embryonic and adult stem cells……15

Figure 1-4. Schematic representation of CRISPR-Cas9-mediated genome engineering……17

Figure 1-5. Schematic representation of SCF…….23

Figure 1-6. F-box genes contributions in hallmarks of cancer……..24

Figure 1-7. Classification of F-box genes based on the different repeated domains…….25

Figure 1-8. Role of FBXO31 in various signalling pathways links to cancer progression……30

Figure 1-9. Schematic anatomy of the large and small intestine……..31

Figure 1-10. The schematic of the small intestine and colon epithelium……...35

Figure 1-11. Schematic presentation of canonical Wnt Signalling Pathway…38

Figure 1-12: Culturing the Human Intestinal organoid…….44

Figure 1-13: Consensus molecular subtyping of CRC……..48

Figure 2-1. Procedure for Mini prep for isolation and purification of DNA plasmid……..85

Figure 2-2. Procedure for obtaining PCR-ready DNA using QuickExtract™ DNA Extraction Solution…….86

Figure 2-3. Schematic of RT^2 Profiler PCR array plate containing 84 Wnt signalling associated genes and related internal control housekeeping genes..90

Figure 2-4. The procedure for performing the RT^2……91

Figure 3-1. Representative images of morphology alteration in organoids derived from normal tissues adjacent to tumours……..99

Figure 3-2. Growth heterogeneity within tumour organoids mirror the in vivo counterparts……..101

Figure 3-3. Comparison of morphological alterations in human colon matched tumour and normal organoids……...102

Figure 3-4. Colonic normal derived organoids self-organize into branching multicellular structures……..104

Figure 3-5. Organoid formation in culture for ~3 weeks gave rise to multicellular structure abundant with small crypt invaginations……..105

Figure 3-6. Organoids sustain their altered growth properties after excessive passaging and freezing-thawing……107

Figure 3-7. The phenotypical characteristics of two dominant types of tumour-derived organoids among different patients……109

Figure 3-8. Quantification of the mRNA expression for selected markers including β-catenin, CD44, LGR5 and c-Jun.109

Figure 3-9. Tumour organoid growth pattern in the presence and lack of Wnt3a……..113

Figure 3-10. WB validation of secreted Noggin from transfected cells (Noggin-conditioned medium)……..114

Figure 3-11.Noggin removal induced growth suppression and subsequent organoid destruction……..115

Figure 3-12. Administration of Noggin did not alter the phenotype of colon cancer cell lines……...117

Figure 3-13. Noggin has no role in modulation of EMT and proliferation in colon cancer cell lines……118

Figure 3-14. Noggin had no impact on E-cadherin and β-catenin expression and localisation in colon cancer cell lines……120

Figure 3-15. Noggin had no impact on cell cycle and proliferation of colon cancer cell lines……...…121

Figure 3-16. Noggin had no remarkable change on migration and also colonosphere efficiency of colon cancer cells……...123

Figure 3-17. Tumour organoid grew indispensable of Noggin……125

Figure 4-1. Determination of Rifabutin cytotoxicity assay in different colon cancer cell lines……...133

Figure 4-2. Rifabutin inhibited the cell-cell aggregation of HT-29 cells…….134

Figure 4-3. Rifabutin induced the cell elongation shape in treated HT-29 and SW620 cells…….135

Figure 4-4. Rifabutin mediates the suppression of colon cancer cell migration in wound healing assay……..136

Figure 4-5. Rifabutin suppressed growth of cystic tumour organoids in culture. A) Cystic tumour organoids underwent 138

Figure 4-6. Rifabutin treatment inhibited growth rate and viability of the organoids in culture……140

Figure 4-7. Rifabutin blocked the growth of budding tumour organoid…....142

Figure 4-8. Significant inhibition of growth and proliferation was evident in tumour organoid treated with Rifabutin……..143

Figure 4-9. TCF-luciferase expression was inhibited by Rifabutin treatment. ……..144

Figure 4-10. Rifabutin administration decreased p-β-catenin and β-catenin expression in SW620 cells……..…145

Figure 4-11: Heat-map representation of 88 differentially expressed genes in cystic tumour organoid upon Rifabutin administration…….147

Figure 4-12. Differential expression of Wnt signalling genes on cystic tumour organoids…….148

Figure 4-13. Gene array revealed potential pathways for Rifabutin's effects in CRC. Genemania was applied to generate the pathway analysis……150

Figure 4-14. Differential expression of Wnt signalling genes upon Rifabutin treatment in colonic cystic tumour organoid……151

Figure 4-15. qRT-PCR validation of Wnt signalling dysregulated genes in budding tumour organoid……..152

Figure 4-16. CXXC4 expression profile in colonic tumour organoids and cancer cells……..154

Figure 4-17. CD44 markedly down-regulated in colonic tumour organoids and colon cancer cell lines…….155

Figure 4-18. Heterogenous expression profile of FZD5 in tumour organoids and colon cancer cells…….156

Figure 4-19. LGR5 demonstrated differential expression pattern in tumour organoids and colon cancer cells……158

Figure 4-20. Schematic outline of the expression pattern of candidate genes in colon cancer cells and tumour organoids treated with Rifabutin……...159

Figure 4-21. WB validation of GSK3 inhibitor (2.5uM BIO) on SW620 cancer cell lines……...161

Figure 4-22. Co-treatment of Rifabutin with BIO significantly decreased the proliferation of SW620 cells……...162

Figure 4-23. Concomitant treatment of Rifabutin and BIO markedly induced apoptotic activity in budding tumour organoid……163

Figure 4-24. Rifabutin and BIO suppressed the growth of normal murine derived organoid in culture……164

Figure 4-25. EMT-mediated regulation of BIO and Rifabutin co-treatment in SW620 colorectal cancer cells……167

Figure 4-26. The schematic diagram for investigating the anti-cancer effect of Rifabutin in colon cancer cell lines and PDOs…….168

Figure 5-1. Validation of the CRISPR gRNA vectors via restriction enzyme digestion and sequencing……181

Figure 5-2. The BFP expression confirmed the correct transgene construct and delivery of F-box gRNA (Fbxo25) in HEK293-T cells……..182

Figure 5-3. LV Generation and validation of CRISPR gRNA library indicate the intense integration of the F-box sgRNAs virus into the cell……..185

Figure 5-4. CRISPR gRNA validation in DLD-1 colon cancer cell lines…186

Figure 5-5. Culture and maintenance of murine intestinal organoid……..188

Figure 5-6. Generation of murine intestinal organoid stably expressing Cas9 endonuclease…….190

Figure 5-7. Western blot validation of stable organoids expressing Cas9...190

Figure 5-8. A Schematic diagram of the experimental procedure for CRISPR/Cas9 screening based methodology in mouse intestinal organoids…..……..……..192

Figure 5-9. Schematic depiction for identification of F-box candidates via CRISPR/Cas9 KO screening……..……194

Figure 5-10. Fbxl18-KO characterized by loss of distinct growth and differentiation……...196

Figure 5-11. Fbxl18 KO developed small size crypt-villus like domain with the absence of distinct budding occurrence……..198

Figure 5-12. Fbxl18-KO suppressed the cell proliferation in murine intestinal organoids……..199

Figure 5-13. Fbxo17-KO organoids developed elongated and non-polarized phenotypical features……..201

Figure 5-14. Phalloidin staining of Fbxo17-KO revealed the presence of various morphological entities……202

Figure 5-15. Loss of Fbxo17 associated with reduced cell viability in murine organoids……...203

Figure 5-16. Fbxl18 and Fbxo17 KOs steered downregulation of proliferation and differentiation markers……...204

Figure 5-17. Generation of FBXL18- and FBXO17-KOs in DLD-1 cancer cells……205

Figure 5-18. The FBXL18-KO characterized by the lack of defined polarized morphology compared to multi-polarised cell shape in control (Cas9 parental cells)……207

Figure 5-19. FBXL18-KO significantly decreased the migration of the cells in DLD-1 colon cancer cell line……209

Figure 5-20. Lack of FBXL18 reduced the proliferation of the DLD-1 colon cancer cells in days 4-6……210

Figure 5-21. The FBXL18-KO inhibited the colony-forming efficiency of colon cancer cells compared to control (Cas9 DLD-1 parental cells)……211

Figure 5-22. Generation of stable Cas9 expressing colon tumour organoid via LV transduction……..213

Figure 5-23. Validation of stable tumour organoid expressing Cas9……..214

Figure 5-24. Loss of FBXL18 did not alter the key aspect of colonic tumour-derived organoids morphology in culture……..215

Figure 5-25. Lack of FBXO17 had no effect on phenotype and growth rate of human colon tumour organoids…….218

Figure 5-26. The schematic diagram of the CRISPR/Cas9 genetic based screening of F-box domain E3 ligase in intestinal organoids……..222

Figure 5-27. The RNA expression profile of FBXL18 in different cancer tissue……...…….226

Figure 5-28. The schematic biological activity of the FBXL18 in CRC cell lines and colonic tumour organoids……...228

Figure 5-29. FBXO17 mRNA expression pattern in 17 types of malignancies. ……..230

List of Tables

Table 1-1. Comparison of different genome engineering tools for target gene editing purposes……20

Table 2-1; Mutational signature of CRC cell lines used in current study…….62

Table 2-2 Solution components (ml) for SDS-PAGE electrophoresis gels……79

Table 2-3 List of primary and secondary antibody used for IHC analysis…..81
Table 2-4. List of primers used for RT-PCR and quantitative real time PCR (qRT-PCR)……87
Table 2-5. The PCR component mix for the Wnt signalling PCR array…….90

Table 2-6: The PCR program condition for the RT^2 assay using LightCycler 480 II instrument (Roche)……92

Table 3-1. The characteristics of CRC patients in the present study……96

Abbreviations

PDO	Patient derived organoid
CRISPR	clustered regularly interspaced short palindromic repeats
gRNA	Guide RNA
sgRNA	Single gRNA
SC	Stem cell
aSC	Adult stem cell
iPSCs	Induced pluripotent stem cells
CSC	Cancer Stem-Like Cells
ISCs	Intestinal Stem Cells
TA	Transient amplifying compartment
SCF	Skp, Cullin, F-box containing complex
β-TrCP	β-transducin repeat-containing protein
BFP	Blue Fluorescent Protein
GFP	Green Fluorescent Protein
3D	3 deimentional
EMT	Epithelial-mesenchymal transition
CXXC4	CXXC finger protein 4
SOX17	SRY-box transcription factor 17
FGF4	Fibroblast growth factor 4
PRICKLE1	Prickle planar cell polarity protein 1
WIF1	Wnt inhibitory factor-1
SFRP4	Secreted frizzled related protein 4
FZD5	Frizzled class receptor 5
Dvl	Disheveled
EGF	Epidermal growth factor
aa	amino acids
LV	Lenti virus
BMP	Bone Morphogenic Protein
bp	base pair
BSA	Bovine Serum Albumin
°C	degrees Celsius
CBCs	Crypt Base Columnar Cells
cDNA	Complementary DNA
cm	centimeter
CMV	Cytomegalovirus
CRC	Colorectal Cancer/Carcinoma
C-terminus	Carboxyl terminus
dH2O	distilled water

DMEM	Dulbecco's Modified Eagle Medium
DMSO	Dimethyl sulphoxide
DNA	Deoxyribonucleic Acid
dNTPs	Deoxyribonucleotide triphosphates
EDTA	Ethylenediaminetetraacetic acid
eGFP	Enhanced Green Fluorescent Protein
EMT	Epithelial to Mesenchymal Transition
FBS	Fetal Bovine Serum
GSK-3β	Glycogen Synthase Kinase-3 Beta
h	hour
kDa	Kilo Dalton
Lgr5	Leucine-rich repeat-containing G-protein coupled Receptor 5
min	minute
ml	milliliter
mM	millimolar
mRNA	messenger RNA
ng	nanogram
IF	Immunofluorescence
IHC	Immunohistochemistry
H&E	Haematoxylin and Eosin
MUC2	MUCIN2
PFA	Paraformaldehyde
PI	Propidium Iodide
WB	Western blotting
qRT- PCR	Quantitative Real Time-PCR
RNA	Ribonucleic Acid
SDS-PAGE	Sodium Dodecyl Sulfate Polyacrylamide Gel Electrophoresis
LRP	lipoprotein receptor-related protein
SRB	Sulforhodamine B
TCF/LEF	T-Cell Factor/Lymphoid Enhancer Factor
TCF4	T-Cell transcription Factor 4
MSI	Microsatellite Instability
CIN	Chromosomal Instability
CBCs	Crypt Base Columnar Cells
FACS	Fluorescence-activated cell sorting

Contents

Declaration ..... **i**

Abstract ..... **ii**

List of publications ..... **iv**

Acknowledgement ..... **v**

List of figures ..... **vi**

List of Tables ..... **xii**

Abbreviations ..... **xiii**

Chapter 1 ..... **1**

General Introduction **1**

1.1 Current Models for Disease and Cancer study **2**

1.1.1 LIMITATIONS OF CELL CULTURE AND ANIMAL MODELS 5

1.1.2 THREE-DIMENSIONAL (3D) MODELS: TOWARDS THE EVOLUTION OF *IN VIVO* NATURAL SYSTEMS 8

1.2 From 3D Cell Culture to Organs-on-Dish: Organoids **9**

1.2.1 MODELLING DISEASE AND CANCERS WITH ORGANOIDS 11

1.2.2 PERSONALISED MEDICINE AND ORGANOIDS 14

1.3 CRISPR/Cas9 mediated Genome Engineering **16**

1.4 F-BOX genes and Hallmarks of Cancer **21**

1.5 Dynamic of the Intestinal Epithelium and Self-renewal in the Intestine . **30**

1.5.2 R-Spondin and Lgr family as regulators of Wnt signalling **38**

1.5.3 Noggin regulates the homeostasis of epithelial stem cells through BMP gradient **41**

1.6 *Ex vivo* Culture of the Intestinal Epithelium: Intestinal Organoid 44

1.7 Colorectal cancer, a Heterogeneous entity and it's Current Therapeutically Approaches 45

1.7.1 TARGETED THERAPY OF COLON CANCER STEM CELLS 50

1.8 Rationale & main objectives 57

CHAPTER 2 Materials and Methods..... 60

2.1 CELL AND MOLECULAR BIOLOGY TECHNIQUES 61

2.1.1 Cell lines 61

2.1.2 Thawing, maintaining, sub-culturing and freezing cells..... 63

2.1.3 Synchronizing the cell cycle 64

2.1.4 Transient transfection of cell lines..... 64

2.1.5 Lentivirus production and transduction 64

2.2 ORGANOID CULTURE.....67

2.2.1 Isolation and culture of human colonic crypts..... 67

2.2.2 Murine intestinal crypt isolation and culture 68

2.2.3 Production of Wnt 3A-conditioned medium 69

2.2.4 Production of R-spondin1-conditioned medium 70

2.2.5 Preparation of Noggin-conditioned medium..... 71

2.3 HISTOLOGY.....71

2.3.1 Organoid preparation..... 71

2.3.2 Hematoxylin and eosin (H&E) stain 72

2.4 FUNCTIONAL ASSAYS.....73

2.4.1 Luciferase reporter assay..... 73

2.4.2 Cell cycle analysis and Propidium iodide (PI) staining 74

2.4.3 Cytotoxicity assay..... 75

2.4.4 Colony-forming assay 75

2.4.5 Cell migration and wound healing assays 76

2.4.6 Colonosphere formation assay..... 76

2.4.7 Organoid viability assay 77

2.5 PROTEIN EXPRESSION.....77

2.5.1 Protein extraction and quantification from cell lines 77

2.5.2 Protein extraction from organoid cultures..... 78

2.5.3 SDS-PAGE and Western blotting (WB) analysis..... 79

2.5.4 Immunofluorescence (IF) and Phalloidin staining..... 81

2.5.5 Phalloidin staining..... 82

2.6 DNA PREPARATION.....83

2.6.1 Bacterial transformation & plasmid DNA amplification 83

2.6.2 Isolation of the plasmid DNA..... 84

2.6.3 Genomic DNA extraction..... 85

2.6.4 RNA extraction from human tissues 86

2.6.5 Complementary deoxyribonucleic acid (cDNA) synthesis..... 88

2.6.6 Quantitative real-time PCR (qRT-PCR) 89

2.7 PRINCIPLE AND PROCEDURE FOR RT^2 PROFILER PCR ARRAY.....89

2.8 STATISTICAL ANALYSIS.....92

Chapter 3..... 93

Establishment of small number of CRC patient derived organoid (PDO) lines and studying the role of Noggin in cultured PDOs and CRC cell lines 93

Brief Introduction..... 94

3.2 Results 95

3.2.1 NORMAL HUMAN DERIVED INTESTINAL EPITHELIUM ADJACENT TO TUMOURS GAVE RISE TO MULTI BRANCHED ORGANOID STRUCTURE.....95

3.2.2 TUMOUR ORGANOIDS REPRESENT DIFFERENTIAL PHENOTYPICAL MORPHOLOGY IN CULTURE.....100

3.2.3 PHALLOIDIN STAINING OF NORMAL DERIVED ORGANOIDS AND THEIR MATCHED TUMOUR TISSUE.....103

3.2.4 LONG-TERM MAINTENANCE (PASSAGING AND FREEZING-THAWING) OF NORMAL/TUMOUR ORGANOIDS IN CULTURE REPRODUCES THE MAIN FEATURES OF ORIGINAL ORGANOID.....106

3.2.5 TUMOUR ORGANOIDS DISPLAY DIVERGENT GROWTH FEATURES AND MORPHOGENESIS.....108

3.2.6 *CTNNB1, LGR5* AND *CD44* GENES EXPRESSION UPREGULATED IN CYSTIC COMPARED TO BUDDING TUMOUR TYPE ORGANOIDS.....110

3.2.7 COLONIC TUMOUR ORGANOID GREW INDISPENSABLE OF WNT-3A AND NOGGIN SUPPLEMENT.....112

3.2.8 THE ROLE OF NOGGIN IN PATIENT-DERIVED ORGANOIDS AND HUMAN COLON CANCER CELL LINES.....114

3.2.8.1 LACK OF NOGGIN CAUSED PERTURBATION OF HUMAN COLONIC AND MURINE INTESTINAL ORGANOIDS.....114

3.2.8.1 NOGGIN DID NOT AFFECT CELL ARCHITECTURE AND MORPHOLOGY OF CULTURED COLON CANCER CELL LINES.....116

3.2.8.2 NOGGIN IS NOT ASSOCIATED WITH PROLIFERATION OR EMT ACTIVITY OF COLON CANCER CELL LINES.....118

3.2.8.3 NOGGIN DOES NOT AFFECT CELLULAR LOCALIZATION AND EXPRESSION OF E-CADHERIN AND B-CATENIN.....119

3.2.8.5 NOGGIN ADMINISTRATION DID NOT ALTER THE WOUND-HEALING, AND COLONOSPHERE EFFICIENCY OF HCT-116 AND SW480 CELL LINES.....122

3.2.8.6 NOGGIN IS CRUCIAL FOR THE MAINTENANCE OF STEM CELL NICHE IN NORMAL DERIVED ORGANOIDS BUT NOT TUMOUR COUNTERPARTS.....124

3.3 Discussion 126

CHAPTER 4 131

4.1 Brief Introduction 132

4.2 Results 133

4.2.1 CYTOTOXICITY ASSAY OF RIFABUTIN IN HT29 AND SW620 COLON CANCER CELLS.....133

4.2.1.1 RIFABUTIN SUPPRESSED THE COLON CANCER CELLS GROWTH.....134

4.2.1.2 RIFABUTIN SUPPRESSED THE MOTILITY AND INVASIVENESS OF THE SW620 AND HT-29 CELLS.....135

4.2.2.1 ANTICANCER EFFECTS OF RIFABUTIN IN BUDDING TUMOUR ORGANOIDS.....141

4.2.3 RIFABUTIN IMPEDED WNT/B-CATENIN SIGNALLING MEDIATED CANCER CELL GROWTH.....144

4.2.4 RIFABUTIN INFLUENCED THE EXPRESSION OF VARIOUS WNT SIGNALLING GENES ASSOCIATED WITH CANCER HALLMARKS IN TREATED CYSTIC TUMOUR ORGANOIDS.....145

4.2.4.1 VALIDATION OF CANDIDATE GENES IN CYSTIC AND BUDDING TUMOUR ORGANOIDS.....151

4.2.4.2 VALIDATION AND EVALUATION OF CANDIDATE GENES IN COLON CANCER CELLS USING REAL-TIME QUANTITATIVE PCR.....153

4.2.5 COMBINATION TREATMENT WITH RIFABUTIN AND GSK-3 INHIBITOR SENSITIZES A RAPID APOPTOSIS ACTIVITY IN COLONIC TUMOUR ORGANOIDS.....159

4.2.5.1 RIFABUTIN SIGNIFICANTLY INHIBITED THE GROWTH OF SW620 IN A SYNERGISTIC MANNER WITH BIO 160

4.2.5.2 EFFECT OF BIO AND RIFABUTIN COMBINATION TREATMENT IN MURINE DERIVED ORGANOIDS.....163

4.2.5.3 DOWN-REGULATION OF EMT-MEDIATORS, STEM CELL MARKERS AND ONCOGENIC DRIVERS OF CRC CELLS BY BIO/RIFABUTIN TREATMENT 165

4.3 Discussion 167

CHAPTER 5 176

5.1 Brief introduction..... 177

5.2.Results
5.2.1 Validation of CRISPR gRNA library constructs; 178

5.2.1 Restriction enzyme digestion and nucleotide sequencing analysis of representative F-box LV gRNAs constructs confirmed the validity of the gRNA library 178

5.2.2 Further Validation of F-box gRNAs in human HEK293-T and colon cancer DLD-1 cell lines 181

5.2.3 GENERATION OF LV LIBRARY OF F-BOX GRNA-BASED VECTORS 182

5.2.3.1 The specific integration of the gRNA in the genome of colon cancer cell lines 183

5.2.4 CULTURING AND EXPANSION OF MURINE INTESTINAL ORGANOIDS AS A PLATFORM FOR CRISPR-CAS9/GRNA SCREENING 186

5.2.4.1 Generation of a stable murine intestinal organoid line, expressing exogenous Cas9 endonuclease 188

5.2.5 A CRISPR/CAS9-MEDIATED MUTAGENESIS METHOD FOR SCREENING OF THE F-BOX GENES 190

5.2.5.1 Fbxl18-KO organoids lack the branching morphogenesis 194

5.2.5.2 Phalloidin staining for F-actin filaments confirmed the compact and smaller morphology in Fbxl18-KO organoids 196

5.2.5.3 Fbxl18-KO organoids impeded the proliferation and viability in WST-1 cell proliferation assay 198

5.2.5.4 Fbxo17-KO mouse organoids formed non-polarized and semi-colonoid morphology 199

5.2.5.5 Fbxo17-KO organoids reproduced by morphologically asymmetric growth pattern 201

5.2.5.6 Fbxo17-KO reduced cell viability in murine intestinal organoids.... 203

5.2.5.7 Loss of Fbxl18 and Fbxo17 is associated with downregulation of proliferation and differentiation markers in intestinal organoids 203

5.2.6 FUNCTIONAL CHARACTERIZATION OF FBXL18 AND FBXO17 KOS IN HUMAN CANCER CELL LINES 205

5.2.6.1 FBXL18-KO developed non-polarized shape with lack of directed protrusions..... 206

5.2.6.2 Loss of FBXL18 reduced the mobility of the DLD-1 colon cancer cells in Wound Healing Scratch Assay 208

5.2.6.3 Loss of FBXL18 impeded the proliferation of the DLD-1 colon cancer cells 209

5.2.6.4 The FBXL18-KO suppressed the colony-forming capacity of DLD-1 colon cancer cells 210

5.2.7 CRISPR/CAS9 MEDIATED DELETION OF FBXL18 AND FBXO17 IN PATIENT TUMOUR ORGANOID 212

5.2.7.1 Generation of intestinal tumour organoid expressing Cas9 212

5.2.7.2 Lack of FBXL18 expression did not affect colon tumour organoids 214

5.2.7.3 Coexistence of loss of FBXO17 and CRC tumour driver genes did not alter the phenotypical features of colonic derived organoids..... 216

5.3 Discussion 220

CHAPTER 6 232

GENERAL DISCUSSION 232

6.1 OVERVIEW 233

6.2 Patient derived organoids reflect the origin tissue in a dish..... 234

6.4 CXXC4 as potential targets of Rifabutin anticancer activity in PDO.... 236

6.3 Screening the role of F-box genes with CRISPR-Cas9–modified organoids genome 237

6.5 CONCLUSIONS, EXPERIMENTAL LIMITATIONS AND FUTURE PERSPECTIVES.....240

References 243

Appendix 279

Chapter 1

General Introduction

1.1 Current Models for Disease and Cancer study

Several preclinical platforms have been introduced to model human diseases and cancer progression. These models enable researchers to elucidate the mechanisms underlying disease development and respond to the specific treatment. Researchers could investigate while manipulating a complex disease process using these platforms in a way infeasible to perform in a patient. In this regard, the development of *in vitro* cell culture and animal models have allowed rapid and facile evaluation of the molecular features and pathogenesis of various malignancies and as well as the prognostic and therapeutic value of several drugs (1, 2). Cancer cell lines have significantly improved our understanding of human cancer biology within the last fifty years. Cell lines are invaluable tools for experimental manipulation and high-throughput applications providing some very important insights into tumour progression while representing an immense range of tumour types (3-6). Cell lines allow researchers not only to study the mechanisms of actions in tumour suppressor genes and oncogenes in cancer development but also enabling the assessment of therapeutic value of several candidate components and further mapping of tumour susceptibility traits (1). HeLa, known as the first human cancer-derived cell line which was originally derived from a cervical tumour of Henrietta Lacks in 1951 (7). Ever since, a broad range of cell lines have gradually burgeoned in either *in vitro* or *in vivo* manner and used extensively to predict, identify and validating gene functions, novel tumour biomarkers, defining molecular and cellular events in disease and cancer progression (8).

However, to what extent cancer cell lines mirror the genetic heterogeneity of parental tumours remains controversial. In the 70s, Nelson-Rees et al. revealed that several cell lines used to study various types of cancers were derived from HeLa cervical cancer cell line and not from relevant cancers (9-11). Through their cytogenetic studies, they proposed that the application of the HeLa cell lines might not be suitable to study the biology of other cancers.

In addition, several animal models from vertebrates to invertebrates have been also developed to study various types of diseases and tumorigenesis. Among the vertebrate, the murine have been extensively applied to study several aspects of cancer progression. Mice models provided numerous benefits over cancer-derived cell lines and despite the evolutionary differences of the human and mouse, the genome properties of both species have been significantly conserved through evolution. Approximately 95-98% genome similarity has been identified between human and mice and the aetiology of the disease in both human and mice are similar in the majority of the cases. Furthermore, the genome of laboratory mice models has been broadly characterized, thereby can be exploited for different research purposes. Moreover, the majority of cancer signalling pathways can be also introduced in mice models. Overall, numerous individual alterations or in combination fashion can be established into such mice and be investigated according to the research project. In this regard, Xenografts have been used to generate the human cancer models in which animal or human tumours/cell lines or cell suspensions implanted or injected into the receipt mice. In order to prevent or

abrogate tumour rejection, the receipt mice should be either nude or possess severe combined immune deficiency (SCID).

The injected tumour/cell line will be propagated and enable the study of tumour behaviour and response to a particular treatment. To further enhance the capability of xenografts to mimic the environment of the primary tumours, the cells can be injected into the equivalent organ from which the tumour is originated. This is known as orthotopic xenografts. Whereas, in ectopic xenografts, the tumour derived cells are implanted in a non-relevant physiologic site in host counterpart (12). Generally, several studies indicated that the tumour-derived cells which to be injected, the location of injection, the age of mouse and genetic background of the mice would potentially affect the results of the research study on these models (13, 14). Furthermore, the advent of genetically engineered mouse models (GEMs) has opened up a new exciting avenue to study the variety of conditions in a whole organism. Conditional or germline transgenic models of GEM can be generated according to the research of interest. For example, several laboratories have applied homologous recombination to model the adenomatous polyposis coli (APC) inactivation using embryonic stem cells (ES) of mice (15, 16).

Altogether, the application of preclinical models including cell lines and animal models for selection of potential therapeutics is the initial step to evaluate the efficacy of the candidate drug. Of note, basic science studies and clinical trials are two fundamental components in cancer drug screening. In this regard, the first study carried out by the National Cancer Institute (NCI) in the 50s evaluated the efficacy

of specific drugs on these preclinical models. These screening approaches were mainly on murine allograft tumours, with emphasis on leukaemia (17-19).

However, over time, a limited success observed in screens to mimic the chemotherapy response in the clinic using these models. The differences in chemotherapy response in clinics led to the emergence of a panel to reduce this variability. Therefore, more than two decades ago, the NCI introduced a "disease-oriented" drug screening approach based on 60 human cancer cell lines originated from nine different cancers including colon, lung, melanoma, brain, breast, leukaemia, ovarian, renal and prostate (20). This approach was introduced to help the conduction of high-throughput screening of several numbers of drugs with proper sensitivity and specificity so that only a small number of drugs would be targeted for following preclinical evaluation in xenograft models. Despite the wide usage of cell lines and animal models to study multiple aspects of disease modelling, ever since numerous limitations have been noted which will be discussed further in the next part.

1.1.1 Limitations of Cell Culture and Animal Models

Generally, the move toward *in vivo* models and considering less attention in the cell lines application in the last few years are due to; ***1)*** It has been noted that cell lines eventually go through genetic and mRNA alteration while they are in culture condition (21-23). ***2)*** As the cancer cell lines have been constantly sub-cultured *in vitro* for several years they might become totally different from the

tumour they were originally derived (24). Therefore, it has been reported that the genetic and molecular profile of the cell lines have been modified over time in comparison to the primary tumour they were derived. ***3)*** Cell lines lack the components of the tumour microenvironment; one of the fundamental limitations in the application of cell lines as a cancer model is the fact that they do not mimic the complexity of the tumours in regards to their environment and the lack of stromal signals and matrix interactions might affect the accuracy of the research. In addition, the cell line's environment can modify tumour epigenetics properties. The lack of immune components in cells lines as another important issue hampers recapitulating the immunology of tumours and their response toward epithelium micro/macro environment (25). Furthermore, ***4)*** cell lines used to modulate tumours may not be an appropriate representative of the *in vivo* tumours and patients with particular aberrant mutations. For example, CRC cell lines commonly used in research studies usually possess microsatellite instability (MSI), however, it has been demonstrated that the MSI phenotype represents ~15% of all CRCs and they are less common in advanced stages (with less than 5% in the metastatic cases) (26-28). Hence, MSI cell lines do not mimic the clinical aspects of all individuals with CRC. Moreover, ***5)*** tumours which are selected for cell line generation, grow fast, so they might not be a suitable platform to study cancers with the slow-growing state in origin like neuroendocrine tumours, which are scarcely introduced as cell line (29). Therefore, although thousands of cell lines have been generated so far, there is still a need for the proper *in vitro* cancer models to describe the heterogeneity and diversity of the cancer cells.

Thus, all these limitations question the reliability of the application of cell lines as a model to study the disease and cancer development. On the other hand, transplantation CRC models, xenografts and genetically engineered mouse models (GEM) also represent some critical limitations. The major issue with the latter is the use of immune-deficient hosts in xenograft models. The role of microenvironment and immune cells in tumorigenesis has encouraged researchers to develop immunocompetent models for better understanding of immunological compartments of related tumours in cancer studies. Despite the emergence of immune-competent hosts, generating of these GEM based models are still time-consuming, expensive and there are also research ethics limitations (30-33). Moreover, recent studies have also indicated that human tumours possess more heterogeneity than their genetically engineered mice counterpart models (34, 35). All these challenges and related limitations in these models highlight an urgent need for the establishment of models mimicking the heterogeneity of individual patient. As the solid tumour and its microenvironment encompass multiple and various types of cells and not only the cancer cells, this model should mimic this heterogeneity of tumours and modulate the complexity of cellular structure. The model thereby, should also closely resemble the *in vivo* tissue or organ system and preferably designed for personalized medicine cancer research projects in which the treatment is based on an individual's genetic profile and medical history.

1.1.2 Three-Dimensional (3D) Models: Towards the Evolution of *In vivo* Natural Systems

The development of a 3D culture system comprises all multiple cell types within a tissue provide a unique opportunity to investigate various intra and intercellular signalling pathways in a tumour. The 3D systems have overcome several limitations of 2 dimensional monolayer conditions by closely recapitulating the cellular heterogeneity and intercellular communications of tumour cells with their environment. In a normal condition, 2D culture system has 3 μm thick, however, the 3D culture has approximately 10-30 μm thick (36). Moreover, in synthetic plastic culture plates, the cells grow, adhere and propagate in a completely different and unnatural way than *in vivo* condition in a way that half of their surface area interact with the medium while other 50% are being exposed to the cell culture plate which is not the case of 3D culture systems. Generally, in 3D culture models, almost all of the cells attached to each other and the cells are in close interact or exposed to the extracellular matrix (ECM). The ECM in 3D culture is similar as *in vivo* counterpart and it is the place of several essential biological processes including, molecular signalling, cell-cell communication and receptor function (37). Cellular behaviour including proliferation, differentiation and metabolism is significantly affected by the cellular microenvironment (38-40). The 3D culture models can be used to study several aspects of cellular process in diseases such as cancer progression. For example, modelling the early steps of oncogenic events and metastasis can be easily programmed and examined in 3D cultures which might be impossible to be recapitulated in monolayer 2D systems.

In addition, 3D cultures have been successfully applied to study the Epithelial-Mesenchymal Transition (EMT) which is the major event in the acquisition of migratory and metastasis of tumours (41, 42). Angiogenesis is another hallmark requires for growth and invasion of tumours, which can be studied in 3D culture systems (43). In fact following the outgrowth of the tumour and invasion to the lymph nodes, the tumour requires oxygen and the sufficient nutrition to grow in the process of metastasis. In vitro organoid vascularization can be achieved via co-culturing with endothelial cells using microfluidic chip and in VEGF and hypoxia gradients (44). In order to establish a model that resembles both the morphology and physiology of an organ with the advantages of cell line application, several 3D cultures have been introduced so far. These models have been generated from a wide range of sources including tissue segments and explants (45), spheroids generated from cancer cell lines (16), or 3D organoid structures derived from the tumour or adjacent normal samples that mimic the tissue morphology and differentiation (46, 47).

1.2 From 3D Cell Culture to Organs-on-Dish: Organoids

In the last few years, there have been considerable efforts towards developing a sophisticated three-dimensional culture system known as "organoid" (48-52). Organoids are 3D cell culture systems comprising all existing multiple cell types within a tissue. They resemble *in vitro* in a variety level, the morphology and composition of their *in vivo* counterparts. The organoids are capable of self-

organizing and they can differentiate to form tissue-specific cell lineages. They can be generated from pluripotent stem cells (ESCs or iPSCs), as well as adult stem cells (AdSCs).

Numerous attempts have been made to generate 3D cultures capable of recapitulating the tissue organs from primary samples, however, the establishment of intestinal organoid by Sato et al. in 2009 was a hallmark in the history of 3D culture (53). In this method, the endogenous signalling pathways surrounding the intestinal stem cell niche at the bottom of the crypt were simulated *in vitro* in order to induce the adult stem cells to form an organ-like structure on a dish. In the latter attempt, the researchers established a long-term condition of a culture system capable of generating villus-crypt like domain from single intestinal crypts. They further demonstrated that single sorted of LGR5+ cells as a recognized cycling intestinal stem cell could also drive the organoid formation *in vitro*. Using the specific scaffold known as Matrigel for organoids, to simulate the ECM (54), and supplementation with essential niche factors allowed the growth and development of this sophisticated *in-vitro* 3D model. Following the establishment of organoid principles by Sato and colleagues, multiple studies have carried out to re-produce the organoids from different types of mammalian tissues (Figure 1-1). Ever since, the organoid system has been generated from the breast, colon, pancreas, stomach, liver, lung, oesophagus, brain and kidney and they have been used to study a wide range of biological events within cells (55-64).

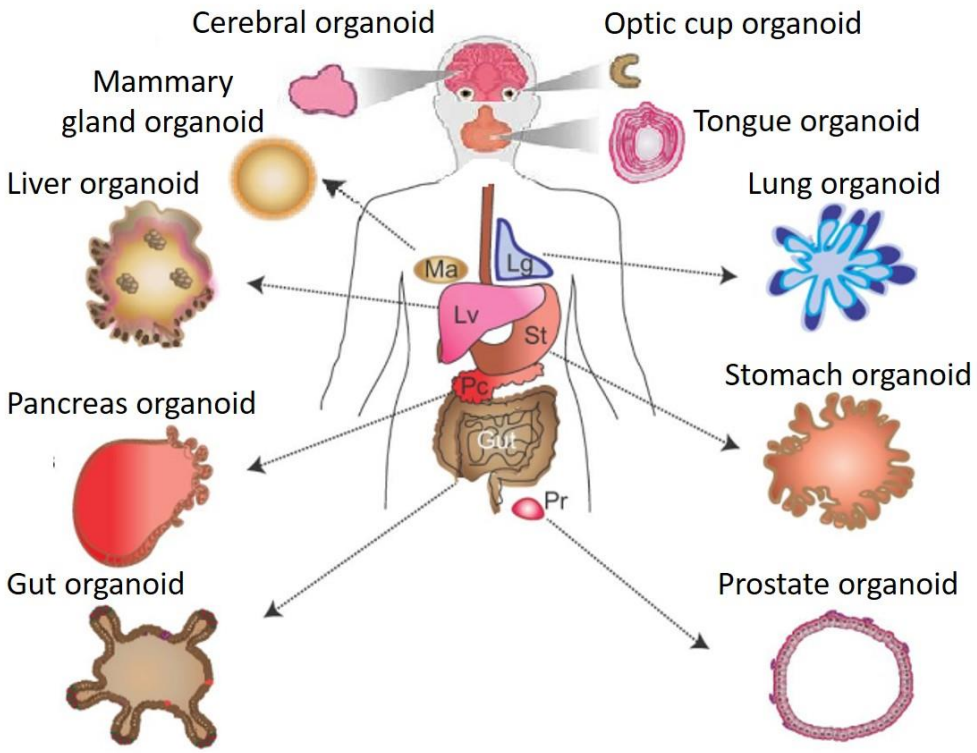


Figure 1-1. Generation of organoids from various human organs. Since its first establishment of in 2009, organoids have been developed form different tissue organs (adapted from Huch and et al, Development; 2015).

1.2.1 Modelling Disease and Cancers with Organoids

Both adult stem cells (aSC) and induced pluripotent stem cells (iPSCs) derived organoids can be used as models to study tissue development, disease and cancer progression (65). The tremendous translational capacity of the organoids and its applications enables bridging the current gaps between the basic researches to clinical trials, therefore providing a promising source to modulate several types of diseases and malignancies in an *ex-vivo* setting (Figure 1-2) (66-69).

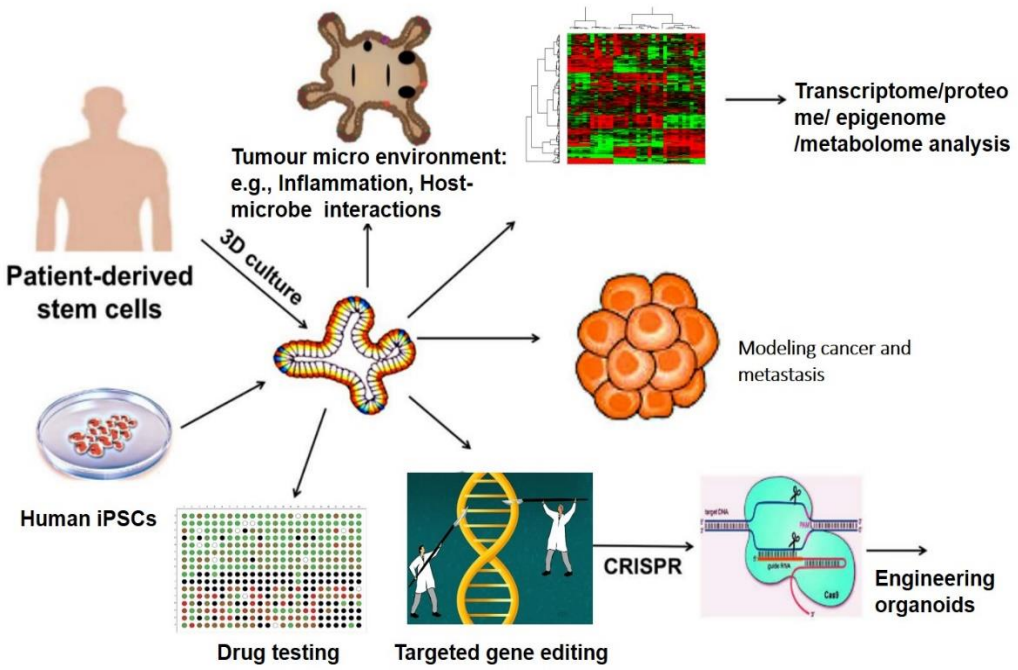


Figure 1-2. Multiple application of organoids in disease modelling and cancer study. Organoids have immense applications in several research areas including developmental and regenerative studies, disease modelling and cancer research. (Adapted from Ho BX et al. International journal of molecular sciences; 19, 2018).

Striking recent studies on host-microbe interactions in organoid co-cultures, indicates their potentials in modelling various infections with pathogens. For example, gastric derived organoids have microinjected with *H pylori*. to evaluate the epithelial respond to the infection, in which the induction of NF-κB–driven inflammatory response in infected organoids have observed (68). Organoids have been also used to study inflammation and tumorigenesis. Prolonged exposure to inflammatory cytokine tumour necrosis factor-α (TNF- α) led the transformation of the normal ovarian organoid to malignant tumours (66). In another study, Zhang et

al. used the mouse intestinal organoid culture to investigate the bacterial-epithelial interaction by *Salmonella* (70). They revealed that the bacteria disrupted the tight junctions in the organoids. Interestingly, they also indicated that the number of LGR5 and Bmi1 stem cells was considerably decreased upon *Salmonella* infection. Furthermore, the application of the organoids in modelling the host-parasite and virus interactions have been also reported previously (71, 72). Finkbeiner and colleagues used the human intestinal organoids to culture and study the fecal rotavirus (72). They co-cultured the organoids with the simian SA11, a strain of rotavirus and they detected that the virus infection was not only restricted to the intestinal epithelium, but also the mesenchymal compartment (72). In addition, with the emergence of genome engineering tools, the genotype of several different types of disease and cancers can be studied through modelling the organoids derived from normal tissues. These approaches can be defined in a setting of virus transduction and the clustered regularly interspersed short palindromic repeats (CRISPR/Cas9) technique which has been successfully performed on organoid models (73, 74). Modelling the early events in carcinogenesis has been always a big challenge. As cell lines generated from normal tissue are very rare, hampering the study of the early process of genetic alterations in tumours. The organoid, however, can be used to introduce the first stages of tumorigenesis to elucidate the initiating events in carcinogenesis. For example, gain and loss-of-function alterations can be exploited to generate oncogenic events in organoids. In addition, the organoids genomes, and transcriptomes and epigenomes can be altered and then they can be evaluated whether these modifications drive the tumourigenesis in the organoid model.

1.2.2 Personalised medicine and organoids

The hallmark of cancer is defined by the constant activation of proliferative signalling pathways, mutations in growth suppressor genes, cell death resistance, activation of angiogenesis and eventually the metastasis (75). Investigating this advanced diversity of tumours requires the presence of a promising model that allows resembling tumour structure while providing the platform for the high-throughput study and analysis. Organoid system is an appropriate model for functional validation of several data derived from basic research studies. Interestingly, organoids are genetically stable and this provides researchers with a great opportunity for drug screening and personalized medicine approaches (Figure 1-3). The establishment of a cancer biobank of organoids from tumour and adjacent normal tissues and following molecular analysis of each organoid derived from individuals, provide a new window in personalized medicine approaches (76). For example, these advances allow researchers to test the potential drugs in patients diagnosed with cancer before the initiation of actual treatment. Subsequently, this may maximize the efficacy of treatment. The fundamental step in cancer therapy is the personalized treatment design which cannot be recapitulated by current platforms. In this regard, van de Wetering and colleagues established a living organoid biobank from 20 patients with colorectal cancer (77). They designed a high-throughput organoid drug screening assay and evaluated all organoids derived from tumour and adjacent normal tissue of patients (77). Based on their findings, they proposed that organoids generated from tumours and normal tissues can be evaluated for clinically approved drugs soon after derivation which this

personalized therapy approach will significantly improve the efficacy of treatment in individuals.

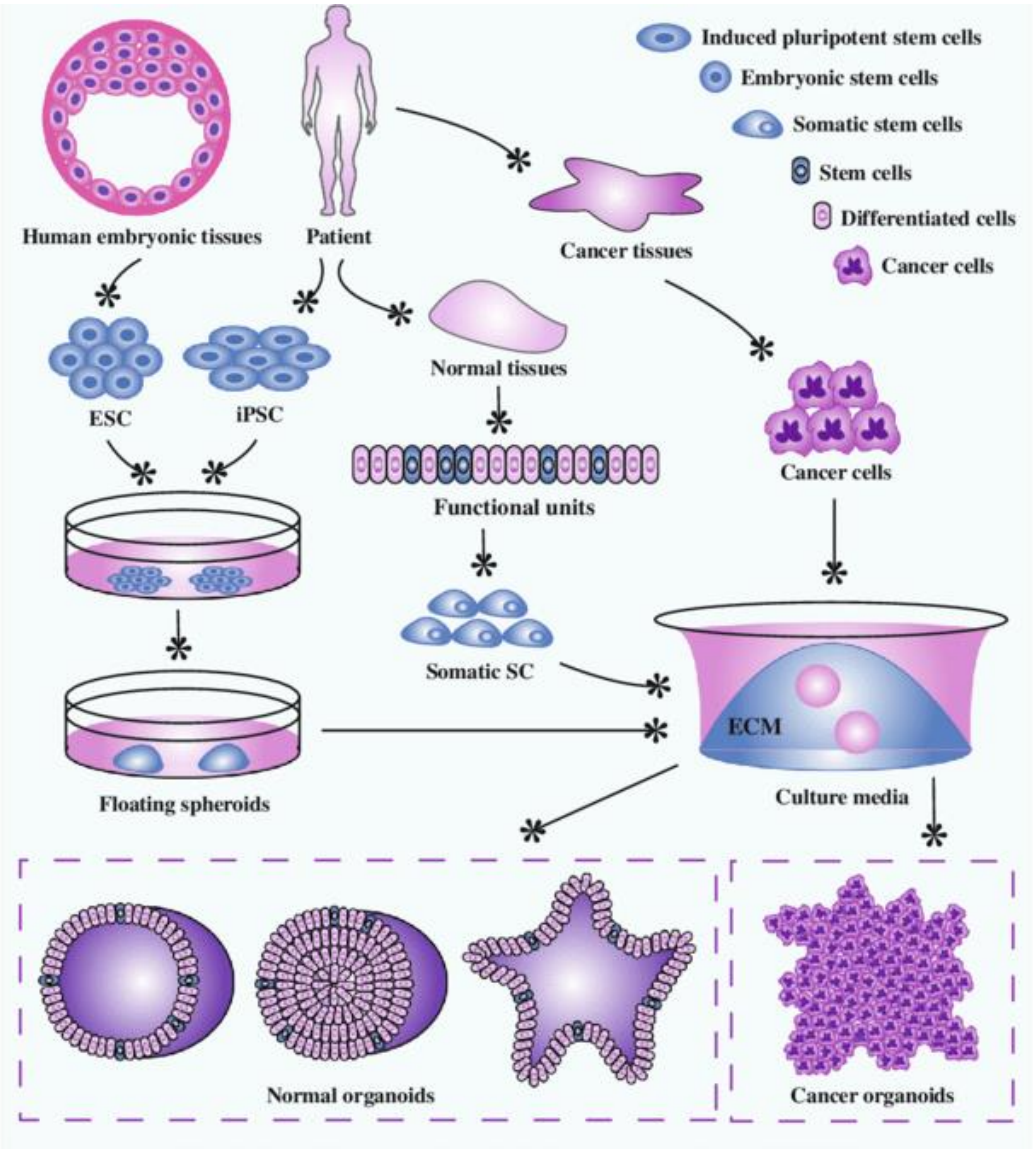


Figure 1-3. Generation of organoids from both human embryonic and adult stem cells. Organoids can be generated from various input material of individuals which highlights their invaluable potential in personalised medical approaches. (Reproduced from Xu H et al. Journal of hematology & oncology; 11, 2018).

1.3 CRISPR/Cas9 mediated Genome Engineering

A fundamental aim in the genetic analysis is to determine which genes contribute to peculiar biological phenotypes and diseases. Clustered regularly interspersed short palindromic repeats (CRISPR) was initially identified in E. coli in 1987 (78) and was further reported in several other bacteria species (79). For around twenty years the role of these repeated sequences was elusive. In 2005 multiple research groups, however, reported the existence of these sequences in phage DNA, indicating their potential contribution in the prokaryotic adaptive immune system (80, 81). Subsequent studies revealed that the CRISPR and its CRISPR-associated proteins (Cas) are components of prokaryotic adaptive immunity against bacteriophage invasion and DNA transfer (82). This advanced versatile genome engineering tool consists of two biological compartments: the RNA-guided DNA endonuclease Cas protein and a single guide RNA (sgRNA). The sgRNA molecule includes both a CRISPR RNA (crRNA) and a trans-activating crRNA (tracrRNA) component, which attaches to Cas9 endonuclease and guides it to a genomic sequence of interest to be cleaved (83, 84).

Upon exposure of the bacteriophage, the genetic elements of the invaders integrate into the host genome at the cite known as CRISPR repeat-spacer array locus (Figure 1-4). This provides the host genome with a genetic record of the prior infection and allows the organism to prevent the future invasion of the same invaders (85). Following transcription of the CRISPR array, the pre-CRISPR RNA is generated and subsequently undergo the enzymatic process to become a functional mature form so-called CRISPR RNA (crRNAs). Simultaneously the Cas9 endonuclease

and trans activating CRISPR RNA (tracRNA) is transcribed. The tracrRNA:crRNA hybrid recruits Cas9 endonuclease to cleave the foreign DNA guided by spacer sequences within crRNA (86). The resultant double-strand breaks (DSBs) are subsequently repaired either by nonhomologous end-joining (NHEJ) or by homology-directed repair (HDR) upon the existence of a donor template.

A laboratory-based single engineered RNA molecule combining crRNA and tracrRNA, further facilitated the application and guidance of Cas endonuclease to cleave a target site of 20n in targeted genes. Interestingly, the type II system of CRISPR family uses a single Cas protein to identify and target a DNA sequence and, thereby has gained considerable attention as a genome editing tools (87). Since 2013 onward, and the first application of type II Cas protein derived from Streptococcus pyogenes (SpCas9) and its combination with sgRNA to site-specific editing of DNA in eukaryotic cells, numerous studies have applied the similar approaches to target a distinct DNA site in different biological models (88, 89).

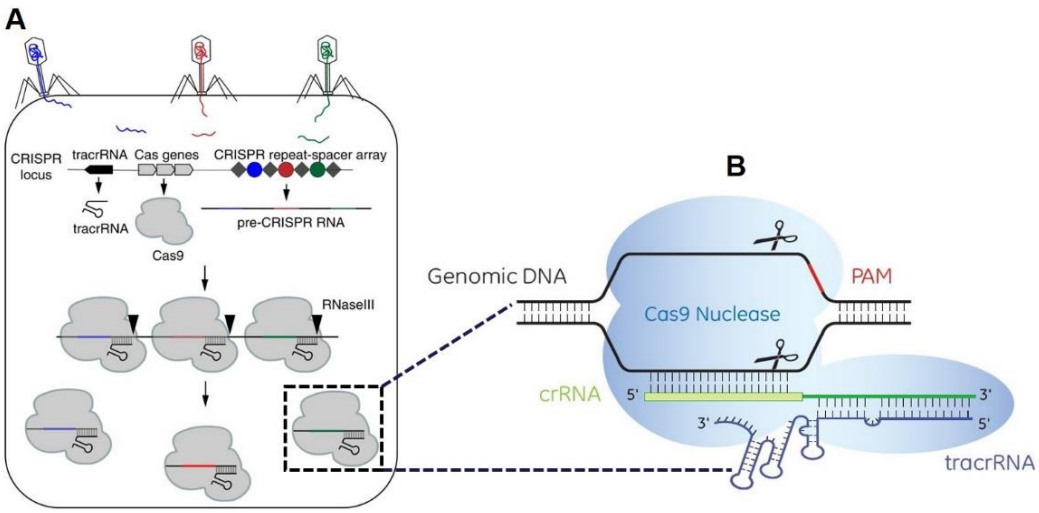


Figure 1-4. Schematic of CRISPR-Cas9 genome engineering system. A) CRISPR locus and the procedure of foreign DNA integration. **B)** Complex of Cas9/sgRNA for induced DNA double-strand break at target sequence using PAM. (Adapted from Dai WJ1 et al; Mol Ther Nucleic Acids; 5, 2016).

Cas9 endonuclease induces the DSBs approximately three nucleotides upstream of the protospacer adjacent motif (PAM) sequence (90). These breaks are identified and subsequently repaired by the cells' DNA damage repair system via two ways: 1) he error-prone non-homologous end-joining (NHEJ) system, which results in the formation of small insertions and frameshift mutations (indels) whit in the coding region of the genes and subsequent generation of the premature stop codon (91). This further produces a knock-out of the targeted genes expression. 2) The second mechanism in which cells deploys to repair the induced DSBs is HDR pathway. In case the single or double-stranded DNA is provided, this can be used as a donor template which will lead to accurate DNA repair modification (92).

Altogether, the CRISPR/Cas9 provides several advantages over conventional protein guided genome engineering tools such as zinc finger nucleases (ZFNs) and transcription activator-like effector nucleases (TALENs) (93).

Unlike the ZFNs and TALENS the DNA recognition by CRISPR/Cas9 is not mediated by protein and through protein-DNA interactions but rather by the 20-nt guide RNA sequence (94). This profoundly prevents a need for designing the domain requires for each specific DNA target site and thereby enhances their application for the large-scale screening purposes (95, 96). Moreover, the RNA sequence is much easier to be synthesized, designed and transfer into a cell than

protein domains (Table 1-1). The widespread use of conventional nuclease-based gene-editing tools like ZFNs and TALENs, therefore, are restricted by their time-consuming designing and complexity. In addition, with CRISPR/Cas9 multiplexing ability, multiple sites of the genome can be targeted in parallel (88). Overall, the CRISPR/Cas9 system is regarded as a more facile and efficient alternative tool to target genetic alterations in any biological systems (93).

	ZFN	TALEN	CRISPR/Cas9
Design	Protein engineering for every target site	Protein engineering for every target site	sgRNA of 20 nucleotide
Targeting mechanism	Protein-DNA hybrid (less prediction)	Protein-DNA hybrid (less prediction)	DNA-RNA hybrid (Highly predictable)
Delivery of the system	Two ZFNs around the target sequence are required	Two TALENs around the target sequence are required	sgRNA complementary to the target site with Cas9 endonuclease
Multiplexing*	Challenging	Challenging	Highly feasible
Library construction and for genome wide screens	Challenging	Challenging	Highly feasible
Affordability	Recourse intensive and time consuming	Affordable but time consuming	Highly affordable

* Capable of incorporating into multiple target sites simultaneously

Table 1-1. Comparison of different genome engineering tools for target gene editing purposes. (Adapted from Eid et al. Experimental & Molecular Medicine. 2016; 48).

1.4 F-BOX genes and Hallmarks of Cancer

Protein metabolism, posttranslational modifications and degradation is a fundamental process within cells to the immediate response to particular signalling or recycling of amino acids/protein axis (97, 98). Any disruption and deregulation in the balance of steady-state levels in this process may cause disease or cancer development. In general, there are two major intracellular pathways associated with protein degradation. The lysosome pathway and the ubiquitin-proteasome system (UPS)(99). The lysosome is involved in the degradation of extracellular proteins, whereas the UPS activity is limited to cytoplasm and nucleus. The proteolysis of proteins via UPS system known as ubiquitination and it is highly specific which orchestrates multiple main signalling pathways related to normal homeostasis and disease (100). A highly conserved ubiquitin (Ub) protein is consist of a 76 residue polypeptide. In general, the UPS targeted protein degradation consist of two well-established steps. 1) The covalent conjugation of multiple Ub proteins to the substrate and 2) the recognition and subsequent degradation of tagged protein via 26S proteasome system (101). Once a substrate is tagged with poly UBs, the 26S proteasome complex identifies it.

The eukaryotic 26S proteasome complex is consist of two subunits: the 19S regulatory unit and the 20S core particle. Following polyubiquitination of substrates

covalently, they are directed to the proteasome. Regulatory particle activity is to recognize, unfold, deubiquitylate, and transfer substrates into the core component, which contains the proteolytic sites of the proteasome (102). Of note, the ubiquitination is a reversible process and another class of enzymes so-called deubiquitylating enzymes (DUBs) mediate the breaking of the linkages thus paly important role in ubiquitin function. UPS exerts its activity via 3 enzymatic cascades mediated by ubiquitin ligases. The ubiquitin-activating E1 enzyme, the ubiquitin-conjugating E2 enzyme and the ubiquitin-protein E3 ligase. In humans, there are two E1 enzymes and approximately 30 E2 enzymes, however, there are ~600 of E3 enzymes (103). The specificity of proteolysis for any particular substrate is determined by its association with a specific E3-receptor subunit. The largest family of E3 ligase is Cullin-RING Ligase (CRL), in which the CRL1, also known as Skp1-Cul1-F-box-protein (SCF) complex is the well-characterized one (103, 104).

F-box proteins are the substrate recognition components of the Skp1-Cul1-F-box-protein (SCF) E3-ubiquitin ligases. The F-box is a protein motif of approximately 50 amino acids that functions as a site of the substrate-binding protein to the SCF-complex (105-107) (Figure 1-5). Despite their regulatory activity and importance for biology and medicine, the functions of most of the F-box proteins have not yet been fully defined so far. The Cullin backbone (Cul1) as a scaffold, binds to the RING-domain containing protein, Rbx1, which interacts and recruits a ubiquitin-conjugating E2 enzyme. Cul1 also attaches to Skp1, which binds with the F-box motif in FBPs. F-box proteins regulate substrates in diverse biological pathways,

including cell growth, development and differentiation, signalling responses, and cell survival/death (103, 108). Therefore, dysregulation of F-box protein-mediated ubiquitylation, which can occur via multiple distinct mechanisms, has been implicated in many pathologies including cancer (103, 108).

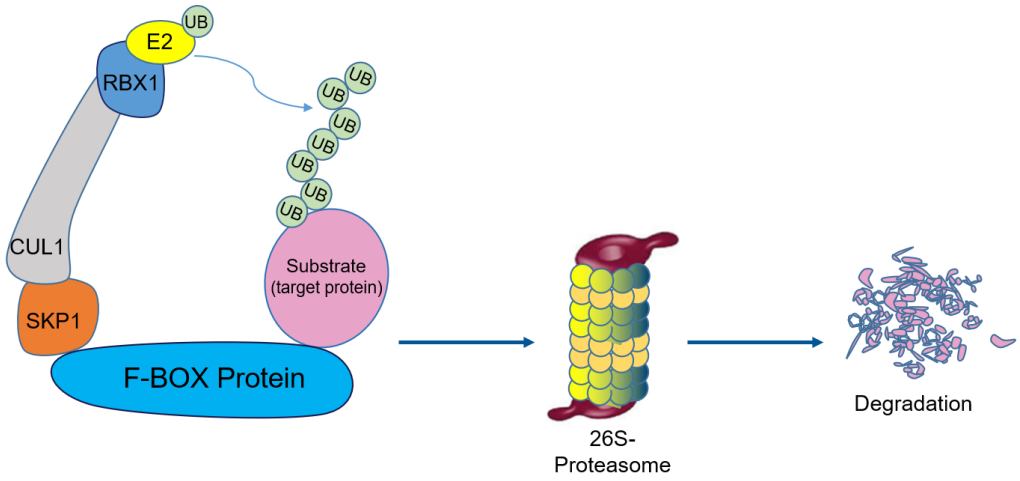


Figure 1-5. Schematic representation of SCF. F-box protein as part of the SCF complex play a significant role in recruiting the substrate for further ubiquitination and degradation by UPS. (Adapted from Dai WJ1 et al; Mol Ther Nucleic Acids; 5, 2016).

Accordingly, F-box proteins can function as oncoproteins when overexpressed (if their substrates are tumour suppressors) or as tumour suppressors (if their substrates are oncoproteins), thus playing their roles in different signalling pathways associated with tumorigenesis (Figure 1-6).

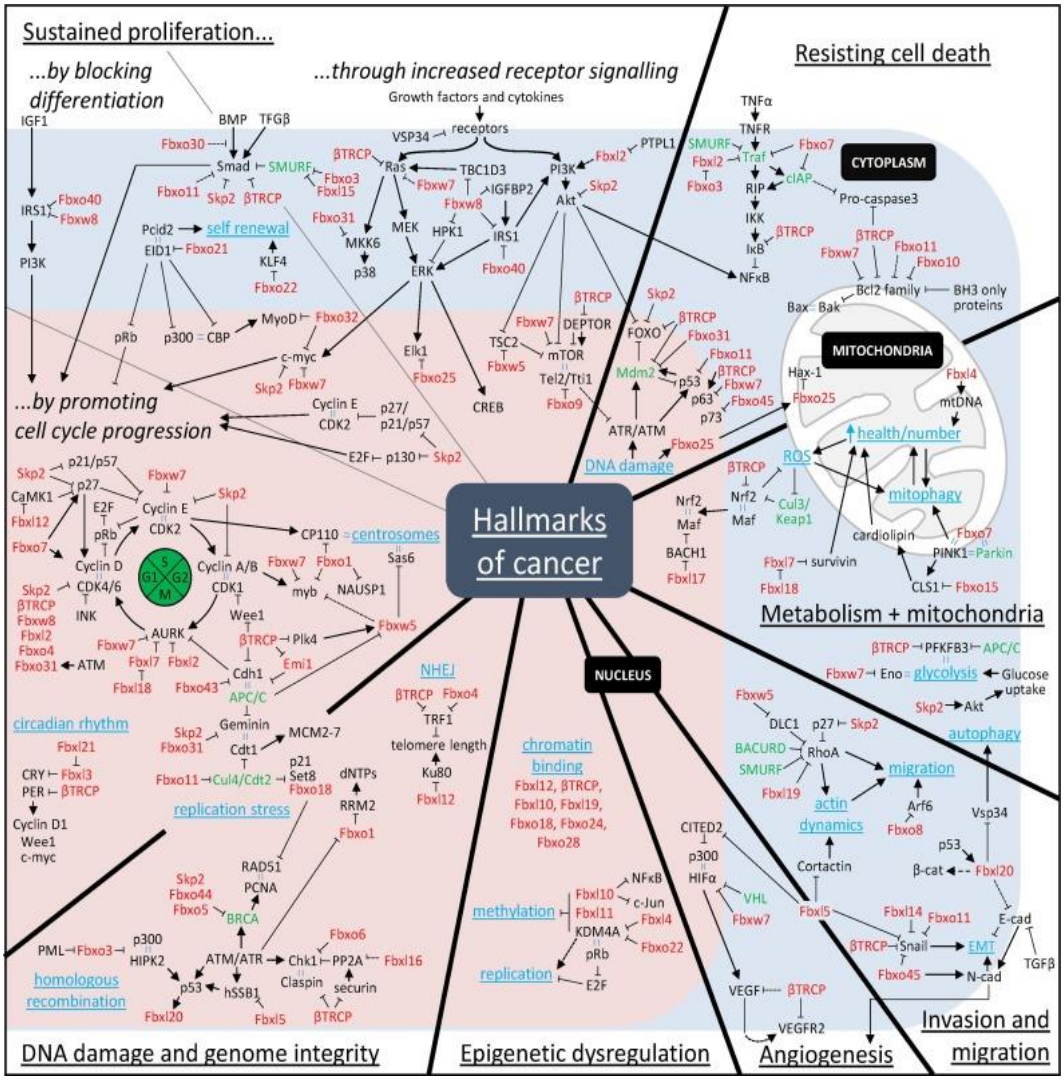


Figure 1-6. F-box genes contributions in hallmarks of cancer. (Adapted from Suzanne et al. Seminars in cancer biology; 36, 2016).

The FBPs physically interacts with substrates, using different domains including Leucine Rich Repeats, WD40 motifs, and other domains, which is also the basis for their classification into 3 sub-groups, FBXW, FBXL, and FBXO, respectively (109). Among the 69 F-box proteins identified in the human genome (110), the FBXW subgroups consist of 10 proteins and contain WD40 repeat domains, the FBXL proteins subgroups have 22 members that could be tumour

suppressors or oncoproteins. And the remaining 37 F-box proteins are known as FBXO proteins (Figure 1-7).

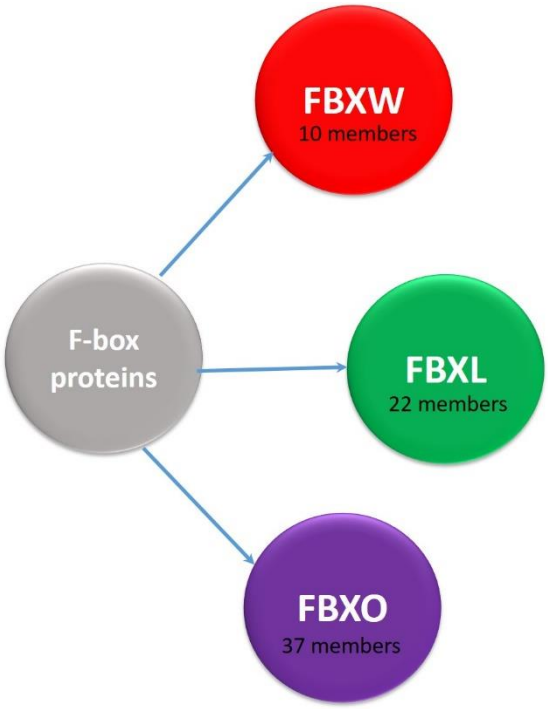


Figure 1-7. Classification of F-box genes based on the different repeated domains. (Adapted from Suzanne et al. Nat Rev Cancer; 14, 2014).

Among FBXW family member, FBXW7 with 36 substrates, and β-Trcp1/2 (Fbxw1/Fbxw11) with 75 substrates were extensively reported and studied in various malignancies (103, 111, 112).

FBXW7

The most frequently mutated F-box protein family in cancer, FBXW7, functions as is a tumour suppressor in various malignancies. FBXW7 specifically involves in the degradation of several oncoproteins such as c-MYC, NOTCH, KLF5, cyclin E, c-JUN, and MCL1 (113, 114). The *FBXW7* gene is located at chromosome 4q31q.3, and it encodes a protein about 707 amino acids and molecular mass of 79663 Da (115). The *FBXW7* has three isoforms known as FBXW7α (present in nucleoplasm), FBXW7β (endoplasmic reticulum), and FBXW7γ (nucleus) and they all have three crucial domains including (i) dimerization domain, (ii) the F-box domain and (iii) 7 tandem WD40 repeats and only differs in their amino terminal domain. *FBXW7* also involved in the maintenance of normal stem cells and progenitors. Previous studies revealed that the heterozygous loss of *FBXW7* impeded the differentiation of goblet cell in mice (116). The most common prevalent types of mutations in FBXW7 are located in hotspots region of binding domain and codons R505, R465 and R479 and accounts for 25.41%, 9.29% and 13.40% of all FBXW7 mutations respectively (117, 118). In a study by Babaei-Jadidi et al the conditional loss of both alleles in the intestine steered the formation of adenomas and accumulation of multiple Fbxw7 substrates (119). In addition, contaminant loss of Fbxw7 and p53 in the intestine resulted in the development of highly penetrant, aggressive and malignant adenocarcinoma (120).

Low level of FBXW7 expression correlated with poor prognosis in CRC patients (121). Recent study by Ning Li et al, demonstrated that the FBXW7 interacts and degrades the EMT-inducing transcription factor ZEB2 directly in a

phosphorylation-dependent manner in CRC (122). FBXW7 increased EMT, CR-CSC properties and metastasis (123). Different isoforms of FBXW7 is regulated differently within the cells. p53 known as one of the regulators of FBXW7(115). The previous study reported the overexpression of FBXW7 via induced upregulation of P53 by radiation (124). Moreover the expression of FBXW7 inhibited in p53−/− mice (125) In another study on 100 cases with gastric cancer (GC), Yokobori and et al, showed that GC patients with low FBXW7 expression and aberrant p53 mutation had a significantly poor prognosis in comparison with other subgroups (126). Emerging evidence on regulation of the FBXW7 also indicated the role of Non-coding microRNA (miRNA) and long non-coding RNA (lncRNA) in the activity of *FBXW7* gene. These are including miR-223, miR-25, miR-27a, miR-182, miR-503, miR-129-5p, and miR-92a (127-129). Some other studies also demonstrated that FBXW7 can be regulated epigenetically via DNA and histone modifications including DNA methylation (130, 131). In addition, simultaneous lack of p53 and FBXW7 correlated with chromosomal instability (CIN) of intestinal cancer, tumorigenesis and advanced trait (132).

β-TrCP

β-transducin repeat containing E3 ubiquitin protein ligase (β-TrCP) as another important member of FBXW family has oncogene role in different malignancies.

It has been reported that the overexpression of β-TrCP1 is detected in more than 50% of CRC samples. The suppression of β-TrCP1 inhibited the progression of

human breast cancer cells (133). In addition, β-TrCP1 is also upregulated in pancreatic cancer (134) and hepatoblastoma tissue samples (135). Among FBXL subfamily, the Skp2 (FBXL1), FBXL10, FBX11 has characterised well in different malignancies (136). Emerging and accumulating recent evidence, however, demonstrated the FBXL5 (F-box and leucine-rich repeat protein 5), also known as FBL4 and FBL5 as new and promising gene contributed to tumorigenesis of multiple cancers (137-139).

FBXL5

FBXL5 (F-box and leucine-rich repeat protein 5), also known as FBL4 and FBL5, is an iron and oxygen-regulated SCF-type E3 ubiquitin ligase (137). In our recent study, we found a lower expression of FBXL5 in normal tissue adjacent to colon tumours (138). We also demonstrated that antibacterial AM404 inhibited the expression of FBXL5, and FBXL5 attenuated AM404-induced anticancer activity in colonospheres derived from CRC-SC (138). FBXL5 physically interacts with Snail1 in the nucleus and promotes its polyubiquitination, thus influencing Snail 1 protein stability and subsequent activity (139). Of note, FBXL5 is extremely sensitive to stress conditions and is downregulated by iron depletion and γ-irradiation (139). FBXL5 oncogenic activity modulated the progression of colon cancer via regulating PTEN/PI3K/AKT signalling (140). FBXL5 interacts with Snail1 and suppressed Snail1 to inhibit the GC cell invasiveness and metastasis (141). In another study In gastric cancer, loss of FBXL5 elevated cisplatin resistance of gastric cancer cells via ERK and p38 activation (142). FBXL5 was

also involved in GEPR-regulated stability of Snail protein in osteosarcoma cells (143). G-protein-coupled estrogen receptor 1 (GPER) treatment of osteosarcoma cells (MG-63 and U2OS) significantly increased the expression of FBXL5 (144). This steered the subsequent degradation of Snail. On the other hand, knockdown of FBXL5 reversed the G-1-induced downregulation of Snail in osteosarcoma cells (143). Among FBXO subgroup, FBXO31(145, 146), Cyclin F (FBXO1)(147) and FBG2 (FBXO6)(123) , has been reported in various types of cancers. Here we highlight the function and potential tumour suppressor activity of FBXO31 as one of the important members of FBXO subgroups.

FBXO31

FBXO31 serves as a member of F-box family and located at chromosome 16q24.3. Previous reports indicated that the FBXO31 involved in DNA damage pathway via degradation of cyclin D and induce G1 arrest following the DNA damage (148, 149) (Figure 1-8). The FBXO31 is upregulated in lung cancer tissue and increased level of FBXO31 promoted growth, metastasis and invasion in lung cancer cell lines (150). FBXO31 suppressed gastric cancer progression via suppressing the epithelial–mesenchymal transition (EMT) transcription factor Snail1 (SNAI1) (146). BXO31-knockdown cells demonstrated hypersensitive to replication stress-inducing compounds and displayed profound genomic instability (151). Overall, FBXO31 is downregulated and may function as tumour suppressors in hepatocellular carcinoma (152) breast cancer (153)and gastric cancer(154) oesophagal squamous cell carcinoma(145) and lung cancer (150).

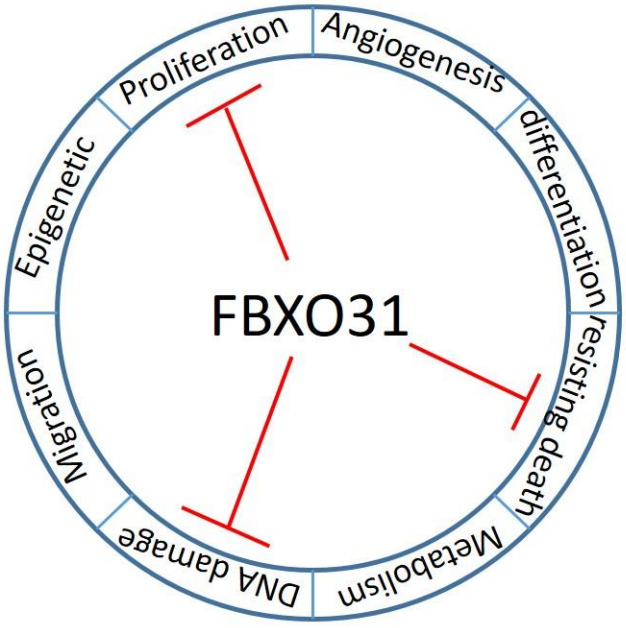


Figure 1-8. Role of FBXO31 in various signalling pathways links to cancer progression. (Adapted from Suzanne et al. Seminars in cancer biology; 36, 2016).

1.5 Dynamic of the Intestinal Epithelium and Self-renewal in the Intestine

The human large intestine contains 4 main compartments, 1) ascending colon, in which it is connected to the ileum via cecum junction, transverse colon which is characterised by its horizontal shape, the descending colon, at the left side of the abdomen and sigmoid colon which ends up to the rectum (155, 156) (Figure 1-9). On the other hand, the small intestine is divided into three regions, duodenum, in which it is attached with the pyloric of the stomach and it is located at the upper side of the small intestine. The jejunum and subsequently ileum at the end of the small intestine. The intestinal wall is comprising of four layers. The mucous layer

which consisted of three sub-layers including columnar epithelium, lamina propria (generates the basement membrane of the epithelium) and muscularis mucus Lamina propria. Muscularis mucosa comprising of two layers of smooth muscle fibres (155, 156).

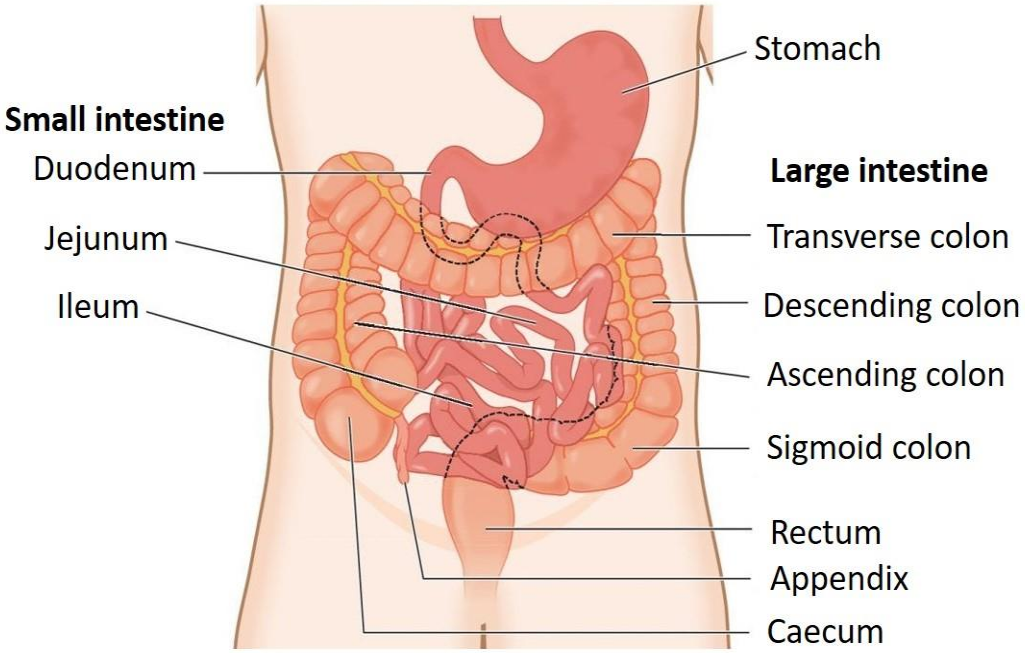


Figure 1-9. Schematic anatomy of the large and small intestine. (Adapted from Nigam Y et al. Gastrointestinal tract 4: anatomy and role of the jejunum and ileum; 9, 2019)

The columnar epithelium in the small intestine is replete with villi which provide a huge area to increase the absorption rate. The second layer is submucosa comprising collagenous connective tissue and blood vessels and also nerve cells (157). The serosa is the third main layer which is connective tissue. Epithelial cells form a barrier from the external environment in the mammalian gastrointestinal tract. Besides acting as a physical barrier, epithelial cells also play a significant role in

the activity of the immune system and digestion of the food. The immune compartment of the epithelial mucosa is able to respond to pathogen activity. The epithelium of the intestine has the largest surfaces containing a layer producing the crypts and villi (155, 158). There are millions of villi in the intestinal mucus which encompass 4 different types of cells. Enterocytes which are the absorptive progenitors and contain the digestive enzymes. Goblet cells as another important secreting cell types producing mucus. Enteroendocrine cells secreting the intestinal hormones. Tuft cells which produce and secrete endorphins and also prostaglandin. The intestinal epithelium renews every 4-5 days and this active process of cell proliferation and differentiation is fuelled by the stem cell pool (159, 160). The crypts are the home of intestinal stem cells which give rise to several putative progenitors of the intestinal epithelium. In the setting of the small intestine, the intestinal stem cells (ISCs) will terminally differentiate into five major cell types including enterocyte, goblet, enteroendocrine cells, Tuft and also Paneth cells (157).

Stem cells at the crypt base divide and give rise into daughter stem cells. These daughter stem cells enter the transient amplifying compartment (TA) and gradually migrate along the crypt while they differentiate toward fully differentiated intestinal cells. While they are differentiating, they pushed up the older differentiated cells until these progenitors reach the top of the villi and undergo apoptosis and subsequently shed to the lumen (Figure 1-10; A). The Paneth cells are only present in the small intestine and CD24+ cells are considered as their equivalent in the large intestine (161). In addition, the mesenchymal compartment around the ISCs which

regulates its activity is known as the niche. The maintenance of stem cells at the crypt base is governed by the interaction of several signalling pathways in the stem cell niche. The microenvironment of niche is crucial for ISC maintenance and self-renewal of the intestine which is mediated by paracrine signalling of several molecules including Wnt, bone morphogenetic proteins (BMPs), epidermal growth factor (EGF) and R-Spondin (RSPO) (162, 163). Generally, two models have been proposed for the intestinal stem cell compartment so far.

1) The crypt base columnar (CBC) ISCs: these cycling stem cells are highly proliferative and positioned at the crypt base among the Paneth cells. They are identified by their specific marker of LGR5. Besides the LGR5, Lrig1 as another stem cell marker is also broadly detected in descending colon as well as in small intestine (164). 2) Another slowly cycling stem cells known as DNA-label-retaining cells which are located at the "+4" position from the crypt base and initially proposed by Potten and colleagues (165, 166), (Figure 1-10; B). Several markers have been demonstrated for LRCs including Bmi1, Tert, Hopx and Lrig1 (167-170). Of note, Bmi1, Tert, Lrig1 and also Hopx are not only restricted to +4 cells and they have been detected by lower expression level in CBC cells as well (171, 172). The '+4' cells can differentiate toward fully differentiated cell including the Paneth cells and enteroendocrine cells (173). Stem cells in the colon and small intestine are marked with different stem cell markers. In comparison to the small intestine, a few studies have been accomplished to identify normal colonic stem cells.

Although LRCs have the quiescent state, it has been noted that in certain conditions the LRCs can gain proliferative status (174). There have been several roles linked

with the LRCs; 1) They are co-present with other rapidly cycling stem cells including LGR5 in a dynamic equilibrium fashion (175). 2) they are considered as reserve group of stem cells and they are active in case of damage and can replace other proliferative cycling stem cells (176). 3) They could differentiate terminally toward Paneth cells (177). Similar to other cell lineages within the crypt, the so-called '+4' cells are generated from LGR5+ stem cells. They are known as LRCs as they have been identified by the retention of DNA labelling dyes (178, 179).

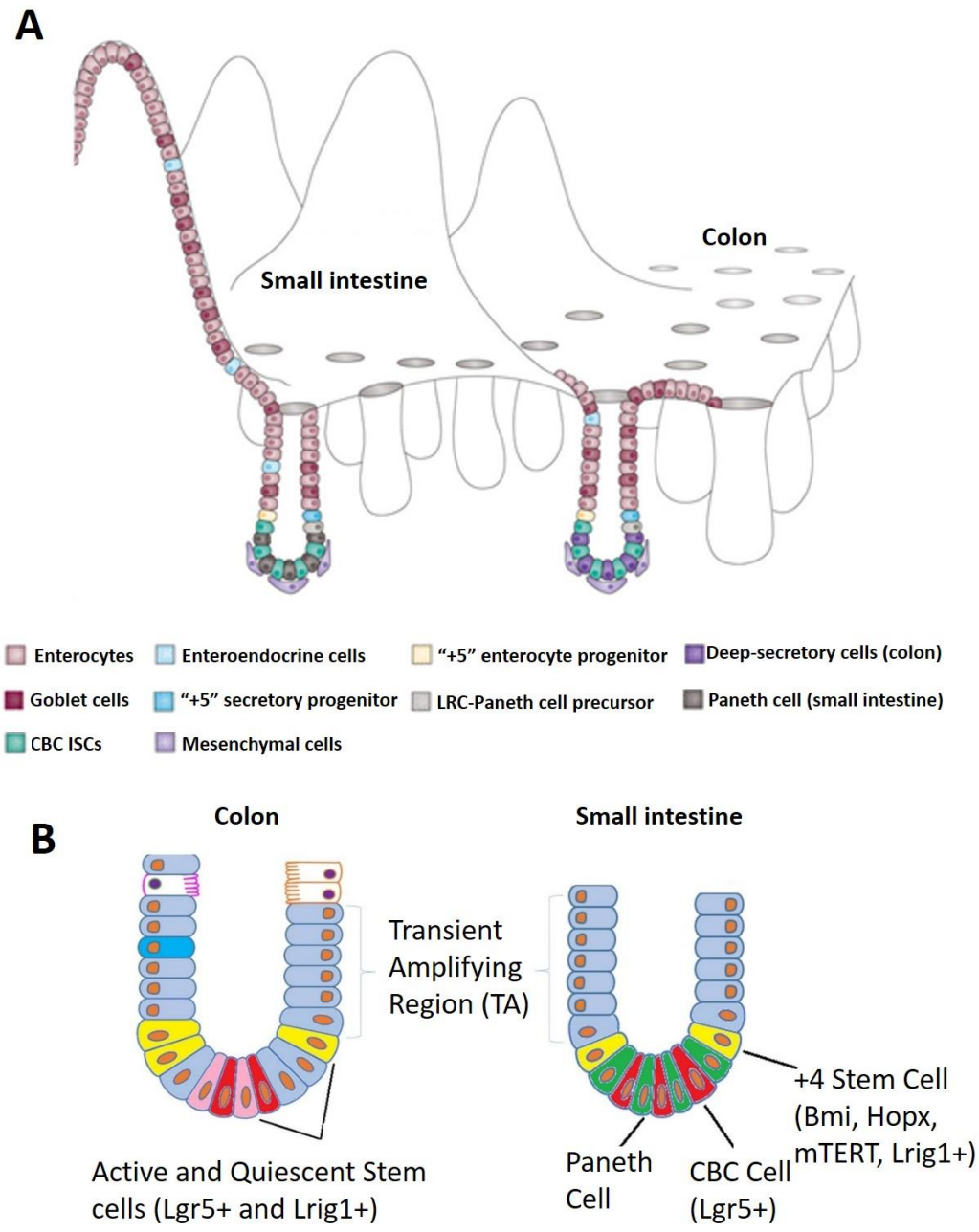


Figure 1-10. The schematic of the small intestine and colon epithelium. A) In both colon and small intestine epithelium, the stem cells are located at the crypt base. Stem cells at the bottom of the crypt divide while they are migrating along with the crypts and they differentiate toward fully differentiated lineages including absorptive and secretory cells as well as progenitor cells. **B)** The number and nature of the stem cell in small and colon intestine are different. The LGR5+ cycling cells and Lrig1+ quiescent cells are present in the crypt of colon epithelium. On the other hand, several stem cell markers including Bmi1, Tert, Hopx and Lrig1 beside

LGR5 have shown to mark the stem cells in the small intestine crypt. (Reproduced from Vermeulen L et al.Nat Rev Cancer; 2014; 14, 2018).

1.5.1 The Wnt Signalling Pathway in Intestinal Epithelium

The homeostasis of intestinal stem cells is mainly regulated by four crucial signalling pathways including Wnt, EGF, BMP and Notch. Among putative pathways, Wnt components are the most important players in maintaining the stem cell fate and the proliferation of stem cell progenitors in the intestinal crypt (180). The interaction of Wnt ligands with their receptors/co-receptors result in initiating of the cascade which leads to the maintenance of stem cells (181). In embryonic development, Wnt ligands are involved in several cellular processes including cell fate, proliferation, differentiation, cell movement, cell polarity and tissue regeneration (182). In adult tissue homeostasis, Wnt, however, is fundamental to the growth and regulation of stem cells. In the case of the Wnt pathway inhibition, the tissue renewal will be disrupted (183). There are mainly two signalling pathways related to Wnt activity (184-186):

1) The canonical Wnt/β-catenin pathway, in which its function is dependent on β-catenin.

2) Non-canonical pathway.

In the canonical Wnt pathway, cytoplasmic β-catenin is phosphorylated by a GSK-3/APC/Axin complex which is known as a destruction complex (Figure 1-11). Once the β-catenin have marked with this complex, it will undergo ubiquitination and

subsequent degradation by the ubiquitination/proteasome complex (187, 188). On the other hand, the presence of Wnt ligand in the environment stabilizes the level of cytosolic β-catenin as a main mediator of the canonical pathway. Upon binding of Wnt ligands to N-terminal extra-cellular domain of Frizzled (Fz) receptor which often requires a presence of co-receptors such as lipoprotein receptor-related protein (LRP)-5/6, results in activation of Dishevelled (DSH) and subsequent inhibition of ubiquitin degradation process. The accumulated β-catenin enters the nucleus and interact with T-cell factor (TCF)/Lymphoid enhancer (LEF) transcription factors and create a nuclear transcriptional complex. This transcriptional complex subsequently displaces the transcriptional inhibitors such as Groucho and allows the expression of downstream Wnt target genes such as *C-Myc*, *Axin 2*, *Cyclin D* and *LGR5*. These activated target genes are involved in different processes of cell proliferation and differentiation (189, 190). The principal regulatory role of the Wnt/β-Catenin in the homeostasis of adult stem cells is through TCF/LEF of transcription factors. As it has been indicated previously, the deletion of β-Catenin from the mice crypts resulted in rapid loss of TA cells (191). Fevr etal. reported that the stem cells were induced to differentiate toward fully differentiated cells as the consequence of this event (191). It has been also reported that the aberrant mutation in Tcf7l2 encodes the TCF4, resulted in intestinal stem cell loss and subsequent tissue malfunction (192). In the condition of β-catenin degradation and the lack of Wnt stimuli, the TCF protein interacts with transcriptional repressor including groucho/TLE from TCF to prevent the expression of Wnt target genes. The noncanonical Wnt pathway on the other hand, is independent of β-catenin/TCF or β-catenin/LEF and characterized by using

mediators downstream of the β-catenin complex. The noncanonical Wnt signalling varies according to the WNT receptors/co-receptors and their downstream regulators. Two well-characterized pathways are the planar cell polarity (PCP) pathway and the WNT–Ca^{2+} pathway (193, 194).

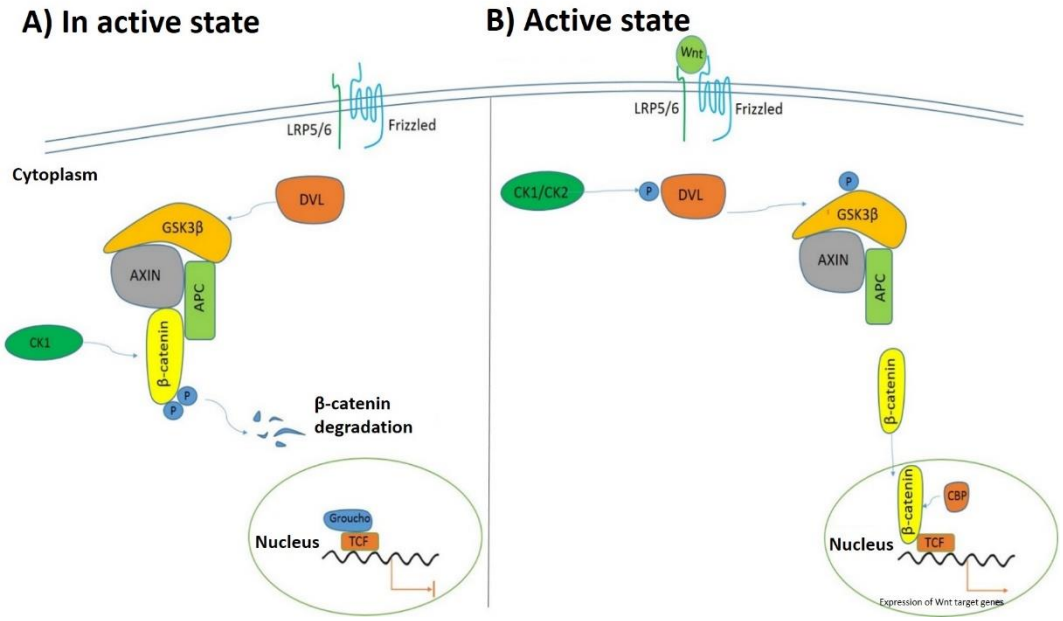


Figure 1-11. Schematic presentation of canonical Wnt Signalling Pathway. A) In non-stimulated cells, cytoplasmic β-catenin is tagged by a GSK-3/APC/Axin complex, consequently undergo the ubiquitination and subsequent degradation by the ubiquitination/proteasome system complex. **B)** Whereas, the presence of Wnt ligand results in the stabilization of the cytosolic β-catenin level. Therefore, the accumulated β-catenin move to the nucleus and interact with TCF)/ LEF transcription factors and create a nuclear transcriptional complex (1).

1.5.2 R-Spondin and Lgr family as regulators of Wnt signalling

In addition to Wnt/β-catenin canonical pathway role in the homeostasis of intestinal stem cells, the hallmark of Wnt signalling pathway in stemness activity is also

explained by the expression of ISC markers including LGR5 (195). Intestinal stem cells give rise and differentiate into different epithelial cell types. The SCs first divide into a daughter stem cells which they will subsequently differentiate toward terminally differentiated epithelial cells. LGR5 is expressed in several tissues (196-198). Previous studies noted LGR5+ cells as fast cycling stem cells in colon, stomach and also the hair follicles (197, 198). Since they are highly proliferating and there is limited space for cells at the bottom of the crypt, therefore, a particular number of stem cells remain in the crypt base while 50% of them exit the stem cell zone and enter the TA region and gradually differentiate into fully differentiated cells.

The determination of stem cells fates to remain at stem cell zone and become daughter stem cells or enter to the TA region is not fully identified and it is regarded as "neutral competition" between LGR5 stem cells which dividing symmetrically. The CD24 cells in the colon may be the equivalent of the LGR5 cells in the small intestine (161). Recent data suggesting that CBC cells within the nearest position to the crypt base have a higher chance of remaining as stem cells than those reside at upper regions. The regulation of stem cells and this competition is not fully characterized, however, some studies indicating the Paneth cells as the regulator of stem cell maintenance in stem cell niche (199). Furthermore, it has been demonstrated that R-Spondin, as a growth factor, binds to the LGR5 receptor which subsequently regulates the stem cell maintenance. Both R-Spondin/LGR and Wnt ligands directly bind to Frizzled (Fzd)-LRP-receptor and activate further downstream signalling pathways. R-Spondins, are belong to a superfamily of

thrombospondin type 1 repeat (TSR-1)-containing proteins. R-Spondins have a fundamental role in stem cell growth via their agonist activity in both canonical and noncanonical Wnt/PCP pathways (200-202). R-Spondins bind to LGR family of transmembrane receptors including LGR 4/5/6. Upon binding to their receptors of LGRs, they enhance canonical β-catenin signalling (203, 204). Generally, once Wnt ligand binds to its receptor, approximately 100 downstream genes will be activated which are including *cMyc*, *Cyclin D*, *LGR5*, *ZNRF3* and *RNF43*. In 2012, Koo and colleagues reported that RNF43 and ZNRF3 transmembrane E3 ubiquitin ligases (Wnt signalling negative regulator) ubiquitinate the frizzled receptor on the cell surface, which results in the reduction of Wnt activity (205). Following the loss of RNF43 and ZNRF3 leads to high activation of Wnt target genes (205). The intracellular interaction of Rnf43/Znrf3 with of Fz/LRP complex, results in inactivation and endocytosis of the Fz/LRP complex which subsequently breaks down the Wnt cascade (206). In addition, LGR4 and ZNRF3 construct a receptor complex for R-Spondin binding. It has been reported that in the presence of R-Spondin, the R-Spondin binds to its corresponding receptors of Lgr 4/5/6 and leads to the removal of the Rnf43/Znrf3 from the membrane which enhances the Wnt signalling. Particularly, it has been noted that the R-Spondin enhanced Wnt activity via inhibiting ZNFR3, therefore, prevents ubiquitination of frizzled receptor (207).

The LGR5 cells are squeezed between the Paneth cells and they have the particular structure which increases the shared membrane between these two cells which mechanically results in decreasing the cross-talk between the homologous (Paneth-Paneth or LGR5+-LGR5+) cells. Indeed, this morphology indicating the

associating between the Paneth cells and LGR5+ cells (199, 208). Depletion of Paneth cells has also shown to decrease the number of ISCs which implies the association between the LGR5 stem cells and Paneth cells. On the other hand, however, some studies reported that the stem cell population size and its regulation in stem cell zone are not restricted only to the presence of Paneth cells in *in vivo* condition and several other modulators may play roles in stem cell regulations (209, 210).

1.5.3 Noggin regulates the homeostasis of epithelial stem cells through BMP gradient

Noggin, a 64kD secreted homodimer glycoprotein, governs a diverse cellular and molecular event from homeostasis of adult/embryonic stem cells and neurogenesis, to recent data, suggesting the differential activity of Noggin in the progression of various malignancies (211-215). Noggin expression is required for the patterning of embryo, whereas, the lack of Noggin is prenatally lethal and manifests a numerous profound developmental abnormality in mice. Initially identified as a dorsalizing factor in the Spemann organizer of Xenopus embryos (216), Noggin along with other inhibitors such as Chordin and Follistatin, orchestrates a variety of signal transduction pathways in the development of embryo axes (217, 218). Direct antagonizing of bone morphogenetic proteins (BMPs) in extracellular space enables secreted Noggin to interfere with the BMPs-mediated signalling pathway.

BMP signalling as a fundamental pathway in the homeostasis of stem cells mediates the epithelial differentiation and negatively regulates the number of ISCs. BMPs are a member of the transforming growth factor-β (TGF-β) superfamily and they

are involved in a variety of cellular functions consist of intestinal development, proliferation and also differentiation of epithelial cells in the intestine (219). Approximately 30 BMP proteins have been identified which some of them have been well described and characterized in previous reports including the BMP2, BMP4 and BMP6. As demonstrated by Hardwick and etal. the BMP2 is expressed by the epithelial cells of the human and mouse intestine (220). They also reported that the BMP2 also play as a tumour suppressor promoting apoptosis factor in mature colonic epithelial cells. In addition, BMP4, as another member of this family is considered as a Wnt target gene in canonical Wnt signalling pathway (221). Generally, the regulatory mechanism of the BMP components begins via their interactions with their receptors on the cell surface. Upon binding of BMP ligands to their corresponding receptor known as BMP receptor type I (Ia/Ib) and II the signalling will be activated. When BMP recruited to BMP receptor II, it results in the phosphorylation of BMP receptor I. This consequently phosphorylates the group of SMAD proteins known as R-SMADs (SMAD1, SMAD5 and SMAD8) which enable them to constitute a complex with co-SMAD (SMAD4). The R-SMAD/co-SMAD complex will translocate into the nucleus in which it binds to a specific DNA binding protein and eventually plays the role as a transcriptional enhancer. The BMP pathway is extensively expressed in differentiated progenitors. Generally, BMPs are mainly produced by mesenchymal cells in the intestine, however, some members of this family can be generated in the epithelium as well. On the other hand, the expression of BMP inhibitor molecules consisting of Noggin or Gremlin is required for the normal self-renewal activity of ISCs (222, 223). Noggin as a secreted protein which plays as an extracellular negative regulator of the BMP

signalling and it is crucial for intestinal organoid maintenance in long-term. For example, as Sato et al. demonstrated, upon the depletion of Noggin, the organoid loss the expression of LGR5 stem cells which leads to the abrogation of proliferation (53). Despite the lack of mesenchymal compartment in organoid culture *in vitro*, in which there are no exogenous BMP signalling surrounding the crypt, the presence of Noggin as a BMP signalling inhibitor is still essential, indicating the expression of BMPs by the epithelium of the intestine which needs to be suppressed by the Noggin activity (199, 224). Furthermore, *in vivo* Noggin inhibitory activity is essential for the generation and maintenance of BMP gradient in intestinal stem cell epithelium at the stromal niche adjacent to the crypt base. Of note, *in vitro* exogenous Noggin administration is also required for the establishment of an advanced self-organizing 3D model known as organoids.

In the context of malignancies, Noggin suppressed the motility and invasion via PI3K/Akt pathway in gastric cancer cells expressing BMP-2 (211). In another study Noggin initiated and promoted skin tumourigenesis through stimulation of Wnt and Shh signalling in K14-Noggin mice (213). Noggin was also identified as a specific breast cancer bone metastasis supporting gene and promotes the metastatic of breast cancer cells (225). Noggin overexpression via retroviral transduction in prostate cancer cells (PC-3) restrained the tumour growth following transplantation. Noggin also antagonized BMP activity and decreased the proliferation of tumour cells *in-vivo* (226). Altogether, the direct effect of Noggin in colon cancer cell lines and PDOs are mainly elusive and requires further investigation.

1.6 *Ex vivo* Culture of the Intestinal Epithelium: Intestinal Organoid

Hans Clevers laboratory established 3D organoids from both murine and human intestinal epithelium (227, 228). In this condition, growth factor and inhibitor compounds have exploited to recapitulate the signalling pathways surrounding the intestinal stem cells. In order to expand the intestinal organoid from human intestinal epithelium, the crypts were isolated and seeded on a submerged extracellular collagen rich matrix known as Matrigel. Following culturing the crypts on this scaffold, Wnt-3a and the Wnt agonist R-Spondin1 along with several substantial growth factors and inhibitors including the EGF and the BMP antagonist Noggin were gradually administrated (227, 228). These signallings are applied to mimic the exogenous signalling around the stem cells which are required for the growth of crypts *in vivo* (Figure 1-12).

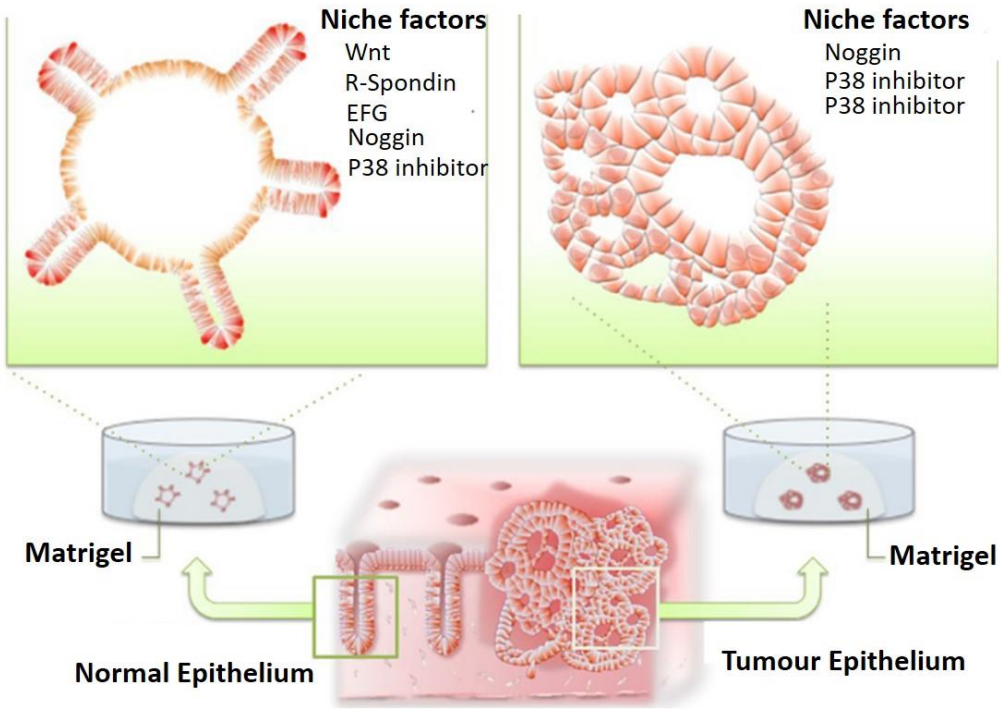


Figure 1-12: Culturing the Human Intestinal organoid. The crypts and tumour fragments were isolated and seeded on Matrigel and organoid culture medium containing the stem cell niche requirements was added for growth and expansion of the organoids (Ohta Y and et al. Intestinal Tumour in a Dish. Frontiers in Medicine; 1, 2014).

Applying the precise functional concentration of each component is essential for the expansion of intestinal organoids *in vitro* culture. Altogether, the organoid culture method has been used for serial passage and growth of both human and mouse intestinal organoids. The so-called WENR components (Wnt-3A, EGF, Noggin, R-Spondin) are the essential intestinal niche factors and the growth and expansion of intestinal organoid culture in vitro requires the presence of latter components(229). These stem cell niche factors are though tissue-specific and each mammalian organs have peculiar stem cell niche. Of note, the stem cell niche in some tissues and organs yet to be identified. For example, skin and ovarian and their stem cell regulators have not been fully characterised.

1.7 Colorectal cancer, a Heterogeneous entity and it's Current Therapeutically Approaches

Colorectal cancer (CRC) is the third most prevalent type of cancer and the fourth cause of cancer-related death worldwide after lung, liver and gastric cancer with approximately 1.4 million new cases diagnosed and almost 700 000 deaths were reported in 2012 (230). In European countries including the United Kingdom, CRC has the second mortality rate both in male and females (231). Approximately

446,000 new cases of CRC diagnosed in Europe each year. CRC usually arises from benign neoplasms known as adenomas and serrated polyps and in case they remained un-resected, they will eventually transform into malignant tumours within the next several years. In general, it is the accumulation of aberrant mutations results in the transformation of normal epithelial cells into invasive adenocarcinomas which is called adenoma to carcinoma sequence model (232). The model was first proposed by Vogelstein and colleagues which highlighted the formation of benign neoplasms (adenomas/sessile serrated polyps) and subsequent progression to more advanced lesions and invasive carcinoma (232). In general, two models have been suggested for the carcinogenesis of CRC so far. In the stochastic model of CRC development any cell types have the equal chance of initiation of malignancy while in a cancer stem cell model, only a small subpopulation of cells known as colorectal cancer stem cells are capable of developing CRC. CRC tumours display a high level of heterogeneity. This heterogeneity is due to the correlation between the genomic properties of tumours with their environment (233). Indeed, based on this heterogeneity, each cell harbour different intracellular mutation pool which interacts with their extracellular environment. Thus, the fraction of cells may survive and continue to grow and they somehow escape from common therapeutic approaches. According to the latter model, this subpopulation of stem cells further results in recurrence of tumours, drug resistance, and subsequent metastasis. On the other hand, genomic instability is recognised as a major genetic event in CRC progression (234). There are three main pathways of genomic instability linked with CRC development (235). 1) Chromosomal instability (CIN); 2) microsatellite instability (MSI) which defined

with a molecular signature deficient in a mismatch repair system and a 3) is the CpG island methylator phenotype (CIMP) which is characterised with CpG islands methylation in promoter regions resulting in inactivation of tumour suppressing genes (236). Up to seventy percent of sporadic CRC cases show CIN which is the instability of chromosomes and can often results in aneuploidy (237). In the setting of CRC, this pathophysiological event is probably orchestrating initiation and further tumorigenesis (238).

Generally, So far, four consensus molecular subtypes (CMSs) with defined molecular trait has been proposed in CRC tumours (239) (Figure 1-13). CMS1, so-called microsatellite instability immune accounts for 14% of tumours, characterized with hypermutation (defined based on whole-exome mutation, >180 events per exome), microsatellite unstable, strong immune activation, having BRAF mutation and extremely worse survival following the relapse. CMS2, known as canonical subtype and consist of large amounts of tumours (37%), defined with somatic copy number alterations high (CSNA) along with activated WNT and MYC. CMS3 or metabolic pathway, defined with low CIMP and SCNA and mixed MSI features and accounts for the 13% of tumours. The last subtypes consist of stromal infiltration, activated TGF-β and angiogenesis. The tumour display high SCNA and worse both disease and overall free survival and proposed for 23% of CRC tumours. Of note these grading were based on the different molecular trait and the present of immune components and reproducing the same condition in organoids requires applying the genome engineering based modelling or co-culturing approaches with of fibroblasts, tumour microenvironment or immune components.

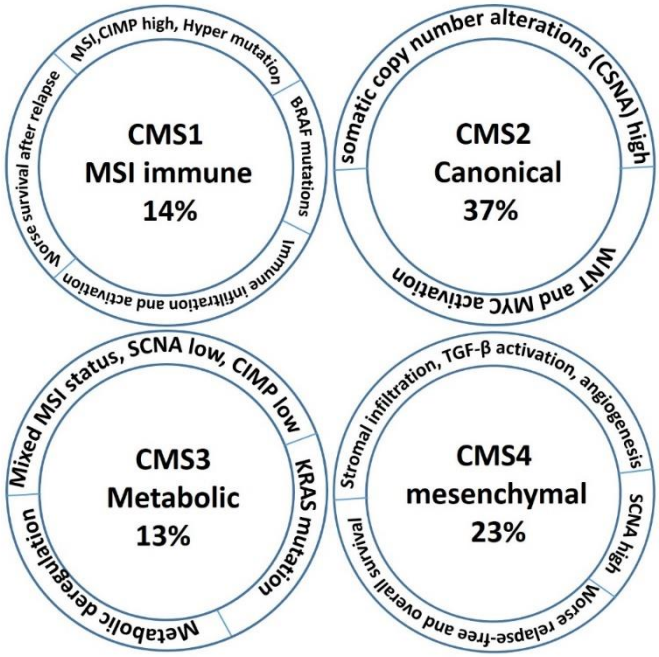


Figure 1-13: Consensus molecular subtyping of CRC. (Adapted from Guinney et al.; 21, 2015).

The curative resection is the frontline plan of action in a newly diagnosed patient with localized tumour (70-80% of patients). Chemotherapy may be applied prior to operation (neoadjuvant chemotherapy), or following the surgery (adjuvant chemotherapy) or in cases with unresectable metastatic disease (20-30% of the cases) (240).

In addition, a considerable proportion of patients (40%–50%) experienced disease recurrence after surgical resection or may develop metastatic disease, and typically in the liver or lungs. Though, it is yet common for the 40-50% of patients to develop recurrence or metastasis following the surgical resection. It has been reported that the 5-year survival rate of patients diagnosed with the early stage of CRC (stages I and II) is 90%. However, because more than 50% of cases are diagnosed at or

beyond stage III (presence of distant metastasis) this drops the 5-year survival rate to 70%. Current common therapeutics for CRC treatment consists of platinum-based chemotherapeutic compounds such as oxaliplatin and cisplatin and biologic agent 5-Fluorouracil (5-FU). Overall, chemotherapeutic intervention coupled with surgery is the major approach in metastatic CRC and the only way of increasing patient survival. 5-FU is an analogue of uracil tagged with a fluorine atom (241) which can integrate into RNA and DNA (242) leading perturbation in nucleoside metabolism and subsequent cytotoxicity and cell death (243). 5-FU has improved median survival of advanced CRC patients in the last three decades (244). Oxaliplatin a third-generation platinum agent as a semisynthetic inhibitor of topoisomerase mediates mitotic arrest in the cells.

5-FU has remained a standard therapy for advanced CRC tumours, however due to their lack of specific toxicity against cancer cells the application of chemotherapy and biological agents such as 5-FU has contributed to further complications and related side effects (245). In addition, the resistance of CRC tumours and cells to chemotherapy regimen has contributed to lower survival rates of CRC patients (246). This resistance feature is a major issue in patient outcome, therefore identification of drug resistance mediators as well as the generation of novel therapeutics is of significant value for future patient care. Therefore, novel therapeutic compounds are required to deal with the high incidence of CRC cases, to improve the efficacy of chemotherapy and alternative regimens. In this regard, cancer treatment has gained considerable attention for the applications of several emerging compounds including antibiotics to evaluate their effects in cancer treatment and patient's survival. In the context of wider literature, antibiotic

application in adjuvant therapy has been reported in several malignancies including CRC (247-249). Kan et al. reported the anti-metastatic activity of fluoroquinolone antimicrobial agent Gemifloxacin (GMF) in colon cancer cells (250). They demonstrated that GMF significantly suppressed the migration and invasion of SW620 and LoVo colon cancer cells (250). In another study, the penicillin-streptomycin cocktail suppressed the sphere-forming ability in suspension culture of 6 colon cancer cells (251). In our recent work, we demonstrated that AM404, a metabolite of acetaminophen with antibacterial activity, showed high potential in suppressing CRC-SC trait, such as stemness/de-differentiation, migration and drug-resistance (252). Altogether, identify the new uses for current existing drugs including the antibiotics with well-characterised profiles in other diseases and exploring their potential value in the prevention of malignancies would help to open a new therapeutic window in cancer treatment.

1.7.1 Targeted therapy of colon cancer stem cells

In colorectal cancer, the metastasis remains the main cause of mortality. Although the surgical approach is the gold standard and effective treatment in the majority of localized tumours in early stages (I/II), however, surgery and adjuvant chemotherapy are effective in only 30% of the CRCs in stage III with regional lymph node metastasis. In patients with advanced stages (IV) and metastasis, the majority of patients die due to the metastasis and the putative approaches are not efficacious (234, 253, 254). On the other hand, the lack of information about the underlying mechanisms leading to metastatic hampering the identification and targeting of driver genes and related pathways in CRC patients. Therefore,

exploring related biomarkers and potential prognostic factors for CRC tumours with metastasis will improve the patient survival especially in late stages (255). Several studies have been carried out to identify the potential regulators of metastasis and recent works have suggested a possible contribution of cancer stem-like cells CSCs in metastasis mechanism. The notion underlying this is that 1) the CSCs have the tumour-initiating capacity which is the first and fundamental characteristic in order the tumour forms in distant locations (256). In addition, 2) recent studies noted the presence of epithelial–mesenchymal transition (EMT) markers in CSCs, which indicates their migratory and subsequent invading capacity (257).

It has been noted that identification and following characterization of stem cells for the therapeutic purposes are difficult. The exact normal stem cell number differs from every individual. Another potential factor which may affect the stem cell pool is the age. It has been demonstrated that the number of stem cells decreases by aging. In addition, the ratio between normal stem cells and differentiated progenitors as well as cancer stem cells and tumour cells is not defined so far exactly. Although previous data revealed the CSCs fraction as a small subpopulation of tumour balk (258), however, recent studies suggesting that the percentage of cancer stem cells may constitute any proportion of the tumour mass. The more the percentage of the CSCs the more risk of the metastasis and tumour recurrence.

Therefore, application of tumour/adjacent derived organoids containing high yield of normal/tumour stem cells would provide an informative source to study several aspects of personalised medicine, and drug efficiency. Normal and cancer stem cells possess several common characteristics including 1) self-renewal activity, 2) active

telomerase expression 3) active anti-apoptotic pathways 4) high membrane transporter activity and 5) having migratory and following metastasis ability. Cancer stem-like cells and tumour-initiating cells terms are widely used in the field of cancer stem cell study. Generally, cancer stem cells are the stem cells derived from normal stem cells and have achieved several mutations which enable them to drive tumour formation and drug resistance. Although, they still share common pathways with normal stem cells. On the other hand, tumour initiating cells referred to CSCs capable of initiating tumour development after transplanted in an animal model (259). It has been demonstrated that CSCs can give rise to all cell lineages within the tumour bulk. They have the self-renew activity and capable of generating cells without stem cell properties which together build the tumour structure. This CSCs can be determined by transplantation of the tumours into genetically engineered models. The cancer stem cell niche is also an important factor in regulating cancer progression and they could even give distinct trait to differentiate cancer and normal stem cells. In the colon, colon cancer stem cells are characterised by the enhanced expression of markers such as CD133 (260, 261), LGR5 (262, 263), CD166 (264), and also present high level of ALDH1 (265) and Wnt signalling components expression within the cells (266).

In comparison to other cells within tumour bulk, cancer stem cells have the highest ability in maintaining and also the progression of the tumour. Lgr5 cells which present in approximately 10% of all tumours in mouse intestine, have been reported to be responsible for the progression of adenoma (267). CSCs were initially identified in acute myeloid leukaemia (AML). Since then, several markers have been used to identify CSCs in various types of cancers including colon (268),

leukaemia (269) brain (270), breast (271), pancreas (272) and lung (273), prostate (274). Recently, interestingly, it has been demonstrated that the normal committed terminally differentiated epithelial cells are also capable of dedifferentiation and generating stem cells (275). Altogether, exploring the gene expression dataset linked to cancer stem-like cells (CSCs)/normal stem cells for primary and matched tissues from colon cancer patients would provide an informative source in order to analyse the genes differentially regulated in these two samples. As the organoids enrich with stem cells they are the valuable source to study the genetic signature and compare the differences between the spheres drive from tumours and normal primary samples. In the setting of colorectal cancer and according to the current theory of CSC, small subpopulation of cancer cells within the tumour has this particular capability to i) divide and ii) grow to form the colonospheres. They also enable differentiating to other differentiated cell lines in the population as well. CSCs and tumour-initiating cells are a fraction of cancer cells with self-renewal activity. In comparison to most of the cancer cells which have restricted proliferation ability, CSCs can grow, differentiate and also contribute to metastasis and subsequent drug resistance and recurrence.

The contribution of CSCs in tumour progression, metastasis as well as resistance to treatment has been already demonstrated in several studies (276-278). Therefore, efficient cancer therapy approaches are required to specifically 1) identify and 2) targeting the CSCs to reduce the possible subsequent recurrence. In fact despite the identification of CSC with current markers, variety in phenotype and morphology of CSCs hampers their application in many studies (279, 280). In fact, the conventional chemotherapy approaches are based on targeting the highly

proliferative and differentiated cells. However, a fraction of stem cells are not metabolically active and they are in the quiescent state, thus, they are not being targeted by the conventional radio and chemotherapy approaches and contribute to regrowth of tumour and relapse in related patients.

Formation of the new tumour by CSCs have been functionally validated through transplantations of CSCs in immune-deficient mice by various concentrations [19]. The principle underlying the attribution of CSCs in metastasis is relying on the regulatory activity of Wnt pathways both in EMT and stem cell maintenance (281). Similar to stemness activity, EMT process is also mediated by Wnt and transforming growth factor β(TGFβ) pathways components in which both of these pathways are dysregulated in tumours (282). As Michl etal. demonstrated on a series of CRC tumours, there was a significant correlation with aberrant regulation of Wnt/β-catenin-signalling and high expression of CSC markers including CD44 and CD133 with liver metastasis (283). In another study on CRC tumours by Ordóñez-Morán et al. revealed that high expression of HOXA5 (a promising gene in differentiation of normal intestinal stem cells) can drive differentiation of colorectal cancer stem cell via suppression of Wnt signalling pathway (284). In another study, Pang et al. (285) identified that patients lack the metastasis at the time of presentation but higher expression of CD26+ in their tumours, developed the distant metastasis on further follow-up procedure which indicates the significant clinical relevance of this cancer stem cells expressing CD26 (285). On the other hand, as the main objective of chemotherapy is to induce the apoptotic cascade in target cells, another mechanism of chemo/radio resistance of CSC could also be due to high expression of anti-apoptotic genes including Bcl-2, NF-kB, Survivin and

multidrug resistance ATP binding cassette (ABC) transporters. Drug resistance of CSCs via ATP-binding cassette transporters is mediated by an intriguing pathway of ABC transporter system (286-289). The ABC transporters family consist of 49 members in which three protein of this family have been reported to be highly associated with multidrug resistance [32] and [33]. The role of ATP proteins in drug resistance has been reported in several malignancies including breast (290, 291) glioma (292), hepatocellular carcinoma (293), CRC (294, 295), melanoma (286) acute leukaemia(296). In this regard, as in a study by Frank NY revealed that ABCB5 contributed to the chemo-resistance in human malignant melanoma. The expression level of ABCB5 was significantly high in cells marked with CD133+ stem cells in related tumours (286). Previous studies indicated that in a purified population of CD133+ sorted stem cells the expression of ABCB5+ were significantly elevated in approximately half of the tumour cell population (297-299). The ABC proteins mediate the translocation of several molecules through the membrane including metabolic products, peptides and proteins and lipids inorganic and organic ions (300). The energy requires for the activity of the ABC transporter is provided by the hydrolysis of ATP (301). Interestingly, the multidrug resistance pattern in colorectal cancer stem cells somehow follows a completely different model in which differentiated cells in tumour mass rather than CSCs play the significant role in drug resistance and extensive-expression of ABCB1 have shown to mediate this activity. This indicates that the subpopulation of differentiated cells provides an environment which preserves CSCs from penetrance of chemotherapy agents (302).

In one study expression of stem cell markers, EpCAM has been detected in the majority of the CRC tumours which was associated with high expression of ABCG5 and poor prognosis in CRC patients which might be due to the drug resistance of CRC tumours (303). As indicated previously, colorectal cancer stem cells are replete with cell markers CD133+, CD44 and CD166 (304, 305) and CD44+/CD166+ (306). It has been demonstrated that human colorectal cancer tumours treated with 5-fluorouracil and oxaliplatin display the high level of CD133+ and these tumours have been resistance to putative chemotherapy reagents (307, 308). In addition, the CD44+/CD166+ enhanced expression has been observed in CRC CSCs treated with Irinotectin (309). Regarding the radiotherapy resistance activity of the CSCs, they exploit four major mechanisms to escape from the ionizing radiation effects (310, 311). The mechanisms are including 1) development of advanced DNA damage system and achieving more checkpoints, 2) altering the cell cycle phase in which they are prone to be quiescent rather than the proliferative state such as mitotic phase (312), 3) repopulation and 4) intra-tumour hypoxia. In fact, after radiation, the surviving tumours experience re-oxygenation and this hypoxic fraction of tumours gain more oxygen during this process which is due to the destruction of aerobic population (313, 314). In addition it has been noted that repopulation of the tumour cell is one of the major factors of radiation and chemotherapy treatment failure. Generally surviving cancer cells and cancer stem cells divide and proliferate during treatment intervals which result in regrowth of the tumour.

1.8 Rationale & main objectives

The advanced capacity of organoid in recapitulating the native architecture and morphology of their counterpart tissues cited them as the most reliable tools than any traditional models for studying several aspects of cellular and molecular events of diseases progression (315). The broad scope of organoid applications from both normal and tumour-derived organoids encouraged us to establish these 3D models in-depth, and in longer-term to define a consensus stemness signature in normal and colon cancer relevant to clinical outcomes, and eventually to assess their potential in modelling CRC, prediction and treatment capability in our laboratory as part of my PhD research project.

Herein, upon the previous establishment of murine small intestinal organoids in the lab (119, 122);

Aim 1) Adapt and optimizing the culture conditions to normal/tumour patient-derived organoid (PDO) from intestinal/colonic epithelium. Technical challenges is the critical starting parameter for establishment of colonic PDOs and it requires the application of several compounds (growth factors and inhibitors) with optimum concentration including the conditioned medium Noggin, Wnt3a and R-Spondin.
So far, some essential aspects of organoids including the morphological alterations and the growth pattern of the matched tumour and their normal derived organoids have received less attention. Therefore in chapter 3 we will also focus on culturing matched normal and tumour organoids from the same patient with colorectal cancer (CRC) and assessed their timed growth and structural differences on a daily basis.

Aim 2) Generating a small PDO biobank and profiling/capturing the phenotypical alterations of different colonic tumour organoids and their adjacent normal tissue in culture.

Moreover, since the effects of Noggin, as extra cellular negative regulator of BMP signalling in the homeostasis of the normal intestinal epithelium, is not fully characterized in malignant condition, we aimed to:

Aim 3) Exploring the role of Noggin administration in a various colorectal cancer cell lines, and PDO system via analysis for morphology changes, immunofluorescence, cell cycle, migratory and stemness activity of treated CRC cell lines.

The development of new therapeutics and identification of new molecular targets for diagnosis and treatment of CRC is always of significant clinical value.

In recent years, drug repurposing has emerged as a viable strategy toward disease progression and cancer treatment. In this regard, we have recently screened the anti-cancer activity of a small molecule anti-bacterial/ inflammatory library compound from NIH (707 small molecule) and the promising candidate identified through initial in vitro screen including Rifabutin and AM404 (316).

Aim 4) In chapter 4 we further aimed to explore the anti-cancer activity of antibiotic Rifabutin and further mechanism of action in colorectal cancer cell lines and PDOs using various biochemical and molecular cell assays.

Considering the promising findings on phenotypical significance modelling application of organoids growth, we decided to combine the organoid culture with genome editing technology, CRISPR/Cas9 to introduce a versatile modelling platforms for rapid and facile screening and identification of large number of genes with unknown biological function in the intestinal epithelium for the first time.

Screening-based method of generating CRISPR/Cas9 knockout organoid lines may represent significant step forward in reducing and replacing the use of animal models in research.

Aim 5) Thus, chapter 5 is investigating the loss of F-box genes function in murine intestinal organoid cultures using CRISPR/Cas9 technology.

CHAPTER 2

Materials and Methods

2.1 CELL AND MOLECULAR BIOLOGY TECHNIQUES

2.1.1 Cell lines

Six human CRC cell lines were used throughout this thesis; SW480, HT29, DLD-1, HCT116, SW620 and LS-174T adenocarcinoma cell lines harbouring different mutational profile (Table 2-1). In addition, transformed human embryonic kidney cells (HEK293-T), (a kind gift from professor Gordon Peters: Molecular Oncology Lab, CRUK- London Research Institute), was also used in this study after the validation. HCT116, SW480, HT29, DLD-1, LS174T and SW620 and DLD-1 were originally purchased from the American Type Culture Collection (ATCC). Human colorectal carcinoma HCT116 cell line harbouring FBXW7 deletion on both alleles, HCT116FBXW7$^{(-/-)}$ were kindly supplied by Prof A. Balmain (University of California, San Francisco, CA) (317, 318).

Cell line/Mutation	APC	KRAS	P53	CTNNB1	PIK3CA	BRAF	TGF βR2	SMAD4	FBXW7
SW420	CAG–TAG (stop) (codon 1338)	c.35G>T (p.G12V), G13D	G -> A mutation/codon 273					IVS7 + 5G>C	
SW620	CAG–TAG (stop) (codon 1338)	c.35G>T (p.G12V), G13D	G -> A mutation in codon 273, C -> T mutation in codon 309					IVS7 + 5G>C	
HCT-116		G13D G12V		Exon 3 (codon 45)	H1047R/ exon 20		Homozygous both alleles		
HCT-116 $^{FBXW7(-/-)}$		G13D G12V		Exon 3 (codon 45)	c.3140A>G (p.H1047R)		Homozygous both alleles		Deletion for Exon 5
HT-29	codon 1555		G -> A/codon 273		c.1345C>A (p.P449T)	c.1799T>A (p.V600E)		c.931C>T (Q311X), EX7	
DLD-1	truncated APC1417	p. Gly13Asp	C -> T/codon 241		E545K alteration in exon 9		CTG . CCG (codon 452)		
LS174-T		c.35G>A (p.G12D)		c.134C>T	c.3140A>G (p.H1047R)				

Table 2-1; Mutational signature of CRC cell lines used in the current study. (Adapted from American Type Culture Collection (ATCC))

2.1.2 Thawing, maintaining, sub-culturing and freezing cells

Cell lines were thawed and grown in 75cm2 flasks in RPMI1640 (Sigma; R0883) or DMEM (Sigma Aldrich, D5671) supplemented with 10% fetal bovine serum (FBS, Sigma; F7524) and 2 mM L-glutamine (Thermo Fisher Scientific, 25030-024). Cells subsequently were kept in 37°C, 5% CO_2 incubator. Confluent flasks (80-90%), were selected for subculturing. Cell lines were washed once with 2ml of Phosphate-Buffered Saline (PBS, Sigma; D8537) and then detached by incubation with 1 ml 1X Trypsin/Ethylenediaminetetraacetic acid (EDTA) solution (Sigma; T3924) for 4-8 minutes in 37°C incubator.

For neutralization of Trypsin/EDTA, 6 ml of appropriate medium (DMEM, RPMI) was added and the detached cells were diluted based on the experimental plan. The Neubauer haemocytometer (Marienfeld-Superior, Germany) was used for cell counting procedure. The trypsinized cells were diluted in pre-warmed fresh medium and centrifuged with 400g for 5 minutes. The supernatant was discarded and the pellet was resuspended in new 10ml medium. Staining of non-viable cells was done with 10µl Trypan blue (Sigma; T8154). 10µl of the cell solution was mixed with 10µl of Trypan blue and subsequently, 10µl of this mixture were loaded on the Neubauer counting chamber. The cells were counted and the average count number was multiplied by the applied dilution factors. For freezing of the cells, the cells were detached using trypsin incubation as indicated earlier and then centrifuged for 4 minutes at 400g and the pellet was diluted in 1 ml of 10% dimethyl sulfoxide (DMSO, Sigma; D4540) and 90% FBS. The cells were kept overnight at -80°C and then transferred to the liquid nitrogen tank.

2.1.3 Synchronizing the cell cycle

Cell lines were synchronized in G0/G1 phase of the cell cycle by serum starvation (0.1%-0.5% FBS) prior to chemotherapeutic drug administration and further analyses. Cell culture medium was replaced with RPMI/DMEM medium supplemented with 2 mM L-glutamine (Thermo Fisher Scientific, 25030-024). Depends on the doubling time of the different colon cancer cells, they kept at 37°C, 5% CO2 in a humidified incubator for 18-24 hours prior to the experiment.

2.1.4 Transient transfection of cell lines

The HEK293T/colon cancer cells were grown in 6 well plates or cell culture dishes until they became 70-90% confluent (overnight incubation). The transfection procedure was accomplished using the polyethylenimine (PEI), (Polysciences; 23966-1) in Opti-MEM (Thermo Fisher Scientific, 31985070). The day after, the cells were washed with Opti-MEM and then the mixture of 4-15 µg of DNA plasmid and PEI (4 µl per each µg of DNA) were added to the seeded cells and kept for 6 hours at 37 °C Opti-MEM. After the incubation time, the medium was changed with the related medium (depends on the cell lines used).

2.1.5 Lentivirus production and transduction

2.1.5.1 Lentivirus production using 2nd generation packaging system

HEK293-T cells were seeded in a total of 10 mL DMEM per 75 cm2 flask. The density of cells was around 70-80% on the day of transfection (no greater than

90%). The volumes required for plasmid transfection and PEI was as follow: final volume per plate 15 µg LV construct (F-box LV gRNA), 5 µg pMDG2 packaging, 10 µg pCMV R8.74 packaging plasmid, 1.5 mL Opti-MEM per 75 mL flask. On day one post-transfection, the Opti-MEM/plasmid (packaging plasmid and PEI) were added gently to each flask; and incubated for 6-9h, gently agitated every 2h. Cells were examined after 6-9h, and then the medium changed with complete DMEM. The flask was incubated overnight 37°C. On day two and three, the supernatant was transferred from flasks into 50mL falcon tube and was filtered through 45µm filter unit. If the LV had a fluorescent reporter gene, it checked via fluorescent microscope for transduction efficiency. Following the medium collection, the medium was changed with complete DMEM medium (3 flasks at a time) and incubated for a further 24h. The virus-containing medium was stored at 4°C. On day four, the virus harvesting continued for 3 days [approx. 60mL of virus containing medium per plasmid]. The medium containing-virus transferred to ultracentrifuge tubes containing 1 mL of virus sucrose solution ~7-8 mL viral supernatant per tube. After ultracentrifuge at 25,000-27,000*g* for 4h at 4°C the supernatant was discarded and air dried under the hood. The additional 500 µl of organoid medium or complete ADMEM/DMEM was added to each tube. The tubes were incubated overnight at 4 °C. The next day, the viruses in the tubes were merged and aliquoted 50-60 µl into Eppendorf's. The tubes were further transported on dry ice and stored at -80 °C.

2.1.5.2 LV transduction of the cell lines

The cells were cultured in their complete growth medium 12-18 hours before transduction in a 6 well plate or 75 cm2 flask. The LV thawed and diluted in 1.5ml of complete medium containing Polybrene (8 μg//ml) to increase the transduction efficacy. Cells incubated with lentivirus for 48 hours without disturbances. The cells were checked for fluorescent if lentivirus contains a fluorescent reporter. Subsequently, the media containing the virus discarded and the antibiotic selection carried out until cells in the negative control condition completely died.

2.1.5.3 Lentiviral transduction and generation of organoid lines

Organoids were grown and expanded to sufficient number [typically 10-12 confluent organoids per well, 3-4 well per transduction, a total of 30-40 organoids per transduction]. Organoids were removed from Matrigel, resuspended in 300ml 4°C PBS, and disassociated using a 200µl pipette 20-30x, amalgamated into a single tube and resuspended in 100-300µll concentrated virus medium with polybrene for 4 hours. The mixture of virus and organoids medium was agitated carefully using 200µl pipette every 30-45 minutes. Organoids were subsequently centrifuged for 3 minutes at 300g, the virus medium discarded and organoids seeded to Matrigel at 10-12 organoids per well. The following day, begin using the appropriate drug marker. After LV transduction and seeding of organoids as described, selection antibiotics were added to organoid medium and replaced every 2 days until control/un-transduced

organoids were completed dead. Surviving organoids were sub-cultured and monitored via bright-field microscopy for phenotypical and morphological changes that could be attributed to their engineered genetic state.

2.2 ORGANOID CULTURE

2.2.1 Isolation and culture of human colonic crypts

The tumour and adjacent normal tissue samples of the human colon were collected from Nottingham Health Sciences Biobank (NHSB), Queens Medical Centre, and the University of Nottingham. The tissue was cleaned with chilled PBS. Then the tissue was cut into pieces of around 5-10mm under the hood, (The tissue sample can be also kept overnight in DMEM supplemented with pen/strep and 10% FBS). Colon pieces were washed in PBS and then incubated in 25mL EDTA solution (1mM EDTA in PBS) at 4°C for 40 minutes.

After this incubation time, EDTA solution was removed and replaced with 10ml sterile PBS. The tube was shaken for 20 seconds. The supernatant was discarded (this process should be repeated 2-3 times until the EDTA completely removed and no debris remained). After this process, another 10ml PBS was added to the tube containing the tissue pieces and it was shaken vigorously for 20 seconds. At this time the crypts released from the epithelium to the PBS. The solution containing the crypts was collected and transferred to a new 15ml centrifuge tube. Upon centrifugation for 1 minute (100g) the crypts accumulated at the bottom of the 15ml tube. The crypts were suspended in a PBS and centrifuged again. The isolated crypts then suspended in Matrigel at a concentration of

approximately 50 crypts/25 µL Matrigel. 25µL crypt-containing Matrigel was carefully added to the centre of the well of a 48-well plate using chilled pipette tips. The plate was incubated at 37°C for 5 minutes to allow Matrigel to solidify. The Matrigel was overlaid with 300-350µL of the complete organoid medium. Organoid medium condition for a total volume of 50ml was as follow: Advanced DMEM/F-12 medium (Invitrogen, 12634-028) containing 2 mM L-glutamine, 100 U/ml Penicillin/Streptomycin and 10 mM HEPES (Invitrogen, 15630-122), was supplemented with 5 ml of Wnt-3a (conditioned medium), 2ml of mNoggin (conditioned medium), 2ml of R-Spondin1 as Wnt agonist, B27 supplement; 1ml (50x) (Invitrogen, 12587-010), N-acetylcysteine; 125ul (1.25 mM) (Sigma Aldrich, A9165), murine recombinant epidermal growth factor (mEGF); 25 ul (100 ug/ml) (Invitrogen, PMG8043), TGF-beta inhibitor (A83-01); 5 ul (10 000x, 5mM), p38 inhibitor (SB202190); 5 ul (30mM):, Primocin; 100 ul (500x), Nicotinamide; 250 ul (10 mM).

2.2.2 Murine intestinal crypt isolation and culture

Intestinal crypts were isolated from BL6J mice (approx. 4-6 weeks old). Mice were sacrificed by cervical dislocation and the whole intestine excised from the abdominal cavity. The sample was cleaned with ice-cold PBS, opened longitudinally, divided into 1mm sections and washed with cold PBS several times until PBS became clear. The sample was incubated in 3mM EDTA for 45 mins at 4 °C. Afterwards, the sample was transferred to 10% FBS/PBS at room temperature and repeatedly agitated and filtered through 70µm strainer 3-6 times. Subsequently, the sample was centrifuged at 300g for 5 mins. The

supernatant was removed and crypts re-suspended in ice-cold Matrigel [typically 200-300µl Matrigel per isolation]. 25µL Matrigel containing the crypt was seeded to the centre of a well in 96 well plates and incubated at 37°C until Matrigel solidified. Finally, 300µL fresh mouse organoid medium pre-warmed to 37°C, was added to each well and the plate incubated at 37°C. Organoid growth was monitored by microscopy. Typically, colorectal organoids take 6-9 days post-seeding to grow to maturity with multiple crypt/villus-like domains. Organoids can typically be kept in culture for another 3-5 subsequent days, however increasing size of the organoid and its necrotic core will eventually cause the organoid to rupture and die.

Fresh organoid medium: basal Advanced DMEM/F-12 medium, 2mM L-glutamine, 100 U/ml Penicillin/Streptomycin and 10mM HEPES was supplemented with N2 (Fisher Scientific, 17502048) supplement (1x), B27 (Fisher Scientific, 12585-010) supplement (1x), 1 mM N-acetylcysteine to stimulate cell proliferation, 50ng/mL murine recombinant epidermal growth factor (mEGF, Fisher Scientific, PMG8043) to activate EGF signalling pathway, 1µg/mL R-Spondin 1 (in-house) as Wnt agonist and 100 ng/mL Noggin (in-house) to inhibit BMP pathway (227). "Complete" DMEM= Advanced DMEM/F-12 medium, 2mM L-glutamine, 100 U/ml Penicillin/Streptomycin and 10mM HEPES.

2.2.3 Production of Wnt 3A-conditioned medium

The Wnt3a cell line (L-wnt3a cells, a kind gift from Prof Hans Clevers laboratory) were thawed from liquid nitrogen in 175cm2 flask in 20ml of DMEM

GlutaMAX Supplemented with 10% FBS + pen/Step and Zeocin (Thermo Fisher Scientific, R25001) (1.25ug/ ml). After 2-3 day (80% confluency) the flask was split into 6x175 cm2 flasks in growing medium with FBS and Zeocin was added to only one of the flasks and no Zeocin to the rest (5x175 cm2 flasks). The flask supplemented with Zeocin (1.25µg/ ml) kept as the cell maintenance and was frozen down after two days. After 2-3 days (when the six 175cm2 flasks were confluent), the cells were trypsinized, pooled in 600ml growing medium (glutaMAX) without Zeocin and plated in 30 x 150cm2 dishes for one week. After incubation for one week in the incubator, the medium was harvested. The collected medium containing the Wnt-3a was centrifuged at 400g for 4 minutes and passed through 0.22 µM filter. Then the medium aliquoted in and stored in 50ml tubes at 4 degrees. The activity of the Wnt-3a and R Spondin-1 were measured by TOP/FOP luciferase reporter assay (Section 2.4.1).

2.2.4 Production of R-spondin1-conditioned medium

The HEK 293T-HA-Rspo1-Fc stable cell lines expressing R-spondin1 (R-Spo1) (a kind gift from Prof Hans Clevers laboratory) were thawed and grown in 75cm^2 flasks with DMEM medium (Sigma, D5671), 10% FBS, 2 mM L-glutamine and 100 U/ml Penicillin. After splitting the cells, the cells were selected with 300 µg/ml Zeocin for 3 days. Then the DMEM medium was replaced with advanced DMEM/F-12 medium containing 2 mM L-glutamine, 100 U/ml Penicillin/Streptomycin and 10 mM HEPES for following one week. R-spo1-conditioned medium was then collected and span down at 400g for 4mins and subsequently filtered through 0.22µM filters. The R-spo1 conditioned medium

then was aliquoted and stored at -80°C. Since the R-spo1 is an agonist of Wnt pathway, the activity of the R-spo1 was further assessed by luciferase reporter assay (Section 2.4.1).

2.2.5 Preparation of Noggin-conditioned medium

HEK293T cells were cultured on 10cm^2 plates with RPMI medium. Once the dishes became 50-60% confluent, the cells were transfected with 15µg of Noggin plasmid and PEI (4µl for each µg of DNA) and kept for 6 hours. After transfection, the medium was replaced with Advanced DMEM/F-12 supplemented with 2mM L-glutamine, 100 U/ml Penicillin/Streptomycin and 10 mM HEPES and kept in the incubator for one week for preparation of the Noggin conditioned medium. After one week the medium was collected and centrifuged at 400 g for 4 mins and filtered by 0.22µM filters. Noggin conditioned medium was collected into 50ml tubes, centrifuged at 400 g for 5 mins and passed through 0.20µm filters. The medium was aliquoted and stored at -80°C. The presence of Noggin as a secreted protein in a conditioned medium was validated by Western blotting assay (Section 2.5).

2.3 HISTOLOGY

2.3.1 Organoid preparation

Organoids (4 wells containing 15-30 organoids) were fixed by 4% paraformaldehyde (PFA) overnight at 4°C. In the following day and after two washing steps with PBS, the organoids pre-embed in 2% low gelling temperature

agarose (Sigma Aldrich, A9045). Subsequently the organoids transferred into histology cassette for paraffin embedding process (319). The day after, organoids were washed with PBS two times by centrifugation. The last organoid pellet was pre-embedded in samples dehydrated using Leica TP1020 semi-enclosed benchtop tissue processor. Samples were embedded in paraffin blocks to be cut in 10µm-thick sections with a microtome and placed onto polysine glass slides.

2.3.2 Hematoxylin and eosin (H&E) stain

The most commonly used staining system is known H&E (Haematoxylin and Eosin). H&E contains the two dyes haematoxylin and eosin. Haematoxylin as a basic compound interacts and stains acidic molecules including the nucleus (contain DNA), and parts of the cytoplasm that contain RNA in purple. As an acidic compound, eosin, however, stains basic molecules such as protein in pink-orange colour. Subsequently, the sections were dewaxed in xylene twice for 5mins then dehydrated in 100% IMS for 3min and once with 70% IMS. Following rinsing with tab water for 1min, sections were stained in Harris Hx (aqueous, RA Lamb, 230D) for 5-6mins. After 5mins washing with tab water the section stained with Eosin (1%) (Thermo Fisher Scientific, LAMB-100-D) for 5-10 mins. Sections were dehydrated with three 100% ethanol baths for 1 min each and two xylene baths for 3mins. Finally, sections were mounted with DPX (Sigma Aldrich, 317616) neutral mounting medium. For further analysis.

2.4 FUNCTIONAL ASSAYS

2.4.1 Luciferase reporter assay

To evaluate the activity of Wnt-3a and R-spondin1-conditioned medium, TOP/FOP-flash dual-luciferase reporter assay system provided by Promega, E1910 was exploited (320). The TOP-flash is a luciferase reporter plasmid containing two sets of three copies of the TCF/LEF binding site upstream of a *Firefly luciferase* reporter gene (Promega, E1910). On the other hand, the FOP-flash plasmid contains three mutated copies of the TCF/LEF binding site and play as a negative control. In addition, *Renilla* luciferase (under SV40 constitutively active promoter) was exploited to normalise transfection efficiency. HEK293T cells were seeded in triplicate into a 6-well plate ($3x10^5$ cells/well) and kept in incubator overnight. When the cells were 60-80% confluent, they were transfected with both *Renilla* luciferase vector (0.05 µg DNA/well) and, either TOP-flash/FOP-flash plasmids (0.2 µg DNA/well).

After 6 hrs, the medium containing the transfection mixture was replaced with Wnt3a+R-spondin1-conditioned medium and left for 48 hrs. After 48hrs, the medium was discarded and the cells were lysed with passive lysate buffer provided by the kit and according to manufacturer guidelines. The lysis (10 µl/well) were loaded in triplicate in 96 well plate (Thermo Fisher Scientific, MPA-560-040A). Then according to the protocol, 50µl/well of Luciferase Assay Reagent II (LAR II) were added into the wells and the bioluminescence produced was detected by a Luminoskan Ascent Microplate Luminometer (Thermo Fisher Scientific, UK). In addition, the measurement of the *Renilla* luciferase activity

was measured by adding 50µl/well of Stop & Glo® Reagent to the same wells. The obtained data exported to Microsoft Office Excel. The *Firefly* luciferase readings were normalised to *Renilla* luciferase readings and then to the activity of the control samples.

2.4.2 Cell cycle analysis and Propidium iodide (PI) staining

Cell cycle analysis was performed by the evaluation of DNA content via propidium iodide staining. Cell lines were synchronized in G0/G1 phase by serum starvation prior to administration with Noggin. Prior the cell fixation, the cells were treated with Noggin protein and incubated at 37°C, 5% CO2 incubator up to 48 hrs for further evaluation. Then, cells were trypsinized and single-cell suspension transferred into Fluorescence-activated cell sorting (FACS) tubes (Falcon, 352054) and followed the fixation process by adding 1ml of ice-cold 70% ethanol (Sigma Aldrich, E7023). The ethanol was carefully discarded and cells were washed with PBS twice by centrifugation. Subsequently, cells were incubated with 50µg/ml propidium iodide (Sigma Aldrich, 4864) and 100µg/ml RNase A (Sigma-Aldrich, 6513) solution for 30mins in dark. DNA content was measured by FC500 flow cytometer (Beckman Coulter) and data were analysed by Weasel 3.2.1 software. The assay was performed at least three times in triplicate.

2.4.3 Cytotoxicity assay

For cytotoxicity assay, cells were seeded in 96-well plate (3000cells/well) and synchronized by serum starvation as indicated earlier. The serum-free medium was replaced with a various dose of Rifabutin (from 20 to 80µM) for a period of 72 hrs. Sulforhodamine B (SRB) colorimetric assay was applied to determine the cytotoxicity (321-323). For the fixation step, 50µl of cold 30% (w/v) trichloroacetic acid (TCA, Sigma Aldrich, T4885) was added to each well and incubated for 60mins at 4°C. Then, fixed cells were subsequently washed with tap water, air-dried and stained with 0.4% SRB (Sigma Aldrich, 230162) in 1% acetic acid (Sigma Aldrich, 320099) for 20 mins at room temperature (RT). After five washing steps with 1% acetic acid and air drying, the SRB was dissolved by adding 200µl of 10 mM Trizma base (Sigma Aldrich, 93349). The absorbance of each well was measured at 540nm of wavelength by microplate reader (321). Data were elaborated by using Microsoft Office Excel and GraphPad Prism 8 software.

2.4.4 Colony-forming assay

The colony-forming assay was performed to estimate the ability of a single cell to proliferate and grow into a colony. Colon cancer cells were seeded in 6-well plates (500 live cells /well) and grown for ten days. The medium replaced with complete medium every four days. Subsequently the colonies were fixed by 4% PFA for 20 mins at RT. Staining performed using 0.1% crystal violet (Sigma Aldrich, 0775).

2.4.5 Cell migration and wound healing assays

CRC cells synchronized in G0-phase of the cell cycle by serum-free starvation for 18hrs before cell motility assays. Prior to scratches, the cells were treated with the drug and incubated for 44-48h. Scratches closure were assessed every 24h for a similar position. Migration quantifications were performed as described previously (324). The assays were performed at least three times in triplicate.

2.4.6 Colonosphere formation assay

To evaluate the stemness activity of CRC cells upon particular treatment or generation of KO cells, cancer stem cells (CSCs) were cultured as 3 dimensional (3D) spheroids, also known as colonospheres, according to the protocol (325, 326). The colonosphere formation efficiency assay of cell lines was performed in treated and non-treated condition or KO versus control cells for 200 cells/well. Approximately 2000-3000 cells were pooled in triplicate into a 6-well plate and cultured in 300µl of stem cell medium for 14days. Stem cell medium was made by supplementing DMEM/F-12 medium (Invitrogen, 11320-074) 100U/ml Penicillin/Streptomycin (Invitrogen, 15140-122) with 1xN2 supplement (Invitrogen, 17502-048), 10ng/ml human recombinant basic fibroblast growth factor (bFGF, R&D systems, 233-FB-025) and 10ng/ml human EGF (Sigma Aldrich, E4127-.1MG). For Noggin treatment, the cells were kept for 14 days to form the colonospheres and the efficiency in colonosphere formation was measured by counting the number of colonospheres after treatment with/without Noggin for 72h.

2.4.7 Organoid viability assay

The WST1 assay (Merc, cat; 5015944001) was performed to measure the proliferation of the KO and treated organoids in comparison to the control group. Organoids were seeded in 5-6 wells (20-50 organoids/well) for per day of the experiment (depends on the types of organoids; murine or PDOs and the nature of the experiment). To measure the viability of the tumour derived organoids upon Rifabutin treatment, the organoids were treated with Rifabutin as described in 4.2.2. Of note, the amount of formazan dye formed directly correlates to the number of metabolically active cells in the culture. Every day/two days, 6 wells of already cultured organoids were evaluated for the viability by adding 30µl/well cell proliferation reagent WST-1 directly to the 6 wells. After incubation for 2 hours the absorbance were recorded within the wavelength (420-480nm) using the spectrophotometer. The duration of the experiments depends on the types of organoid and the nature of the experiments.

2.5 PROTEIN EXPRESSION

2.5.1 Protein extraction and quantification from cell lines

To collect proteins from cells, the monolayer cell was washed with PBS (1ml). To release all the proteins, cells were incubated with Radio immunoprecipitation assay buffer (RIPA buffer; containing 150mM sodium chloride, 1% NP-40 and 1% sodium dodecyl sulphate) and containing 1xprotease inhibitor cocktail (Sigma Aldrich, P8340) for 20 mins in 4°C. Subsequently, the cells were scraped and the lysate was collected and purified by centrifugation at 10-12K g for 10

mins at 4°C. The upper phase containing total protein lysate was collected into a new Eppendorf tube and stored at -20°C. Following the protein extraction, the protein concentration was determined using, Bradford assay. Five protein standards (50, 100, 150, 200, 250 µg/ml) was prepared from a stock solution of 2 mg/ml BSA in distilled water. The experimental sample was further diluted 1:50. Next, 20 µl of distilled water, BSA standards and diluted experimental samples were added in triplicate into a 96-well plate. Following loading of 200 µl of 5x diluted Bradford reagent (Sigma Aldrich, B-6916) to each well, the absorbance was measured at 595 nm of wavelength by spectrophotometer (Bio-Rad). The standard curve and the protein concentration were analysed by Microsoft Office Excel software.

2.5.2 Protein extraction from organoid cultures

Western blot validation requires a sufficient number of organoids as input material (at least 6 wells of 15-30 mature organoids). When the organoids are grown for 6-9 days, they were collected as previously described (2.1.5.3). The organoid pellet was re-suspended and incubated in 70-80µl of RIPA buffer for further 20 min in 4°C, while rocking [20 oscillations/minute]. The organoids were lysed and homogenised using a 21-25G BD syringe needle occasionally within the incubation time. The lysate was used directly for the western blot analysis.

2.5.3 SDS-PAGE and Western blotting (WB) analysis

Sodium dodecyl sulphate-poly acrylamide gel electrophoresis (SDS-PAGE) separates proteins according to their molecular weight. SDS-PAGE is consisting of two parts: stacking: the upper part and the resolving (bottom part). Both stacking and resolving gel were made according to the instructions (Table 2-2). The resolving gel percentage was selected based on the size of the secreted protein.

	Resolving gel (10 ml)				Stacking gel (5 ml)
	8%	10%	12%		5%
H_2O	4.6	4.0	3.3	H_2O	3.4
30% acrylamide mix	2.7	3.3	4.0	30% acrylamide mix	0.83
1.5M Tris (pH 8.8)	2.5	2.5	2.5	1.0M Tris (pH 6.8)	0.63
10% SDS	0.1	0.1	0.1	10% SDS	0.05
10% ammonium persulfate	0.1	0.1	0.1	10% ammonium persulfate	0.05
TEMED	0.006	0.004	0.004	TEMED	0.005

Table 2-2 Solution components (ml) for SDS-PAGE electrophoresis gels.

The protein lysate was mixed with 5x loading buffer (250 mM Tris-HCl pH 6.8, 10% SDS, 50% glycerol, 5% β-Mercaptoethanol and 0.05% bromophenol blue) and denatured for 5 mins at 95°C to facilitate a run. To ascertain the size of the protein bands, the Precision Plus Protein™ Dual Colour Standards ladder (Bio-Rad, P7711S) was loaded alongside with the experimental samples.

The running buffer (25 mM Tris-HCl pH 8.3, 192 mM glycine and 0.1% SDS) were added the outside and inside the compartment of electrophoretic tank (Mini-PROTEAN® Tetra Vertical Electrophoresis Cell, Bio-Rad, 1658004) and the gel was run for approximately 1 hr at 80 volts (V). Using the semi-dry

transfer method, the separated protein within the gel were transferred to a hydrophobic polyvinylidene difluoride membrane (PVDF, GE Healthcare, RPN303F). The transfer compartment (sandwich) was consist of filter paper, gel, membrane and filter paper. The transfer buffer (25 mM Tris HCl, 192 mM glycine and 20% methanol) was applied to soak the filter papers before placing the prepared sandwich into a Semi-Dry Electrophoretic Transfer Cell (Bio-Rad). The membrane containing the transferred protein the incubated with Tris-buffered saline (20 mM Tris 7.6 pH, 135 mM NaCl) 0.1% Tween 20 (TBS-T) with 3% BSA, was for 1 hr at RT to prevent non-specific protein. Then the primary Ab was added in 5ml of 2% BSA and the membrane was blotted over night at 4°C (Table 2-3). The day after, the membrane was washed 3 times (10 mins) with TBS-T and the corresponding horseradish peroxidase (HRP)-conjugated secondary antibody was added for 1 hr at RT. Then, the membrane was washed twice for 5 mins with TBS-T. At the end, the visualisation of the protein was done after addition of the detection reagent (Millipore, 10776189) that activates the chemiluminescent reaction catalysed by HRP enzyme.

Primary Antibody	Supplier	Cat No	Source	Dilution factor	
				WB	IF
β-catenin	BD Biosciences	610154	mouse	1:5000	1:150
E-cadherin	BD Biosciences	610181	mouse	1:5000	1:150
Noggin	Santa Cruz Biotechnology	560170	mouse	1:1000	NA
BMP4	Santa Cruz Biotechnology	sc-393329	mouse	1:5000	1:150
Cas9 Antibody (7A9-3A3)	Santa Cruz Biotechnology	sc-517386	mouse	1:5000	NA
FBXL18	Proteintech	11556-1-AP	Rabbit	1:5000	NA
FBXO17	Proteintech	12844-1-AP	Rabbit	1:5000	NA
β-actin	Abcam	Ab6276	mouse	1:5000	1:100
Secondary Antibody	**Supplier**	**Cat No**	**Source**	**Dilution factor**	
				WB	**IF**
Alex Fluor 594 anti-mouse	Life Technologies	A-21155	goat	NA	1:500
Anti-mouse HRP	Santa Cruz Biotechnology	sc-2005	goat	1:5000	NA
Anti-rabbit HRP	Santa Cruz Biotechnology	sc-2004	goat	1:5000	NA

Table 2-3. List of primary and secondary antibody used for IHC analysis.

2.5.4 Immunofluorescence (IF) and Phalloidin staining

10^5 cells were seeded on top of a coverslip. When the cells became 70-90% confluent, the cells were treated with 20% of Noggin and kept in the incubator for 42-48 hours along the control group (free Noggin medium).

Cultured cells were fixed with 1 ml of 4% PFA for 30 mins and permeabilizing was with 500 µl/well of 0.1% TRITON X-100 solution (Sigma Aldrich, 93443). After blocking with 3% bovine serum albumin (BSA) the primary antibody was added, and the cells incubated overnight. The next day, unbound antibodies were

removed by washing with 1% BSA 0.1% Tween 20 solution and fluorochrome-conjugated secondary antibodies were applied in a dark room for 1 hr at RT. After 4 washing steps, slides were mounted with Vectashield mounting medium with DAPI (Vector Laboratories, H-1200). The day after, images were taken with a Leica DMI3000 B fluorescence microscope (Leica Microsystems).

2.5.5 Phalloidin staining

2.5.5.1 Phalloidin staining of CRC cells

Phalloidin is a dye commonly used to determine the cell morphology via labelling actin filaments in the cell. Cells seeded onto coverslips were fixed with 4% PFA, permeabilised with 0.1% TRITON X-100 and incubated with fluorochrome-conjugated phalloidin (Sigma Aldrich, 1951) for 40 mins at RT. Following washing steps with PBS for 10 mins (twice), slides were mounted with Vectashield mounting medium with DAPI and incubated overnight at 4°C in dark. The day after, images were taken by fluorescence microscope.

2.5.5.2 Phalloidin staining of organoids

5-6 confluent wells with mature organoids (6-8 days old; 15-30 organoids/well) were selected and 500µl of 4% PFA was added to each well. The organoids were incubated overnight in 4°C.

The day after, the PFA was discarded gently, the organoids were collected in a tube (15ml falcon). Subsequently organoids were washed twice with chilled PBS (this step repeated twice). Following the last washing step, the organoids

permeabilized with 500µl of 0.5% TRITON X 100 on the tube for 30min at RT; The pellet was washed twice and 800µl of PBS contains the Phalloidin (Sigma Aldrich, 1951; 1:400 dilution) were added in the tube and the tube kept in 4°C for 40 minutes. Organoids were washed twice with PBS and mounted with DAPI and incubated overnight at 4°C in dark. The images were taken using the fluorescence microscope from the next day.

2.6 DNA PREPARATION

2.6.1 Bacterial transformation & plasmid DNA amplification

The heat shock method was applied for the introduction of the DNA plasmid(s) in chemically competent *Escherichia coli* (*E. coli*) cells. 50µl of competent *E. coli* cells were mixed with 100ng of plasmid DNA and incubated on ice for 30mins. Subsequently, the heat shock was done at 42°C for 1 min, then incubated on ice for 10 mins and then the mixture was added to 500µl of Luria-Broth medium (LB) (Sigma Aldrich, L3022). Then, bacteria were incubated for 1 hr at 37°C in a shaking incubator. The bacteria then transferred to a bigger volume of the LB for the amplification (5ml) and 5µl of the ampicillin was added for the selection of the competent cells as the plasmid vectors retained the *AMP* resistance gene. The mixture was incubated in a shaking incubator for 6 hours until the bacteria grew and the medium became cloudy. The mixture was transferred to the bigger volume (100ml) of LB medium supplemented with 100 µl of AMP and left overnight for amplification. In order to isolate the plasmid DNA, the Midiprep kit was used.

2.6.2 Isolation of the plasmid DNA

In order to isolate the DNA plasmids (100-200µg) and also gRNA construct of the F-box library (*Appendix 2 & 3*), the Genopure Plasmid Midi Kit (Roche, 03143414001) was exploited. According to the manufacturer's instructions. The bacteria were spun down at 5000g for 10 mins at 4°C, then re-suspended with 4 ml of cold Suspension Buffer supplemented with RNase and subsequently lysed with 4 ml of Lysis buffer. Then the tube containing the lysis was incubated for 2-3 minutes at RT allowing the lysis of the bacteria cell walls. Then chilled Neutralization Buffer (4ml) was used to deactivate the Lysis buffer and incubated on ice for 5 minutes. The bacteria containing the Neutralization Buffer Centrifuged for 40 mins at 4°C (10,000g). Simultaneously the columns were placed in chambers and 2.5 ml of Equilibration Buffer was loaded to the filter (Figure 2-1).

The lysate then was loaded to the filter and left until it emptied by the gravity. 5 ml of the wash buffer was added to the column and allowed to be empty by the gravity. Then 2.5 ml of Elution buffer was loaded to the column and the DNA plasmid was collected to a 50ml of conical tube. Then 3.5 ml of isopropanol (Sigma Aldrich, I9516) was added to the DNA plasmid and it was centrifuged at 10,000 g for 30 mins at 4°C. The 3 ml of chilled 70% ethanol was used to wash the DNA pellet which followed centrifugation at 4°C for 10 mins (10000 g), then, it air-dried and 100 µl of DNase/RNase free water was added to re-suspend the precipitated DNA. Nanodrop 2000 spectrophotometer (Thermo Scientific) was used to measure DNA purity. The DNA samples were stored at -20°C.

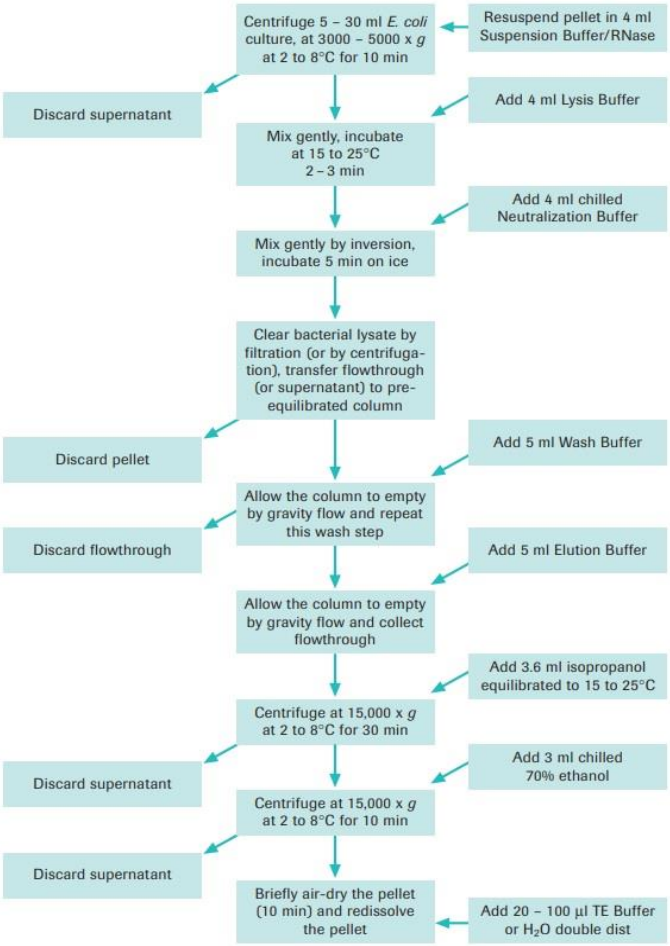


Figure 2-1. Procedure for Mini-prep for isolation and purification of DNA plasmid.

2.6.3 Genomic DNA extraction

Genomic DNA was extracted from both human cancer cells and PDOs using the QuickExtract™ DNA Extraction Solution kit (BioSearch Tech; catalogue number QE0905T /QE09050). The 6-8 days organoids (3 wells of 10-15 mature organoids) were collected into 15ml tubes and followed the centrifugation and washing steps as described in Figure 2-2. The pellet was incubated with 30ul of the DNA Extraction Solution for 6mins at 65°C. Subsequently the pellet was heated for 2mins 98°C. The extracted DNA is suitable for PCR analysis.

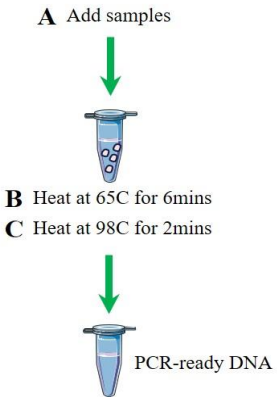


Figure 2-2. Procedure for obtaining PCR-ready DNA using QuickExtract™ DNA Extraction Solution.

2.6.4 RNA extraction from human tissues

The RNA was isolated from CRC cell lines using TRIZOL® Reagent (Invitrogen, 15596-018) according to the manufacturer's instruction. The cell lines were cultured in 6 well plate and washed with PBS twice. Then, the cells were incubated with 1 ml TRIZOL reagent for the maximum 10 mins in RT. Subsequently, 0.2 ml of chloroform was added to the samples, mixed by pipetting up and down and followed by 3 mins incubation at 15-30°C. Following centrifugation at 12000g for 15 mins at 4°C the mixture was separated in 2 layers. A red lower layer of chloroform and a clear aqueous layer (containing the RNA) at the top. The aqueous layer containing the RNA was collected and transferred to a new tube containing 0.5ml of isopropanol alcohol (Sigma Aldrich, I9516) for precipitation stage. The samples containing the RNA and isopropanol were incubated in room temperature for 10mins and centrifuged at 12g for 15mins at 4°C. Following the centrifugation, the pellet washed with 1 ml of 75% ethanol twice and centrifuged at 10000g for 5mins. The RNA pellet was air-dried, dissolved in RNase-free water and stored immediately at -80°C.

Gene	Primer	Sequence
CTNNB1	**hCTNNB1-F**	5’ -GCGCGGCTACAGCTTCA
	hCTNNB1-R	5’ -CTTAATGTCACGCACGATTTCC
β -Actin	**hβ-actin-F**	5′-AGGTGACAGCATTGCTTCTG
	hβ-actin-R	5′-AGGGAGACCAAAGCCTTCAT
FBXW7	**hFBXW7-F**	5’ -TGCAAGTGATAGAACCCCAG
	hFBXW7-R	5’ -TGTCTTCAGCCAAAATTCTCC
C-Myc	**hC-Myc-F**	5′-AAAACCAGCAGCCTCCCGC
	hC-Myc-R	5′-GGCTGCAGCTCGCTCTGC
LGR5	**hLGR5-F**	5′-GACAACAGCAGTATGGACG
	hLGR5-R	5′-GCATTACAAGTAAGTGCCAG
E-Cadherin	**hE-Cadherin-F**	5’-TGGAGGAATTCTTGCTTTGC
	hE-Cadherin-R	5’-CGTACATGTCAGCCAGCTTC
Vimentin	**hVimentin-F**	5’-TGTCCAAATCGATGTGGATGTTTC
	hVimentin-R	5’-TTGTACCATTCTTCTGCCTCCTG
FLYWCH1	**hFLYWCH1-F**	5′-GCAAAGGTCGAAGACCAGGA
	hFLYWCH1-R	5′-TTCCTGGTGTACGAGTCCTT
CD44	**hCD44-F**	5′-AGAAGGTGTGGGCAGAAGAA
	hCD44-R	5′-AAATGCACCATTTCCTGAGA
SFRP4	**hSFRP4-F**	TCAAGTCCTCATCACCCATC
	hSFRP4-R	AACTGTTCTCCGCTGTTCC
CXXC4	**hCXXC4-F**	ATGCACCACCGAAACGACTC
	hCXXC4-R	GCAGTGTTCAGGGGATAAGGT
DVL1	**hDVL1-F**	GCGGGAGATCGTTTCCCAG
	hDVL1-R	CGGCGCTCATGTCACTCTT
FGF-4	**hFGF-4-F**	TATGGCTCGCCCTTCTTCAC
	hFGF-4-R	TCGGTTCCCCTTCTTGGTCTTC
WIF1	**hWIF1-F**	AACACCATTCTCCAAACACC
	hWIF1-R	TCACACAAAGTCCACCATTC
FZD5	**hFZD5-F**	CACACCCGCTCTACAACAAG
	hFZD5-R	AGATGAAGCACAGCACCGAC
PRICKLE1	**hPRICKLE1-F**	AGGTACGGTATTGCCAGTCTT
	hPRICKLE1-R	CGAACACTGCAACTTCACCTC
PPARD	**hPPARD-F**	AAGAGGAGGAGAAAGAGGAAG
	hPPARD-R	TGAACACCGTAGTGGAAGC
SOX17	**hSOX17-F**	TCGGGGACATGAAGGTGAAG
	hSOX17-R	ACTTGCCCAGCATCTTGCTC
FBXL18	**hFBXL18-F**	TCCGGGCTGGTCAATATCG
	hFBXL18-R	CGCTTGCAGTGCTTCAACA
FBXO17	**hFBXO17-F**	CTGACCCGG TCCTTCAGTG
	hFBXO17-R	CTCCCGTACTGCTCAAAAGATAC

Gene	Primer	Sequence
Fbxo17	**mFbxo17-F**	CCTGGTAGATGGCCCAAGTAT
	mFbxo17-R	GCAGAATGGGAACTCGTCGT
Fbxl18	**mFbxl18-F**	GAACTGATCGGGTCCAATTTCT
	mFbxl18-R	GTTGGGCTAGAGTCAGGTGC
Ctnnb1	**mCtnnb1-F**	ATGGAGCCGGACAGAAAAGC
	mCtnnb1-R	TGGGAGGTGTCAACATCTTCTT
CD44	**mCD44-F**	ACTTTGCCTCTTGCAGTTGAG
	mCD44-R	TTTCTCCACATGGAATACACCTG
Olfm4	**mOlfm4-F**	TGTGTCTCAGCCACTTTCCA
	mOlfm4-R	TACTCGGACCGTCAGGTTCA
Lgr5	**mLgr5-F**	CCAGTCTCCTACATCGCCTC
	mLgr5-R	ATCTAGGCGCAGGGATTGAA
Cryp1	**mCryp1-F**	TCAAGAGGCTGCAAAGGAAGA
	mCryp1-R	ACCCTTTCTGCAGGTTCCATT
Chga	**mChga-F**	CCAAGGTGATGAAGTGCGTC
	mChga-R	GGTGTCGCAGGATAGAGAGGA
Muc2	**mMuc2-F**	AGGGCTCGGAACTCCAGAAA
	mMuc2-R	CCAGGGAATCGGTAGACATCG
Muc2	**mβ-Actin-F**	GGCACCACACCTTCTACAATG
β-Actin	**mβ-Actin-R**	GGGGTGTTGAAGGTCTCAAAC

Table 2-4. List of primers used for RT-PCR and quantitative real time PCR (qRT-PCR).

2.6.5 Complementary deoxyribonucleic acid (cDNA) synthesis

Total RNA was reverse transcribed into cDNA using PrimeScript RT Reagent Kit (Takara-Clontech Laboratories, RR037A) according to the manufacturer's recommendations. In brief, in an RNase-free Eppendorf tube, 1-5µg of RNA was added to a mixture containing 1µl oligo dT primer (25pmol), 50pmol of random six-mers primers and 1x Prime Script buffer with 0.5 µl of reverse transcription (RT) enzyme and distilled water. The reaction incubated at 37°C for 15 mins for

the cDNA synthesis and at 85°C for 5 sec, to terminate the reverse transcriptase. cDNA was collected and stored at -20°C until use.

2.6.6 Quantitative real-time PCR (qRT-PCR)

The qRT-PCR was applied to evaluate the mRNA expression of the genes in cells and organoids. Both cDNA and primers were diluted 1:10 prior the experiment with nuclease-free water (final concentration of primers was 10 μM) (Table 2-4). All reactions were conducted in triplicates in a 96-well plate (Roche, 04707516001) and the emitted fluorescence was evaluated by LightCycler 480 II instrument (Roche). For a final reaction of 10μl, 2μl of cDNA template, 5μl of 2X lightCycler® 480 SYBR Green I Master Mix (Roche, 04707516001), 5pmol/μl of primers and 1μl of DNase/RNase free water was used (Table 2-4). The expression of β-actin or glyceraldehyde 3-phosphate dehydrogenase (GAPDH) was used for normalisation.

2.7 Principle and procedure for RT^2 Profiler PCR Array

The 96-well RT^2 Profiler PCR Array (human Wnt signalling, Cat. no. 330231 PAHS-043ZA) was used to evaluate the effect of Rifabutin in expression in 84 genes linked to Wnt signalling pathway in comparison to untreated control. Each well of the Profiler PCR Array plate consists of a primer for a specific Wnt signalling gene (*Appendix 1*). Along 84 genes, one well contains a genomic DNA control, 3 wells contain reverse-transcription controls, and 3 wells contain positive PCR controls were also included (Figure 2-3). 5 housekeeping genes also included in the arrays for normalization of data.

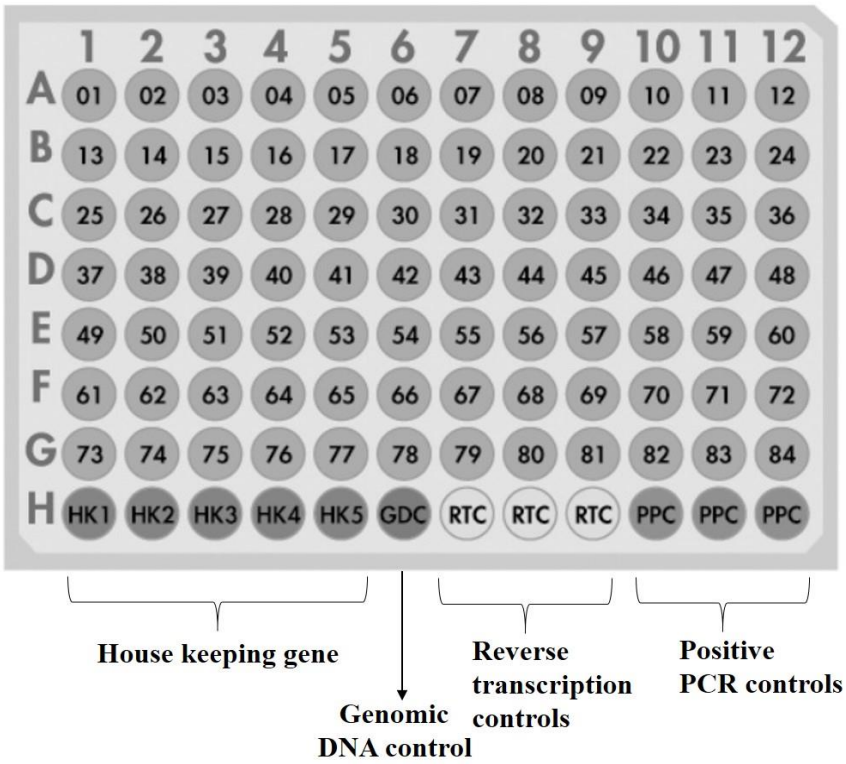


Figure 2-3. Schematic of RT^2 Profiler PCR array plate containing 84 Wnt signalling associated genes.

During the procedure, the cDNA is mixed with the RT^2 master mix and subsequently added to individual well. The total amount of the SYBR Green, cDNA and RNase-free water is presented in table 2-5. 25µl PCR component mix was added to each well of PCR array plate. This provides an excess volume of 300µl from master mix to allow for pipetting errors.

Array format	96-Well (F)
SYBR Green Mastermix	1350 µl
cDNA synthesis reaction	102 µl
RNase-free water	1248 µl
Total Volume	2700 µl

Table 2-5. The PCR component mix for the Wnt signalling PCR array.

After RNA purification from experimental samples (treated and non-treated control organoids), the cDNA is generated as described earlier (2.6.5). Subsequently the cDNA is mixed with the appropriate amount of cyber green and 25µl of Mastermix is loaded in each well. PCR is performed and finally, relative expression is determined using data from the real-time cycler and the ΔΔCT method (Figure 2-4).

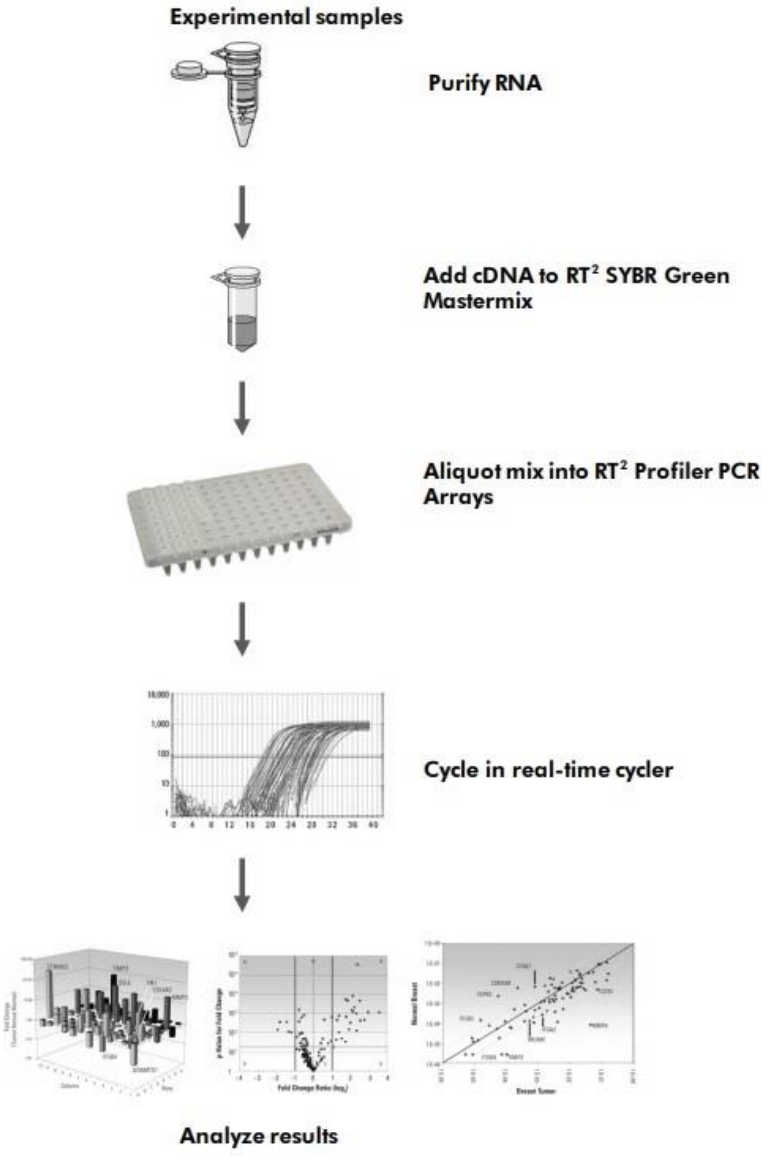


Figure 2-4. The procedure for performing the RT^2. (Adapted from QIAGEN.https://www.qiagen.com/be/products/discovery-and-translational-research/lab-essentials/plastics/rt2-profiler-pcr-arrays/#orderinginformation).

The cycling conditions for LightCycler 480 II instrument (Roche) used for RT^2 assay is as follow (Table 2-6).

Cycles	Duration	Temperature	Comments
1	10 min	95°C	HotStart DNA Tag Polymerase is activated by this heating step
45	15 s	95°C	
	1 min	60°C	Perform fluorescence data collection

Table 2-6: The PCR program condition for the RT^2 assay using LightCycler 480 II instrument (Roche)

2.8 Statistical analysis

All statistical analysis was performed using Microsoft Office Excel 2010 and GraphPad Prism 8 software. All experiments were performed at least 2-3 times on independent occasions and all results are indicated by mean ± standard deviation (STDEV) unless otherwise mentioned in the text. The significance of differences between mean and median was determined using the Students t test and $P < 0.05$ (*) is considered as significant, $P \leq 0.01$ (**) as highly significant and $P \leq 0.001$ (***) as very highly significant.

Chapter 3

Establishment of small number of CRC patient derived organoid (PDO) lines and studying the role of Noggin in cultured PDOs and CRC cell lines

Brief Introduction

As outlined in Chapter 1, organoids have a broad application in many fields ranging from modelling human development and disease, personalised medicine, drug screening, etc. (327, 328). Moreover, in the last few years, several studies have evaluated the capacity of the organoids as transplantation sources for therapeutic approaches and regenerative medicine (329). So far, some crucial aspects of organoids, including the morphological alterations and the growth pattern of the matched tumour and their normal (normal adjacent to a tumour) derived organoids have received less attention. To our knowledge, there was no systematic study that compares the pattern of organoids growth/structure from normal and matched tumour tissue derived from one patient or comparison with another patient. Therefore, this chapter was initially focused on culturing matched normal and tumour organoids of patients with CRC and assessed their timed growth and structural differences daily. Based on our observations, the morphology characteristics of the organoids derived from colorectal cancer tumour and adjacent normal tissues from the same patient differed markedly. The investigation of phenotypical changes in tumour and matched normal organoids after administration of candidate therapeutics impact a vital role in the selection of appropriate treatment before actual therapy. Thereby, in a personalised targeted-based approach, capturing organoid morphological differences upon drug treatment (in both tumour and normal adjacent derived organoids) is of significant importance in patients who diagnosed with CRC. Part of this chapter has been published as original research recently (330).

On the other hand, Noggin inhibitory activity is essential for the early stage of embryo patterning, while the loss of Noggin has shown to be perinatally lethal in mice (331). Noggin is a glycoprotein which is secreted as a 64 kD homodimer (332). In the colon and small intestine, Noggin inhibitory-mediated maintenance of normal stem cells is through the bone BMP gradient in the crypt base. Considering the significance of secreted Noggin activity in intestinal homeostasis and their potent contribution in cancer progression, we aimed to examine the effect of Noggin treatment in a series of colon cancer cell lines including HCT-116, SW480, DLD-1 and HCT-116 with and without FBXW7 E3 ligase gene (119).

3.2 Results

3.2.1 Normal human derived intestinal epithelium adjacent to tumours gave rise to multi branched organoid structure

After culturing the isolated normal organoids crypts in the Matrigel, the complete organoid growth medium was supplemented as outlined in M&M chapter, section 2.2.1. The clinicopathological characteristics of patients included in this study presented in Table 3-1. Of note, 17 patients have been successfully generated from both tumour and matched normal adjacent sample of colonic cancer tissues from different patients (successful rate; 63%). Approximately 10 samples failed to grow and develop into organoids as either due to bacterial contamination in 4 cases or application of low expressing Wnt3a supplement (failure rate: 37%).

Patient Number	Age	Gender	Diagnosis/history	Staging	Organoid generation/passage
1	67	M	Colonic carcinoma - poorly differentiated adenoma carcinoma	T3 N1 M0	Successful/two vial frozen from passage 3
2	69	F	Colonic carcinoma - moderately differentiated adenoma carcinoma	T4 N2 M0	Successful/two vial frozen from passage 4
3	51	M	Mid-rectal cancer with no interval liver or lung metastasis	T3 N0 M0	Successful/two vial frozen from passage 2
4	35	F	Sigmoid colon polyp - tubular adenoma with focal high grade dysplasia	n/a	Successful/two vial frozen from passage 3
5	79	M	Colonic cancer - moderately differentiated adenocarcinoma	T2 N0 M0	Successful/two vial frozen from passage 4
6	62	F	Colonic tumour - also got some lung nodules on the CT scan	T3 N2 M0	Successful/two vial frozen from passage 4
7	68	F	Sigmoid colon cancer- moderately differentiated adenocarcinoma	T2 N0 M0	Successful/two vial frozen from passage 3
8	83	M	Hepatic flexure cancer - moderately differentiated adenocarcinoma	T3 N1 M0	Successful/two vial frozen from passage 2
9	72	F	Colonic carcinoma - moderately differentiated adenocarcinoma	T3 N3 M0	Successful/two vial frozen from passage 3
10	52	M	Colonic cancer - moderately differentiated adenocarcinoma	T2 N0 M0	Successful/two vial frozen from passage 2
11	55	M	Colonic cancer - moderately differentiated adenocarcinoma	T2 N0 M0	Successful/two vial frozen from passage 3
12	68	M	Colon tumour with evidence of low GI cancer	T1 N0 M0	Successful/two vial frozen from passage 2
13	59	M	Caecal carcinoma - poorly differentiated adenocarcinoma	T3 N0 M0	Successful/two vial frozen from passage 3
14	83	M	Sigmoid cancer - Moderately differentiated adenocarcinoma	T3 N0 M0	Successful/two vial frozen from passage 4
15	62	M	Rectal cancer - Moderately differentiated adenocarcinoma	T3 N1 M0	Successful/two vial frozen from passage 4
16	64	F	Colon cancer - poorly differentiated adenocarcinoma	T3 N1 M0	Successful/two vial frozen from passage 3
17	69	F	Colon cancer - moderately differentiated adenocarcinoma	T3 N1 M0	Successful/two vial frozen from passage 2
18	58	F	Colonic carcinoma - poorly differentiated adenoma carcinoma	T3 N0 M0	Failed/contamination in passage 1

19	64	M	Sigmoid colon cancer- moderately differentiated adenocarcinoma	T2 N0 M0	Failed/contamination in passage 1
20	57	F	Colonic carcinoma - poorly differentiated adenoma carcinoma	T2 N0 M0	Failed/contamination in passage 2
21	66	F	Colonic carcinoma - moderately differentiated adenocarcinoma	T2 N0 M0	Failed/contamination in passage 1
22	79	M	Colonic cancer - moderately differentiated adenocarcinoma	T3 N1 M0	Failed/technical issue
23	85	M	Colonic carcinoma - poorly differentiated adenoma carcinoma	T3 N0 M0	Failed/application of low activated Wnt3a
24	84	F	Colonic carcinoma - moderately differentiated adenocarcinoma	T2 N0 M0	Failed/application of low activated Wnt3a
25	73	M	Colonic cancer - moderately differentiated adenocarcinoma	T2 N0 M0	Failed/application of low activated Wnt3a
26	66	F	Colonic carcinoma - poorly differentiated adenoma carcinoma	T3 N0 M0	Failed/application of low activated Wnt3a
28	59	M	Colonic carcinoma - poorly differentiated adenoma carcinoma	T3 N0 M0	Failed/application of low activated Wnt3a
27	70	M	Sigmoid cancer - Moderately differentiated adenocarcinoma	T3 N1 M0	Failed/application of low activated Wnt3a

Table 3-1. The characteristics of CRC patients in the present study.

The morphological alterations and growth pattern were visualised on a daily basis (Figure 3-1). From days 2 to 4 post-culturing, the crypts acquired an enclosed central lumen and started budding into new regions with crypt-like structures known as colonoids. The frequency of cryptogenesis enhanced rapidly during days 5 and 7, and the colonoids underwent excessive expansion which accompanied with an augment in the size of the organoids. As previously indicated (333), these morphogenesis events mediated formation of new

multicellular and branched domains containing stem cells and differentiated cells. This multi-lineage differentiation capacity of the organoids facilitated the development of a miniature intestine as an *in-vivo* culture. The resulting organoids then constantly self-renewed and self-organized into a mature organoid comprising numerous crypt-like protrusions in the organoid outer layer. Each of this small crypt-like domain forms spheroid-like organoids after passaging and could give rise to a new mature organoid (Figure 3-1; inset). The day zero crypts are representative images of cultured colonic crypts after seeding on the Matrigel, and it is not similar to the organoids showed for days 1 to 7. The central region of the organoids so-called necrotic core contains dead and apoptotic cells resembling the intestinal lumen. During days 6-7, the size of the organoid elevated more than 3-4 folds (Figure 3-2; day 7). At this point, mature organoids were either utilized for assays or further expanded in culture for freezing purposes.

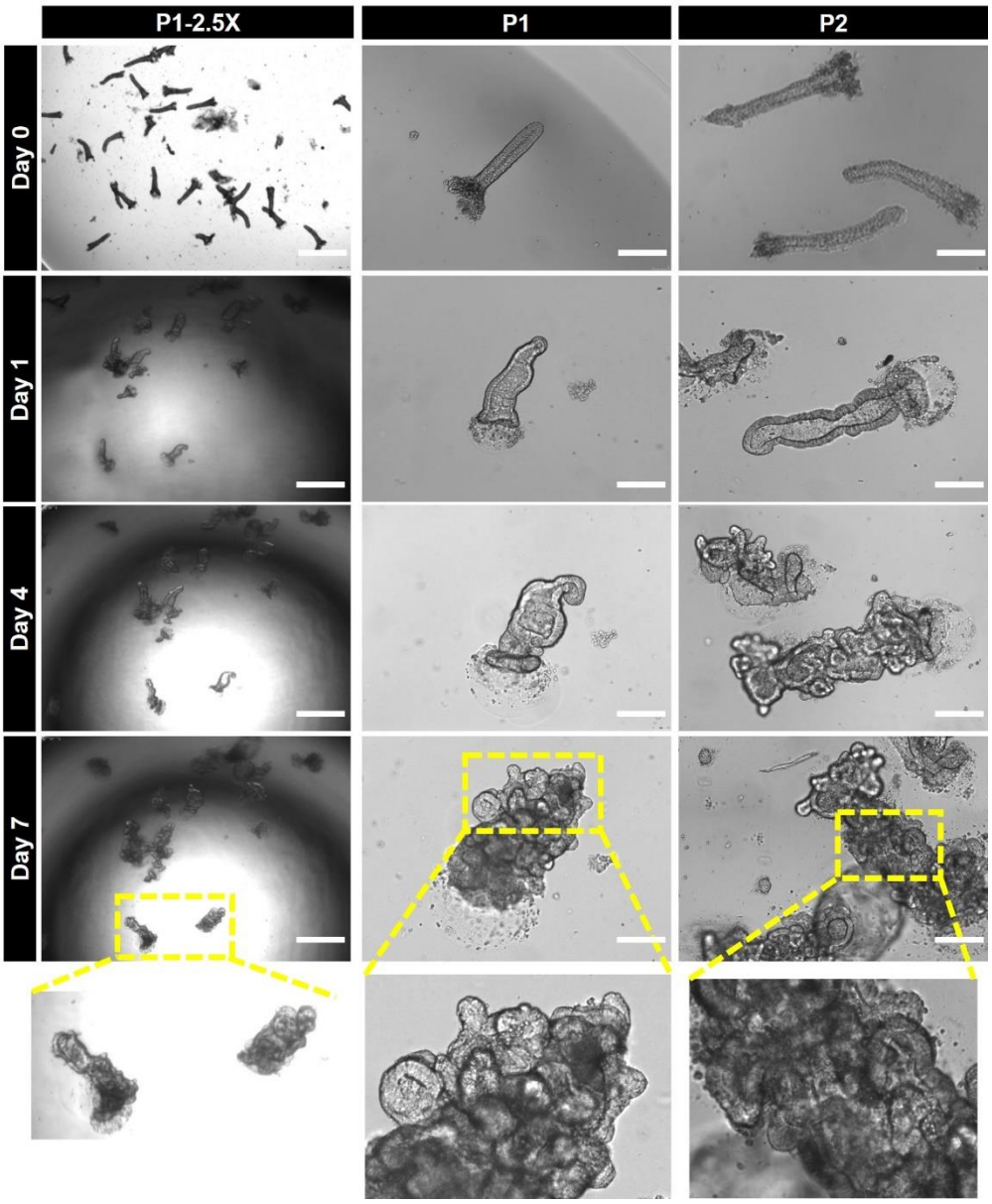


Figure 3-1 Representative images of morphology alteration in organoids derived from normal tissues adjacent to tumours. The three panels represent, the growth of normal organoids from two different patients (P1, P2) with CRC. The left panel shows the gradual growth of organoids derived from the normal human colon tissue from patient 1 (P1), day 0 to day 7 with 2.5X magnification (Scale bar, 250μm). The organoid expanded rapidly and the developing crypt actively grew and differentiated while branching. On day 7, further outgrowth created a mature organoid, comprising numerous new regions of crypt-like domains; P1 and P2, two right panels (Scale bar, 75μm).

3.2.2 Tumour organoids represent differential phenotypical morphology in culture

After seeding the tumour cells into Matrigel and adding organoid culture medium, a few cystic-like shape bodies (representing the tumour-derived organoids) with uneven borders appeared. Unlike the adjacent normal epithelium at day zero, no finger-like invaginations were resembling the intact crypt structure in colonic tumour samples post isolation, whereas, there were some small aggregated structures formed by a subpopulation of cells mimicking the primary origin tumour (Figure 3-2). The tumour organoids demonstrated broadly different phenotypical features. The size, morphology and growth pattern of the tumour-derived organoids extensively varied from one tumour sample to another in which three main types of tumour-derived organoids were identified. The first and most prevalent types of tumour organoids with relatively rapid growth rate was characterised by cystic morphology and defined lumen (Figure 3-2, right panel, inset). The second type was the small-sized compact organoids without luminal area and remarkably decreased growth rate across all types of tumour organoids (Figure 3-2, left two panels, inset and red arrowheads indicating their remarkable small size compared to other tumour organoids). The third and most scarce type of colonic tumour organoids distinct by restricted budding morphogenesis surrounded the surface area and low growth rate so-called budding tumour organoid. This heterogeneity of tumour organoids might be due to the genetic background and characteristics of the patient, number of CSC and normal stem cells, treatment regimen, and also location of the tumour (334, 335).

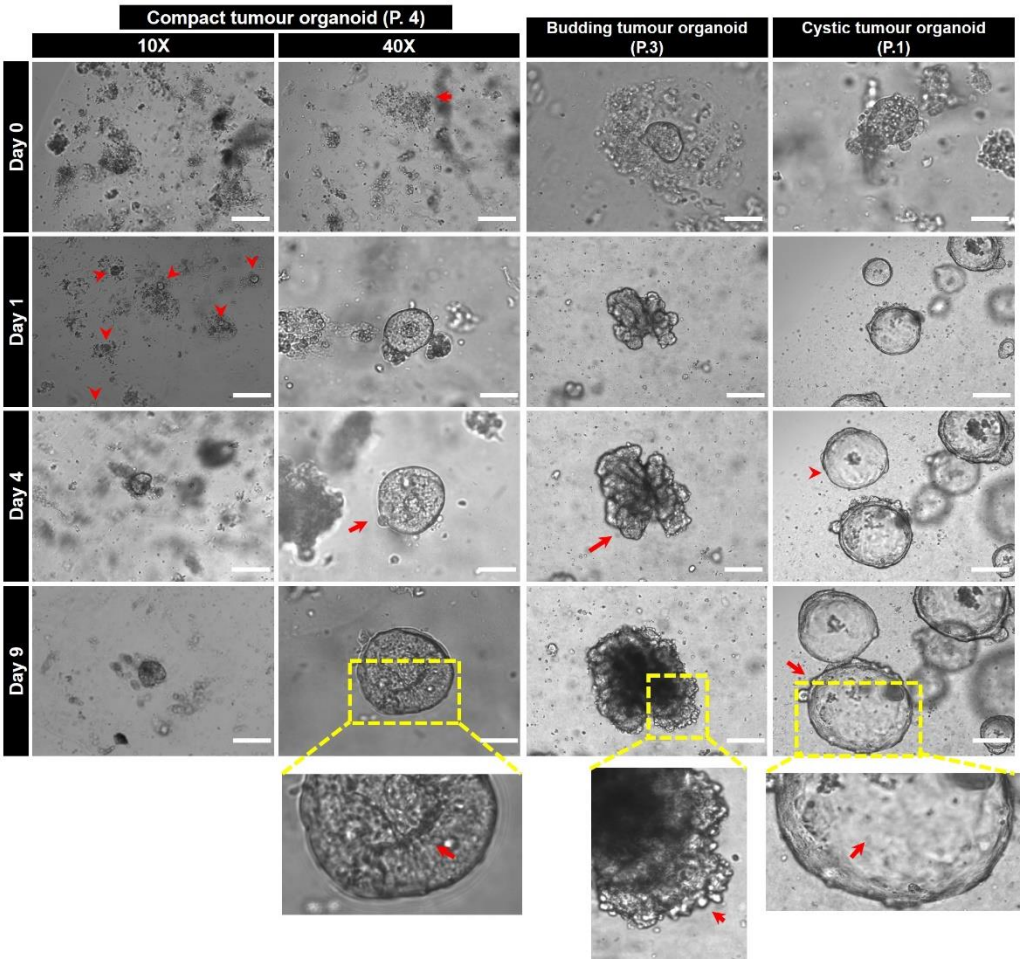


Figure 3-2. Growth heterogeneity within tumour organoids mirrors the *in vivo* counterparts. The four above panels are representing the 3 major types of colonic tumour organoids derived from different patients (P.1, 3, 4 are related to patients no1 no 2 and no 3 from the table 3-1). The phenotypical features, growth pattern and growth rate of tumour organoids differed from rapid growing cystic tumour organoids forming a rounded morphology with apical lumen (right panel) to compact aggregated small tumour organoids without distinct lumen region (left two panels). The rare type of tumour-derived organoids (third panel; budding tumour type) acquired very limited cryptogenesis with multiple budding units and low growth rate. Left panel scale bars; 25µm and 75µm, all other represented panels; 75µm.

Differences in the morphology and growth pattern of organoids derived from tumour/adjacent normal tissue of patients with colon cancer within seven days

implied the presence of underlying differential cellular and molecular events. Overall, in contrast to normal derived organoids with evident branching outgrowth (Figure 3-3), these cystic-like tumour organoids failed to develop budding or significant crypt-like units over one week. The cystic-like can be due to the higher rate of mitotic failures, cell death, deregulation of essential signalling pathways required to maintain the colonic crypt proper function and growth rate, as previously indicated (328, 336, 337).

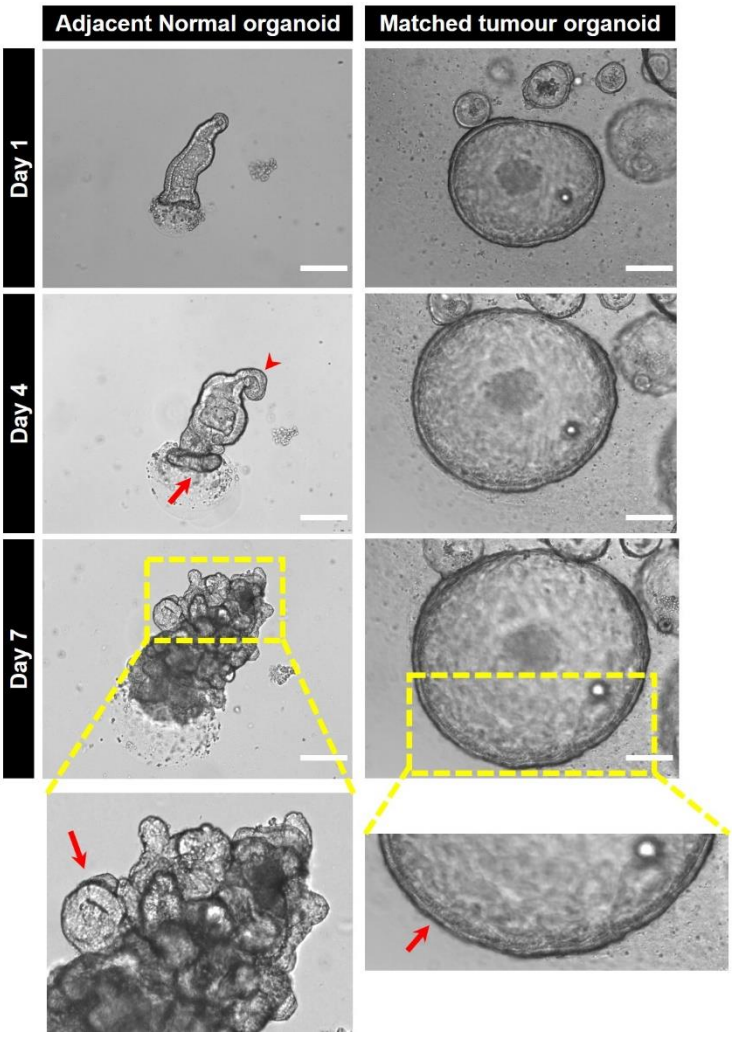


Figure 3-3 Comparison of morphological alterations in human colon matched tumour and normal organoids. The growth pattern and size of tumour-derived organoids and their matched normal tissue were significantly different. Left panel represents the development of normal organoids and right

panel indicates the growth pattern of a matched colonic tumour organoids in culture. In comparison to the normal organoids, there was no finger-like extrusions (crypts) or branching events in a fraction of tumour organoids. Scale bar, 75µm.

3.2.3 Phalloidin staining of normal derived organoids and their matched tumour tissue

The tumour and adjacent normal derived organoids were co-stained with Phalloidin conjugated with Alexa 568 to reveal F-actin and DAPI to demonstrate the nuclei using whole-mount embedded sections. Phalloidin functions by binding and stabilising filamentous actin (F-actin). The lack of budding and following cystic outgrowth is the main characteristics of tumour organoids while the normal derived organoids formed multiple crypt-like units capable of developing to the new budding crypt and mature organoids (Figure 3-4; A and yellow arrowheads).

Furthermore, to investigate whether organoids with a disrupted and dark morphology (necrotic core) in the bright-field microscope, represent dead cells, the live/dead staining assay was performed. Hoechst 33342 dye, a popular cell-permeant nuclear counterstain for live-cell staining, and Propidium iodide (PI), which stain dead cells (338), were used on whole-mount samples, both normal and tumour organoids respectively (Figure 3-4). This data shows that cell death responses and the number of dying cells in the normal and tumour organoids are primarily different from each other. Also, a tumour crypt culture possessed the cystic organoid structure with no cellular segregation and polarisation.

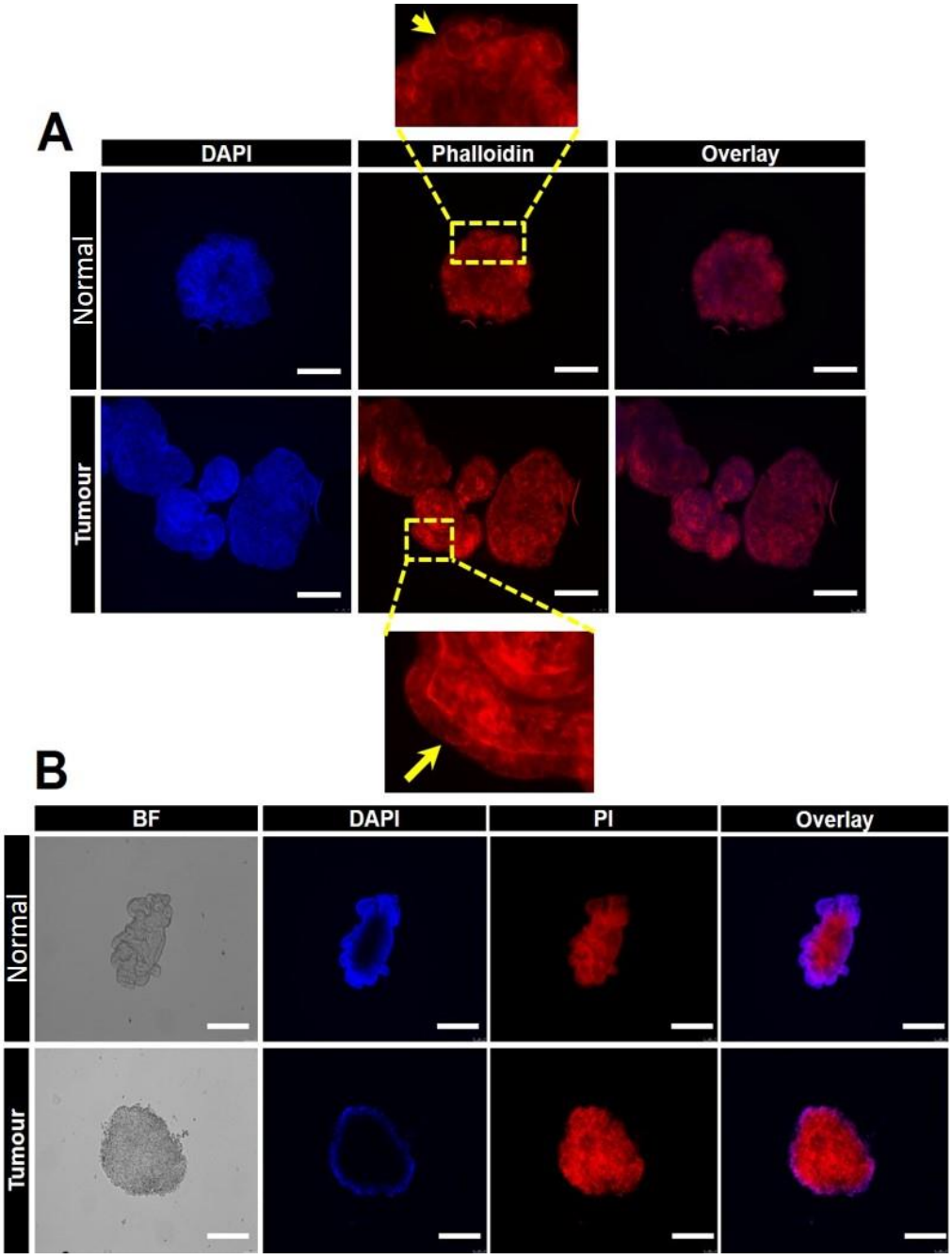


Figure 3-4. Colonic normal derived organoids self-organize into branching multicellular structures. A) Analysis of the phalloidin staining revealed the presence of multilayer fragments and budding units scattered throughout the organoid structure in normal derived organoids compared to tumour counterparts. The lack of multiple branching units was a dominant characteristic across all tumour-derived organoid types. Scale bar 75μm **B)** Dead/live staining of organoids using the PI dye also verified the accumulation

of dead cells in central atypical luminal part (necrotic core) in both tumour and matched normal organoids. Scale bar, 75µm.

Furthermore, the adherent/constant growing of ever-expanding normal derived organoids in culture without passaging over two weeks resulted in the formation of a gigantic organoid containing hundreds of crypt-like units. These crypt-like structures contain both stem-cell and differentiated-cell compartments, as previously indicated (339). At the expense of prolonged organoid expansion, each of this crypt-like domain was capable of growing, budding, and further give rise to new organoid, similar to the isolated crypt on the day zero (Figure 3-5). At this stage, these grown, normal organoids can go under freezing methods for patient's organoid biobank maintenance.

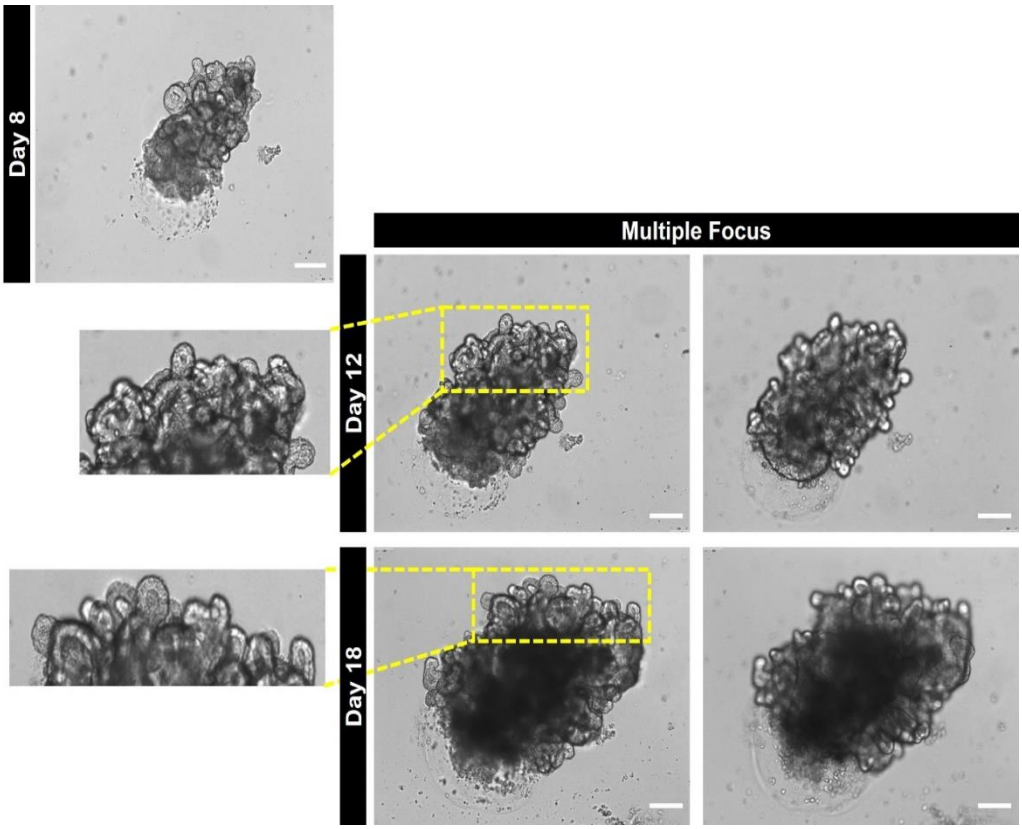


Figure 3-5. Organoid formation in culture for ~3 weeks gave rise to multicellular structure abundant with small crypt invaginations. Expansion of the organoids in culture over two weeks (18 days) steered the formation of a very large mature organoid comprising hundreds of crypt-like domains. Each of this individual small crypt-like domain can develop to a new mature organoid after re-culturing. At this stage, the organoid can be broken apart, and a single domain can be pooled in culture to form a new organoid, or it can be used to proceed the freezing process. Scale bar, 75µm.

3.2.4 Long-term maintenance (passaging and freezing-thawing) of normal/tumour organoids in culture reproduces the main features of original organoid

Both tumour and matched normal adjacent organoids can be cultured indefinitely and cryopreserved for further biobank purposes. Previous studies indicated that the organoids stably retained the molecular features of primary tissue after an intense process of prolonged passaging. The figure 3-6; A-B, demonstrates the re-culturing of organoids in both tumour and matched normal adjacent for 9 days. To further investigate the extent of the regenerative potential of normal and matched tumour organoids upon on freeze-thawing, the frozen organoids were recovered from two different patients in the organoid biobank. Both tumour and normal derived recovered organoids maintained the main morphological features similar to primary isolated crypts and subsequently self-renewed and self-organized into mature organoids in the following weeks. The growth rate, size and pattern of tumour organoids varied from one tumour to another with a typically rounded shape was the dominant trait. The presence of an apoptotic fraction of cells surrounding the recovered organoids was the dominant feature

in day one post-recovery of both normal and tumour-derived organoids (Figure 3-6; C, insets and red arrowheads). In the process of organoid formation in the following days, the organoids revived and underwent a similar growth pattern and morphology when compared to the driven organoids initially.

The survival rate of the recovered, normal human organoids varies from 40-70%. The growth rate and morphological pattern of recovered organoids are heterogeneous, and they required two adherent passages to revive completely and to restore stable status before initiation of any further experiments.

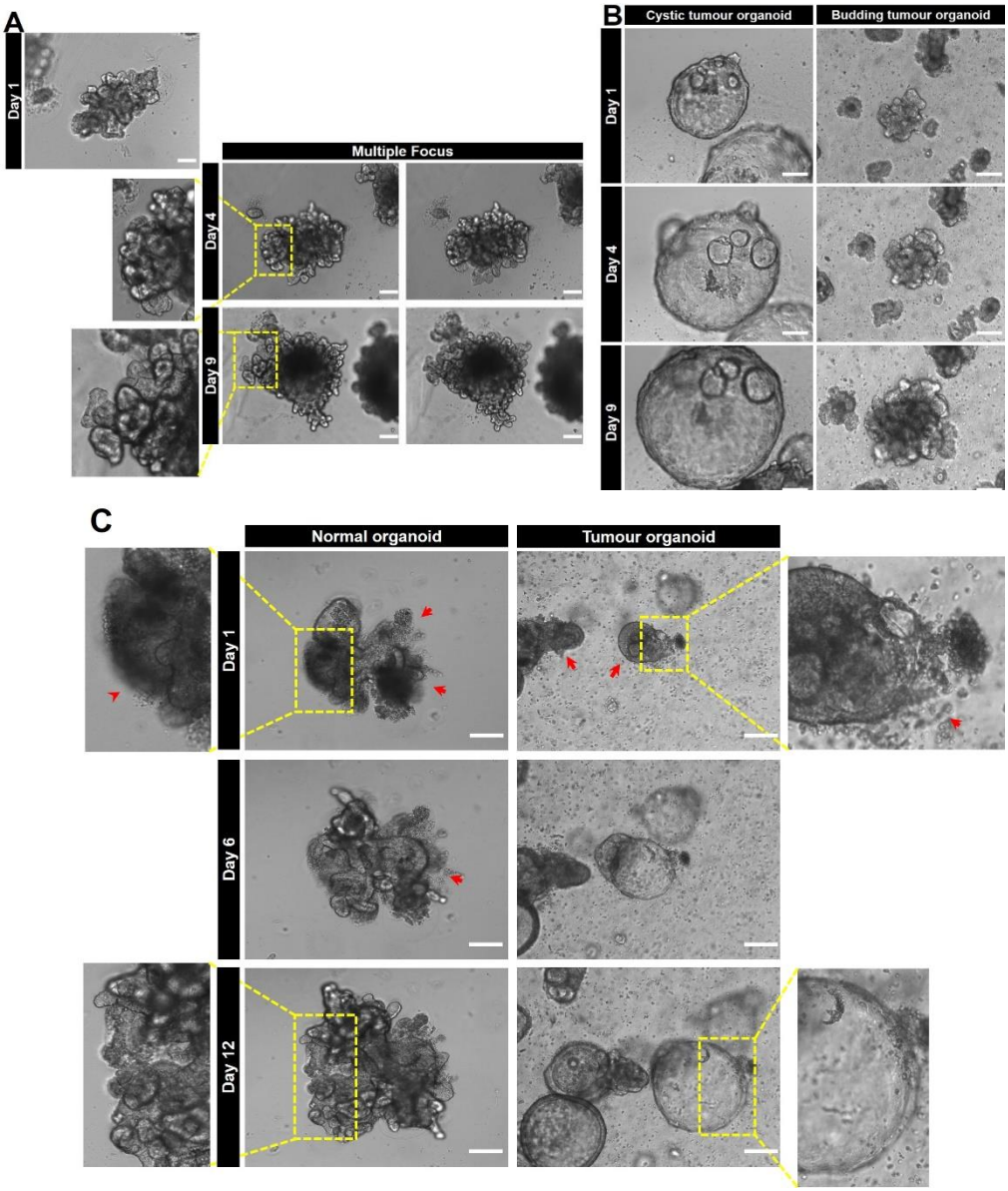


Figure 3-6. Organoids sustain their altered growth properties after excessive passaging and freezing-thawing. A) Representative bright-field images of a single normal organoid that grew in culture for further 9 days after passage. **B)** Similar normal organoids, the tumour organoids can be passaged for a long-term state, while can actively differentiate and show heterogeneous phenotypes and morphology. **C)** The capability of organoids to ever grow and freeze-thaw in culture nearly infinitely makes them a suitable 3D *in-vitro* model for a broad range of developmental and disease studies. The culture contains an apoptotic subpopulation of cells distributed around the organoids in first days after recovery in both normal and tumour-derived organoids (insets and red arrow-heads). Scale bars for all panels; 75µm.

3.2.5 Tumour organoids display divergent growth features and morphogenesis

Further characterization of the differences between the two main types of tumour-derived organoids (cystic and budding form) from 17 patients are presented in Figure 3-7. The Phalloidin and haematoxylin and eosin (H&E) staining of the tumour organoids revealed a distinct differential pattern between the major colonic tumour organoids. The budding tumour organoids characterized by small lobular structures surrounding the surface area (Inset and yellow arrow-heads). Following staining of budding tumour-derived organoids embedded tissue with H&E confirmed the presence of multiple small follicular structures distributed around the laminar region. Unlike the budding tumour type, however, the rapidly growing cystic tumour organoid had no visible lobular domains and were prone to form a large rounded structure with a lack of any cryptogenesis (Figure 3-7, right panel). Further investigating of H&E staining also confirmed the presence of large apical area without morphogenesis in cystic tumour organoids compared to budding type.

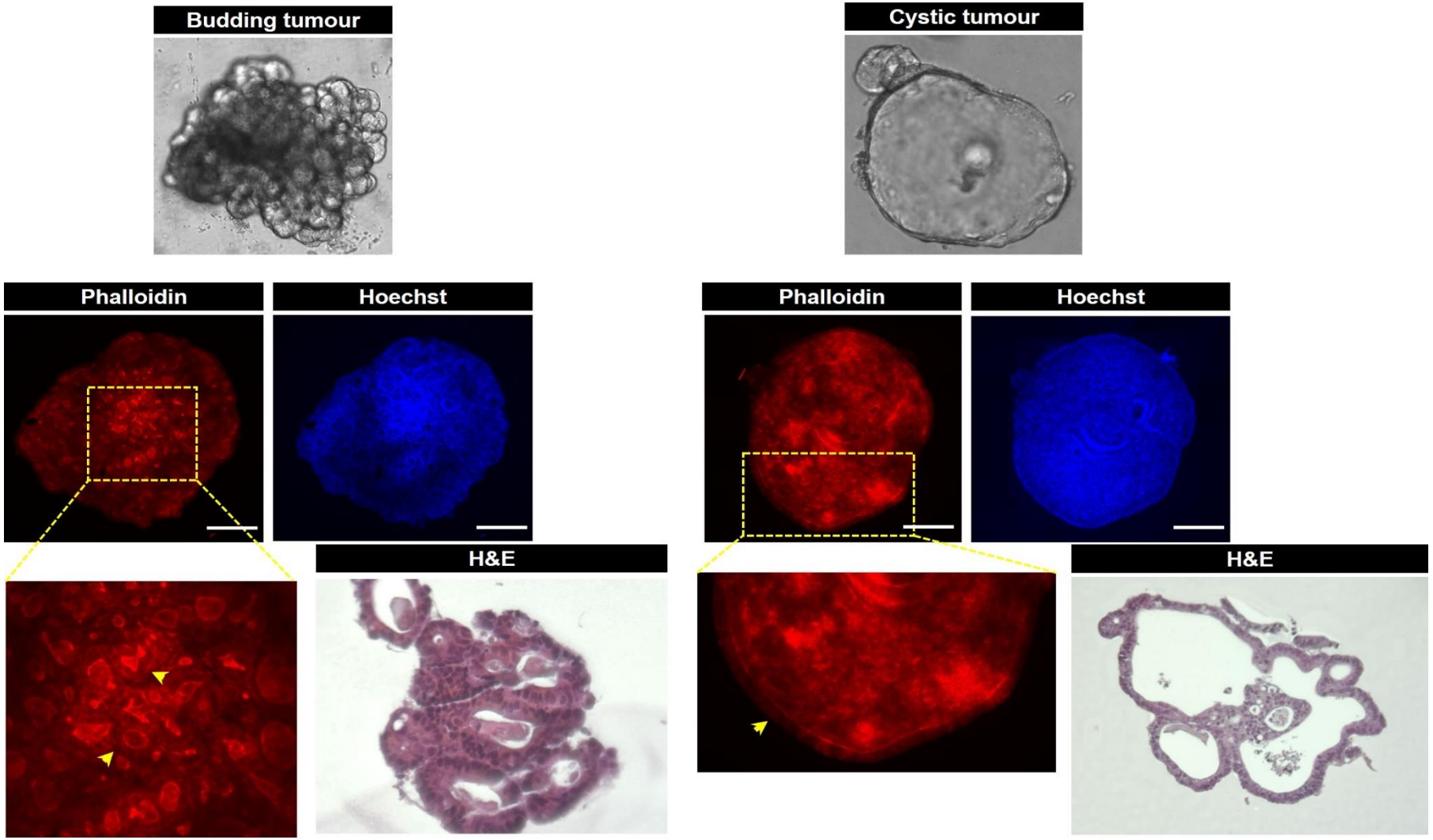

Budding tumour
Cystic tumour
Phalloidin
Hoechst
Phalloidin
Hoechst
H&E
H&E

Figure 3-7. The phenotypical characteristics of two dominant types of tumour-derived organoids among different patients. The cystic tumour-derived organoids characterized by the lack of branching events (right panel) compared to budding tumour type in which the organoids replete with numerous small lobular structures localized around the surface area (insets and yellow arrowheads). Further microscopic appearance on haematoxylin and eosin staining confirmed the existence of extensive multi-vesicular compartments in budding tumour organoid vs cystic type. Scale bar, 75μm.

3.2.6 *CTNNB1, LGR5* and *CD44* genes expression upregulated in cystic compared to budding tumour type organoids

Further characterisation of the cystic vs budding tumour organoids was performed via qRT-PCR for various markers including *CTNNB1*, and its downstream target genes including *LGR5*, *CD44* and *c-Jun* (Figure 3-8). *CTNNB1* mRNA expression was upregulated significantly in cystic tumour-derived organoids compared to a budding tumour. The lack of budding morphogenesis and induction of proliferation is the main characteristics of cystic tumour organoids. In addition, the formation of hyper-proliferative units is the feature of Wnt/β-catenin mutant organoids. Drost et al. have recently demonstrated that CRISPR/Cas9 mediated of normal colon derived organoids (simultaneous mutant for *APC*, *KRAS*) developed cystic form phenotype in culture (340).

Furthermore, relative fold-change in mRNA expression levels of *CD44* in budding derived organoids markedly decreased compared to cystic tumour organoids (mean ≥1.5-fold change), this may indicate the enrichment of *CD44* gene expression in cystic tumour-derived organoids compared to budding type

potentially providing a resistance trait to chemotherapeutic treatments. In addition, the *LGR5* expression was remarkably upregulated by more than 4-fold in cystic tumour-derived organoids compared to budding tumour organoids. The *LGR5* expression has already indicated as a poor prognosis factor in CRC tumours. Moreover, further investigation for *c-Jun* expression, revealed that the budding tumour organoids associated with markedly enhanced relative mRNA expression when compared to cystic organoid type (mean ≥3.5-fold change).

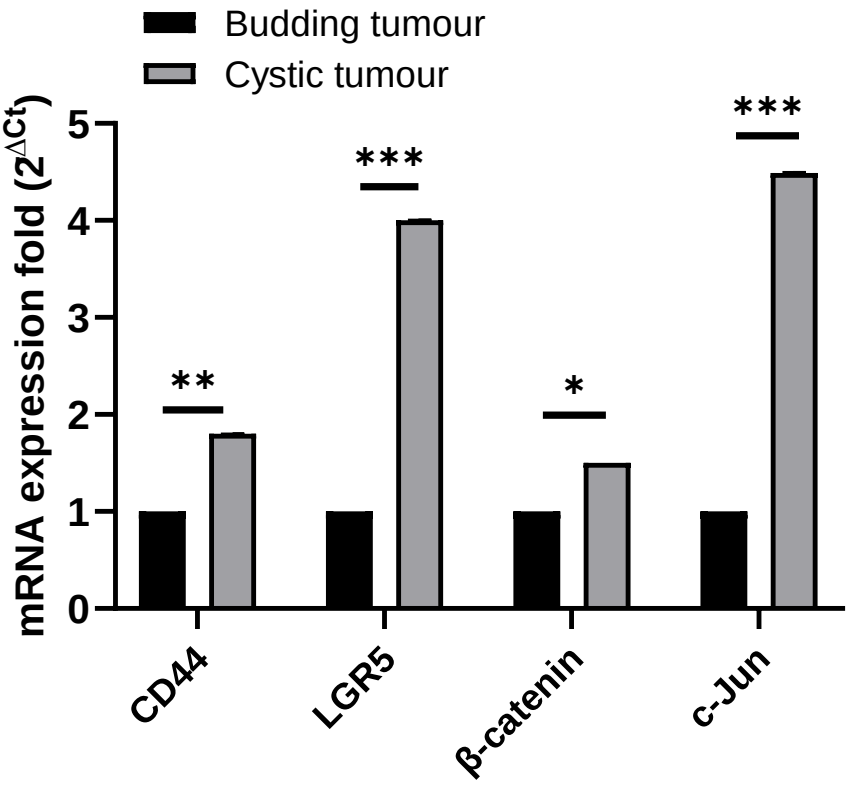


Figure 3-8. Quantification of the mRNA expression for selected markers including β-catenin, CD44, LGR5 and c-Jun. qRT-PCR analysis of mRNA expression for *CTNNB1* and *CD44* showed remarkable downregulation in budding tumour organoids compared to cystic. All values represent means ± SD. $^{*}p < 0.01$, $^{**}p < 0.01$, $^{***}p < 0.001$ denote significant differences between the groups, N=3.

3.2.7 Colonic tumour organoid grew indispensable of Wnt-3a and Noggin supplement

To further characterize the cystic and buddying tumour organoids, both tumour-derived organoids cultured independence of Wnt-3a and Noggin niche supplement (Figure 3-9). Of note, previous studies demonstrated that *APC* mutant tumour organoids grew independence of Wnt3a supplement while *SMAD4* mutant organoid can grow in culture lack of Noggin (51). Positive selection of both tumour organoids by removal of the Noggin and Wnt3a revealed that tumour organoids are aberrant for *APC* and *SMAD4* mutations. A recent finding on the library of 55 colorectal tumour organoids from a range of histological subtypes and clinical stages also supports this observation that the activated Wnt-3a signalling pathway promotes the colon tumour organoid formation in Wnt Niche-independent signalling manner, and the abolition of canonical Wnt signalling improved their differentiation potential (341). Altogether, the actual mutation status of the main tumour derived organoid lines in this study is not known.

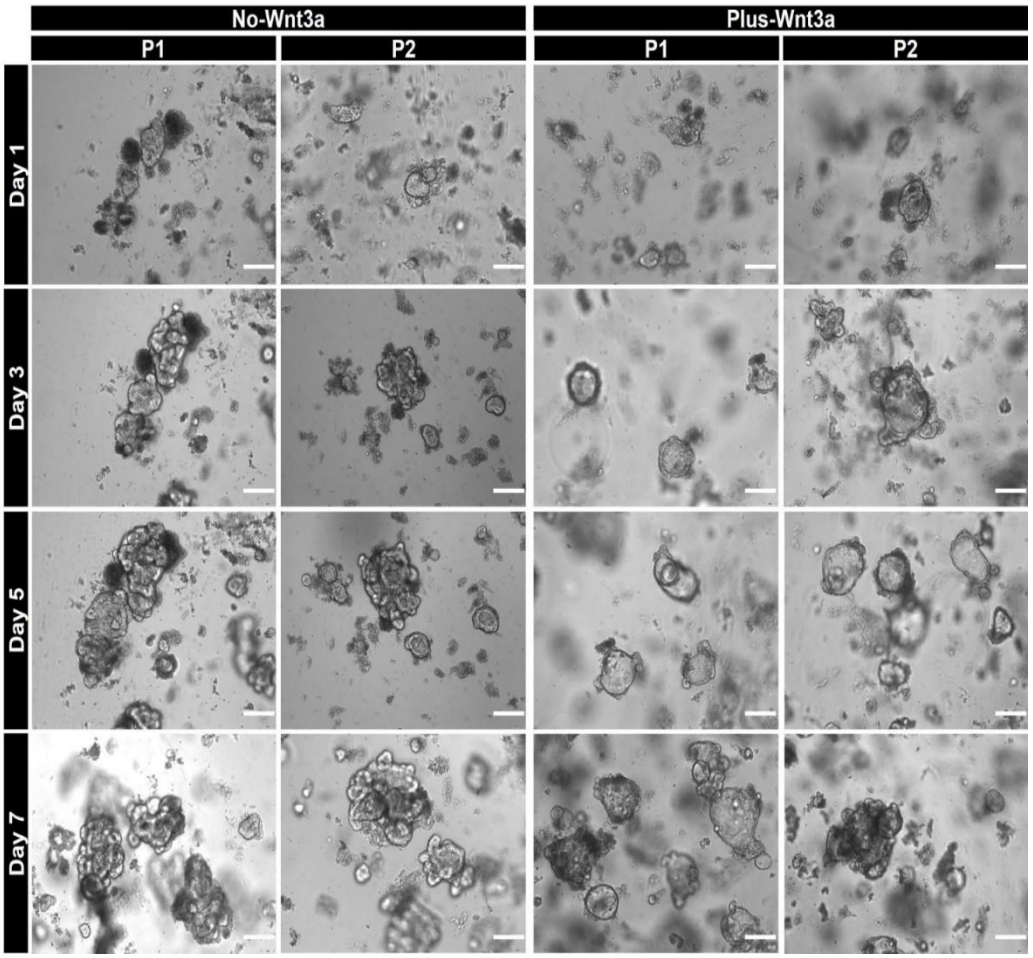


Figure 3-9. Tumour organoid growth pattern in the presence and lack of Wnt3a. Unlike adjacent normal derived colon organoid, the removal of Wnt-3a and Noggin from tumour organoid medium did not impact the phenotypical morphology of both tumour-derived organoids (cystic and budding types). The augment tumour organoid size and increase in the number of buds/lobes from their original cystic/budding shape bodies was determined in a growth medium with lack/presence of Wnt-3a and Noggin in both conditions. Scale bar, 75µm.

3.2.8 The role of Noggin in patient-derived organoids and human colon cancer cell lines

3.2.8.1 Lack of Noggin caused perturbation of human colonic and murine intestinal organoids

Noggin is a small glycoprotein produced as a homodimer. Noggin is post-translationally modified when it is secreted as disulphide-bounded homodimer glycoprotein (64 kDa) (332).

The Noggin-conditioned medium was produced, harvested and validated as previously described (Figure 3-10) (342).

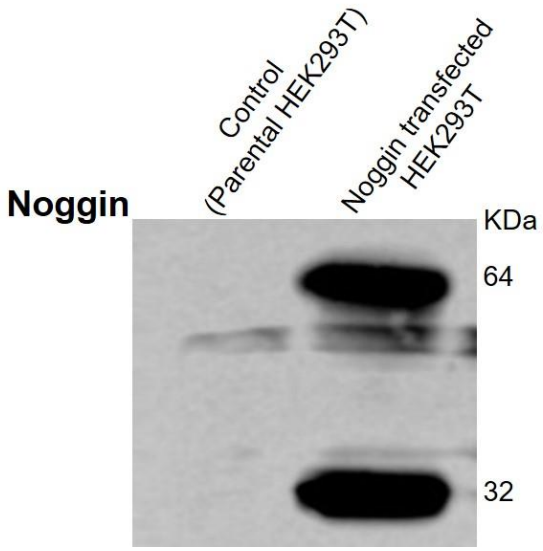


Figure 3-10. WB validation of secreted Noggin from transfected cells (Noggin-conditioned medium). The secreted Noggin were collected from medium of transfected HEK293T cells. WB analysis shows strong expression of both Noggin isoforms.

The biological activity of the Noggin was further determined by removal of the Noggin from the normal human colon and murine intestinal organoid culture medium (Figure 3-11, A-C). Absence of Noggin significantly impeded the organoid growth in the majority of the organoids and led a formation of compact multilayer architecture lacking the typical budding and branching morphogenesis as a control. Removal of the Noggin induced the organoid disruption and subsequent lethal phenotype in both human and murine intestinal organoids in following days. Measuring the growth rate of organoids supported our findings on morphological alterations upon removal of Noggin. Viability assay also determined the marked reduction of proliferation activity in -Nog vs +Nog conditions (Figure 3-11; D).

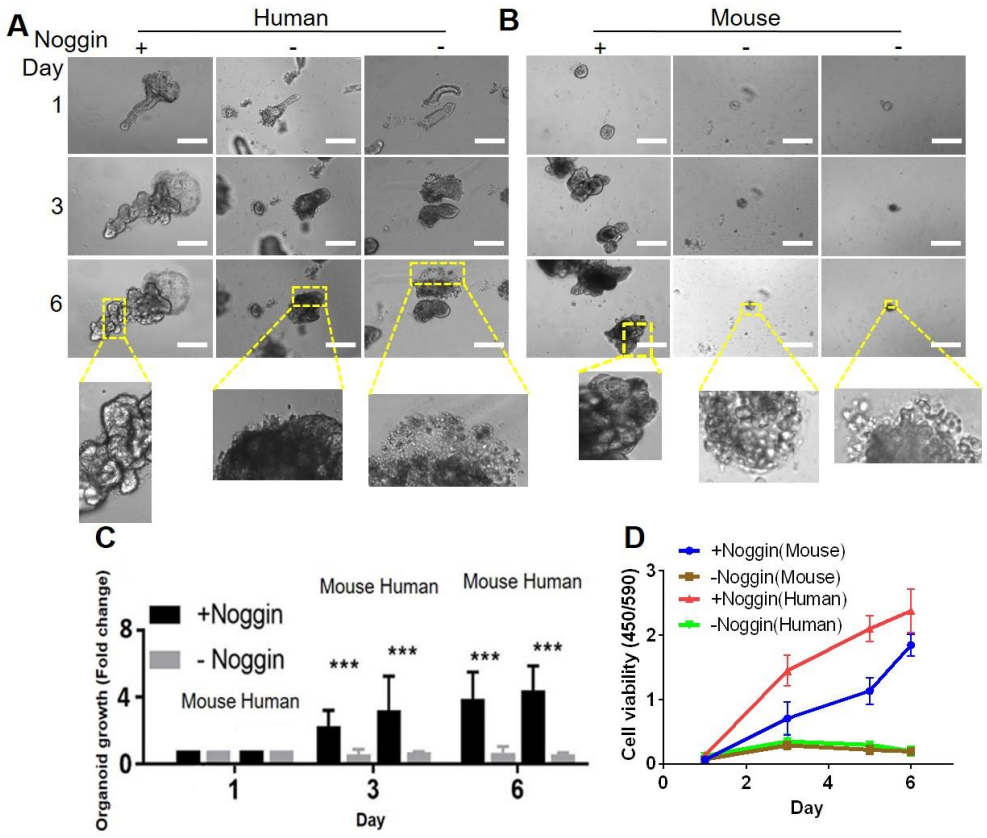


Figure 3-11. Noggin removal induced growth suppression and subsequent organoid destruction. A-C) Demonstrates the expansion and growth of the normal human colonic and murine derived intestinal organoid in the presence and absence of the Noggin supplement for 6 days. Lack of Noggin resulted in the development of cystic structure in the majority of the organoids and failure of cryptogenesis. This led the subsequent disruption of the organoids in day 6-7 (inset). Image-J software was applied to measure the circumference of each organoid (5-6 organoids). Subsequently the circumference growth of selected organoids was averaged and graphed. The expansion rates were calculated with the formula (Present Day Area / First Day Area) *100 as previously reported (343-345). D) The organoid viability assay confirmed the significant reduction of proliferation and the presence of viable cells in lack of Noggin condition as compared to the control group over 6 days. All values represent means ± SD. ***$p < 0.001$ denote significant differences between the groups. Scale bar, 75µm.

Considering the biological activity of Noggin in intestinal organoid *in-vitro* and the fatal trait after Noggin depletion, we further aimed to investigate the effect of Noggin on human colon cancer cell lines. Thereby, we treated human colon cells including the HCT-116, SW480, DLD-1 and HCT-116 with loss *FBXW7* E3 ligase gene ($FBXW7^{-/-}$) with functional Noggin conditioned protein (400ng/µl) for 48h.

3.2.8.1 Noggin did not affect cell architecture and morphology of cultured colon cancer cell lines

The exogenous administration of Noggin in SW480, DLD-1, HCT116, and HCT116 $FBXW7^{-/-}$ colon cells for 48h did not significantly influence the shape,

size and morphology of the cells determined in Phalloidin staining (Figure 3-12).

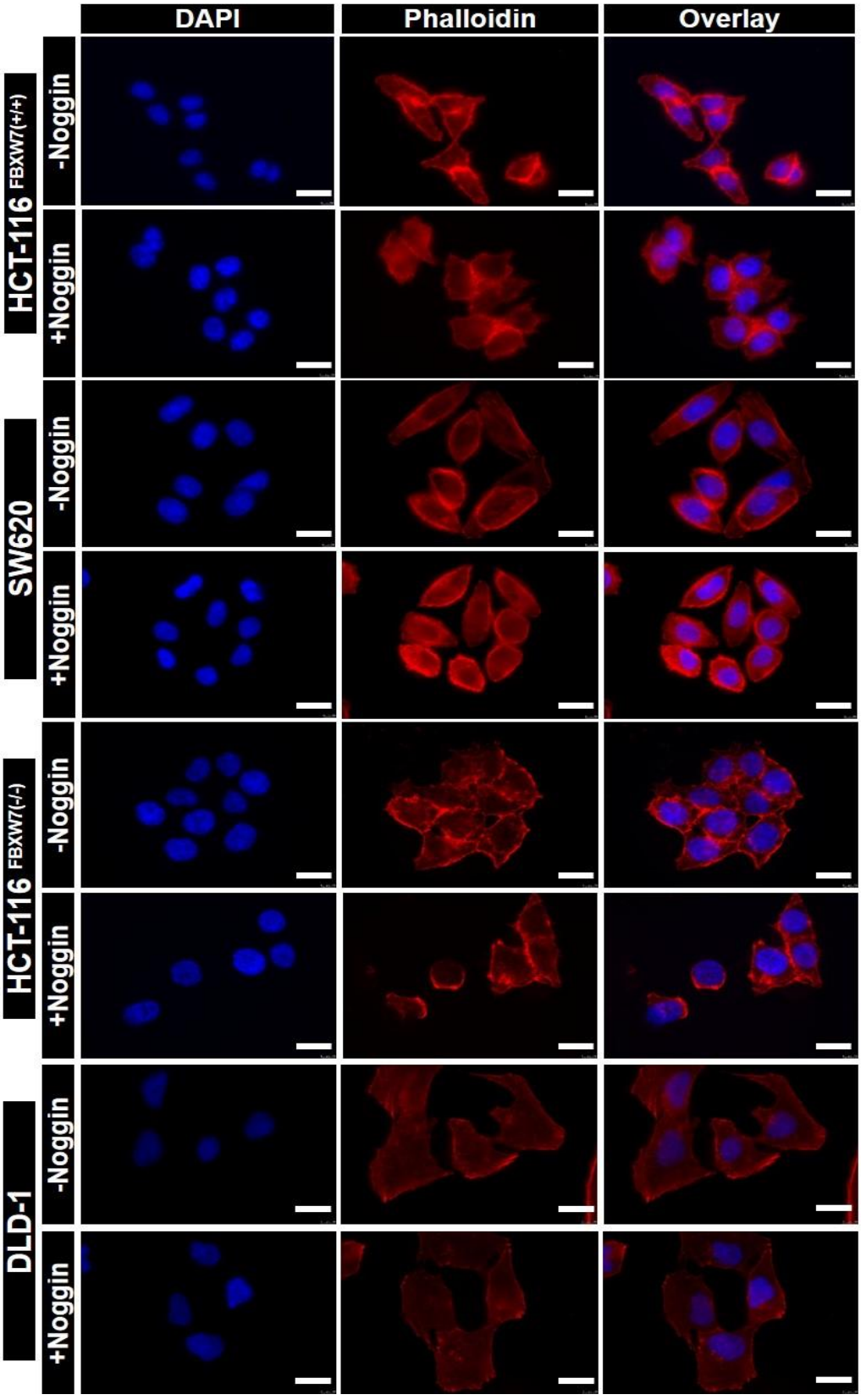


Figure 3-12. Administration of Noggin did not alter the phenotype of colon cancer cell lines. There were no detectable morphological differences in Phalloidin staining of HCT-116, SW480, DLD-1 and HCT-116 FBXW7$^{-/-}$ colon cells treated with Noggin in comparison to untreated controls after 48h. Scale bar, 7.5µm.

3.2.8.2 Noggin is not associated with proliferation or EMT activity of colon cancer cell lines

Western blot analysis revealed that Noggin treatment slightly reduced the level of BMP4 expression in HCT-116, HCT-116 $^{FBXW7\ (-/-)}$ and SW480 cells, indicating the negative regulation of BMP4 by inhibitory Noggin activity (Figure 3-13; top panel). To further investigate the potential interaction of Noggin in cancer proliferation and EMT, β-catenin and E-cadherin expression was assessed in treated and non-treated colon cancer cell lines (Figure 3-13; middle panels).

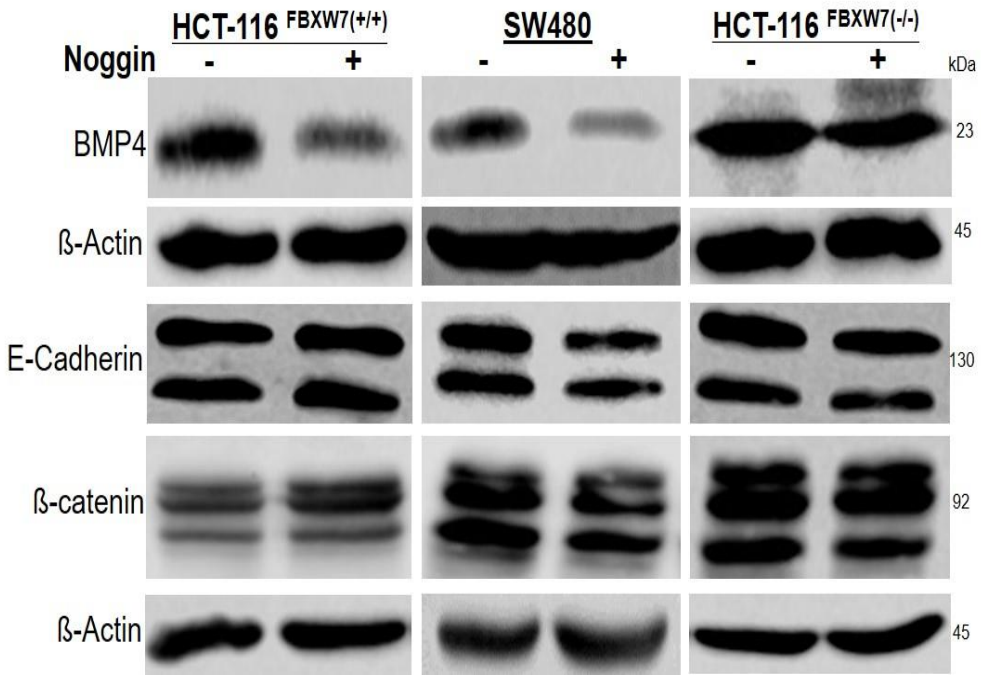


Figure 3-13. Noggin has no role in the modulation of EMT and proliferation in colon cancer cell lines. HCT-116, SW480, DLD-1 and HCT-116 $^{FBXW7-/-}$ cell lines exposed to an indicated dose of Noggin demonstrated a slight reduction in the expression of BMP4 implying that Noggin endogenously reduced the expression of BMP4. In addition, Noggin exposure did not influence the expression of E-cadherin and β-catenin in latter cells suggesting that the Noggin administration may not mediate colon cancer proliferation and EMT via BMP/Wnt/β-catenin pathways.

3.2.8.3 Noggin does not affect cellular localization and expression of E-Cadherin and β-catenin

Following immunofluorescence staining of E-cadherin and β-catenin revealed no significant differences in expression pattern and localization of cells in treated compared to untreated conditions (Figure 3-14).

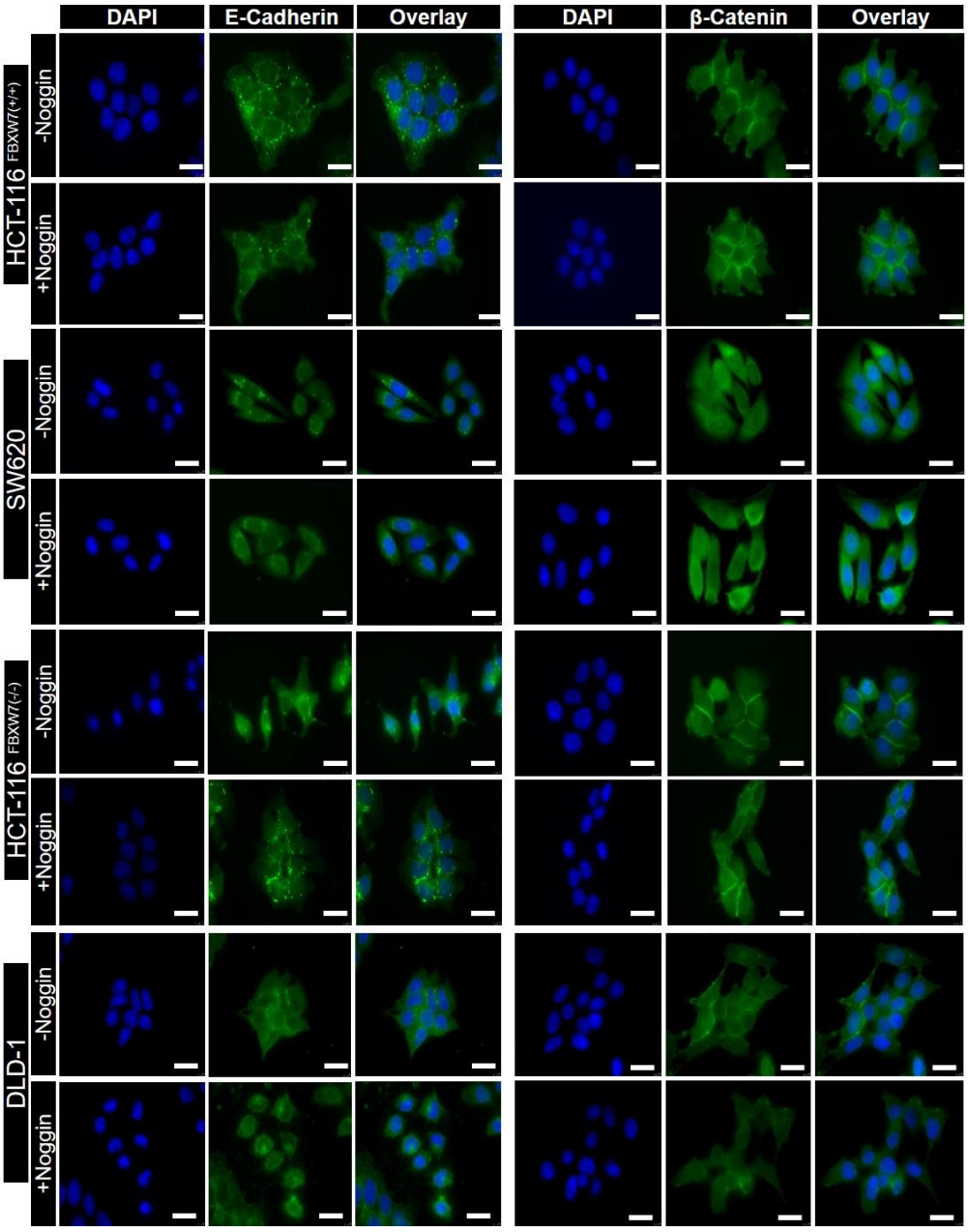


Figure 3-14. Noggin had no impact on E-cadherin and β-catenin expression and localisation in colon cancer cell lines. The IF staining did not reveal any change in E-cadherin and β-catenin expression pattern and their localization in different colon cancer cell lines. Scale bar, 7.5μm.

3.2.8.4 Noggin is not the modulator of cell growth and cell cycle distribution in colon cancer cell lines

To also investigate the effect of commercial Noggin in colon cancer cells, cancer cells were treated with 200ng/µl of commercial Noggin. Analysis of cell cycle by flow cytometry in HCT-116 cells showed that despite a slight decrease in the SubG1 fraction of the cells treated with Noggin, this had no significant impact on overall cell growth and cell-cycle progression (Figure 3-15). In addition, treatment of the SW480 and HCT-116 FBXW7$^{-/-}$ cells did not change the cell cycle distribution, cell growth and cell-cycle progression.

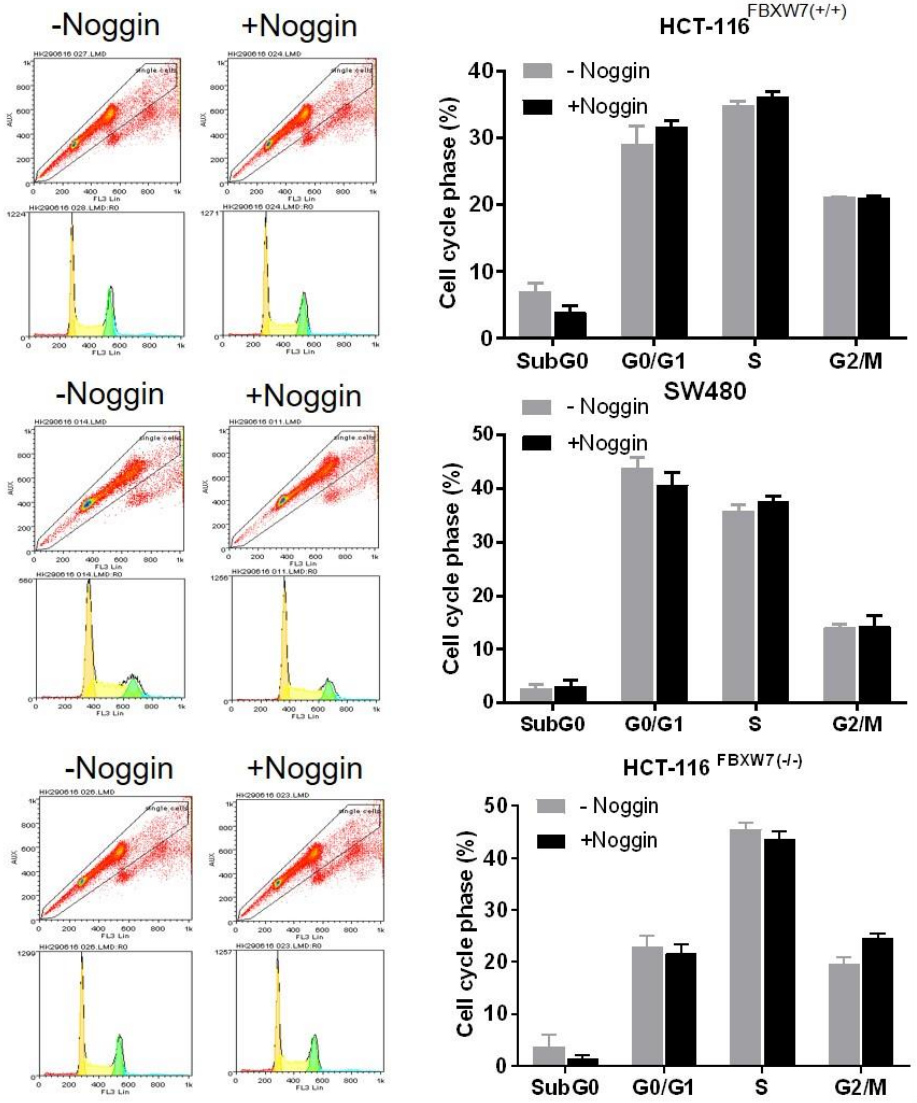
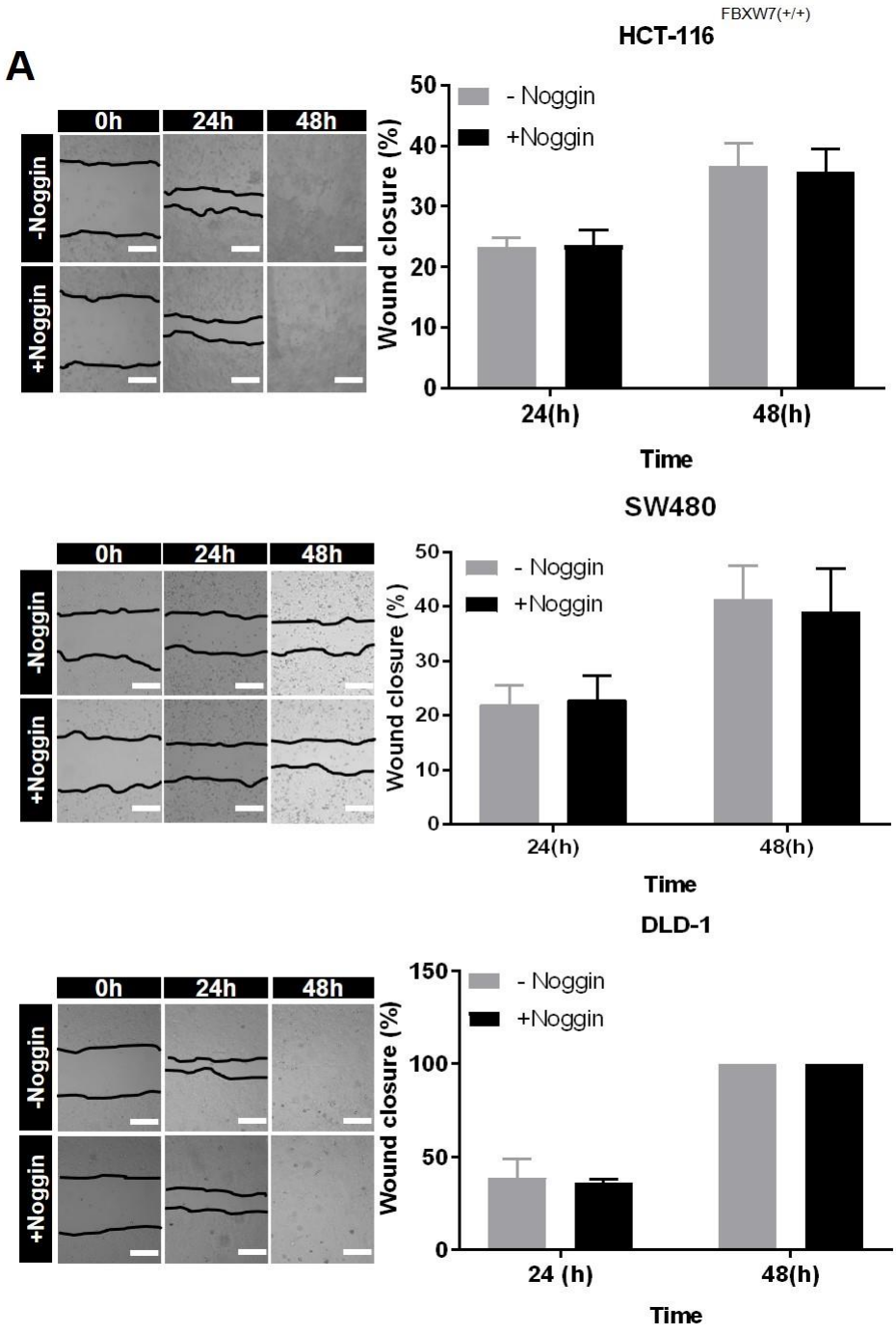


Figure 3-15. Noggin had no impact on cell cycle and proliferation of colon cancer cell lines. Despite a slight decrease in the number of cells in the SubG1 fraction of HCT-116 cells treated with commercial Noggin, this had no significant impact on cell growth or cell-cycle progression of the after 48hr. In addition, similar to HCT-116 cell lines, treatment with Noggin did not change the cell cycle and cell growth of SW480, HCT-116 and HCT-116 $^{FBXW7(-/-)}$ cells. All values represent means ± SD, N=3.

3.2.8.5 Noggin administration did not alter the wound-healing, and colonosphere efficiency of HCT-116 and SW480 cell lines

The effect of Noggin on cell migration and invasion is demonstrated in figure 3-16; A. Based on our findings, Noggin administration did not interfere the cell motility of HCT-116, SW480 and DLD-1 cells in 24 and 48 hours. In addition, HCT-116 and SW480 did not exhibit significant differences in the frequency of colonosphere formation in response to Noggin treatment (Figure 3-16; B). Thus, there was no correlation between colonosphere formation efficiency of the colon cancer cell lines and Noggin treatment.


A
FBXW7(+/+)
HCT-116
0h
24h
48h
-Noggin
+Noggin
Wound closure (%)
- Noggin
+Noggin
24(h)
48(h)
Time
SW480
DLD-1
24 (h)

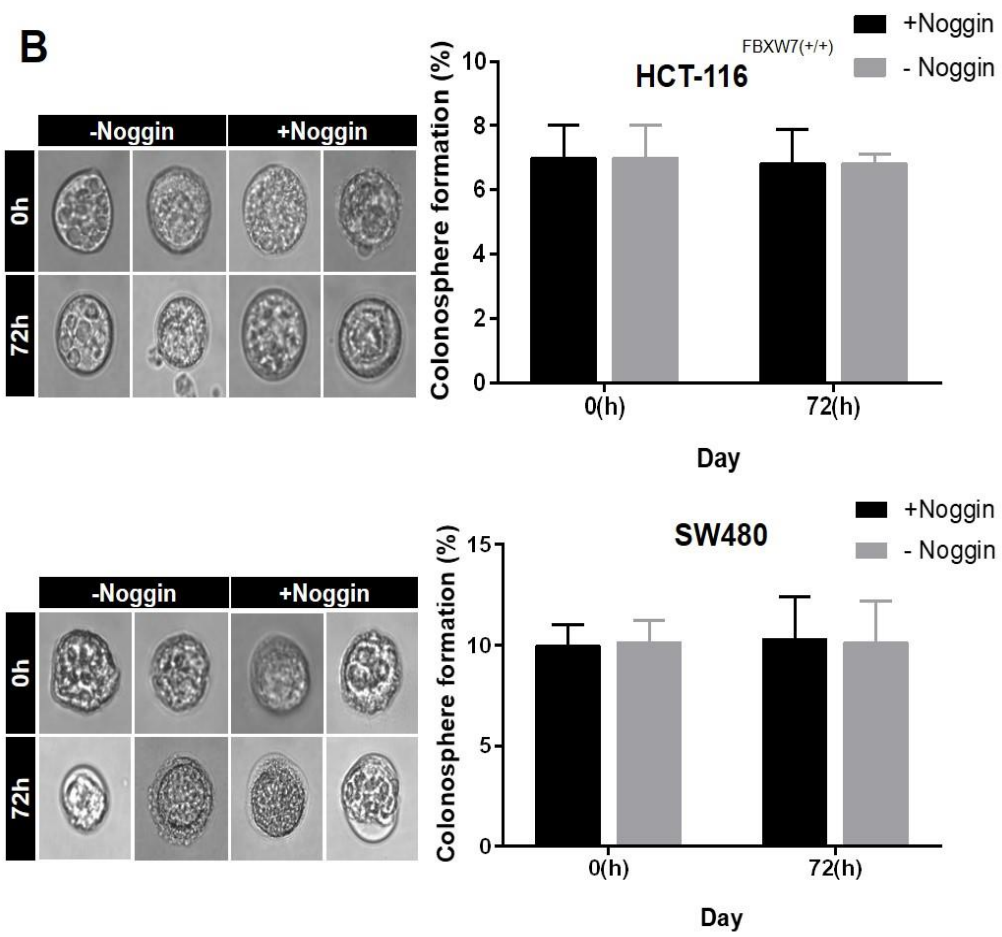


Figure 3-16. Noggin had no remarkable change on migration and also colonosphere efficiency of colon cancer cells. A) Noggin administration didnot alter the cell migration, motility and invasion of HCT-116, SW480 and DLD-1 cell lines after 48 hours. **B)** Noggin treatment did not change colonosphere formation efficiency of colorectal cancer stem-like cells after 72h. All values represent means ± SD. Scale bar, 75µm, N=3.

3.2.8.6 Noggin is crucial for the maintenance of stem cell niche in normal derived organoids but not tumour counterparts

To further validate our findings, we assessed the effect of Noggin in cystic and budding tumour organoids. Unlike the normal derived human/mouse intestinal organoids, the absence of Noggin did not trigger phenotypical changes or

organoid disruption in tumour derived organoids, highlighting the significant regulatory role of Noggin in the maintenance of the non-neoplasm condition (Figure 3-17; A-D). In this study we initially investigated the effect of Noggin with lower concentration 10% (v/v) and as there were no detectable biological effects on colon cancer cell lines the concentration subsequently increased to 20% (v/v). Our results indicate that the Noggin downstream signalling might be activated in CRC cells lines and colonic tumour derived organoids in which it makes them indispensable of the Noggin supplement.

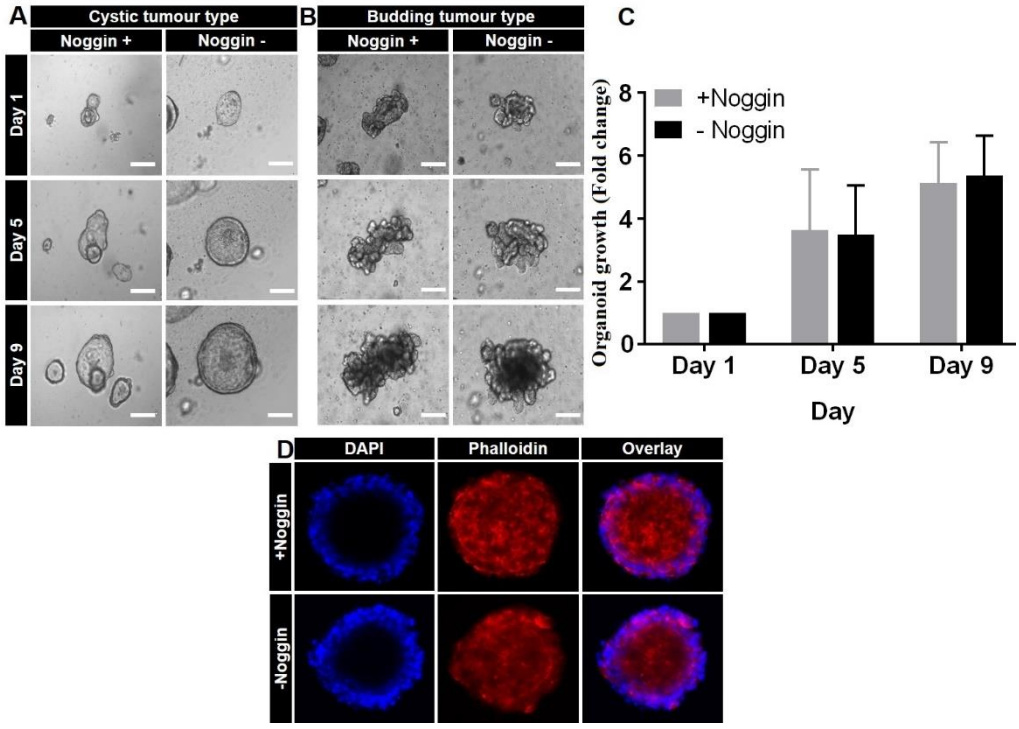


Figure 3-17. Tumour organoid grew indispensable of Noggin. A-C) The administration and removal of Noggin supplement from the tumour organoid culture did not change the growth pattern and phenotype features as their normal derived counterparts. **D)** Phalloidin staining of organoids did not show any significant differences in size and morphological pattern of treated and non-treated organoids. All values represent means ± SD. Scale bar, 75µm, N=3.

3.3 Discussion

The comparison of the morphology, structure organization, dynamic and growth pattern daily may provide fundamental information on PDOs differential phenotypical features, addressing their original molecular and genetic differences. CRC tumours demonstrate broad genetic and phenotypic heterogeneity in comparison to their matched normal tissue. To shed light into this diversity, an advanced *in-vitro* 3D model capable of self-renewal, self-organization and exhibit organ functionality is required. Such a model should allow the propagation of primary tumours and matched adjacent normal tissues *in-vitro* while reserving the whole genome, transcriptome, and proteome profile of the original materials. The recent advent of intestinal/colonic organoids appeared as reliable 3D culture models to recapitulate the cellular and molecular characteristics of the *in-vivo* tissue growth. This model maintains key features from their parental tumours and matched normal tissue. Herein, we demonstrated the phenotypical morphology changes and characteristics of several tumours and their matched normal organoids derived from CRC patients.

In the current study, the tumour organoids displayed divergent phenotypes in which the cystic tumour organoids with rapid growth rate was a dominant type (Figure 3-2). Although it should be noted that one of the weakness of this chapter is the lack of in depth genetic characterisation of tumour derived organoids therefore mutational status of tumour organoid lines are unknown. In comparison to normal derived organoids, the tumour organoids grew independent of niche signalling molecules and failed to develop multicellular

budding morphogenesis (Figure 3-9). These various phenotypical alterations in primary organoid culture were further confirmed with Phalloidin staining analyses (Figure 3-7). Long term maintenance of both tumour and matched normal organoid resulted in the formation of a gigantic structure in culture (Figure 3-5). Organoids also preserved the growth features of initial culture after excessive passaging and freezing-thawing process (Figure 3-6).

It is of note that the tumour-derived organoids did not follow a similar growth pattern in all patients, likely due to differences in patient age, genetic background, and medical history. Therefore, tumour-derived organoids derived from a single patient cannot be applied as a uniform tool across all; however, the improved methodology may greatly increase the practicality of this model. On the other hand, this also implies the significance of organoid in personalised-based approach.

In line with our observations, recent works have revealed the correlation of differential phenotypical manifestations of organoids and their engendered genomic profile reflecting their *in-vivo* origin tissue (346-349). This indicates the importance of the organoid morphological analysis in modelling diseases and cancer progression. In our study, we established a library of normal and matched tumour organoids from 17 patients with colorectal cancer. In this regard, Van de Wetering and colleagues generated an organoid biobank from 20 patients with colon cancer (77). The genomic analysis of tumour and matched normal derived organoids showed the main subtypes of primary CRC tumours. Furthermore, they designed an organoid drug screening platform for therapeutic compounds before going into a clinical trial on patients, highlighting their potential in

personalised medical treatments (77). Similarly, Fujii et al. also established a library of organoids from 55 human CRC tumours and 41 matched normal tissues (350). They confirmed that the growth of tumour organoids is not dependent on exogenous niche components in the prevailing culture, as the Wnt signalling pathway activated in the majority of CRC tumours. These findings are consistent with our current results that tumour organoids can grow indispensable of Wnt-3a and the Noggin (Figure 3-9).

They further confirmed that the organoids were histopathologically similar to the transplanted and origin tumours. Moreover, Cristobal et al. recent study on transcriptome and proteome of tumour and adjacent normal tissue of seven patients with colon cancer revealed that the organoids retained the original characteristics of CRC tumours they were originated (351). Via CRISPR/Cas9 mediated engineering of normal organoid epithelium Matano etal. generated an organoid mutated for the colon cancer driver genes comprising *APC, SMAD4* and *TP53, KRAS* and/or *PIK3CA*. The engineered normal organoids displayed compact and cystic morphology reflecting the phenotype of colonic tumour-derived organoids similar to our findings. Inconsistent with the previous approach, Drost and colleagues also revealed the similar phenotypical alterations in organoids mutated for *APC, KRAS, TP53* and *SMAD4* (340).

On a broader scope, organoids hold a new hope in the area of regenerative medicine, particularly for organ transplantation purposes, where they can be used as a source of autologous tissue, avoiding the potential subsequent immune response and organ rejection upon transplantation. However, entirely successful transplantation could be difficult due to the limitations in the current delivery

systems and the existing extracellular matrix (ECM) scaffolds such as Matrigel. Thus, more data are urgently needed on the reliability and validity of methods toward more reliable clinical or therapeutic practice. Such as the proper design of ECM and their compatibility with patients tissues (352), and the design of reliability studies in applying targeted delivery techniques like small molecules and expansion of organoids and graft survival (353). Together, these studies have provided proof of concept for the regenerative and therapeutic utility of gut organoids and their promising future as a functional transplantable choice in different gastrointestinal (GI) diseases and injuries. Furthermore, Noggin inhibitory activity is pivotal for the early stage of embryo patterning while the loss of Noggin has noted to be perinatally lethal in mice. Based on recent report evidence addressing the effect of Noggin dysregulation in varies malignancies (213, 214, 225, 354), we exposed different colon cancer cell lines with the indicated dose of secreted Noggin.

In the present study, we demonstrated that despite the crucial activity of BMP inhibitor Noggin in the maintenance of stem cell niche in normal human and murine derived intestinal organoids, Noggin did not influence colon cancer cells and colonic tumour organoids. We noted that the treatment of HCT-116 and SW480 cell lines did not significantly alter the expression of E-cadherin and β-catenin. This indicates that the Noggin may have no impact on colorectal cancer EMT or Wnt/β-catenin mediated tumorigenesis. Moreover, there were no differences in cell proliferation and cell cycle profile of colon cancer cell lines treated with Noggin (Figure 3-15). Our findings showed that Noggin did not affect the colonosphere formation activity of the HCT-116 and SW480 cancer

stem cells. Recent data, however, demonstrated that Noggin administration induced the apoptotic activity of CRC cells via the inhibition of BMP signalling under serum-free conditions (214). In another *in-vivo* study on colorectal cancer stem cells (CRC-SCs), Noggin-treated CRC-SCs for 12 and 30 days showed a faster growth rate as compared to control (355).

Noggin overexpression via retroviral transduction in prostate cancer cells (PC-3) restrained the tumour growth following transplantation. Noggin also antagonized BMP activity and decreased the proliferation of tumour cells *in-vivo* (226). Consistent with our study, Kang et al. did not detect any effect of Noggin orthotopic expression in lung cancer cells (212). Altogether, administration of a higher dosage of Noggin or increasing the incubation time might produce a different outcome on colon cancer cell lines.

Our findings demonstrate that despite the significant role of Noggin in the homeostasis of normal stem cells in colonic derived organoids, the administration of Noggin does not follow a similar pattern in colon cancer cells. Thus, there were no significant differences found in growth, cell migration, cell cycle distribution, morphology, colony formation efficacy as well as the epithelial-mesenchymal transition of the HCT-116, SW480, DLD-1 and HCT-116 FBXL7 -/- cell lines upon Noggin treatment.

CHAPTER 4

Antibiotic Rifabutin targets human CRC cells and patients derived tumour organoids via changes in expression level of selected Wnt-associate genes

4.1 Brief Introduction

Rifabutin is a member of the Rifamycins class of anti-mycobacterial (356). As DNA-dependent RNA synthesis inhibitors, Rifamycins block the transcription and protein synthesis in prokaryotes (356, 357). Due to the irreversible character of their binding, Rifamycins reveal a prolonged post-antibiotic effect (358). Rifabutin has previously used for the treatment of *Mycobacterium avium complex* (MAC) infections in immuno-suppressed patients with HIV (359). In general, Rifabutin demonstrates a broad range of activity against a majority of both gram-positive and gram-negative bacteria, including Mycobacterium tuberculosis and non-tuberculous mycobacteria (NTM) (356, 360). Following a single oral dose of 300 mg Rifabutin capsule, it was readily absorbed from the gastrointestinal tract with mean (±SD) peak plasma levels (Cmax) of 375 (±267) ng/mL (range: 141 to 1033 ng/mL) attained in 3.3 (±0.9) hours (Tmax range: 2 to 4 hours). We have recently identified Rifabutin from a NIH anti-inflammatory small molecule inhibitors as a potential anticancer agent on 3D colonosphere (252). Nevertheless, the direct effect of Rifabutin in tumorigenesis of the majority of cancers, including CRC, is still mainly elusive. Therefore, in the present work, we investigated the potent anticancer capacity of Rifabutin in tumour derived organoids and colonic cancer cell lines.

4.2 Results

4.2.1 Cytotoxicity assay of Rifabutin in HT29 and SW620 colon cancer cells

To investigate the effects of Rifabutin on colon cancer cells, cytotoxicity assay was carried out on HT29 and SW620 cell lines (Figure 4-1). The HT29 and SW620 cells were incubated with 6 different dosages of Rifabutin for 72 hours. After the indicated period, the IC50 was obtained via SRB assay as described earlier (Chapter 2, section 2.5.1) (361). The IC50 of 29.7µM and 28µM for HT29 and SW620 respectively were applied for the subsequent related experiments.

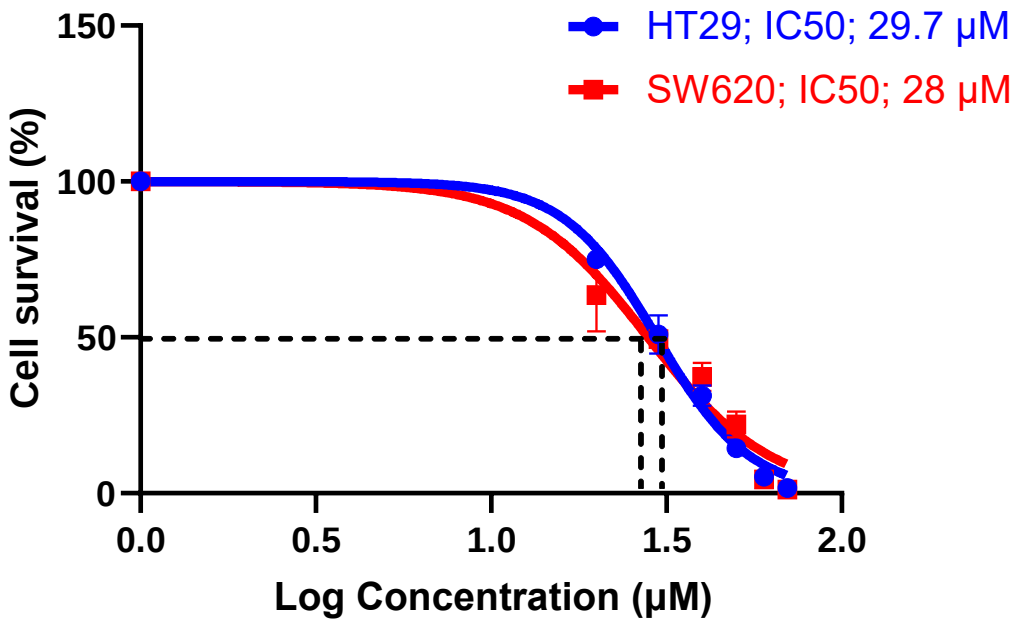


Figure 4-1. Determination of Rifabutin cytotoxicity assay in different colon cancer cell lines. Cell-mediated cytotoxicity of Rifabutin was carried out using SRB assay. The survival curves showing the slight difference in IC50 of HT29 and SW620 cells treated with Rifabutin. Error bars represent mean ± S.D. 0.05 > P > 0.001. Experiments were performed in triplicate for each cell line on at least three independent occasions.

4.2.1.1 Rifabutin suppressed the colon cancer cells growth

The representative bright-field image of HT-29 cells treated with Rifabutin (IC50: 29.7μM) is illustrated in Figure 4-2. In comparison to DMSO, Rifabutin hindered the growth of HT-29 cells and cells developed small clustered colonies in culture (Figure 4-2; insets). The SW620 and HT-29 cells were further assessed for the morphological changes after 48 hours with Rifabutin exposure (Figure 4-3). SW620 and HT-29 cells developed a more linear, stretched and elongated assembly of actin filaments with directional protrusions around the cells compared to control non-treated groups (Figure 4-3; yellow arrow-heads).

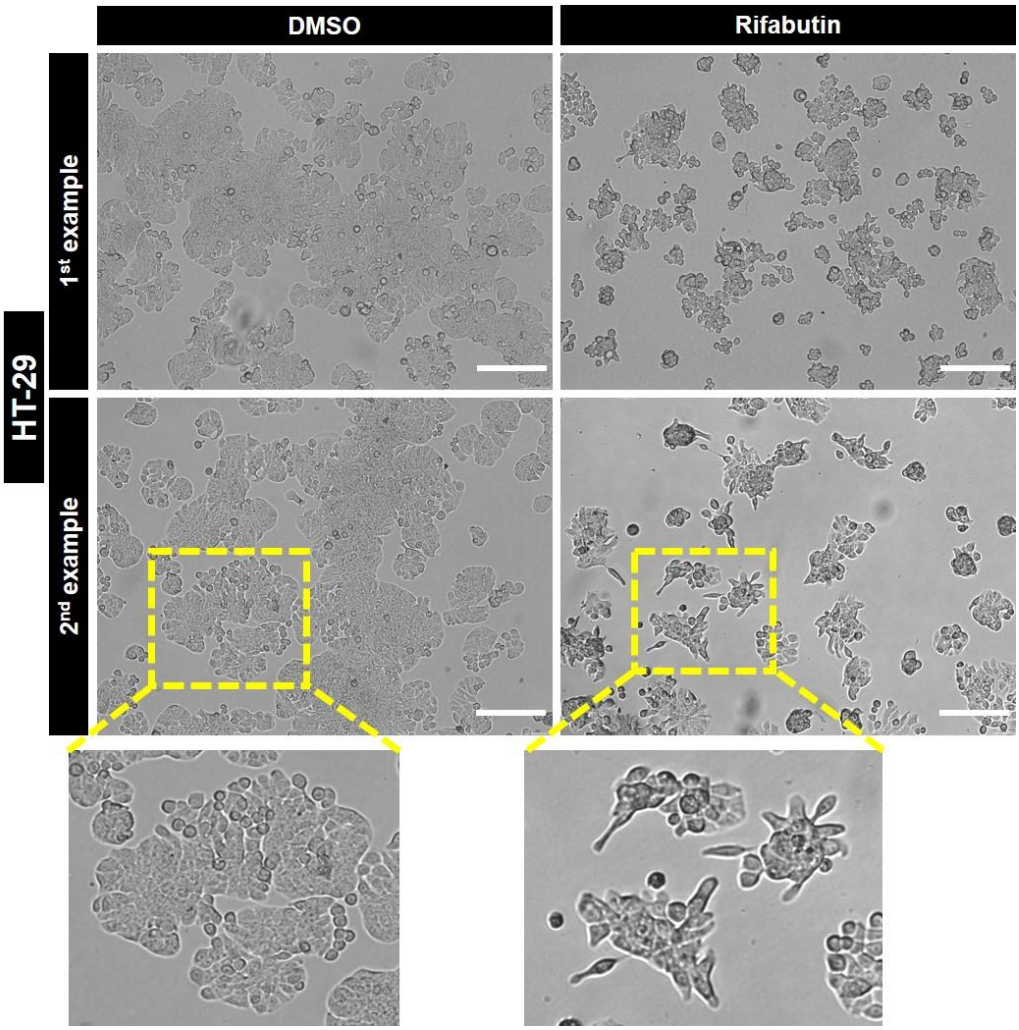


Figure 4-2. Rifabutin inhibited the cell-cell aggregation of HT-29 cells. Rifabutin drastically suppressed the growth of the HT-29 cells after 48 hours compared to the control group. Scale bar: 75µm.

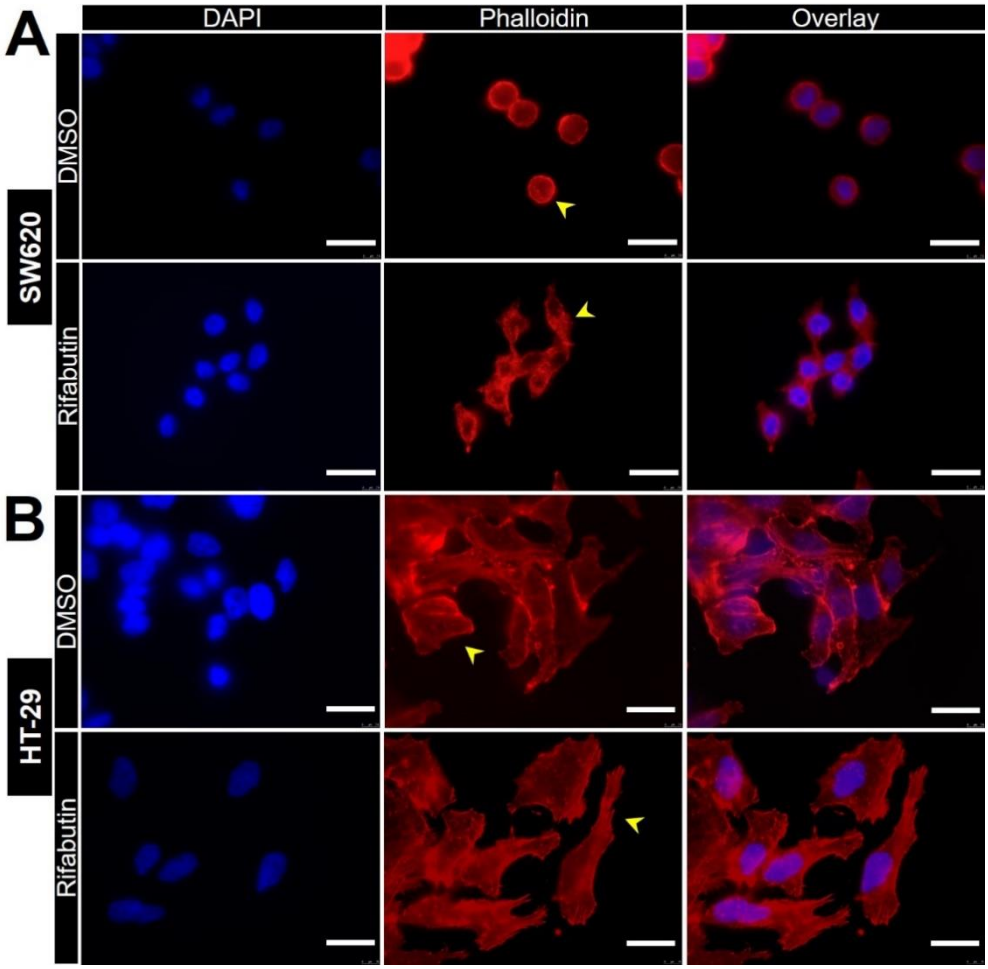


Figure 4-3. Rifabutin induced the cell elongation shape in treated HT-29 and SW620 cells. A-B) Rifabutin treated cells developed elongated spindle-shaped phenotype in both colon cancer cells compared to control untreated group. Scale bar: 7.5µm.

4.2.1.2 Rifabutin suppressed the motility and invasiveness of the SW620 and HT-29 cells

Wound healing assay was performed to determine the cell motility changes of the SW620 and HT-29 cells as two invasive colorectal cancer cell lines upon treatment with Rifabutin. The images were captured immediately after the

wounding, in the presence and absent of Rifabutin 24h and 48h hours after treatment. The parental SW620 and HT-29 cells moved remarkably faster than the treated counterparts indicating the inhibitory activity of Rifabutin in both colon cancer cell lines (Figure 4-4; A&B).

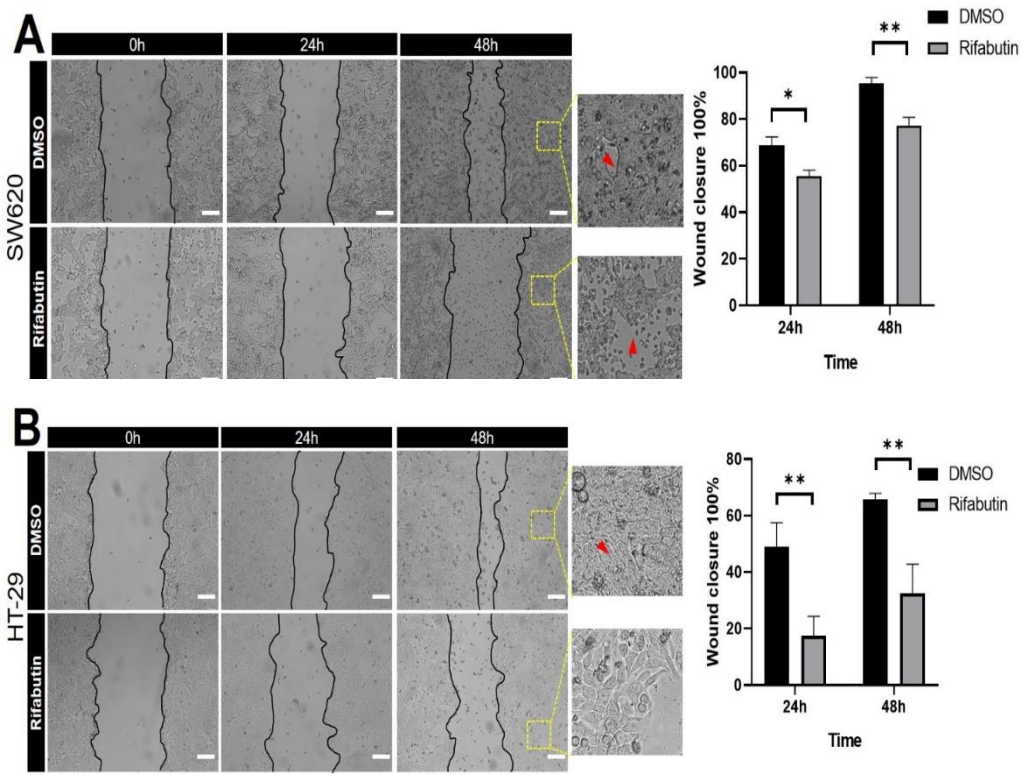


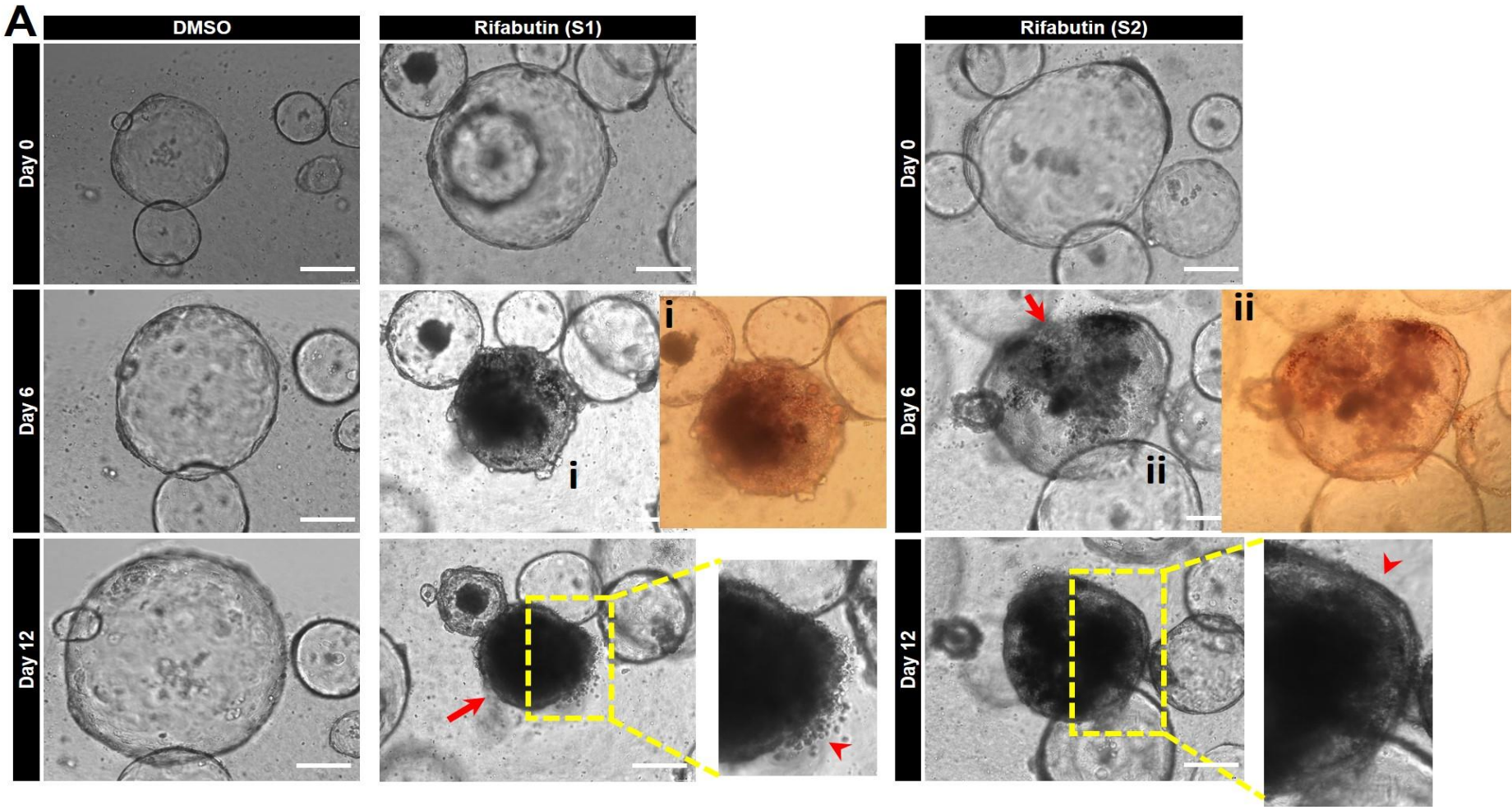
Figure 4-4. Rifabutin mediates the suppression of colon cancer cell migration in wound healing assay. A-B) representative images of wound healing assay in SW620 and HT-29 cells treated with Rifabutin indicated the significant reduction of cell migration compared to the control group. Data presented as mean ± standard deviation. Each experiment in both cell lines performed in triplicate. Error bars represent mean ± S.D. *, P ≤ 0.05; **, P ≤ 0.01. Scale bar: 75μm.

4.2.2 Rifabutin inhibited proliferation and induced the growth arrest in cystic tumour organoid

To further step toward more relevant preclinical system using a three-dimensional tissue-like model of CRC and to highlight the Rifabutin potential

activity in personalised medical treatments, we assessed the drug response on two main types of tumour-derived organoids including cystic and budding tumour organoids (Chapter 3.2.6). Initially, we evaluated the effect of Rifabutin on cystic tumour organoid using the established IC50; 28μM obtained from SW620 colon cancer cells. Organoids were passaged and grew in culture for 4-5 days before initial treatment in both conditions (DMSO and drug). Organoids were treated with drug every 48 hours and the morphological differences were imaged in a daily basis. 2 weeks treatment period was selected based on the majority of treated organoids started to display cell death after the total period of 3 weeks. The tumour organoids were further assessed for several key parameters including integrity, morphology, proliferation, growth and survival.

Rifabutin notably impeded the proliferation of cystic tumour organoid and induced the apoptotic activity (Figure 4-5; A insets and red arrowheads). Under Rifabutin administration, the majority of the organoids displayed growth arrest followed by organoid destruction in subsequent days. Of note, the variety in the magnitude of the apoptosis-mediated phenotype in organoids might be due to the drug penetration, composition of organoid in Matrigel and mutation status of individual organoids. Thus, some organoids were more sensitive to the drug while others showed resistant feature (Figure 4-5; B). Eventually, Rifabutin hindered the growth and all organoids died in culture within 3 weeks.


A
DMSO
Rifabutin (S1)
Rifabutin (S2)
Day 0
Day 6
Day 12
i
ii

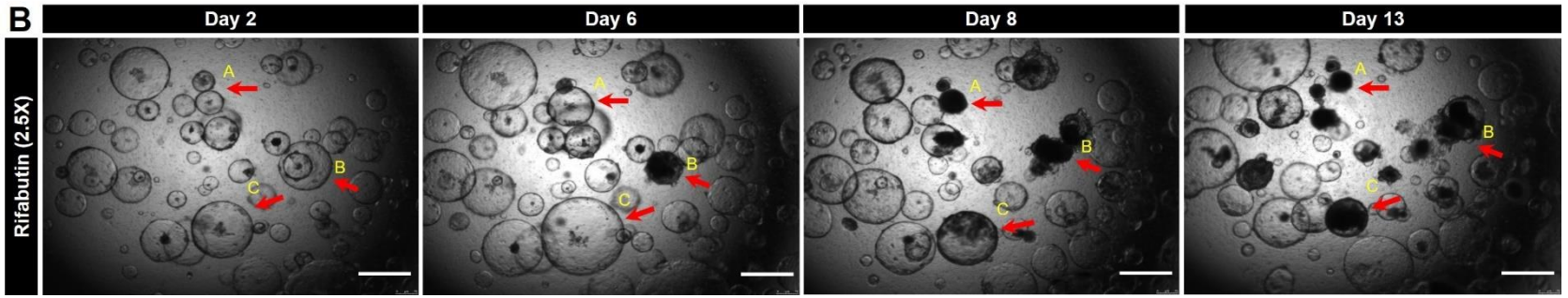


Figure 4-5. Rifabutin suppressed the growth of cystic tumour organoids in culture. A) Cystic tumour organoids underwent Rifabutin treatment for 12 days. Administration of Rifabutin inhibited the proliferation, growth rate and promoted the apoptosis activity of tumour organoids (S1; Sample 1; and S2 is a representative of sample 2). *i* and *ii* are representative colour-full images of corresponding organoids. Scale bar:75µm **B)** To facilitate tracking of Rifabutin effect on cystic tumour organoid, A, B & C as representative individual organoids (display with red arrow-heads) were selected over 13 days. Scale bar: 250µm.

The growth rate analysis of Rifabutin treated organoids also revealed a significant reduction in size in comparison to the control group (DMSO) over 12 days (Figure 4-6; A). Considering the 3D enteroid structures with crypt-like projections, the volume of organoids was measured by taking 3–4 separate diameters for each organoid. Half of the average of this diameter was considered as the radius (r), organoid volume was measured using the following formula: $V = 4/3\pi r3$ as previously reported (138).

WST-1 proliferation assay also determined the viability of tumour-derived organoid exposed to Rifabutin (Figure 4-6; B). The proliferation activity of tumour organoids was assessed at day 0, 2, 6, 8 and 12 of organoid culture. The significant reduction of proliferation and cell viability was evident in tumours treated with Rifabutin compared to non-treated condition (DMSO). Our findings indicate that the Rifabutin, suppressed organoid proliferation and viability while inducing the cell apoptosis.

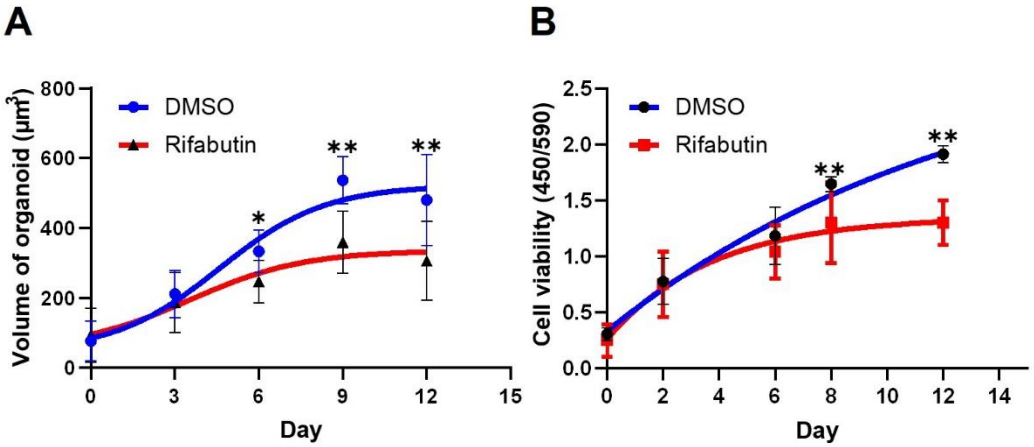


Figure 4-6. Rifabutin treatment inhibited growth rate and viability of the organoids in culture. A-B) Rifabutin significantly suppressed the growth and cell proliferation of cystic tumour organoid in the indicated period which eventually followed by apoptosis and organoid death. Error bars represent mean ± S.D. *, P ≤ 0.05,**, P ≤ 0.01, N=3.

4.2.2.1 Anticancer effects of Rifabutin in budding tumour organoids

To further investigate the effects of Rifabutin administration on another main type of tumour organoid with the distinct morphological trait (budding morphology), budding tumour organoid was exposed to Rifabutin (28μM) as previously described in 4.2.2. The Rifabutin-induced growth inhibition-activity of budding tumour organoids is illustrated in Figure 4-7.

In comparison to cystic tumour organoid, however, the budding tumour organoids displayed a significantly higher sensitivity to Rifabutin. On day one post-treatment with Rifabutin, the outer layer of organoids absorbed the drug which sensitized the disassociation of the organoids to single cells within the next 5-6 days (red arrowheads and corresponding colourful image). In addition, in comparison to cystic type, the budding tumour organoids showed a more homogeneous response to Rifabutin and the majority of organoids (>95%) underwent simultaneous apoptosis within six days. This is partly due to the heterogeneity of the colonic tumour organoids derived from a different patient or organoids harbouring differential mutational background as previously indicated in chapter 3.2.6.

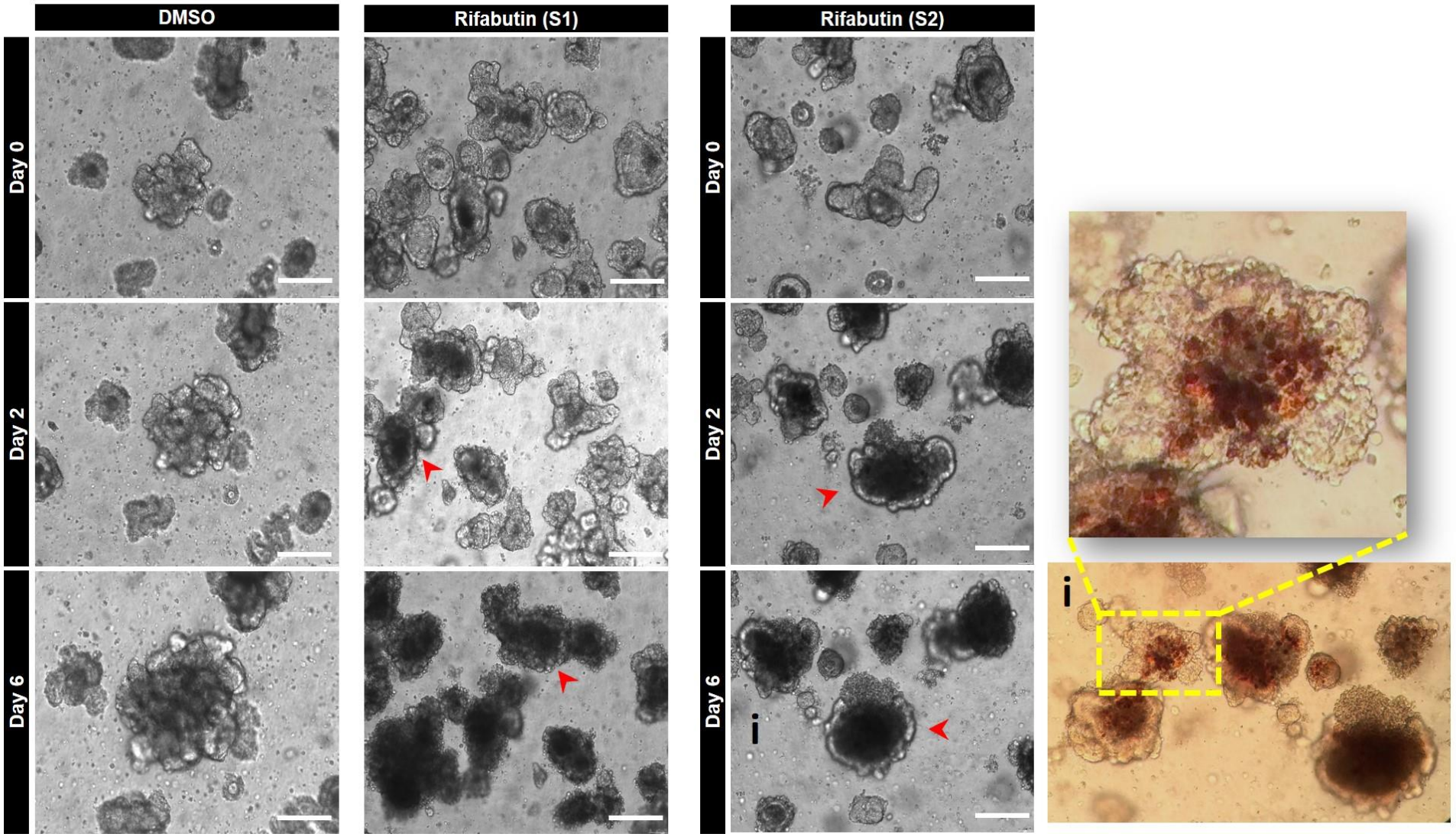

DMSO
Rifabutin (S1)
Rifabutin (S2)
Day 0
Day 2
Day 6
i
i

Figure 4-7. Rifabutin blocked the growth of budding tumour organoid. Rifabutin treatment associated with profound perturbation of the budding tumour organoid in culture. Budding tumour organoid treated with Rifabutin were more susceptible to the drug treatment characterised with immediate apoptotic respond compared to cystic tumour organoids (S1; Sample 1; and S2 is a representative image of sample 2). *i* is a representative colour-full images of corresponding organoids treated with Rifabutin. Scale bar: 75µm.

The growth inhibition rate of organoids significantly correlated with Rifabutin treatment in budding tumour organoid (Figure 4-8; A). The tumour growth-suppressing role of Rifabutin is further supported by WST-1 proliferation assay. In comparison to the non-treated control condition, the Rifabutin administration markedly reduced organoid growth and cell proliferation over eight days (Figure 4-8; B). Our findings indicate that the Rifabutin suppressed the proliferation, growth rate and induces the organoid death via apoptosis in both colon tumour-derived organoids.

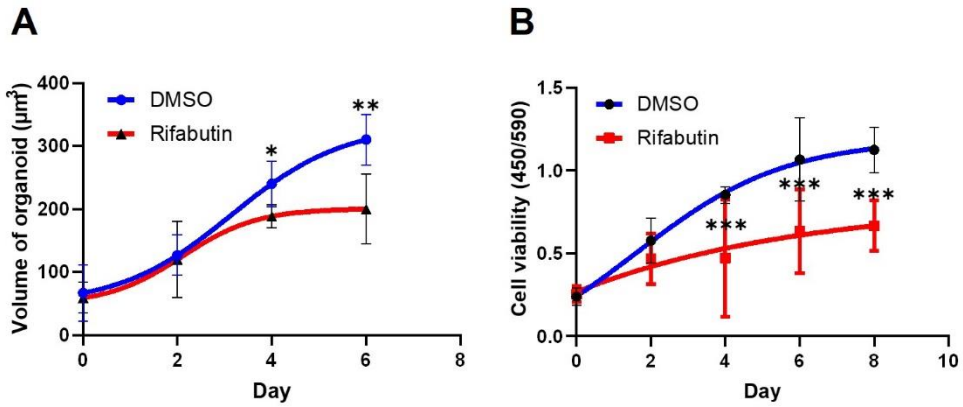


Figure 4-8. Significant inhibition of growth and proliferation was evident in tumour organoid treated with Rifabutin. A-B) Rifabutin-mediated growth inhibition and viability was apparent over 8 days in budding tumour organoid. Similar to cystic tumour organoid, Rifabutin disrupted the growth rate of budding tumour organoid in culture. Error bars represent mean ± S.D. *, P ≤ 0.01, **, P ≤ 0.01, ***, P ≤ 0.001, N=3.

4.2.3 Rifabutin impeded Wnt/β-catenin signalling mediated cancer cell growth

Following the striking inhibitory growth effects of Rifabutin on both colonic tumour organoids (cystic and budding tumour organoids) and colon cancer cell lines, we further aimed to shed light into the mechanism of action of Rifabutin. The TOP/FOP Flash luciferase reporter assay was performed in SW620 colon cancer cells to investigate the potential contribution of Rifabutin in Wnt/β-catenin signalling perturbation as previously described (Chapter 2; 2.4.1). Post transfection of the SW620 cells with TOP/FOP Flash and Renilla luciferase reporters, the cells were exposed to Rifabutin for 48 hours. The Firefly and Renilla luciferase activity were measured 48-hour post-treatment using the Dual-Luciferase Reporter assay (Promega, E1910). Rifabutin significantly inhibits TCF-mediated expression of luciferase in SW620 (Figure 4-9), by 13 folds indicating its inhibitory activity in Wnt/β-catenin signalling.

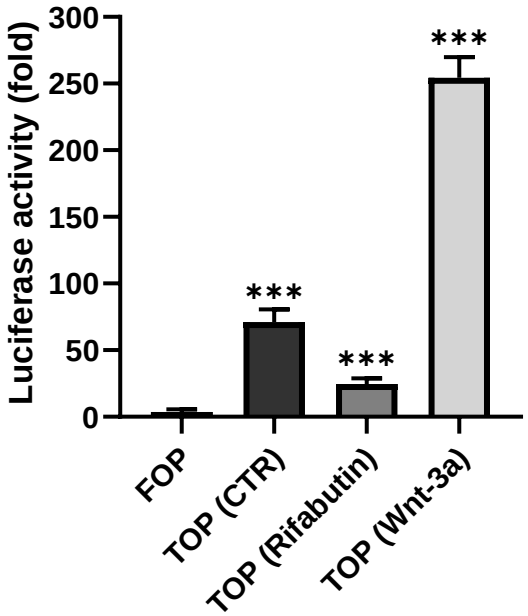


Figure 4-9. TCF-luciferase expression was inhibited by Rifabutin treatment. The stable SW620 cells expressing TOP-Flash and Renilla luciferase were treated with Rifabutin and the luciferase activity was assessed 48h post-treatment. Rifabutin decreased transcriptional activity of TCF-luciferase representing Wnt/β-catenin signalling targets. Measurements of Top/Fop luciferase assay revealed that the luciferase activity significantly reduced following Rifabutin treatment compared to the control group. Error bars represent mean ± S.D. ***, P ≤ 0.001, N=3.

Further investigation for p-β-catenin, β-catenin and E-cadherin expression on SW620 cells revealed no significant changes in expression of p- β-catenin or total β-catenin level upon Rifabutin administration (Figure 4-10). In addition, there was no difference in the expression of E-Cadherin after Rifabutin exposure.

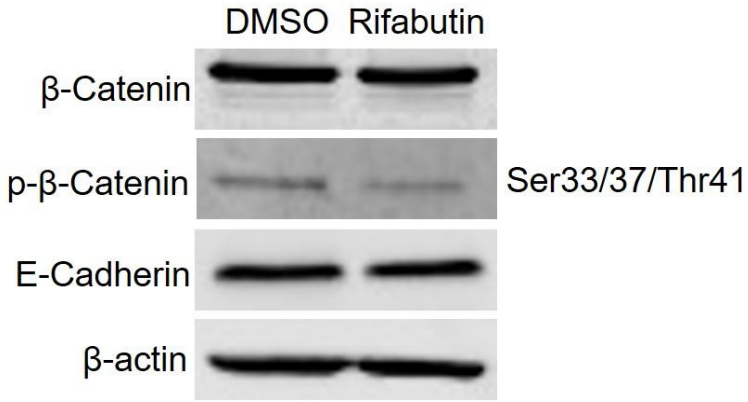


Figure 4-10. Rifabutin did not impact the level of p-β-catenin and β-catenin expression in SW620 cells.

4.2.4 Rifabutin influenced the expression of various Wnt signalling genes associated with cancer hallmarks in treated cystic tumour organoids

To identify the expression of specific genes associated with Rifabutin inhibitory mechanism on CRC, the transcriptome analysis of cystic tumour organoids was performed. Thus, the same passaged tumour organoids were cultured for 4 days

prior to initial treatment with Rifabutin and DMSO. The organoids further underwent 5 courses of treatment (every 48 hours) before RNA extraction. On day 15th of organoid culture, the RNA was extracted from treated and the control untreated (DMSO) and RT^2 Profiler qPCR array were deployed to examine the expression of 84 genes involved in Wnt signalling pathway (*Appendix 1*). Expression array analysis was carried out with commercially available RT^2 Profiler PCR Arrays for the Human Wnt Signalling pathway to investigate a panel of Wnt specific related genes in cystic tumour organoid per manufacturer's instructions. We further detected a discrete difference between Rifabutin and DMSO treated control groups, implying distinct transcriptome signatures for these two populations (Figure 4-11; A-B). Wnt signalling array analysis has revealed dysregulations of multiple genes in Rifabutin treated group (Figure 4-12).

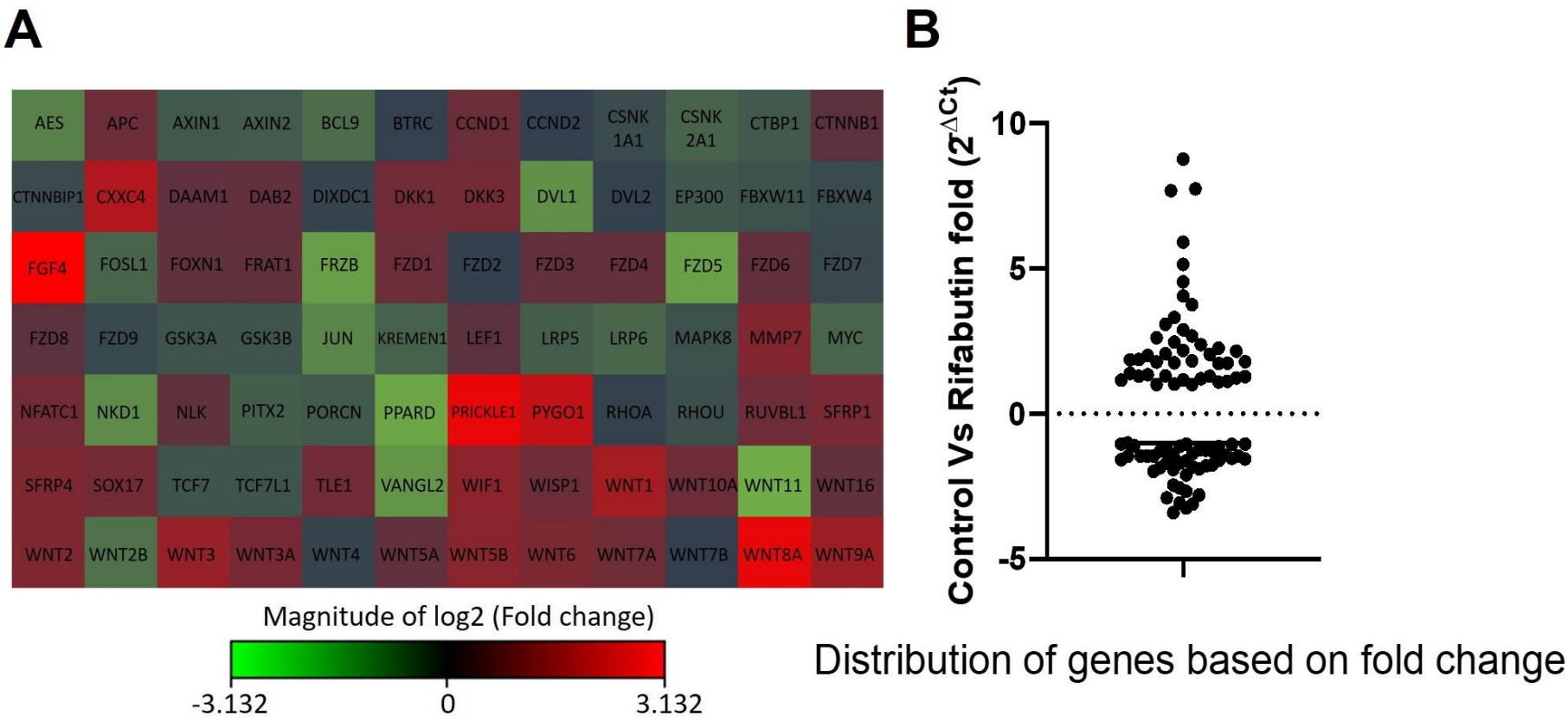

A
AES APC AXIN1 AXIN2 BCL9 BTRC CCND1 CCND2 CSNK 1A1 CSNK 2A1 CTBP1 CTNNB1
CTNNBIP1 CXXC4 DAAM1 DAB2 DIXDC1 DKK1 DKK3 DVL1 DVL2 EP300 FBXW11 FBXW4
FGF4 FOSL1 FOXN1 FRAT1 FRZB FZD1 FZD2 FZD3 FZD4 FZD5 FZD6 FZD7
FZD8 FZD9 GSK3A GSK3B JUN KREMEN1 LEF1 LRP5 LRP6 MAPK8 MMP7 MYC
NFATC1 NKD1 NLK PITX2 PORCN PPARD PRICKLE1 PYGO1 RHOA RHOU RUVBL1 SFRP1
SFRP4 SOX17 TCF7 TCF7L1 TLE1 VANGL2 WIF1 WISP1 WNT1 WNT10A WNT11 WNT16
WNT2 WNT2B WNT3 WNT3A WNT4 WNT5A WNT5B WNT6 WNT7A WNT7B WNT8A WNT9A
Magnitude of log2 (Fold change)
-3.132
0
3.132
B
Control Vs Rifabutin fold ($2^{-\Delta Ct}$)
10
5
0
-5
Distribution of genes based on fold change

Figure 4-11. Heat-map representation of 84 differentially expressed genes in cystic tumour organoid upon Rifabutin administration. A) Array correlation heat map to demonstrate differential genes. Each well represents a single gene. Colour code within the graph represents: red, up-regulated; and green, down-regulated. **B)** The distribution of the Wnt associated genes according to the fold changes.

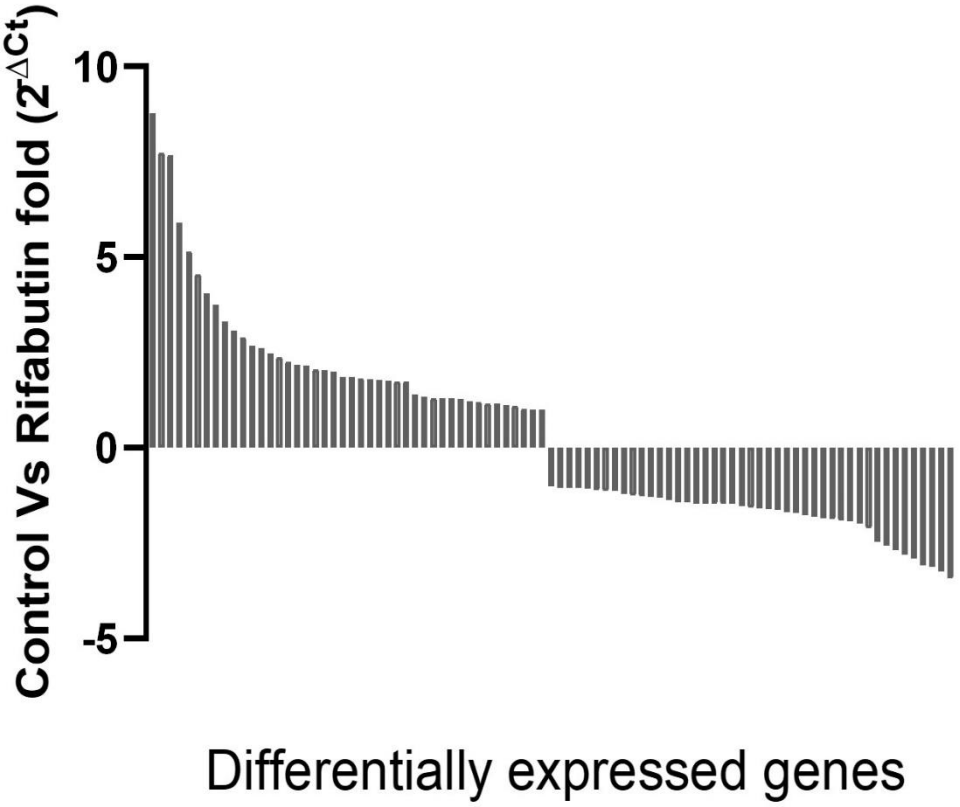


Figure 4-12. Differential expression of Wnt signalling genes on cystic tumour organoids. Each bar represents one gene with relative fold change, down-regulation or up-regulation following the Rifabutin treatments.

Among 84 genes, 29 candidates were further identified with significant differential expression (2-fold expression change and p-value < 0.001) compared to control groups. The panel of 29 genes was including 20 up-regulated and 9 down-regulated genes. Subsequently, the top 8 candidates including CXXC finger protein 4 (*CXXC4*)(362), SRY-box transcription factor 17 (SOX17)(363), fibroblast growth factor 4 (*FGF4*)(364), prickle planar cell polarity protein 1

(PRICKLE1)(365), Wnt inhibitory factor-1 (*WIF1*)(366), secreted frizzled related protein 4 (*SFRP4*)(367), Dishevelled (*DVL-1*)(368), frizzled class receptor 5 (*FZD5*)(369) were selected using literature-based approaches and their relevance to cancer trait for further validation and analysis. Figure 4-13 shows the interaction of these candidate genes with other Wnt signalling pathway genes and mediators.

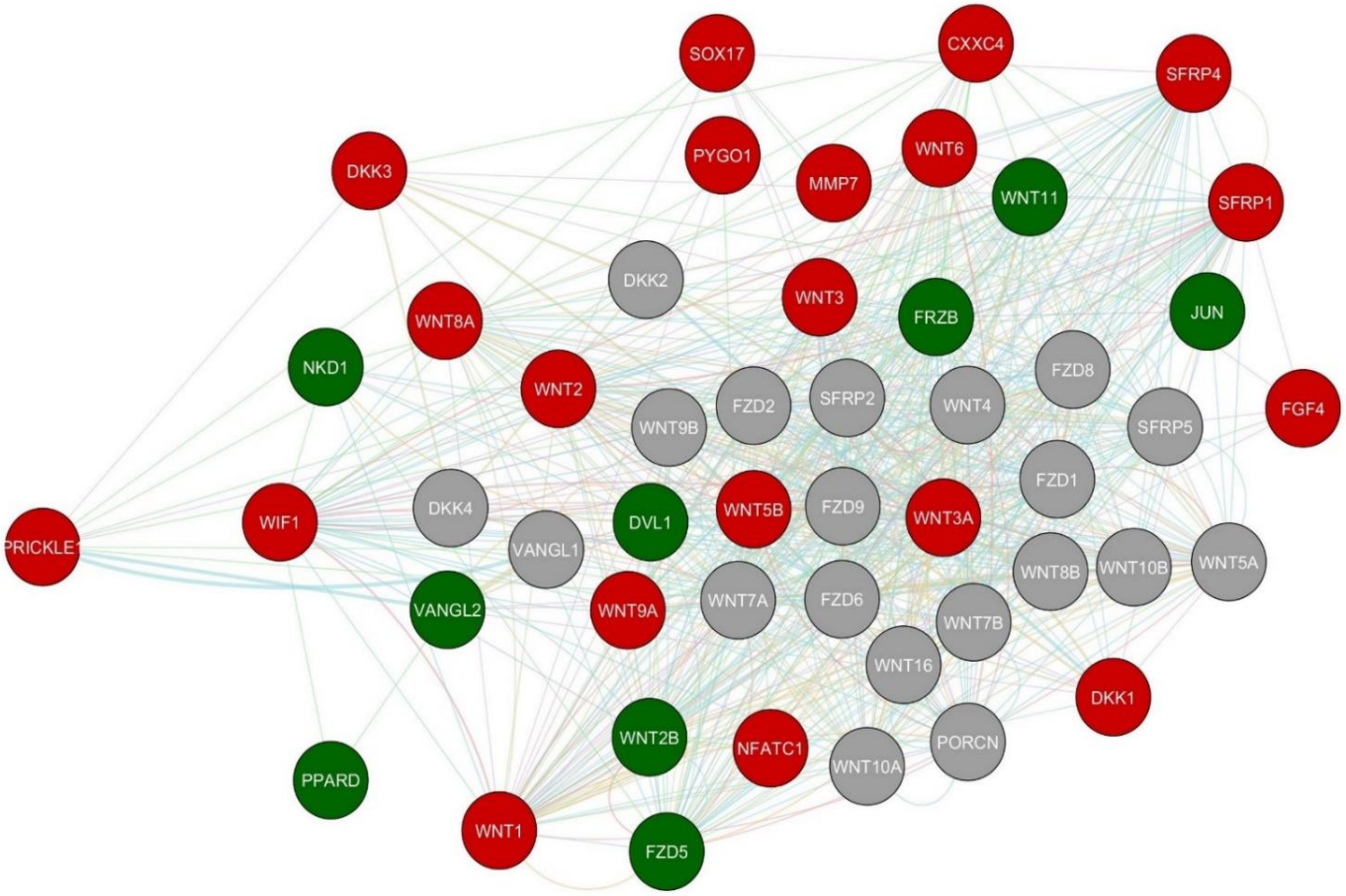

SOX17
CXXC4
SFRP4
PYGO1
WNT6
DKK3
MMP7
WNT11
SFRP1
DKK2
WNT3
JUN
WNT8A
FRZB
NKD1
FZD8
WNT2
FZD2
SFRP2
WNT4
FGF4
WNT9B
SFRP5
FZD1
WIF1
DKK4
DVL1
WNT5B
FZD9
WNT3A
PRICKLE
VANGL1
WNT8B
WNT10B
WNT5A
VANGL2
WNT9A
WNT7A
FZD6
WNT7B
WNT16
DKK1
WNT2B
NFATC1
PORCN
PPARD
WNT10A
WNT1
FZD5

Figure 4-13. Gene array revealed potential pathways for Rifabutin's effects in CRC. Genemania was applied to generate pathway analysis. Genes that are presented in green circles represents 2 or higher fold down-regulation whereas red nodes represent genes with 2 or more-fold up-regulation upon Rifabutin treatment of cystic tumour organoids.

4.2.4.1 Validation of candidate genes in cystic and budding tumour organoids

To further refine the list and to validate the dysregulated genes from the array in cystic tumour-derived organoids, we applied qRT-PCR to evaluate the expression level of top candidate genes from up-regulated and down-regulated panels. In accordance with the preliminary data from the RT^2 Wnt signalling array, the expression of *DVL1* and *FZD5* showed remarkable downregulation while the expression of *CXXC4, SOX17, FGF4, PRICKLE1, WIF1* up-regulated significantly in cystic tumour organoids (Figure 4-14).

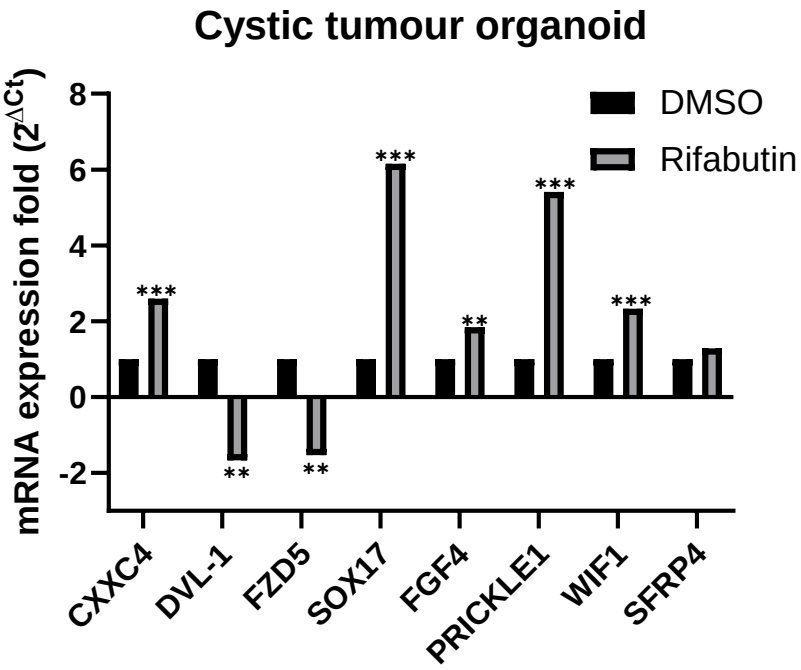


Figure 4-14. Differential expression of Wnt signalling genes upon Rifabutin treatment in colonic cystic tumour organoid. Consistent with data from the array, we obtained similar findings on qRT-PCR validation of the candidate genes including up-regulation of *CXXC4*, *SOX17*, *FGF4*, *PRICKLE1*, *WIF1* and following down-regulation of *DVL-1* and *FZD5*. Error bars represent mean ± S.D. **, P ≤ 0.01; ***, P ≤ 0.001, N=3.

Furthermore, the qRT-PCR validation of candidate dysregulated genes from the array was also carried out in budding tumour organoids (Figure 4-15). Inconsistent with the primary data on the array and following validation on cystic tumour organoids, a similar pattern of mRNA expression was obtained in budding tumour organoids upon Rifabutin treatment except for FGF4.

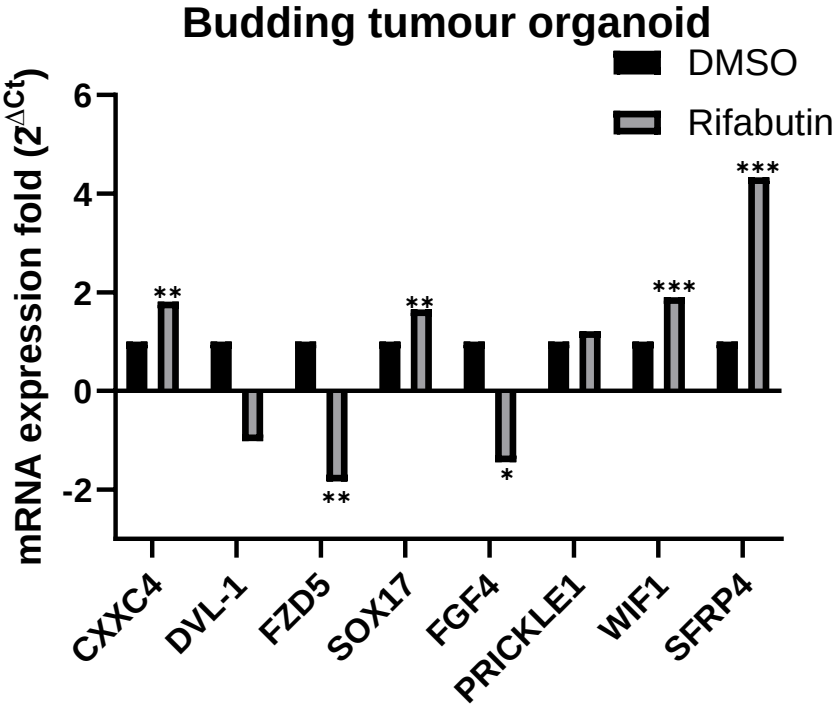


Figure 4-15. qRT-PCR validation of Wnt signalling dysregulated genes in budding tumour organoid. Based on our findings, except FGF4, the dysregulated candidates displayed a similar expression pattern as the cystic tumour organoid. This indicates the potential regulatory mechanism of the Rifabutin via Wnt signalling pathway in colonic tumour organoids. Error bars represent mean ± S.D. *, P ≤ 0.05; **, P ≤ 0.01; ***, P ≤ 0.001, N=3.

4.2.4.2 Validation and evaluation of candidate genes in colon cancer cells using real-time quantitative PCR

To further investigate the effect of Rifabutin in modulation of Wnt signalling and its target genes in colon cancer cell lines, different colon cancers including SW480 (27μM), SW620 (28μM), HT-29 (29.7μM), HCT-116 (27μM), LS174T (26μM) and DLD-1(26μM) were treated with Rifabutin.

From the panel of 8 validated candidate genes in cystic and budding tumour organoid, *CXXC4* and *FZD5* were selected based on their recent contribution in tumourigenesis. *CD44* and also *LGR5* genes as established putative Wnt target genes and potential markers for colorectal cancer stem cells were also included in the assays. Inconsistent with our findings on cystic and budding tumour types, the CXXC4 mRNA levels markedly increased in SW480 and SW620 cell lines, while, the remarkable reduction was determined in LS-174T, HT-29 and HCT-116 cells. Further quantification of endogenous mRNA expression fold change in the untreated and treated condition is demonstrated in Figure 4-16; A. The endogenous expression of *CXXC4* was up-regulated in budding tumour organoids, SW480, LS-174T, HCT-116, and down-regulated in SW620, HT-29 and DLD-1 (Figure 4-16; B-C). Further quantification of CXXC4 mRNA expression in primary colon tumours and matched normal samples are also presented in Figure 4-16; D.

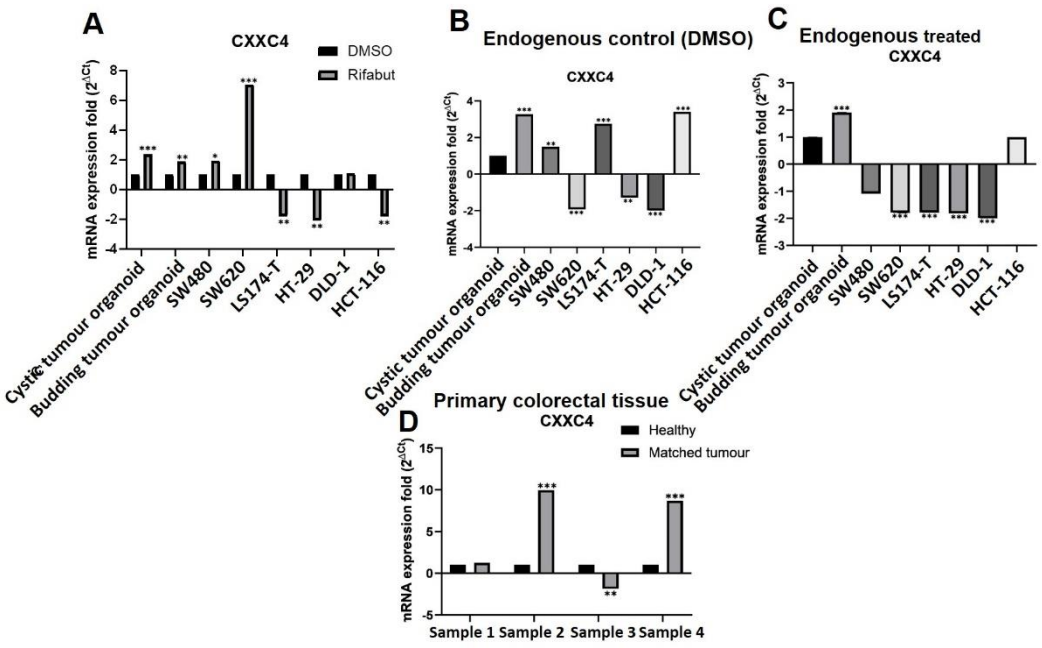


Figure 4-16. CXXC4 expression profile in colonic tumour organoids and cancer cells. CXXC4 qRT-PCR expression revealed heterogeneity across tumour organoids and different colon cancer cell lines. Error bars represent mean ± S.D. *, P ≤ 0.05; **, P ≤ 0.01; ***, P ≤ 0.001, N=3.

Furtheremore, upon Rifabutin administration, the expression of *CD44* remarkably decreased in both colonic tumour organoids and across all colon cancer cells except DLD-1 (Figure 4-17; A). Previous studies have shown that CD44 down-regulation suppressed cell proliferation, migration, invasion and increased apoptosis activity of colon cancer cells in lymphocytes (370, 371). Investigation for CD44 endogenous expression revealed that all cell lines and also budding tumour organoids displayed a strong reduction in mRNA expression compared to cystic tumour organoids (Figure 4-17; B-C). The expression of CD44 in treated cell lines showed significant up-regulation in LS-

174T, DLD-1 and HCT-116, whereas, the budding tumour organoid, SW480, SW620 and HT-29 demonstrated significant down-regulation.

The mRNA expression fold of CD44 in 4 primary tumour and matched normal samples are also presented in Figure 4-17; D. In agreement to previous works the expression level of CD44 remarkably enhanced in tumour tissues compared to normal adjacent samples (372).

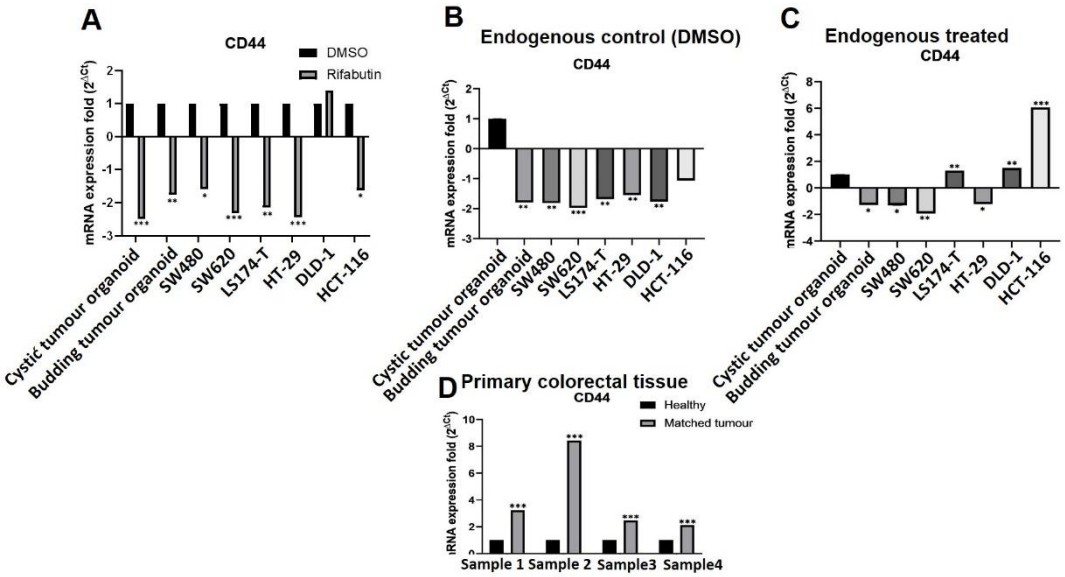


Figure 4-17. CD44 was markedly down-regulated in colonic tumour organoids and colon cancer cell lines. In comparison to the untreated control, the CD44 expression level remarkably down-regulated in all colonic cancer cells and colonic tumour organoids except DLD-1 colon cancer cells. Error bars represent mean ± S.D. *, P ≤ 0.05; **, P ≤ 0.01; ***, P ≤ 0.001, N=3.

Previous works also indicated the interaction of the *FZD5* with various diseases and malignancies (373-379). In ovarian cancer, the *FZD5* increased adhesion of collagen IV, fibronectin and vitronectin as extracellular matrix components (373). qRT-PCR measurements of *FZD5* as Wnt receptor showed heterogeneous pattern across tumour-derived organoids and colon cancer cells with significantly decrease in cystic and budding tumour organoids and HCT-116 to enhanced up-regulation in SW480 and LS174T cells (Figure 4-18; A). Further evaluation of the endogenous expression of *FZD5* is displayed in Figure 4-18; B-C. Based on our result, the endogenous expression of *FZD5* for non-treated group, showed up-regulation in budding tumour organoid, HT-29, DLD-1 and HCT-116, while there were significant down-regulation in SW480 and a slight decrease in SW620. Furtheremore, the *FZD5* endogenous expression in treated condition revealed the strong increase in all colon cancer cells and tumour-derived organoids.

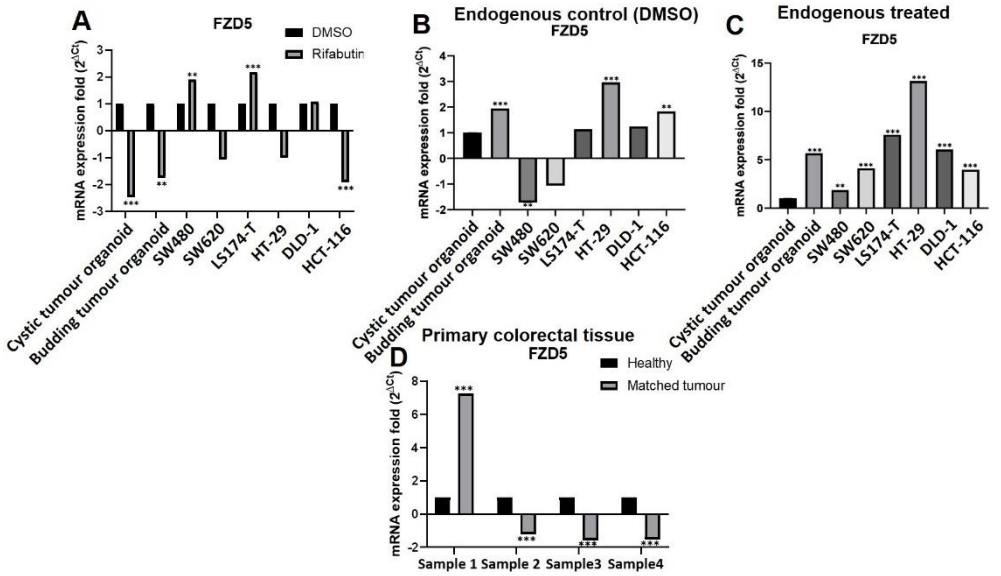


Figure 4-18. Heterogenous expression profile of FZD5 in tumour organoids and colon cancer cells. qRT-PCR analysis of FZD5 demonstrated a significant reduction in cystic, budding tumour organoids and HCT-116 and elevated expression in SW480 and LS174T cells. Moreover, the FZD5 endogenous expression in treated cell lines showed significantly enhanced expression in all colon cancer cells and tumour organoids. Error bars represent mean ± S.D. *, P ≤ 0.05; **, P ≤ 0.01; ***, P ≤ 0.001, N=3.

The *LGR5* is highly expressed in colon cancer tissue and over-expression of *LGR5* correlates with initiation, progression and also poor survival of colon cancer (380). lack of *LGR5* inhibited the growth of cultured CRC cells and induced the fraction of apoptotic cells (381). In the present study, the expression level of *LGR5* was significantly enhanced in cystic tumour organoid, SW480, SW620, whereas, the remarkable reduction was detected in budding tumour organoid, LS-174T, HT-29 and DLD-1 cells in comparison to the control group (Figure 4-19; A).

Moreover, measuring the endogenous expression of *LGR5* in the treated group showed the strong up-regulation in budding tumour organoid, while, there has been a significant reduction in LGR5 expression in all cell lines except LS-174T (Figure 4-19; B-C). Strikingly, we found that the mRNA expression pattern of the *LGR5* and *CXXC4* across the organoids and colon cancer cells followed a similar pattern except in two cases (budding tumour organoids and DLD-1 cancer cells). Moreover, the expression of the *CXXC4* and *LGR5* in SW620 cells were strongly up-regulated in comparison to their controls (7&16 fold change respectively).

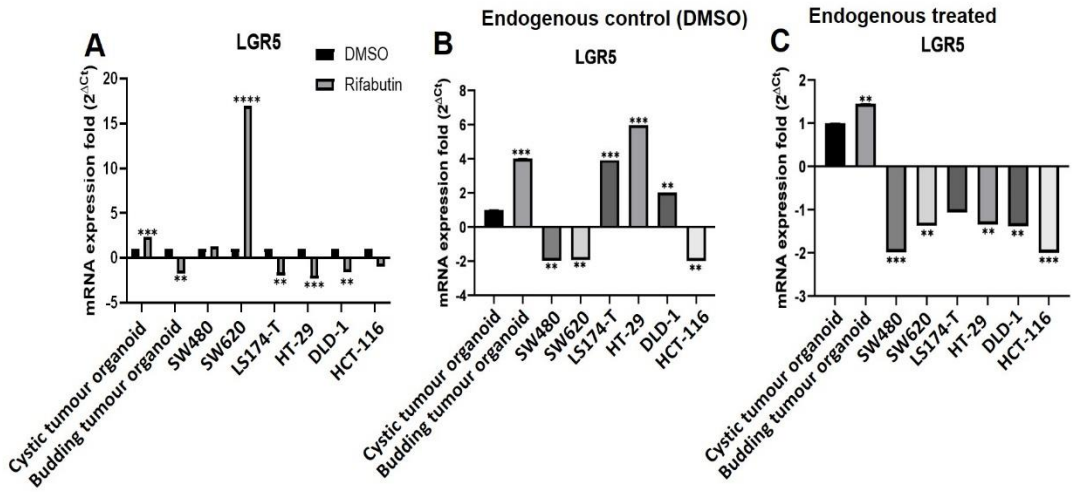


Figure 4-19. LGR5 demonstrated differential expression pattern in tumour organoids and colon cancer cells. The LGR5 expression was up-regulated in cystic tumour organoids, SW480, SW620 while significantly down-regulated in budding tumour organoid, LS-174T, HT-29 and DLD-1 cells after Rifabutin treatment. The LGR5 endogenous expression, based on cystic tumour organoids as control, revealed the significant increase in budding tumour organoid, LS-174T, HT-29 and DLD-1 cells. Error bars represent mean ± S.D. *, P ≤ 0.05; **, P ≤ 0.01; ***, P ≤ 0.001, N=3.

The expression pattern of candidate genes in tumour organoids and 6 colon cancer cell lines is outlined in Figure 4-20. As previously denoted, after Rifabutin exposure, both colonic tumour organoids displayed similar mRNA expression pattern for the candidate genes. In addition, among all colon cancer cells, SW480 and SW620 showed the maximum similarity with the colonic tumour organoids.

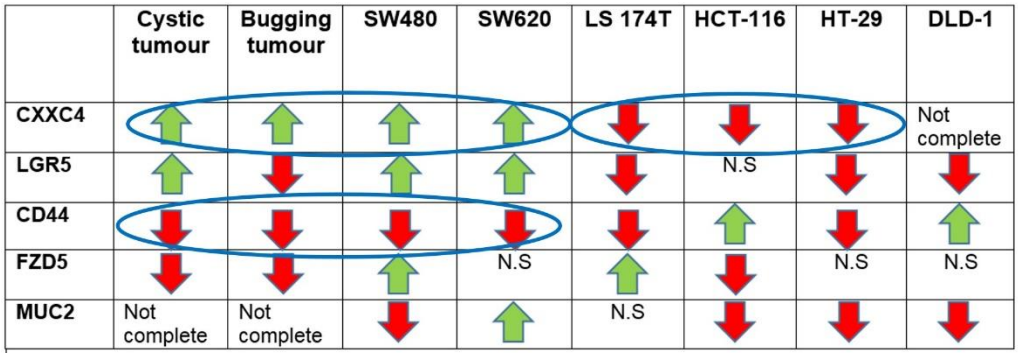


Figure 4-20. Schematic outline of the expression pattern of candidate genes in colon cancer cells and tumour organoids treated with Rifabutin. After Rifabutin treatment, the CXXC4 significantly up-regulated in both tumour derived organoids, SW480 and SW620. Further analysis showed that the CD44 significantly down-regulated in the majority of the colon cancer cells and also both colonic tumour organoids.

Altogether, apart from their main differences of being two versus three-dimensional models, this heterogeneous expression pattern of candidate genes in colon cancer cells vs colon tumour organoids after Rifabutin administration might be due to their differential genetic signature as outlined in chapter 2 (Table 2-1).

4.2.5 Combination treatment with Rifabutin and GSK-3 inhibitor sensitizes a rapid apoptosis activity in colonic tumour organoids

Glycogen synthase kinase-3 (GSK-3) is a member of the protein kinase family. This enzyme modulates the transfer of a phosphate group from adenosine triphosphate (ATP) to serine or threonine residues of its substrates thus it can initiate, elevates, or suppress the activity of a target substrate in a various biological system (382-384). GSK-3 overexpression has been reported in several malignancies (385). GSK-3 functions as tumour suppressors or tumour promoter

in different cancers. It may acts as tumour suppressors by phosphorylation of growth factor-stimulated kinases such as Akt,(386, 387). Moreover, GSK-3 negatively regulates many proto-oncogenic proteins through the Wnt/β–catenin and Hedgehog signalling (388, 389). As their fundamental activity in different signalling pathways involved in disease modelling, development and hallmarks of cancer, the kinase inhibitors have emerged as an attractive target for therapeutic purposes (384). Therefore, to evaluate the potent synergic effect of Rifabutin treatment with GSK-3 inhibitor, 6-bromoindirubin-30-oxime (BIO) in colon cancer cells and PDOs, we have initially treated the SW620 colon cancers with BIO and in combination with Rifabutin.

4.2.5.1 Rifabutin significantly inhibited the growth of SW620 in a synergistic manner with BIO

GSK3 inhibition with BIO reduces the level of GSK3β and induces β-catenin in SW620 cells (Figure 4-21). To further evaluate the effect of single-agent treatment with BIO or Rifabutin and in concomitant treatment comprising administration of both agents in colon cancer cell lines, the SW620 cells were incubated with BIO, Rifabutin or combination treatment of both for 48h (Figure 4-22).

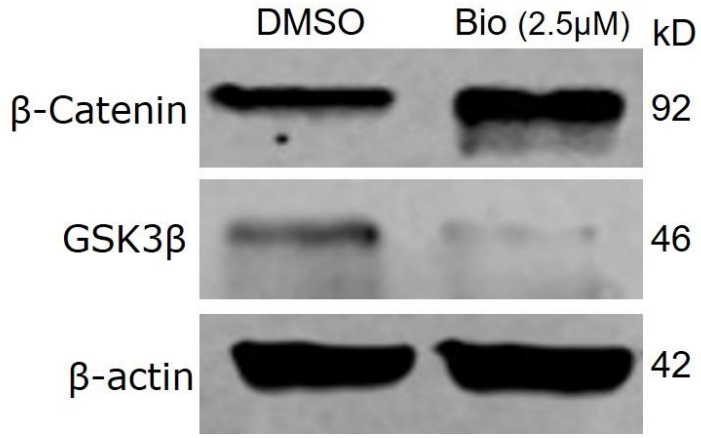


Figure 4-21. WB validation of GSK3 inhibitor (2.5uM BIO) on SW620 cancer cell lines.

Based on our results the combination of both agents yielded better results than single treatment in the suppression of cell growth and induction of apoptosis activity in SW620 cells (insets and red arrowheads) (Figure 4-22). Moreover, the combination treatment of Rifabutin 28μM and BIO; 2.5μM (patent application publication; US20180320144A1) in budding tumour organoid drastically inhibited the organoid growth and induced apoptotic activity compared to control, Rifabutin or Bio treatment alone (Figure 4-23).

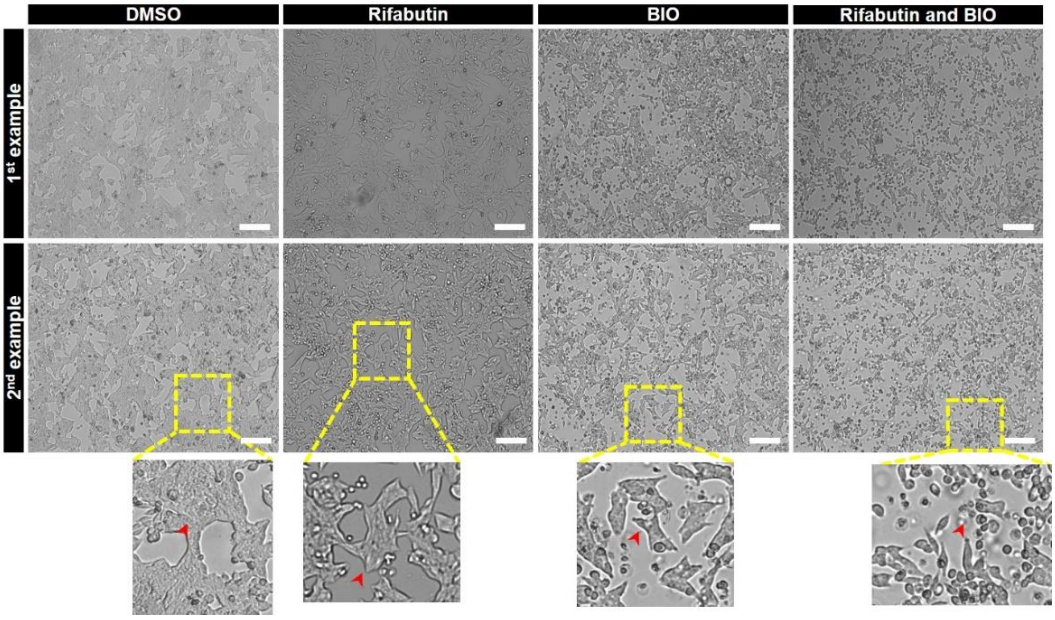


Figure 4-22. Co-treatment of Rifabutin with BIO significantly decreased the proliferation of SW620 cells. The individual treatments with BIO or Rifabutin (middle panels) produced a partial reduction in cell growth compared to control group. Co-treatment with Rifabutin and BIO resulted in reduced cell growth, and induced apoptotic activity of the SW620 cells after 48h (Right panel). These data suggested that the combination treatment of Rifabutin and BIO is effective in the inhibition of cell growth in SW620 cells. Scale bar: 75μm.

Rifabutin and Bio treated organoids growth significantly impeded within 48h after treatment compared to controls. Even though the Rifabutin or Bio single administration inhibited the growth of organoids in following days, the organoids displayed immediate and much more apoptotic reaction to co-treatment with Rifabutin and Bio (Figure 4-23; right panel).

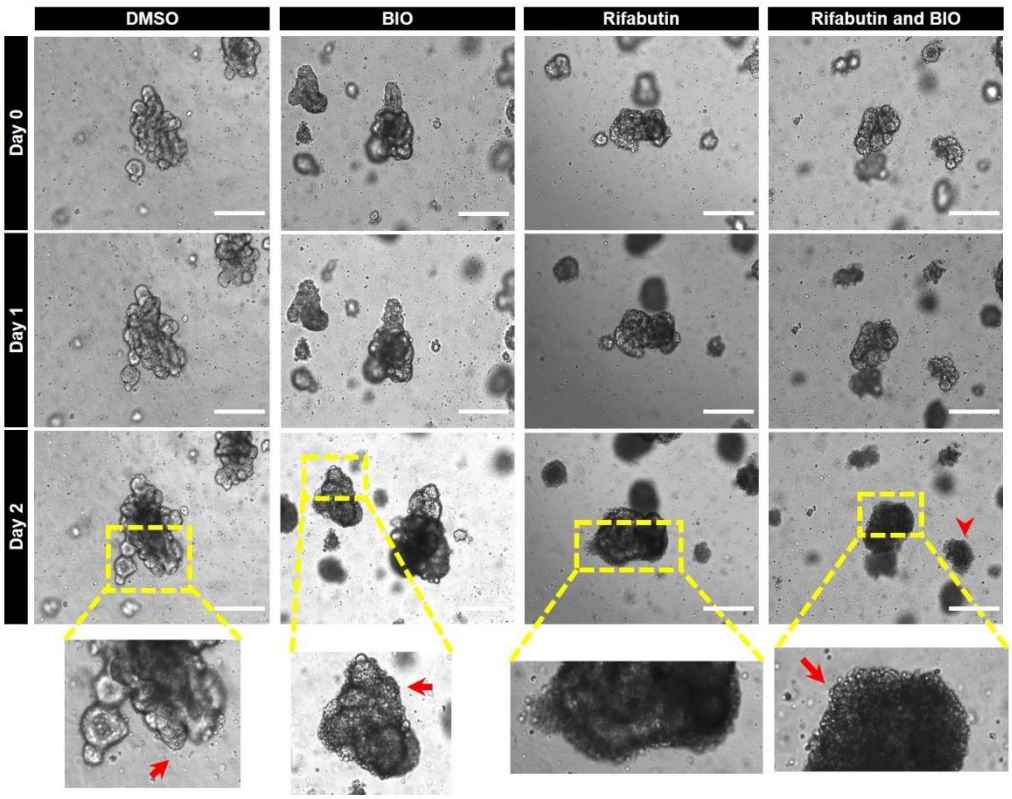


Figure 4-23. Concomitant treatment of Rifabutin and BIO markedly induced apoptotic activity in budding tumour organoid. Treatment with Rifabutin (IC50:28μM) arrested tumour organoid growth rate. The combination of Rifabutin and BIO resulted in inhibition of organoid growth and enhanced apoptosis activity. We conclude that the growth inhibitory potential of Rifabutin significantly enhanced in co-treatment of Rifabutin with BIO. Scale bar: 75μm.

4.2.5.2 Effect of BIO and Rifabutin combination treatment in murine derived organoids

To explore the effect of Rifabutin and in combination treatment with BIO on normal derived organoids, the organoids were cultured from murine intestinal epithelium and treated with the indicated dose of Rifabutin (28μM; obtained from SW620 cell line). As demonstrated in Figure 4-24, the Rifabutin hampered

the growth of normal derived organoids over 5 days compared to the control group (DMSO). Subsequently, the majority of organoids underwent apoptotic activity in the following days. Strikingly, unlike budding tumour derived organoids (Figure 4-7), the normal organoids were more resistant to Rifabutin administration. The murine intestinal organoids were subsequently treated with BIO agent (2.5µM) and in combination manner with Rifabutin. As demonstrated in Figure 4-24, the Rifabutin/Bio co-treatment did not significantly affect the normal organoid growth suppression as in colonic tumour organoids.

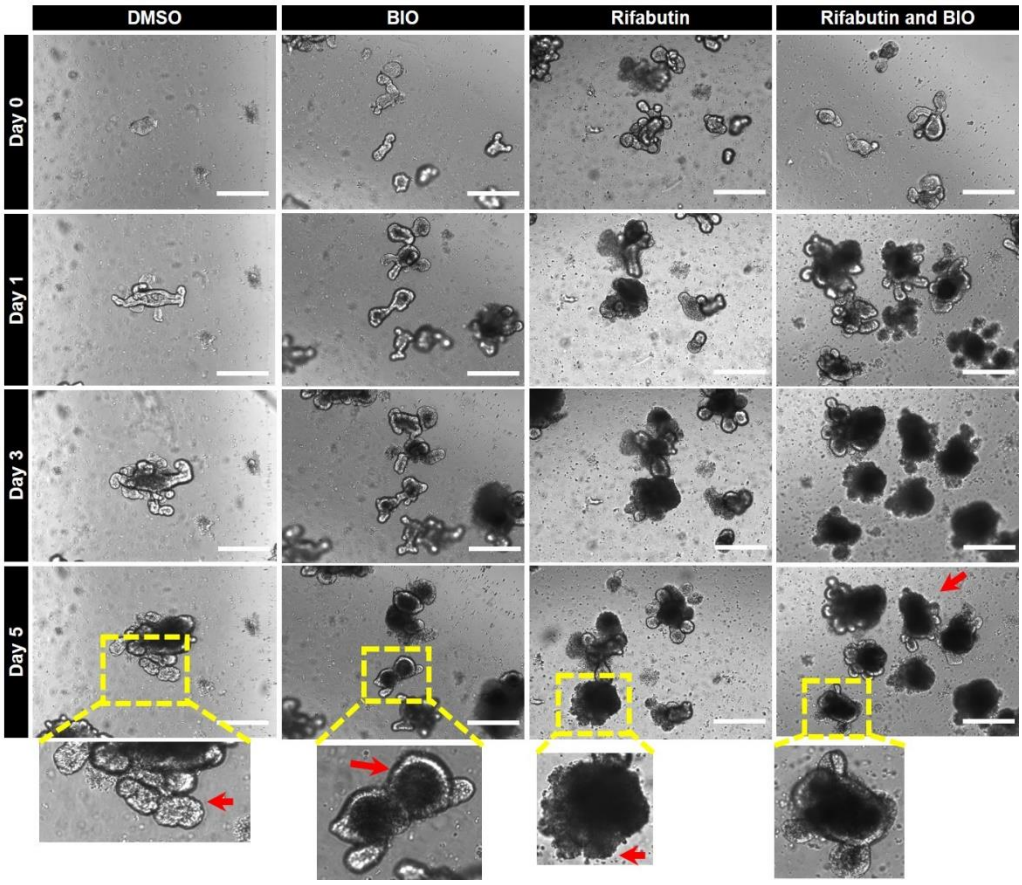


Figure 4-24. Rifabutin and BIO suppressed the growth of normal murine derived organoid in culture. Murine intestinal organoid was incubated with Rifabutin and BIO; 2.5µM and the images were captured on a daily basis. Rifabutin inhibited the organoid growth and steered the apoptosis of organoids

in 8 days. Unlike the tumour-derived organoids, the normal organoids were less sensitive to Rifabutin treatment. Scale bar:75μm.

In the line of our study, a recent study also reported the GSK3 inhibitor and Taxol based therapy synergistically inhibited the growth of NSCLC cells *in vitro* and *in vivo* (390). In another recent study combination of GSK3 inhibitor and gemcitabine induced the pancreatic cancer cell death (391). Taken together relative to a single agent, these results suggest that BIO and Rifabutin in a synergic manner had a significant negative effect on SW620 cell lines and also budding tumour organoids growth.

4.2.5.3 Down-regulation of EMT-mediators, stem cell markers and oncogenic drivers of CRC cells by BIO/Rifabutin treatment

Following the morphological evaluation, qRT-PCR was performed to investigate the differential mRNA signature of SW620 cells in Rifabutin combination treatment with BIO. The mRNA expression of β-catenin and its target genes including *CD44*, *LGR5*, *FLYWCH1*, *C-Myc* and EMT markers including *E-cadherin*, *Vimentin* were also investigated. We also evaluated the level of FBXW7 tumour suppressor, targeting several proteins with critical roles in the hallmarks of cancer including EMT (361).

Co-treatment of the Rifabutin and BIO significantly increased the expression of FBXW7, FLYWCH1, CD44, LGR5 and Vimentin while there has been a remarkable reduction of the β-catenin, C-Myc and E-Cadherin expression level

(Figure 4-25). β-catenin mRNA expression levels were reduced after BIO Rifabutin co-treatment. Enhanced expression of the β-catenin is correlated with the proliferative tumorigenic trait (392), this is in line with our phenotypical findings on co-treatment of BIO with Rifabutin in SW620 cells. In addition, we detected remarkable FBXW7 increase expression level in a co-treatment condition relative to the single BIO/Rifabutin treatment. The previous study demonstrated that the loss of the FBXW7 promoted intestinal tumorigenesis and β-catenin accumulation in adenomas (111). Taken together, this supports the idea that Rifabutin in co-treatment may hinder cancer cell proliferation. In co-treatment of Rifabutin with BIO, CD44 expression also increased by 2-fold. CD44 is also closely associated with cell proliferation, tumour invasion, and metastasis. Previous studies also indicated that overexpression of the CD44 CRC CSC significantly increased the cell proliferation and migration, and induced apoptosis (393). The otherwise 3-fold overexpression of LGR5 was also detected in co-treatment condition. As a target of Wnt signalling pathway, LGR5 is involved in CRC tumorigenesis and progression (394-396). Paradoxically to the traditional view on LGR5 activity, the inhibition of proliferation in CRC through LGR5 has been noted in recent works (397, 398).

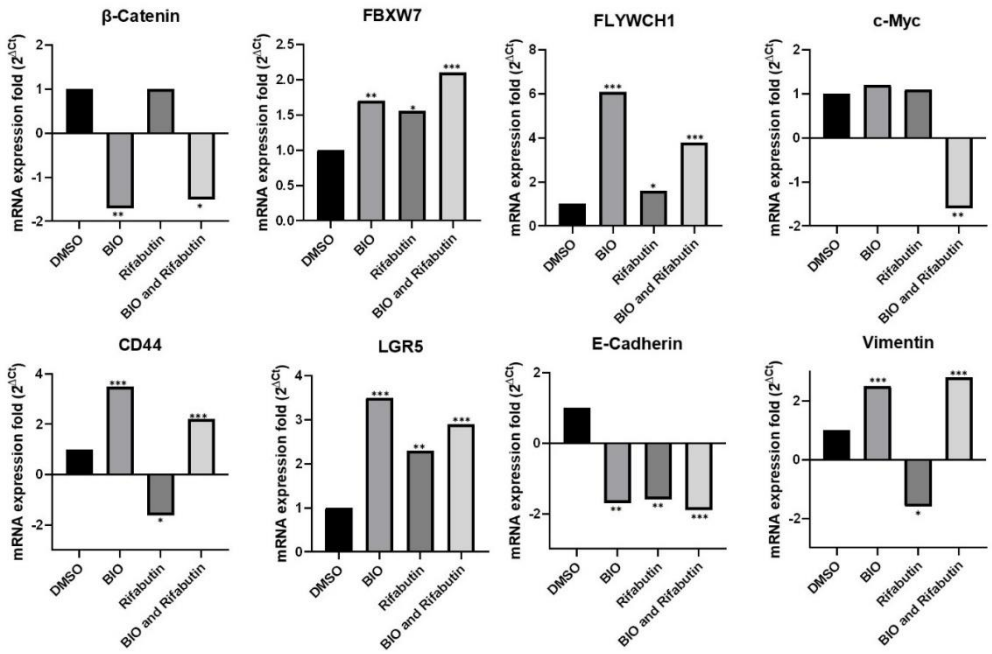


Figure 4-25. EMT-mediated regulation of BIO and Rifabutin co-treatment in SW620 colorectal cancer cells. Co-treatment of the Rifabutin and BIO significantly increased the expression of *FBXW7, FLYWCH1, CD44, LGR5* and *Vimentin* while there has been a remarkable reduction of the β-catenin, C-Myc and E-Cadherin expression level. Error bars represent mean ± S.D. *, P ≤ 0.05; **, P ≤ 0.01; ***, P ≤ 0.001, N=3.

4.3 Discussion

In the current study, we evaluated the anticancer potential effect of Rifabutin in CRC patient derived tumour organoids and colonic cancer cell lines. The procedure for treating colon cancer cells and tumour organoids to repurpose antibacterial drug Rifabutin as anti- colorectal cancer agent is depicted in Figure 4-26.

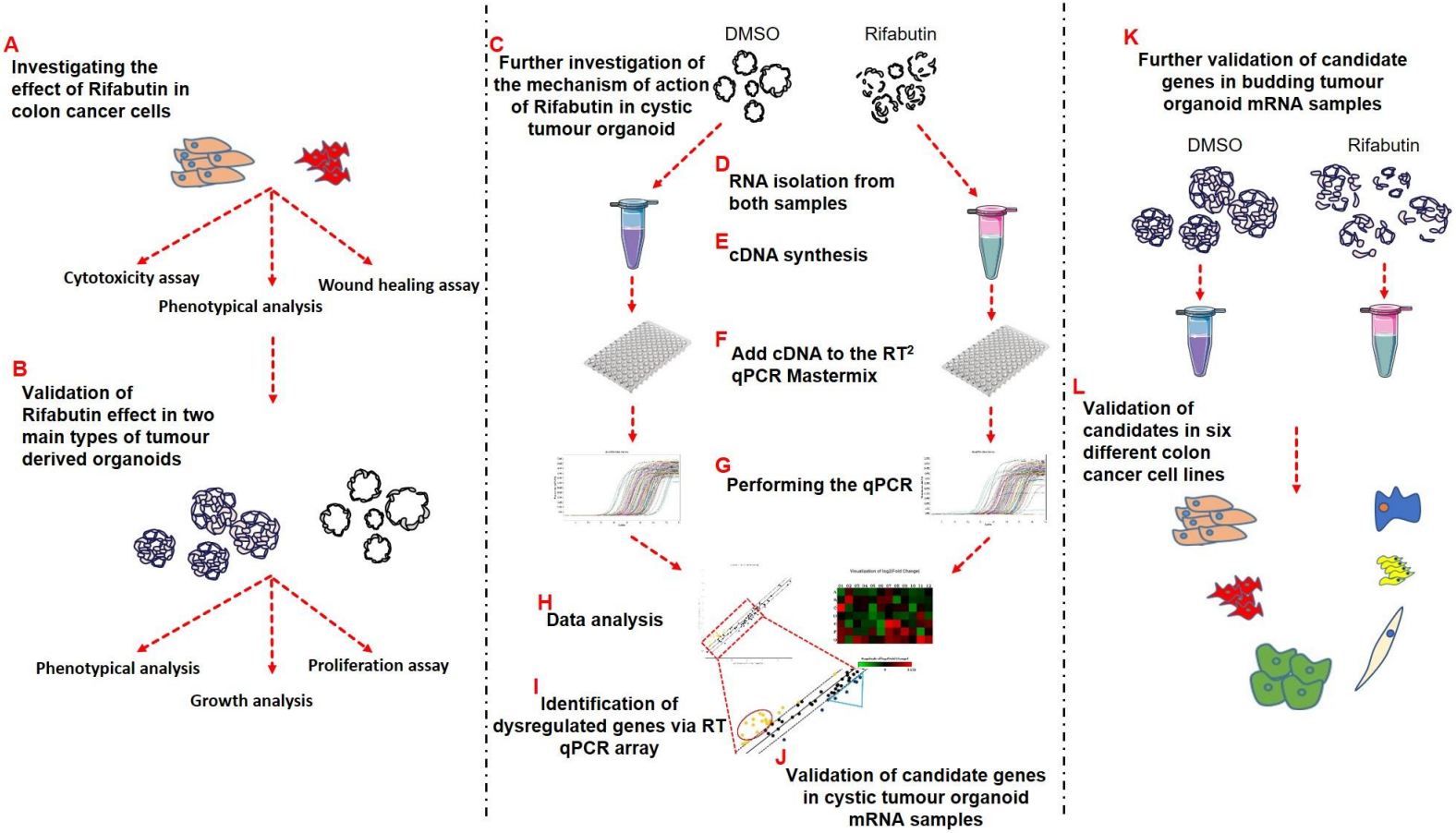

A
Investigating the effect of Rifabutin in colon cancer cells
Cytotoxicity assay
Wound healing assay
Phenotypical analysis
B
Validation of Rifabutin effect in two main types of tumour derived organoids
Phenotypical analysis
Proliferation assay
Growth analysis
C
Further investigation of the mechanism of action of Rifabutin in cystic tumour organoid
DMSO
Rifabutin
D
RNA isolation from both samples
E
cDNA synthesis
F
Add cDNA to the RT² qPCR Mastermix
G
Performing the qPCR
H
Data analysis
I
Identification of dysregulated genes via RT qPCR array
J
Validation of candidate genes in cystic tumour organoid mRNA samples
K
Further validation of candidate genes in budding tumour organoid mRNA samples
DMSO
Rifabutin
L
Validation of candidates in six different colon cancer cell lines

Figure 4-26. The schematic diagram for investigating the anti-cancer effect of Rifabutin in colon cancer cell lines and PDOs. A) After IC50 determination, the colon cancer cells were exposed to Rifabutin and the morphological changes and wound healing assay was assessed. **B)** Investigating the effect of Rifabutin in cystic tumour derived organoid. **C-I)** subsequently, the RNA was isolated from experimental and control conditions and the RT-qPCR array was carried out to identify the dysregulated Wnt signalling pathway associated genes. **J)** The candidate gens expression was eventually validated from treated organoids. **K-L)** Further validation and characteristics of Rifabutin was performed on budding tumour organoid and multiple colon cancer cell lines including SW480, SW620, HCT-116, HT-29, LS-174T and DLD-1.

Based on our finding, Rifabutin significantly perturbated the growth of colon cancer cells and cystic tumour organoids in culture and led subsequent organoid death within 10 days. The viability assay further validated the inhibition of proliferation and increase of cell death in organoids upon Rifabutin treatment. Characterization of the inhibition pathway involved in the mechanism of Rifabutin on tumour organoids, was initially deployed by gene expression analysis from mRNA isolated from cystic tumour organoids. To address this phenomenon, the RT^2 Profiler PCR arrays were carried out to evaluate the expression of 84 genes associated with Wnt signalling pathway. We further validated the dysregulated genes using the cystic tumour organoid mRNA samples.

Subsequently, the Rifabutin effect was evaluated in budding tumour organoids and 6 colon cancer cell lines. Interestingly, the Rifabutin sensitized the formation of elongated spindle-shaped morphology in SW620 and HT-29 cells. SW620 and HT29 cells treated with Rifabutin tended to migrate slowly in Rifabutin treated culture in wound healing scratch assay. In the line of our study, in recent

work on pancreatic cancer cell lines including Panc10.05, Panc215, A6L, Rifabutin profoundly suppressed cell growth in all pancreatic cell lines in 3 dimensions by 80% (399). The TOP/FOP flash luciferase activity further revealed that the Rifabutin drastically suppressed Wnt/β-catenin signalling in SW620 cells. Inconsistent with our findings, Li and colleagues showed that Rifabutin effectively inhibited the proliferation and induced the apoptosis of lung cancer cells and xenograft mouse model (400). Recent data revealed that the Rifabutin inhibited proliferation and inducing apoptosis activity in lung cancer cells via targeting eIF4E-β-catenin axis (400-403). Eukaryotic translation initiation factor 4E (eIF4E), profoundly interacts with two majors signalling, including PI3K/Akt and Ras/MA. In addition, Rifabutin interferes BCL-6 transcription repressor activity (360). As a transcriptional inhibitor, BCL-6 has contributed to the progression of different cancers, including breast and lymphoma (360).

The identification of new molecular targets for the diagnosis and treatment of CRC is of significant clinical value. In our study, we have found that the expression of eight key genes in the Wnt signalling pathway was significantly altered upon Rifabutin treatment in cystic tumour organoids. Among these 8 genes, CXXC4 (362), DVL-1 (368), FZD5 (369), and WIF1 (366) were broadly reported in different types of cancer.

Frizzled is a family of G-protein coupled receptors (GPCRs) and act as a receptor for Wnt ligands (404). GPCRs consist of the largest protein superfamily and accounts for more than 800 members in the human genome. GPCRs all share a common seven-transmembrane α-helical domain which mediating most of the

signal transduction in human cells (405). The Frizzled GPCR family have a cysteine-rich domain (CRD) in their extracellular part and they consist of SMO and ten FZDs. FZDs are the receptors for 19 Wnt proteins that orchestrate the Wnt/β-catenin signalling pathway in the cells (406). When FZD is activated, it recruits Disheveled (DVL) protein in cytoplasm to initiate the Wnt signal transduction. FZD5 overexpression has been reported in several cancers (404, 406, 407). FZD5 has a higher affinity with WNT5A, WNT3A, WNT7A and WNT10B and it is involved in both conical and non-conical pathways.

Inconsistent with our study, previous works in breast cancer showed that Mir-224 suppressed cell growth and migration via FZD5 mediated inhibition of Wnt/beta catenin (375). In another study CRISPR/Cas9 knock-out of FZD5 significantly inhibited cell growth in pancreatic ductal adenocarcinoma RNF43 mutant cells (378). Down-regulation of FZD-5 inhibited prostate cancer *in-vivo* and *in-vitro* (377). Interestingly, recent study on prostate cancer revealed that knockdown of FZD5 and co-treatment with WNT5A further enhanced WNT5A-induced apoptosis in prostate cancer (377). This is in line of our findings on downregulation of FZD5 and increase in expression of WNT5A and further apoptotic phenotype in cystic tumour organoids.

On the other hand, DVL1, as a positive regulator of Wnt signalling, encodes a cytoplasmic phosphoprotein that regulates cell proliferation and acts as a transducer molecule for developmental processes. The complex of FZD-DVL triggers the Wnt/β-catenin signalling by suppressing the Axin-GSK3-APC destruction complex (408, 409). In ovarian cancer, overexpression of DVL1 suppressed GSK-3b activity and further increased the expression of β-catenin

via AKT (409). Of note, two pathways have been proposed for GSK-3b inhibition via DVL1 activity; First is suppressing the catalytic mediated activity of GSK-3β by serine phosphorylation (408, 410), and second is a disruption of the interaction between b-catenin and GSK-3b (411).

Furthermore, CXXC4 plays as a tumour suppressors by negatively regulating Wnt/ β-catenin signalling in colorectal cancers (412, 413), renal cell carcinoma (414), and gastric (415, 416). Expression of CXXC4 is significantly downregulated in colon cancer, gastric and renal carcinoma tissues (412, 413, 415, 416). In gastric cancer tissue, CXXC4 downregulation is correlated with poor outcome of patients (416). Decreased expression of CXXC4 is also associated with metastasis, high tumour grade and a poor survival outcome in renal cell carcinoma (414). As a transcription factor, CXXC4 acts through different targets in various cancers. In colorectal cancer, MiR-629-5p enhanced colorectal cancer progression through targeting CXXC4 (412). Recent work by Yu et al showed that BMI1, a component of the polycomb repressive complex (PRC1) activates WNT signalling in colon cancer by negatively regulating the CXXC4 (413). Overexpression of CXXC4 significantly reduced β-catenin and two WNT downstream targets including cyclin D1 and c-Myc, thus suppressed the growth of the colon cancer cells (413). Inconsistent with our findings on luciferase reporter assay and concomitant up-regulation of CXXC4 and down-regulation of DVL1, recent works on gastric, breast and renal cell carcinoma also revealed that CXXC4 directly interacts with the PDZ domain of DVL1 and disrupt its activity (414, 416, 417). Thus stabilize the β-catenin degradation complex through activation of GSK-3b. Upon CXXC4 mediated inactivation of

Wnt/β-catenin signalling, CXXC4 interfere the nuclear translocation of β-catenin, therefore, inhibits further activation of Wnt beta catenin signalling downstream target genes including cyclinD1, C-Myc and Survivin which play fundamental roles in cell proliferation, apoptosis and cell cycles in cancer progression (413, 417). Furthermore, WIF-1 protein is an important antagonist of Wnt signalling. WIF1 play as tumour suspensor and predominantly epigenetically silenced in different malignancies (366, 418). Reduction of WIF-1 expression activates the Wnt signalling, which subsequently promotes cell growth and proliferation (419). A recent meta-analysis on the diagnosis value of Wif1 in CRC demonstrated that WIF1 hyper-methylation might be also a promising diagnostic candidate for CRC (366).

The overexpression of CD44 confers a selective advantage to resist apoptosis and developed a malignant trait in CRC Cells (2). Our further analysis showed that in comparison to the single treatment of BIO or Rifabutin, the concomitant treatment of Rifabutin with BIO significantly steered the perturbation of SW620 in culture. In comparison to a single treatment, co-treatment of Rifabutin with BIO accelerated the inhibition of proliferation and apoptotic activity in tumour organoid and also SW620 cell line. Further qRT-PCR analysis of SW620 cells upon Rifabutin treatment and in combination manner with BIO revealed the remarkable elevated expression of FBXW7 and down-regulation of β-catenin. FBXW7, function as a tumour suppressor and exerts its activity as recognition subunits of E3 ligase family for ubiquitination and further proteasomal degradation (420). In the line of our study, previous work on APC (adenomatous polyposis coli) deficiency (*ApcMin/+* mice) revealed that lack of Fbxw7

accelerated intestinal tumorigenesis and following death and promoted β-catenin accumulation in adenomas (111).

Previous works have demonstrated a wide range of Rifabutin IC50 values from 5-35.5μM in different cell lines (403, 421, 422). Of note, the recommended clinical dosage of Rifabutin in tuberculosis is 150mg/day. Based on our findings on normal derived organoids, and the resistance phenotype compared to tumour derived organoids, the lower IC50 (22μM) was also applied which was less than the initial target threshold derived from cancer cells (28μM). Interestingly this dosage (22μM) still had the negative effect on budding tumour organoids growth while had less toxicity on normal derived organoids. This indicates that the Rifabutin is well tolerated in lower dosage and makes it as a safe anticancer compound. It should be noted that the phenotypical differences in different tumour organoids upon Rifabutin treatment could be due to Wnt signalling differences and genetic background of the tumours. In addition the Rifabutin concentrations used in the study are slightly above normal therapeutic doses for cancer cells, however simultaneous treatment with 5-FU or other chemotherapeutics may decrease this concentration in synergic manner.

In conclusion, Rifabutin significantly impeded the growth of PDO and colon cancer cell lines. This suggests that on its own Rifabutin can have an anti-cancer effect through significantly interfering migratory capability of cells which will impede the acquisition of invasive and metastatic trait. Taken together, these findings confirm Rifabutin anticancer activity and provide strong evidence to justify further work surrounding Rifabutin and its potential as an adjuvant in CRC. Further investigation is required to elucidate what the direct target of

Rifabutin in cancer cells is and provide more explanations of the observed dynamics.

CHAPTER 5

Screening the role of F-box genes in murine intestinal organoid culture using the CRISPR /Cas9 technology

5.1 Brief introduction

The CRISPR/Cas9 based editing technology, as a robust genome engineering tool, has provided a promising approach for targeted loss/gain-of-function mutations at specific sites in the genome of eukaryotes (423). Of note, previous studies demonstrated that CRISPR/Cas9 engineering of normal organoids for cancer driver genes including APC, KRAS, P53, SMAD4, and PIK3ca genes displayed differential phenotypical features as their in-vivo tumour counterparts (424). This highlights the morphological significance application of engineered organoids for further analysis and validation in disease models and developmental studies.

One of the key cellular mechanisms of regulating the activity of many proteins on a post-translational scale is via protein degradation by the Ubiquitin-Proteasome System (UPS) (108). The specificity of proteolysis for any particular protein substrate is determined by its association with a specific E3-receptor subunit. F-box proteins are the substrate recognition components of the Skp1-Cul1-F-box-protein (SCF) E3-ubiquitin ligases (108, 425). Despite their regulatory activity and importance for biology and medicine, the functions of the majority of the F-box proteins have not yet been fully defined. Herein, we developed a CRISPR/Cas9 mediated system-based screening method in intestinal organoid culture to investigate the role of F-box E3 ligases in intestinal homeostasis and cancer development. We postulate that the CRISPR/Cas9 mutagenesis (loss-of-function) screening method of exploring the phenotypical morphology of large candidate genes with unknown/poorly identified function, facilitates the rapid and reliable identification of new genes that may play a role in gut development and gut-associated diseases including colon cancer.

Given the high efficiency of gene knockout by lentivirus-based CRISPR-Cas9, we transduced lenti-gRNAs expressing F-box genes into a stable Cas9 expressing

organoids to evaluate their effect in organoid growth. Knockout intestinal organoids and their differential phenotypical alterations might be associated with the key biological function of the gene(s) in development, homeostasis, disease progression, and tumorigenesis and also in drug responses. Moreover, our finding provides an example study for other labs for potentially replacing animal models for future studies. The methodology part of this chapter has been accepted for publication at the *Methods in Molecular Biology* (2020) and *F1000Reseaech* (in review by NC3Rs). This chapter has accomplished in collaboration with Nicholas Jinks in the Dr Nateri's laboratory.

5.2.Results

5.2.1 Validation of CRISPR gRNA library constructs;

5.2.1 Restriction enzyme digestion and nucleotide sequencing analysis of representative F-box LV gRNAs constructs confirmed the validity of the gRNA library

All CRISPR gRNA vectors in the library (n=126) contain a similar backbone with a total size of 9Kb, including a 19-21bp gRNA insert (gRNAs provided by the Sanger Institute in Cambridge on a collaboration basis coordinated by Dr Nateri). Restriction enzyme digestion of both copy CRISPR gRNA vector of representative F-box genes (e.g., Fbxw7, Fbxo25) with *Pvu*II and *Nde*I enzymes, generated the same sized fragments on 2% agarose gel (Figure 5-1, A). The left band includes a 1Kb ladder which has ranged from 1000 bp to 10000bp. As expected, representing digested gRNA plasmids with *NdeI* for both Fbxw7 and Fbxo25 generated a 4.2Kb, 3Kb and 1.8Kb fragments. In addition, 4 similar sized fragments were produced upon digestion with *PvuII*, including 3.8kb,

2.5kb, 1.5kb and 1.2kb across all representative F-box vectors. Furthermore, U6 promoter-driven LV gRNA of F-box library enabled the sequencing analysis of the gRNA construct via forward U6 promoter primer (Figure 5-1; B). Following the validation with restriction enzyme digestion, randomly selected LV gRNA of F-box plasmids (Fbxw7, Fbxo25) were sequenced based on U6 promoter (Figure 5-1; B). In this example, both copies of the sgRNAs (Fbxw7, Fbxo25) were exploited for the sequencing process and the findings showed up to 100% homology to their target DNA genes as previously speculated. The list of 126 F-box CRISPR LV gRNA sequence is presented in *Appendix 2*, by which each of the gRNA sequences is BLASTed in the NCBI database, and their specificity is further verified.

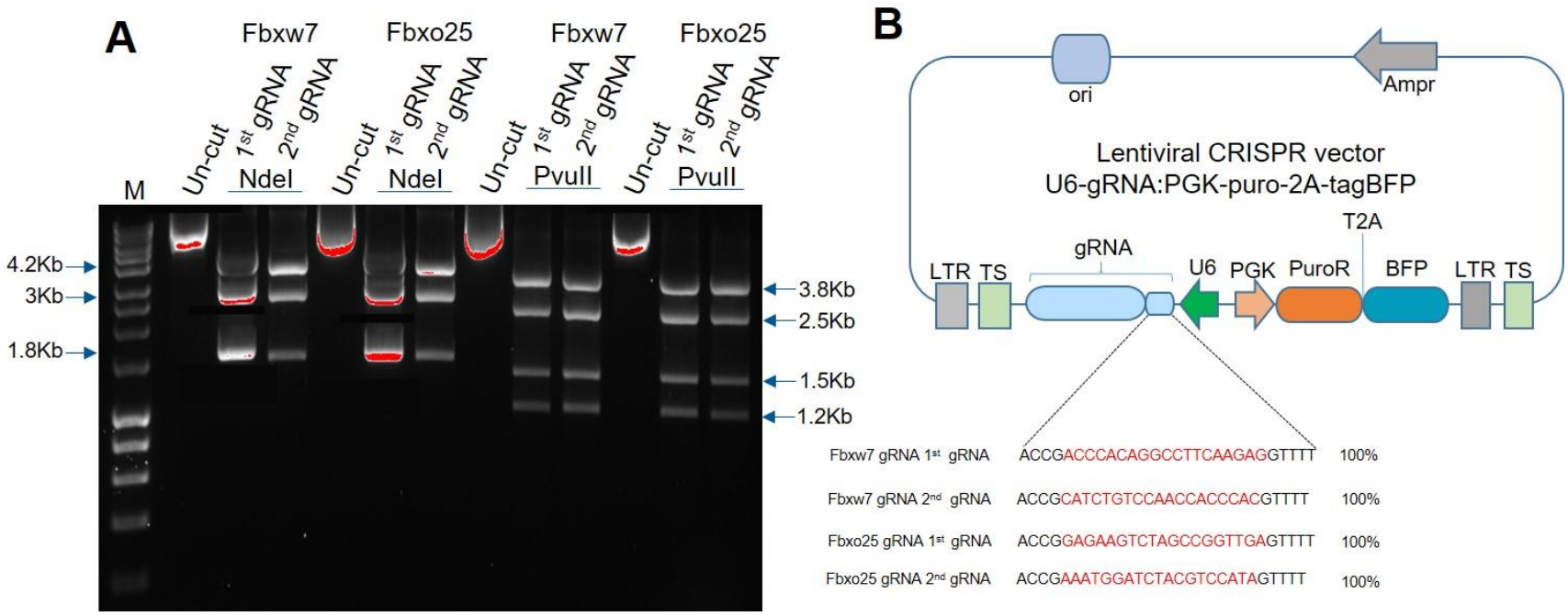

A
Fbxw7
Fbxo25
Fbxw7
Fbxo25
Un-cut
1st gRNA
2nd gRNA
NdeI
PvuII
M
4.2Kb
3Kb
1.8Kb
3.8Kb
2.5Kb
1.5Kb
1.2Kb
B
ori
Ampr
Lentiviral CRISPR vector
U6-gRNA:PGK-puro-2A-tagBFP
T2A
gRNA
LTR
TS
U6
PGK
PuroR
BFP
Fbxw7 gRNA 1st gRNA ACCGACCCACAGGCCTTCAAGAGGTTTT 100%
Fbxw7 gRNA 2nd gRNA ACCGCATCTGTCCAACCACCCACGTTTT 100%
Fbxo25 gRNA 1st gRNA ACCGGAGAAGTCTAGCCGGTTGAGTTTT 100%
Fbxo25 gRNA 2nd gRNA ACCGAAATGGATCTACGTCCATAGTTTT 100%

Figure 5-1. Validation of the CRISPR gRNA vectors via restriction enzyme digestion and sequencing. A) Cleavage of the 2 representative amplified gRNA plasmids including Fbxw7 and Fbxo25 carried out with *PvuII* and *NdeI* enzymes. Of note, we have checked Restriction enzyme digestion for all gRNAs used in this screening and we have only presented two of them here. **B)** Illustrates the representative sequencing findings for 3 pairs of F-box gRNAs including Fbxw7, Fbxo25. The selected gRNA sequence displayed up to 100% homology to their DNA target sequence.

5.2.2 Further Validation of F-box gRNAs in human HEK293-T and colon cancer DLD-1 cell lines

Transgene expression of selected F-box gRNA vectors for validation purposes can be performed via transient transfection into a suitable cell line including HEK293-T cells prior proceeding with the further step. As expected, the blue fluorescent proteins (BFP) were successfully detected in live cells, where expressed 24h post-transfection using fluorescence microscopy. Transfection validation for F-box gRNA plasmids (possess a fluorescent reporter protein) was performed for all F-box gRNA construct used for screening (i.e., 32 F-box LV gRNAs). For example, transfection of representative gRNA F-box (Fbxo25) into HEK293T cells is demonstrated in Figure 5-2. The transfected cells can be further selected by antibiotics or fluorescence-activated cell sorting (FACS).

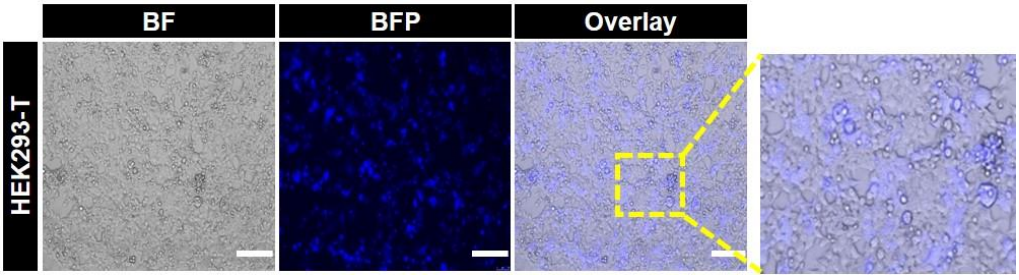


Figure 5-2. The BFP expression confirmed the correct transgene construct and delivery of F-box gRNA (Fbxo25) in HEK293-T cells. Post transfection analysis of HEK293-T cells (24h) and following BFP expression was verified by fluorescence microscopy. Scale bar: 75μm.

5.2.3 Generation of LV library of F-box gRNA-based vectors

To genetically disrupt the expression of F-box genes, with the collaboration of Sanger institute, 2 copies of sgRNAs from each F-box gene were designed as indicated previously (5.2.1). In addition, lentiviral F-box from sgRNA vectors was produced using the second generation of packaging plasmids as previously described in Chapter 2. In F-box CRISPR/Cas9 KO screening of intestinal organoids, the large-scale production, frequent harvest cycles and following validation of the CRISPR gRNA LV was critical. Following the harvesting of the viruses, transduction and titration was performed to assess the titration efficacy for each of the LVs. To address the intensity of virus particles generated in a medium over time (3 days), representative images of day 1 and 3 post-transfection with FBXO25 LV and the GFP control (pLVX-eGFP) are presented (Figure 5-3; A & B). The improved intensity of the BFP and GFP on day 3 compared to the day one indicates the significant increase in the number of infected cells due to the gradual production of virus particles in the medium. Since the LV comprises the gRNA of interest were aimed for further organoid transduction and generation of precise genetic modifications using CRISPR/Cas9 system, the production of the high titer virus was an essential requirement. This enables the acquisition of robust organoid KOs by the CRISPR/Cas9 within a short period.

5.2.3.1 The specific integration of the gRNA in the genome of colon cancer cell lines

The transgene integration during the transduction led the expression of BFP in the transduced cells of LV expression in host cells for example DLD-1 cells (Figure 5-3; C, inset). Furthermore, as it is depicted in Figure 5-3; C, upon the successful transgene delivery of gRNA vector (which contains the puromycin resistant gene) into DLD-1 cells, nearly 100% of the cells exhibited resistance to puromycin in comparison to control non-transduced group.

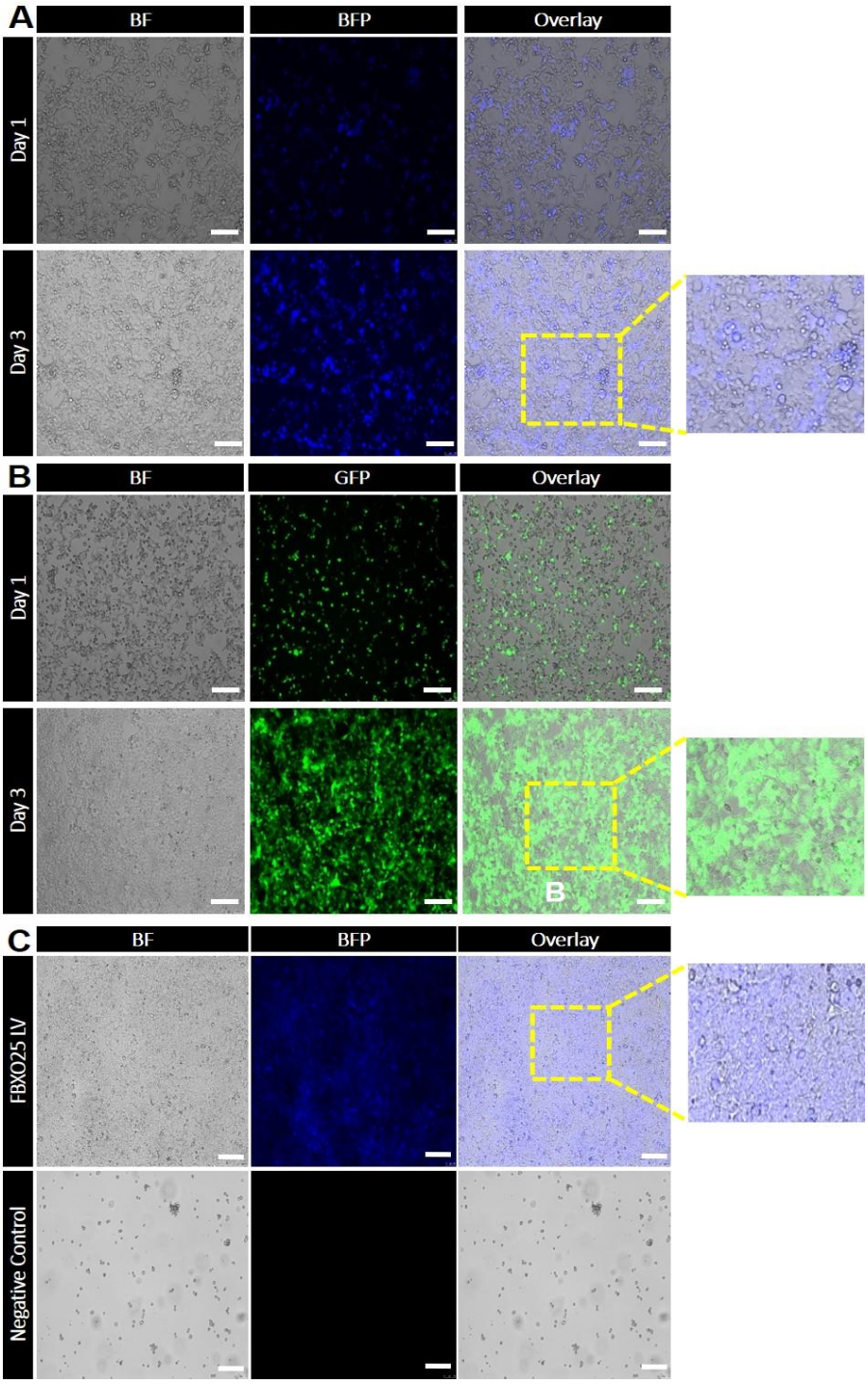


Figure 5-3. LV Generation and validation of CRISPR gRNA library indicate the intense integration of the F-box sgRNAs virus into the cell. A-B) The representative image demonstrating the production of the library of lentiviruses from CRISPR sgRNA of F-box genes and GFP control over 3 days in HEK293-T cells (n=126). Scale bar: 75µm **C)** The validity of the produced LV carried out via transduction of DLD-1 cells using high titer FBXO25 LV. The cells were incubated with the high titer virus for 48h. Inset;

magnified section of the transduced cells with FBXO25 sgRNA LV. To further validate the transduction density, the infected cells underwent antibiotic selection with puromycin and >99% of the cells survived on the selection process, whereas, nearly all cells died in non-transduced control condition after 2 rounds of antibiotic selection. Scale bar: 75µm.

Next, as an example, we validated Cas9 mediated gene targeting of F-BOX genes and the specificity of the gRNA library in cultured DLD-1 colon cancer cells by the generation of FBXO25 knockout cells. To evaluate the efficacy of gene knockout by lenti-CRISPR gRNA, the colon cancer cell lines stably expressing Cas9 was generated using DLD-1 cells and the expression of the Cas9 was further validated via Western blotting (Figure 5-4; A). Subsequently, to investigate the efficiency of the sgRNA library in generating selected F-BOX deficient genes in colon cancer cells, the representative FBXO25 gRNA were further transfected in DLD-1 Cas9 expressing cells. Following selection and generation of the stable cell lines, western blot analysis showed a complete absence of FBXO25 protein expression in the DLD-1 cells stably expressing Cas9 relative to control cells (Cas9 DLD-1), (Figure 4-5; B).

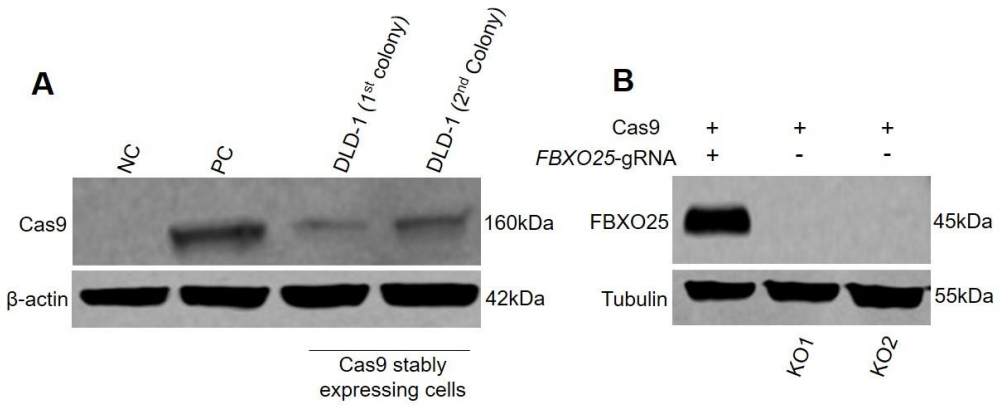


Figure 5-4. CRISPR gRNA validation in DLD-1 colon cancer cell lines. A) Demonstrates the WB validation of stable DLD-1 colon cancer cells for Cas9 expression. **B)** To investigate the efficacy of the sgRNA library at achieving knockout of the endogenous gene of interest and generation of KO cells, the KO of FBXO25 in DLD-1 colon cancer cells were generated. The western blot analysis showed the complete loss of FBXO25 expression in DLD-1 cells compared to the positive control, implying the perturbation of the FBXO25 protein.

5.2.4 Culturing and expansion of murine intestinal organoids as a platform for CRISPR-Cas9/gRNA screening

Following some validation studies of gRNA and Cas9 mediate knockout in cultured cells, as outlined above, we utilized the mouse intestinal organoid for CRISPR/Cas9 screening based methodology. Figure 5-5 demonstrates the culture of mouse intestinal organoids from the isolated crypt (left panel), passaging/re-culturing organoids (middle panel), and right panel represents the recovery of the frozen mice epithelial organoid. In principle, optimizing a robust, stable and reproducible organoid culture from isolation, passaging and the freezing-thawing process is a voluble property of this sophisticated *in-vitro* model. The growth of the organoid from isolation, passaging and thawing in overall, followed the similar pattern over a period of 8 days in which they gave rise into multiple budding units, (Figure 5-5; insets and red arrowheads indicating the similarity of the budding and branching across the organoids). In addition, measuring the comparative growth rates of organoids did not show significant changes over 2 weeks. Of note, organoid recovered from

freezing may require increased time-period for differentiation and expansion immediately post-thawing.

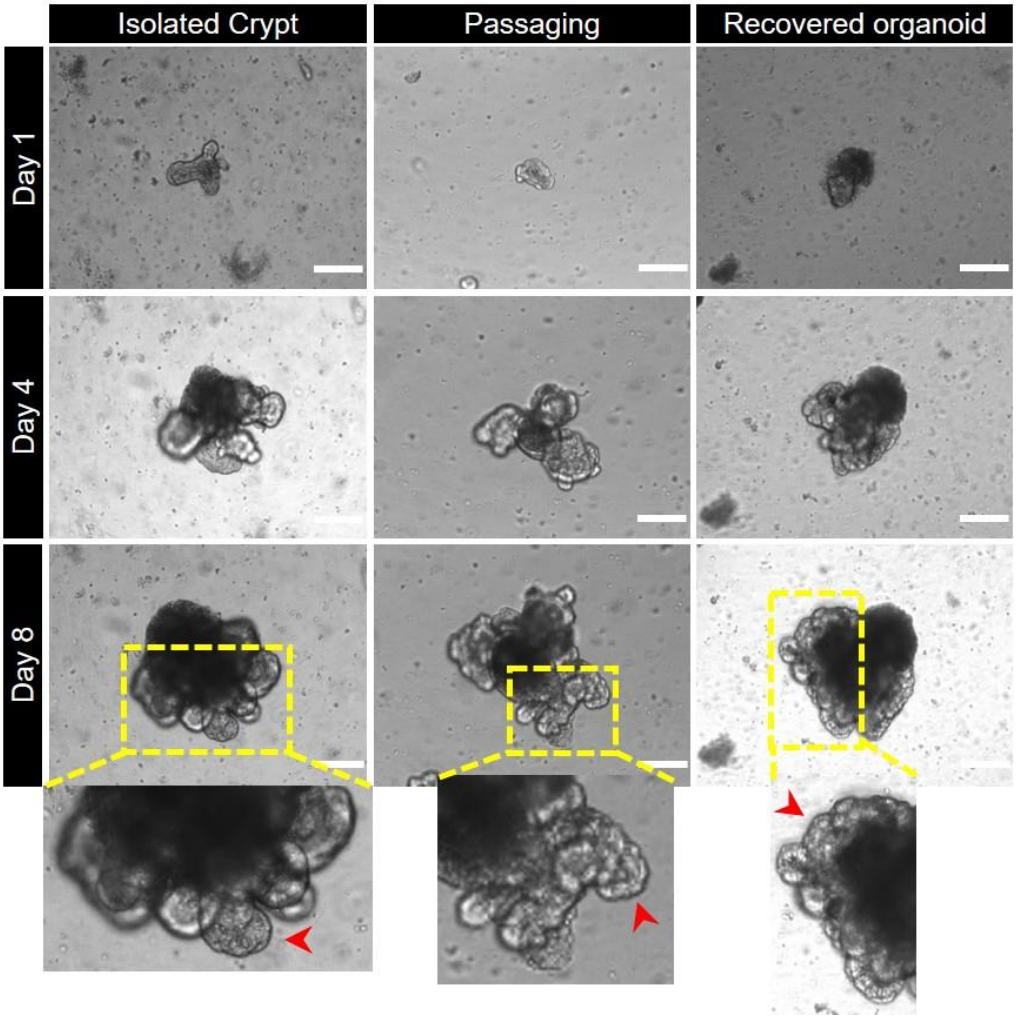


Figure 5-5. Culture and maintenance of murine intestinal organoid. Culture of murine intestinal organoid from the isolated crypt, following the passaging and subsequent recovery of organoids. Typically, the organoids grow with similar growth pattern/rate across all three conditions in a period of 8 days (insets and red arrowheads). Scale bar: 75µm. Note: All the murine derived organoids in this chapter were generated by the author.

5.2.4.1 Generation of a stable murine intestinal organoid line, expressing exogenous Cas9 endonuclease

In the RNA-guided CRISPR/Cas9 system, single guide RNA (sgRNA) is utilized to guide the Cas9 protein to target DNA sequences (36). As an endonuclease, Cas9 induces double-stranded breaks at target DNA sites. Since the CRISPR pooled gRNA library vectors used in the present study were not engineered with Cas9 endonuclease in the same vector, we separately generated a stable intestinal organoid line expressing Cas9 via LV transduction (Figure 5-6). To this, the expanded murine intestinal organoid line, transduced for expressing Lv-Cas9. The transduced organoids further passaged and grew in Wnt-3a supplement to form hyper-proliferative organoids prior to LV transduction (Figure 5-6 A-B). Right top panel shows the representative images of transduced intestinal mouse organoids with Cas9 LV vector after antibiotic selection and expansion (Days 1, and 7) (Figure 5-6 D). Middle panel; positive control, displays the GFP transduced organoids indicating the transduction efficacy. Bottom panel; negative control, the un-transduced intestinal organoids underwent the antibiotic selection with G418 (200µg/ml) and un-transduced organoids died after 2 rounds of antibiotic selection.

The transduced organoids then underwent sequential antibiotic selection for 9 rounds (G418, 200µg/ml) and following 3 passages before expansion for the validation process by western blotting (Figure 5-7). Cas9 expression did not change the growth rate and shape of wild type intestinal organoids. The generation of Cas9-overexpressing organoid line has also reduced the level of nongenetic heterogeneity of growth rate of isolated organoids for screening

purposes of elucidating the loss of F-box genes functions in changing the growth and morphology of them.

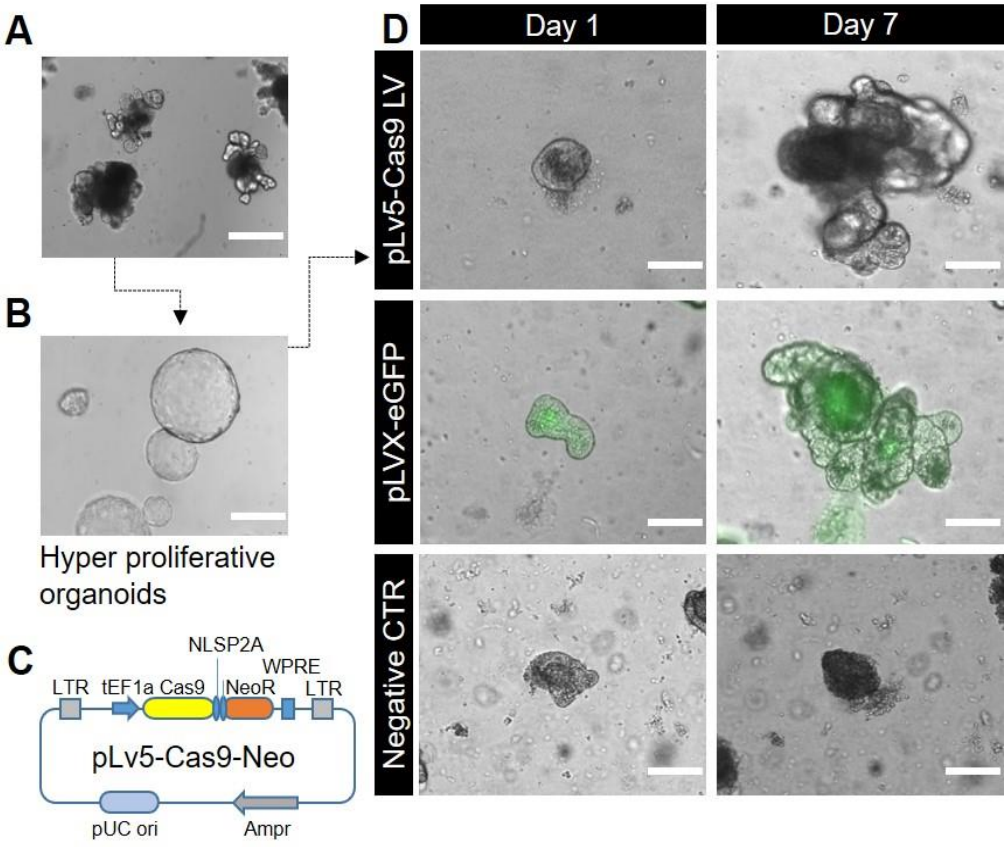


Figure 5-6. Generation of murine intestinal organoid stably expressing Cas9 endonuclease. A) Illustrates the use of expanded murine organoids for LV transduction and production of Cas9 expressing organoids. **B)** Generation of hyper-proliferative organoid structure; prior to LV transduction. **C)** The schematic of the Cas9 LV vector utilized in the present study. **D)** Shows the representative images of transduced intestinal mouse organoids with Cas9 LV vector after antibiotic selection and expansion (Day1, 7). Middle panel; positive control, displays the GFP transduced organoids indicating the transduction efficacy. Bottom panel; negative control, the un-transduced intestinal organoids underwent the antibiotic selection with G418 (200µg/ml) and organoids died after 2 rounds of antibiotic selection. Scale bar: 75µm.

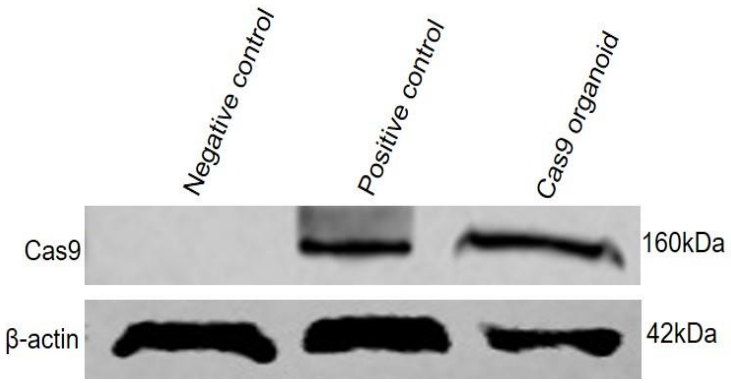


Figure 5-7. Western blot validation of stable organoids expressing Cas9. The selected organoids expanded in free antibiotic medium and protein were lysed and the Cas9 expression verified via western blot analysis (positive control; DLD-1 Cas9 expressing cells).

5.2.5 A CRISPR/Cas9-mediated mutagenesis method for screening of the F-box genes

In this study, we have screened the phenotype and morphology of F-box-E3 ligases knockout (K/O) in murine intestinal organoids (32-genes from 63 gRNAs from gRNA library outlined above). A schematic diagram of the CRISPR/Cas9 screening procedure and the screening results briefly, depicted in Figure 5-8.

CRISPR/Cas9 engineered KOs organoids were assessed for any morphological alterations for every 48h using the light inverted microscopy. The principle for the assessment of organoid KOs was monitoring the organoids growth pattern for varies types of phenotypic traits from; cystic, hyper budded or compact organoids with the absence of the differentiation to elongate or partially differentiated structures (Figure 5-8). This differential phenotypic diversity might be due to an alteration of differentiation, proliferation and death

underlying loss of F-box gene activity. Of note, some organoid KO may not present any obvious phenotypical manifestations due to the functional of related F-box or functional compensation by their paralogues.

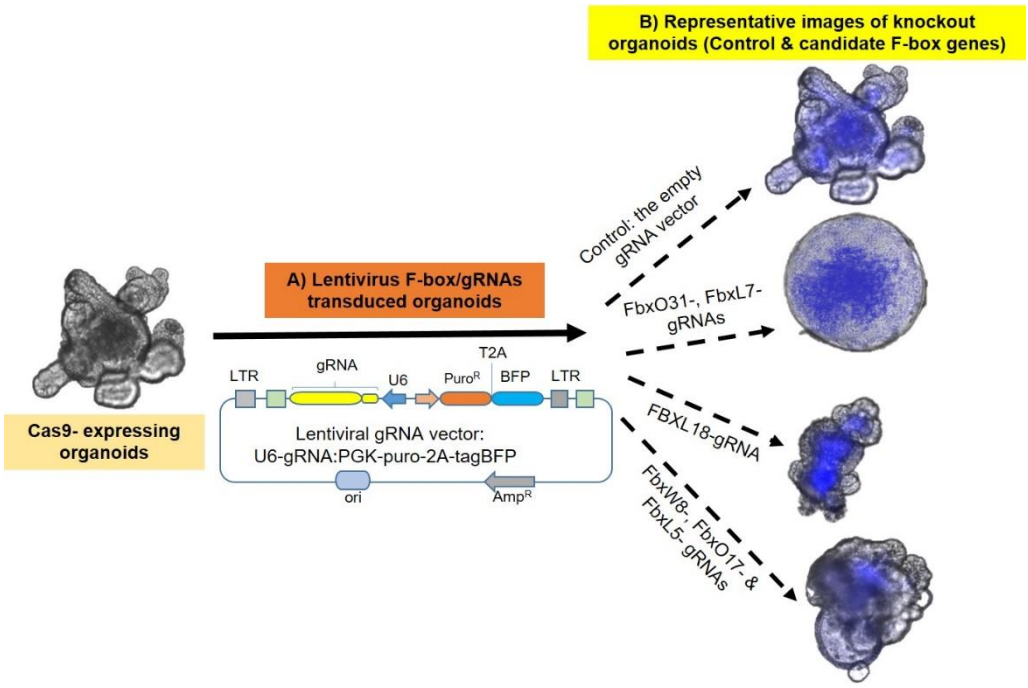


Figure 5-8. A Schematic diagram of the experimental procedure for CRISPR/Cas9 screening based methodology in mouse intestinal organoids. Generation and screening of intestinal F-box (F-BoX) knockout organoids. **A)** Cas9-expressing organoids infected with lentivirus expressing gRNA, validated & sequenced. **B)** Phenotypical analysis of control and the selected F-box knockout organoids (representative images).

This systematic loss-of-function genetic screening methodology facilitates a rapid and potentially accurate approach to identify the genes with unknown/poorly biological activity prior to molecular downstream analysis. Via phenotypical analysis of 32 F-box genes (total 32/69 F-box genes), we initially observed major changes via expressing of gRNAs for; FBXO31, FBXL7, FBXL18, FBXL5, FBXW8, FBXO17, (Figure 5-8). I have then selected F-box

genes Fbxl18 and Fbxo17 for further validation and downstream analysis in my study (Figure 5-9). Representative F-box KO-organoids without significant morphological differences is demonstrated in *Appendix 4*.

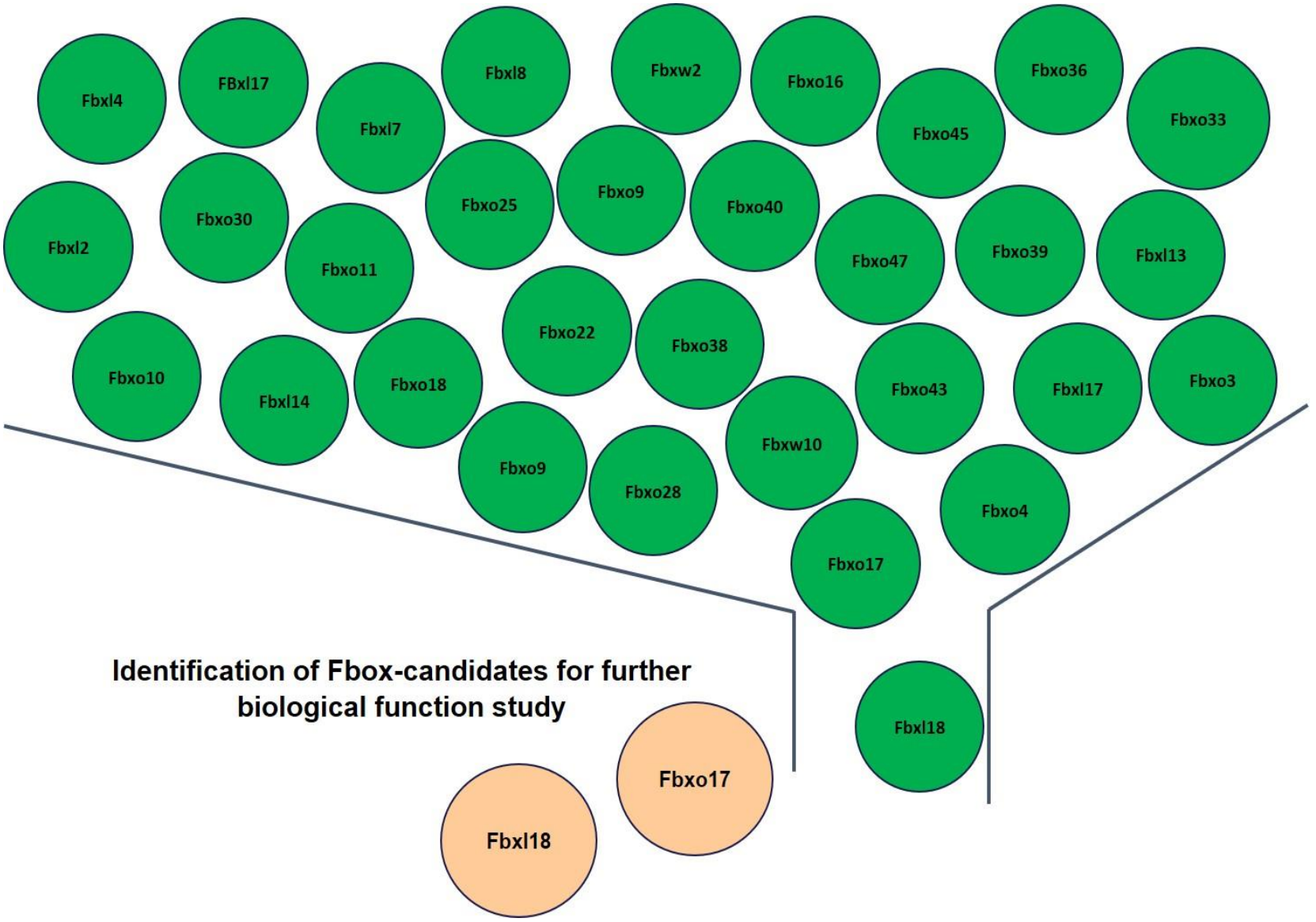
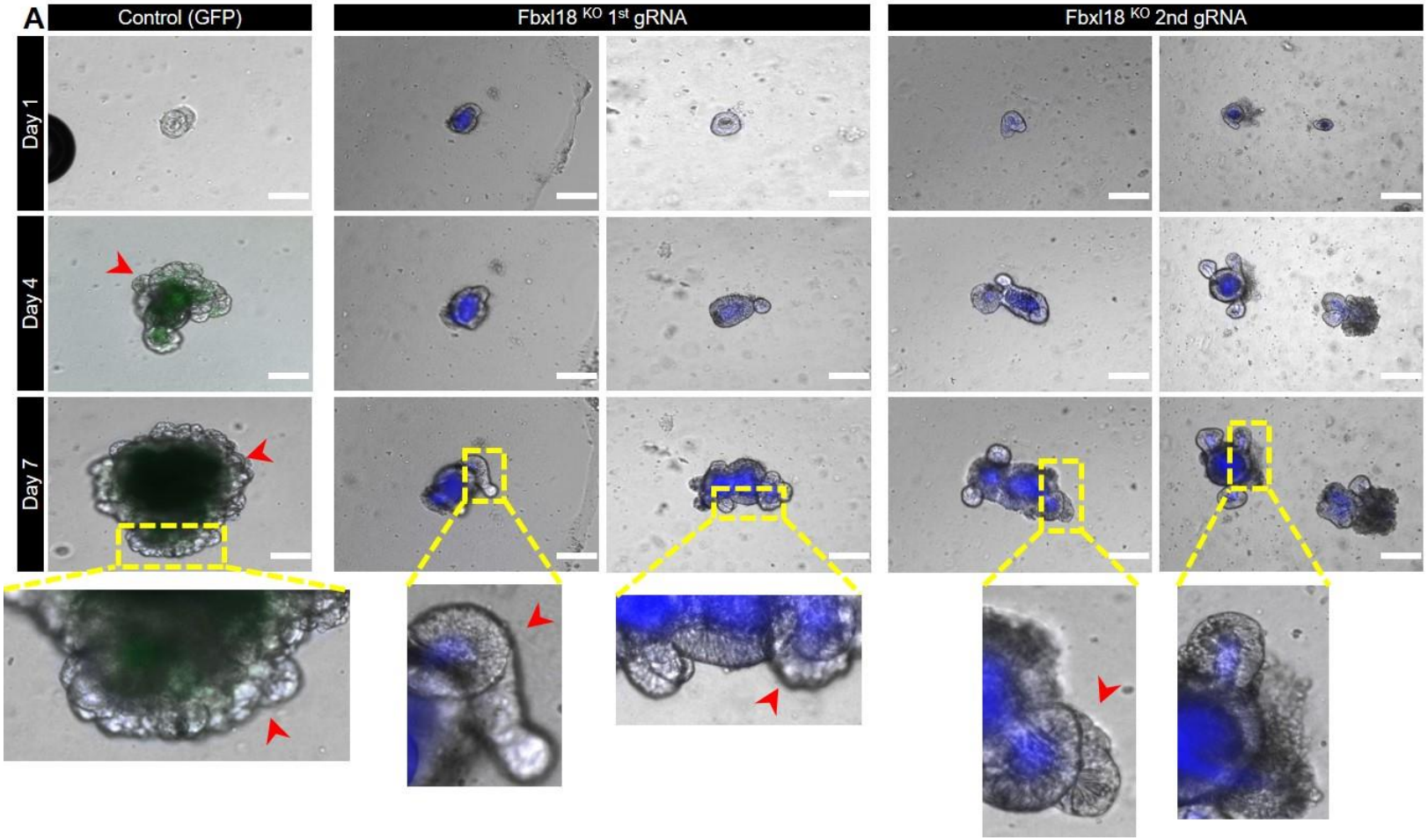

Fbxl4
FBxl17
Fbxl7
Fbxl8
Fbxw2
Fbxo16
Fbxo45
Fbxo36
Fbxo33
Fbxl2
Fbxo30
Fbxo11
Fbxo25
Fbxo9
Fbxo40
Fbxo47
Fbxo39
Fbxl13
Fbxo10
Fbxl14
Fbxo18
Fbxo22
Fbxo38
Fbxo43
Fbxl17
Fbxo3
Fbxo9
Fbxo28
Fbxw10
Fbxo4
Fbxo17
Fbxl18
Identification of Fbox-candidates for further biological function study
Fbxo17
Fbxl18

Figure 5-9. Schematic depiction for identification of F-box candidates via CRISPR/Cas9 KO screening. Following the CRISPR/Cas9 screening of the F-box genes, I followed two F-box genes (fbxo17 and fbxL18) for further investigation of their role in colon cancer cells.

5.2.5.1 Fbxl18-KO organoids lack the branching morphogenesis

Quantification of organoid morphological features over 7 days indicated that in contrast to the growth rate of control organoids (GFP transduced organoids), the Fbxl18-KO organoid typically grew at slower rates and was prone to develop smaller sized units (Figure 5-10; A & B). The phenotypical validation was also carried out via 2nd gRNA copy of Fbxl18 (right panel). The Fbxl18 Organoid KOs failed to differentiate, expand and did not undergo regular cryptogenesis features compared to control organoids. The qRT-PCR determined the markedly reduced expression of the Fbxl18 expression in Fbxl18-KO organoid using both gRNAs, (Figure 5-10; C). Red arrowheads indicate the number and distribution pattern of crypt-villus like domains in Fbxl18-KO vs control organoids (i.e. expressing Cas9). The surface area was calculated only in the expanding horizontal directions. Subsequently, the surface area of selected organoids was averaged and graphed. The surface area of growth (expansion rates) was also calculated for each selected organoid in each well, with the formula (Present Day Area / First Day Area) * 100, as previously reported (343).


A
Control (GFP)
Fbxl18 KO 1st gRNA
Fbxl18 KO 2nd gRNA
Day 1
Day 4
Day 7

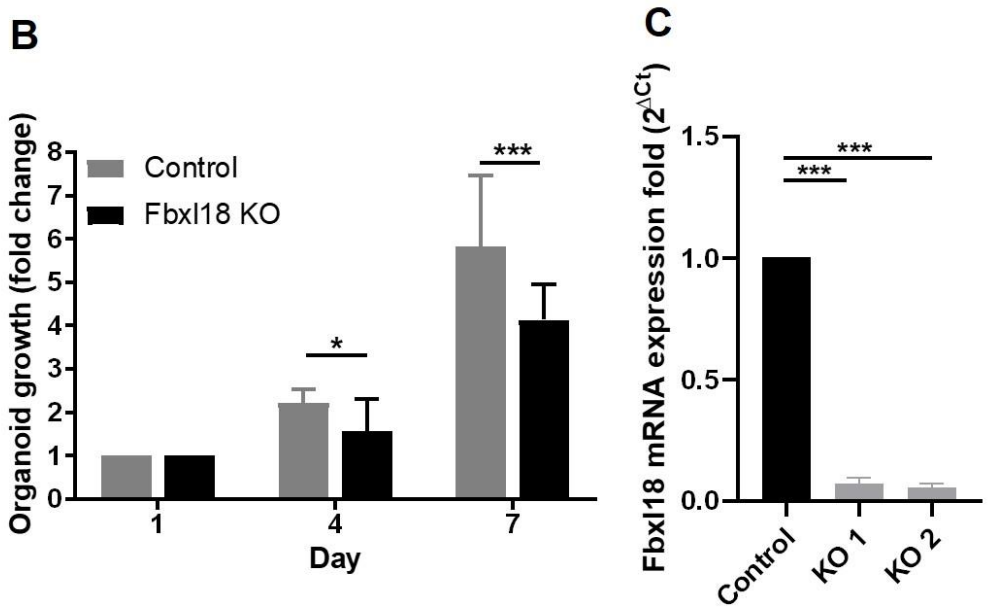


Figure 5-10. Fbxl18-KO characterized by loss of distinct growth and differentiation. A) The Fbxl18-KO organoid is associated with small overall size and significantly reduced budding and branching events in comparison to the control group. Scale bar: 75µm. **B**) The phenotypical and growth analysis indicates that the Fbxl18-KO organoids have slow-growing rate compared to control. The growth rate evaluated as previously described in chapter 3.1.1.1, (N=12) **C**) Validation of mRNA level disruption was done via qRT-PCR for both copy gRNA of Fbxl18 (P<0.001). Error bars represent mean ± S.D. *, P ≤ 0.05,***, P ≤ 0.001.

5.2.5.2 Phalloidin staining for F-actin filaments confirmed the compact and smaller morphology in Fbxl18-KO organoids

To verify the morphological differences of the KO candidate's vs control (GFP transduced organoids), the organoids were co-stained with Phalloidin dyes for cytoskeleton via F-actin staining and DAPI for detection of nuclei. The Fbxl18-KO organoids displayed a reduced size and compact integrity indicating potentially reduced differentiation activity compared to control organoids (Figure 5-11; A). Phalloidin staining revealed the lack of regular

expansion, a morphological characteristic of normal derived organoids, in functional units of Fbxl18 KO. In addition, the live/dead cell staining of Fbxl18-KO organoids using the PI and Hoechst, revealed no significant differences in PI dye uptake of Fbxl18 KO compare to the control group (Figure 5-11; B).

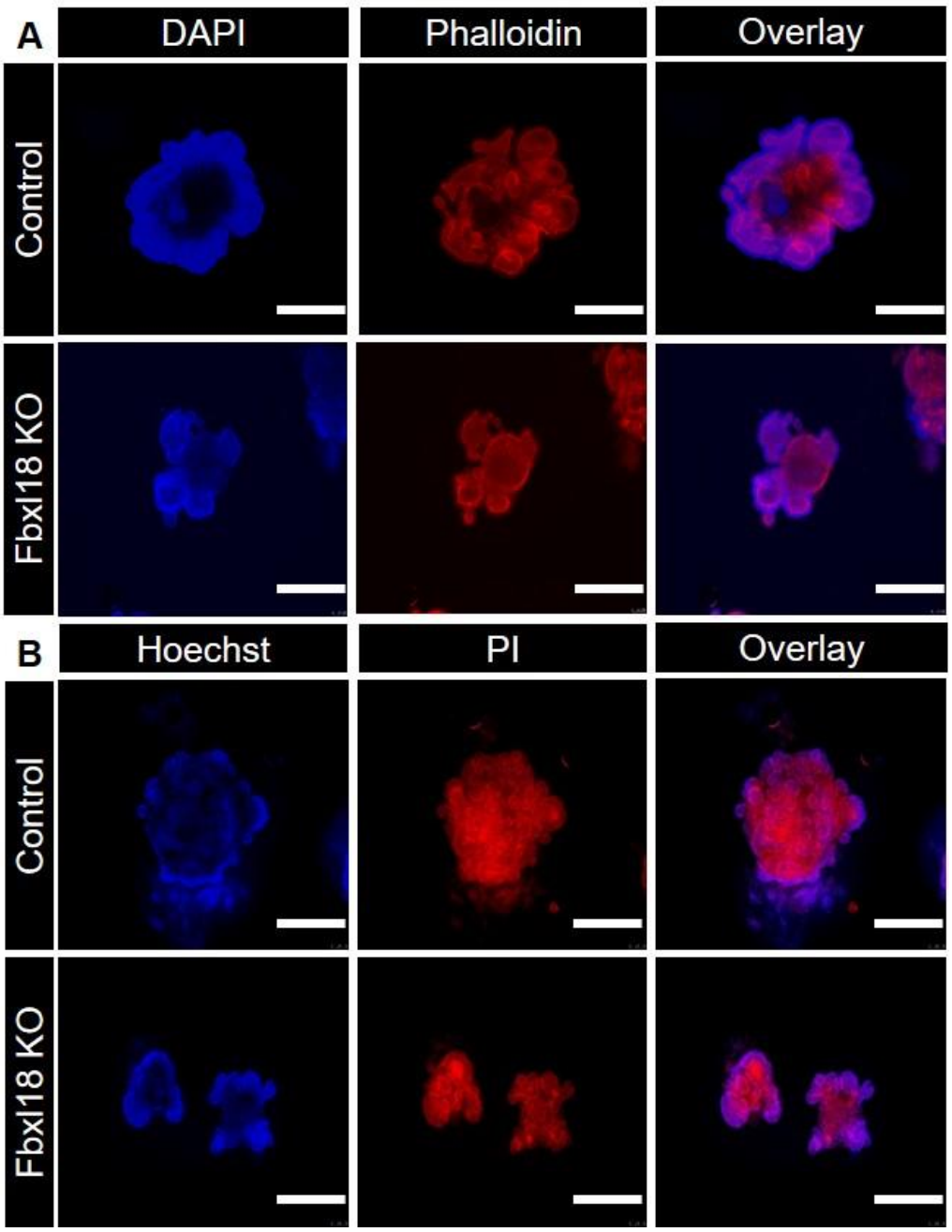


Figure 5-11. Fbxl18 KO developed small size crypt-villus like domain with the absence of distinct budding occurrence. A) To further validate the morphological differences in Fbxl18-KO vs control organoids, the Phalloidin staining was performed. The Phalloidin staining of whole-mount Fbxl18-KO organoids verified the presence of small-sized organoid with lack of branching in comparison to the controls. Scale bar: 75µm**. B)** There were no obvious differences in live/dead staining of Fbxl18-KO organoids compared to the controls. Scale bar: 75µm.

5.2.5.3 Fbxl18-KO organoids impeded the proliferation and viability in WST-1 cell proliferation assay

To further investigate the cell proliferation in organoids *in-vitro*, we exploited WST-1 proliferation assay. The proliferation status of KO and control organoids (consist of 4 wells with 15-30 organoids) were measured at day 1, 4, 7 and 9 of organoid culture (Figure 5-12). The reduced cell viability was evident in Fbxl18-KO organoids over 8 days in comparison to control group ($P<0.001$).

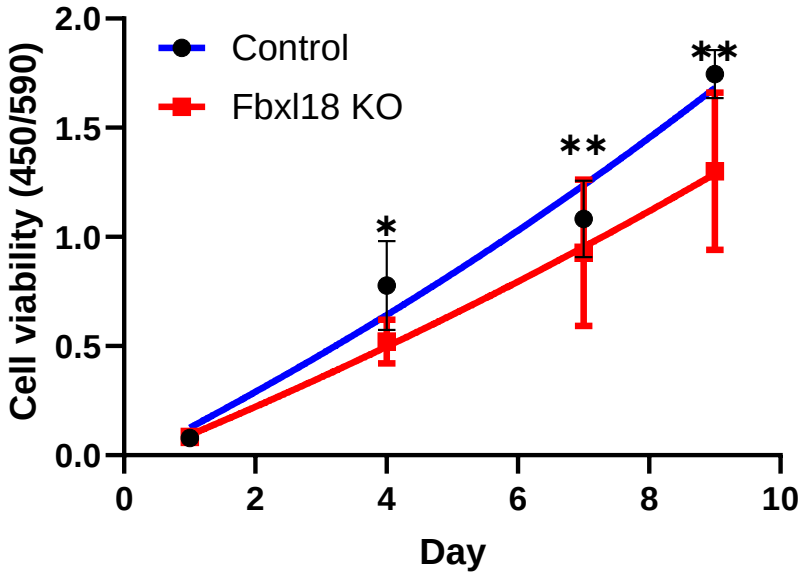
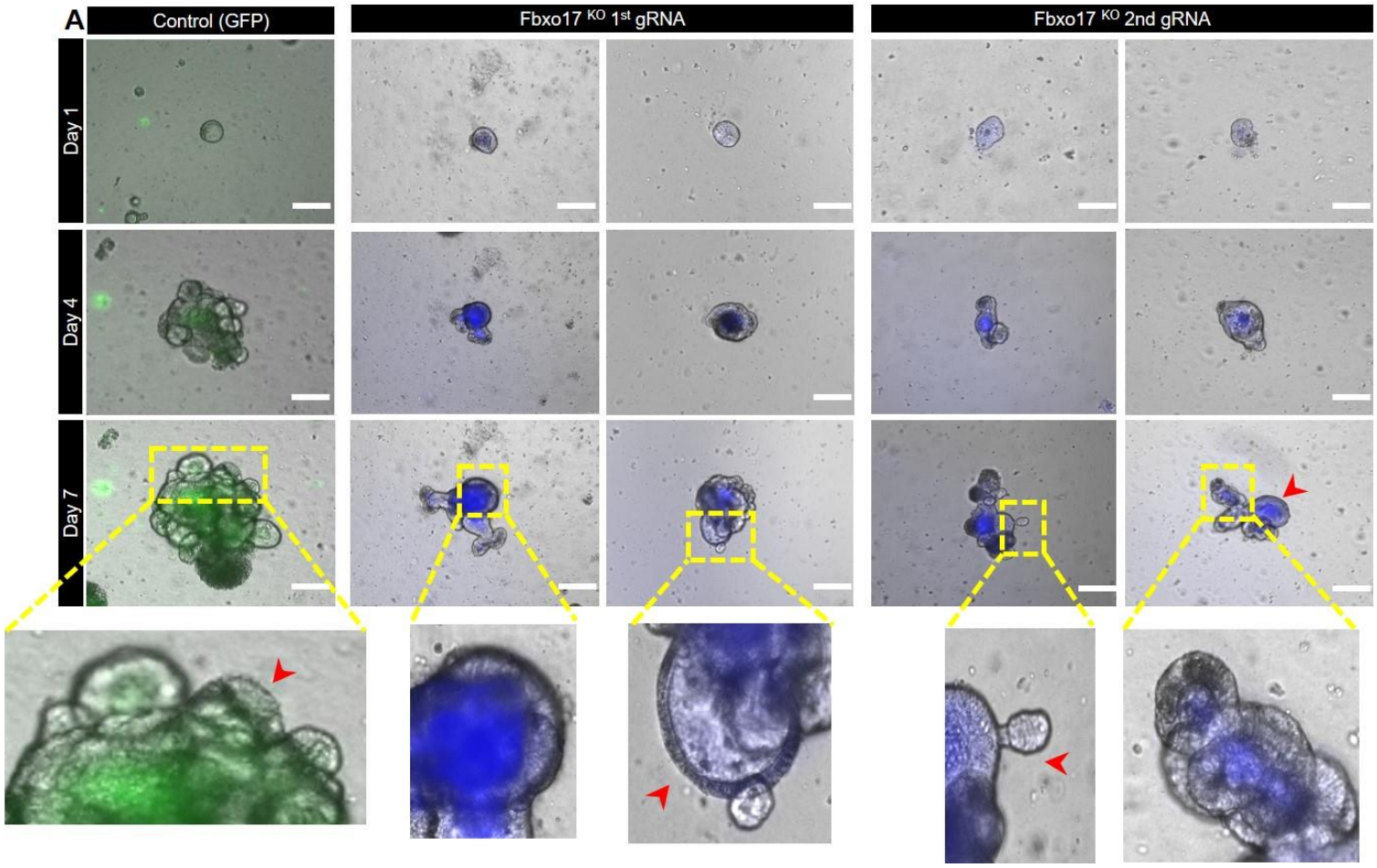


Figure 5-12. Fbxl18-KO suppressed cell proliferation in murine intestinal organoids. WST-1 proliferation assay of Fbxl18-KO organoid was carried out in days 1, 4, 7 and 9 of organoid growth. Our results revealed the significant reduction of cell viability in Fbxl18-KO organoids compared to the control groups ($P<0.001$). Error bars represent mean ± S.D. *, $P \leq 0.05$, **, $P \leq 0.01$.

5.2.5.4 Fbxo17-KO mouse organoids formed non-polarized and semi-colonoid morphology

The crypt-villus like domain showed extensive divergent phenotypical morphology in Fbxo17-KO. The engineered Fbxo17-KO organoids possessed a slow-growing and more elongated morphology or developed into a partially cystic structure with uneven differentiation appearances (Figure 5-13, A-B). Besides demonstrating with significantly reduced growth rate compared to controls, Fbxo17-KO organoids promoted to non-polarized or semi-rounded phenotypical formations. The similar results were obtained in the verification process using the second copy of Fbxo17 gRNA (Figure 5-13, A; right panel). Further qRT-PCR confirmed the remarkable reduction of expression levels in Fbxo17 mRNA relative to expression levels in control organoids (Figure 5-13, C). Red arrowheads indicate the number and distribution pattern of crypt-villus like domains in Fbxo17-KOs vs control organoids.


A
Control (GFP)
Fbxo17 KO 1st gRNA
Fbxo17 KO 2nd gRNA
Day 1
Day 4
Day 7

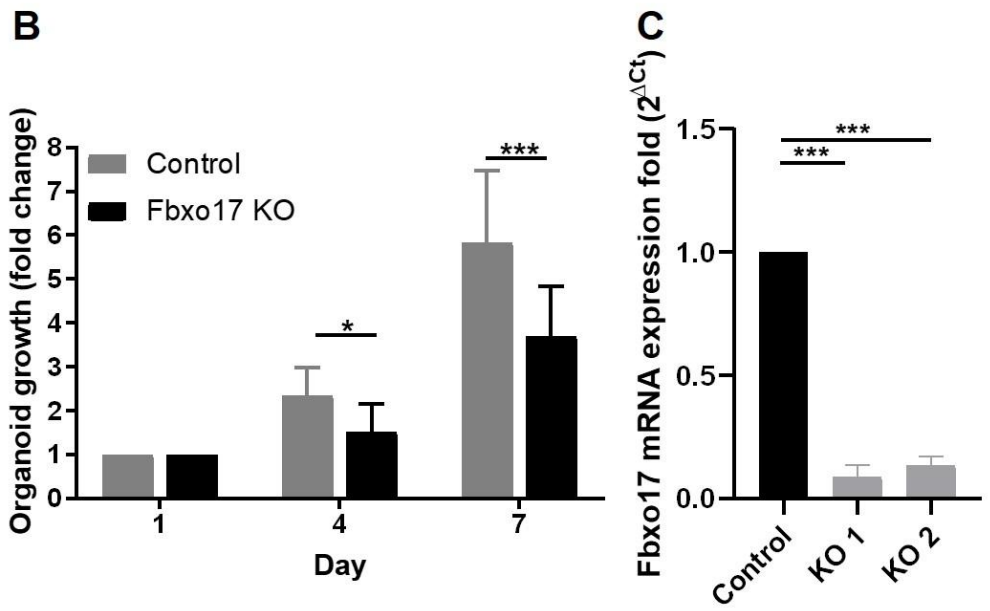


Figure 5-13. Fbxo17-KO organoids developed elongated and non-polarized phenotypical features. A-B) Fbxo17-KO organoids showed differential phenotypes in which the partially cystic or elongated morphology were dominant characteristics. Scale bar: 75µm. **B)** Monitoring and quantification of the growth rate over 7 days revealed evident decreased growth in Fbxo17-KO organoids compared to controls **C)** The expression of Fbxo17-KO was significantly decreased using both gRNA Fbxo17 copies. Error bars represent mean ± S.D. *, P ≤ 0.05, ***, P ≤ 0.001.

5.2.5.5 Fbxo17-KO organoids reproduced by morphologically asymmetric growth pattern

Further Phalloidin staining of Fbxo17-KO organoids demonstrated that the Fbxo17 organoids represented partially cystic or elongated phenotype and gave rise to non-polarized or semi-rounded morphologies as previously indicated in growth pattern analysis (Figure 5-13; A). Analysis of live/dead cell staining revealed no differences in Fbxo17-KO vs controls (Figure 5-14; B).

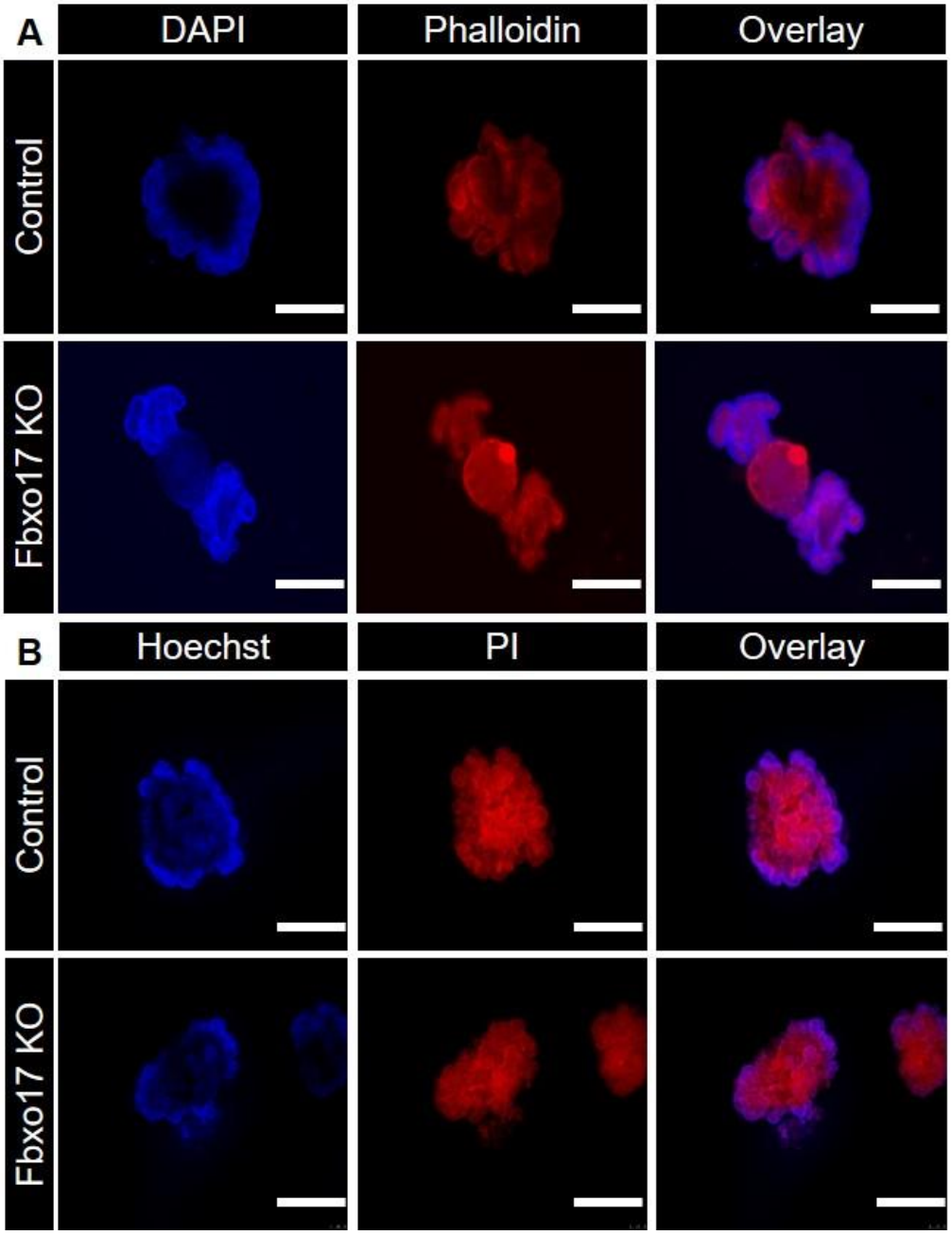


Figure 5-14. Phalloidin staining of Fbxo17-KO revealed the presence of various morphological entities. **A)** Consistent with the phenotypical analysis, immunofluorescence staining with Phalloidin revealed an altered morphology with elongated or partially differentiated or cystic crypt-like domains forming a colonoid structures in Fbxo17-KO organoids. Scale bar: 75 µm. **B)** Further live/dead cell staining of Fbxo17-KO showed no differences compared to control condition (GFP transduced). Scale bar: 75µm.

5.2.5.6 Fbxo17-KO reduced cell viability in murine intestinal organoids

Assessment of cell proliferation in Fbxo17-KO indicated that loss of Fbxo17 significantly decreased the proliferation activity of the engineered organoids in culture (Figure 5-15).

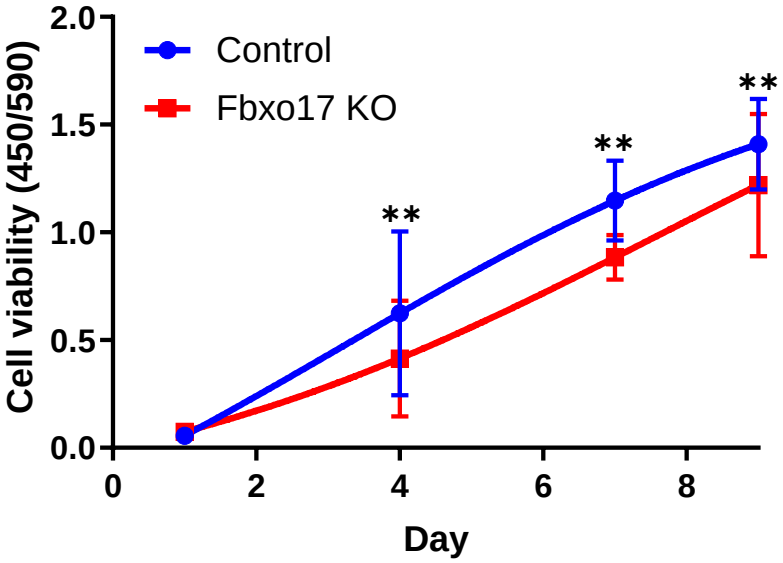


Figure 5-15. Loss of Fbxo17 associated with reduced cell viability in murine organoids. Further investigation of viability assay in Fbxo17-KO organoids indicated a significant loss of proliferation in day 1, 4 and 7 and 9 of organoid culture. Error bars represent mean ± S.D. ***, P ≤ 0.001.

5.2.5.7 Loss of Fbxl18 and Fbxo17 is associated with downregulation of proliferation and differentiation markers in intestinal organoids

Further characterization of Fbxl18 and Fbxo17 KO intestinal organoids were determined via qRT-PCR for cancer stem cells (CSC), proliferation, and differentiation markers including *LGR5*, *CD44*, *CTNNB1*, *Cryp1*, *Muc2*, *Olf4* and *ChgA*. As demonstrated in Figure 5-16, relative fold-change in mRNA

expression levels of all indicated markers significantly downregulated compared to control (mean ≥1.5-fold change), for both Fbxl18- and Fbxo17-KO organoids. The lack of budding morphogenesis and the decrease of proliferation is the main characteristics of both Fbxl18- and Fbxo17-KO organoids. Further investigation revealed that the Fbxl18 and Fbxo17-KO murine organoids associated with significantly decreased relative mRNA expression for differentiation and stem markers.

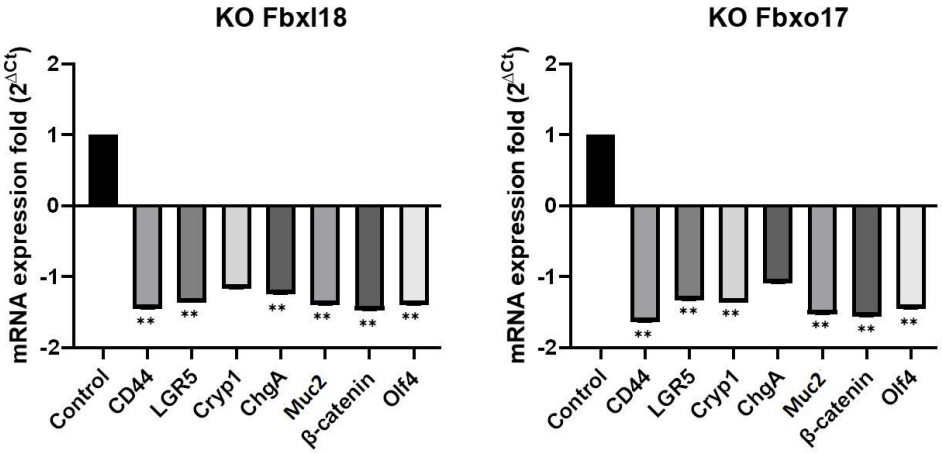


Figure 5-16. Fbxl18 and Fbxo17 KOs steered downregulation of proliferation and differentiation markers. Fbxo17 and Fbxl18 KOs characterized by significant decrease in *LGR5*, *CD44*, *CTNNB1*, *Cryp1*, *Muc2*, *Olf4* and *ChgA* expression levels. The suppression in proliferation and differentiation was apparent in the morphological assessment of Fbxl18- and FBXL18-KO murine organoids. All values represent means ± SD. ∗∗p< 0.01, denote significant differences between the groups, N=3.

5.2.6 Functional characterization of FBXL18 and FBXO17 KOs in human cancer cell lines

In order to characterize the FBXL18 or FBXO17 loss in tumorigenesis of colon cancer cells, the FBXL18 and FBXO17 KOs have been generated in DLD-1 colon cancer cells via LV transduction and following antibiotic selection with puromycin, 4μg/μl, (Figure 5-17). The genomic DNA was extracted from both KO cells and the sequencing validation was performed to validate the deletion via CRISPR gene edit using Sanger sequencing and blasting (Data not shown).

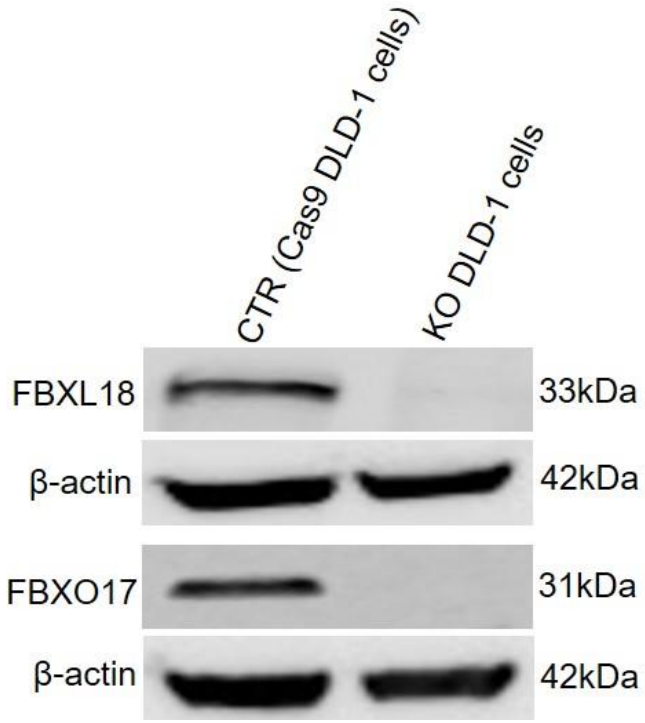


Figure 5-17. Generation of FBXL18- and FBXO17-KOs in DLD-1 cancer cells. The western blot analysis shows the complete absence of FBXL18 and FBXO17 expression in DLD-1 colon cancer cells.

5.2.6.1 FBXL18-KO developed non-polarized shape with lack of directed protrusions

The morphology of the FBXL18-KO and control cells (DLD-1 Cas9) was assessed via Phalloidin staining. Based on our findings, unlike the control cells which acquired multipolar rod shape structures with distinct directional protrusions spread around the edges, the flat and Non-polar cell architecture was dominant in FBXL18-KO cells (Figure 5-18, middle panel, yellow arrowheads).

This might imply the low migratory capacity of the FBXL18-KO compared to control group.

Furthermore, Phalloidin staining of the FBXO17-KO indicated that there were no differences in phenotypical morphology, size and shape of the FBXO17-KO compared to control in which the cells developed more polarized and tend to migrate towards the needle shape structures scattered throughout the cells (inset). Thus, loss of FBXO17 did not affect the cellular morphology of the DLD-1 cancer cells.

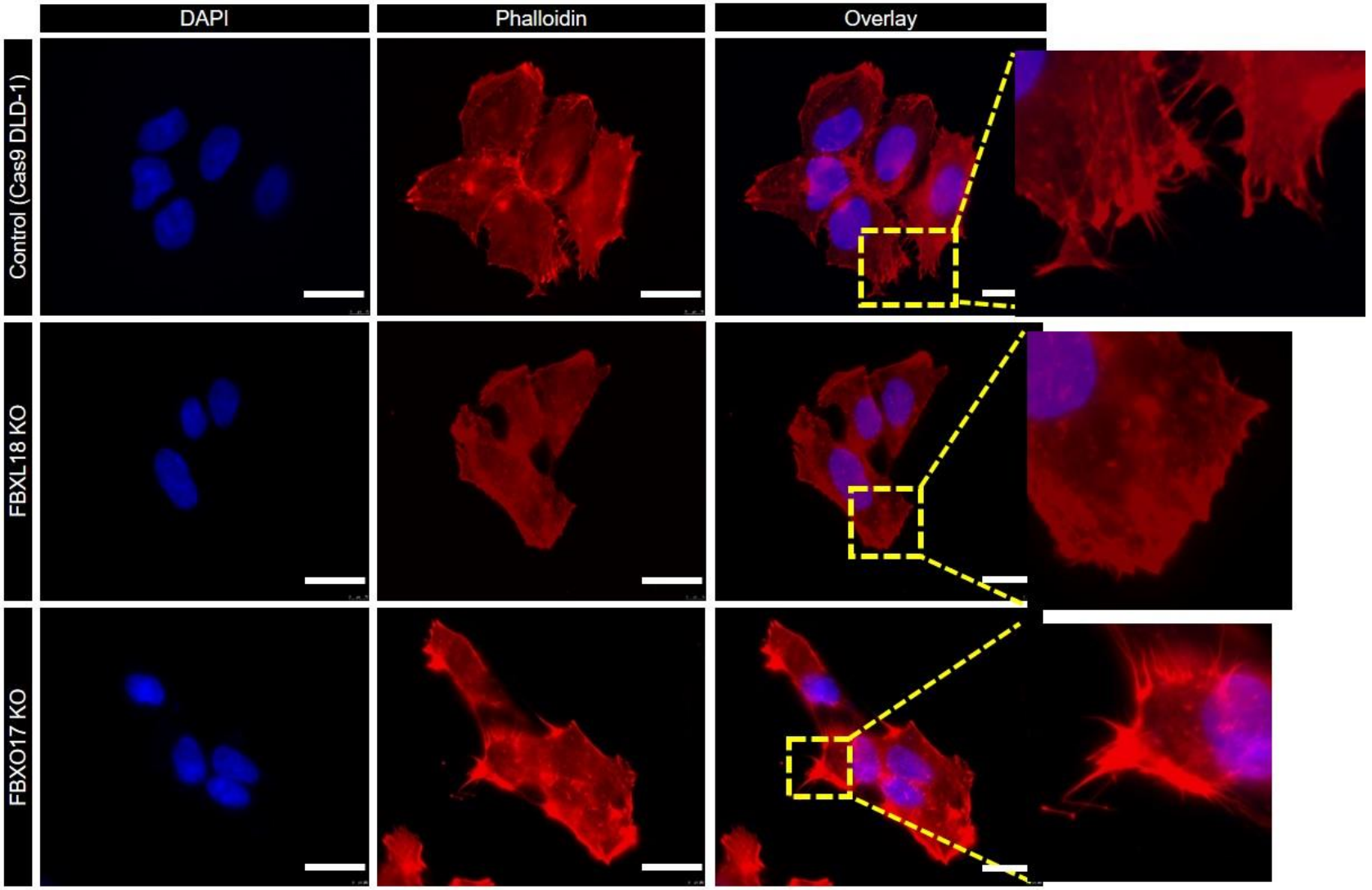

DAPI
Phalloidin
Overlay
Control (Cas9 DLD-1)
FBXL18 KO
FBXO17 KO

Figure 5-18. The FBXL18-KO characterized by the lack of defined polarized morphology compared to multi-polarised cell shape in control (Cas9 parental cells). The morphological analysis of the FBXL18-KO vs control (Cas9 parental cells) via Phalloidin staining revealed that FBXL18-KO cells tend to develop a non-polarised or flattened protrusions phenotype defined with lack of directional protrusions. This may indicate low migration activity of FBXL18-KO cells in comparison to control group. Bottom panel, investigating the morphological differences of FBXO17-KO and control cells revelled that there were no obvious differences in cell shape, morphology and size of the FBXO17-KO vs Cas9 parental cells, insets and yellow arrowheads. Scale bar: 7.5µm.

5.2.6.2 Loss of FBXL18 reduced the mobility of the DLD-1 colon cancer cells in Wound Healing Scratch Assay

The wound-healing assay was performed to evaluate the effect of FBXL18 and FBXO17-KOs on the migration of DLD-1 colon cancer cells. Wound closure was photographed at 0h, 24h and 48 after wounding (Figure 5-19; A). Downstream analysis of the FBXL18-KO for wound healing scratch assay showed a significantly decreased cell migration in 24h and 48h in comparison to control Cas9 DLD-1 cells (Figure 5-19; B). Further investigation of the wound healing closure for the FBXO17-KO compares to control cells revealed that FBXO17-KO did not impact the migration and motility of the colon cancer DLD-1 cells (Figure 5-19; B).

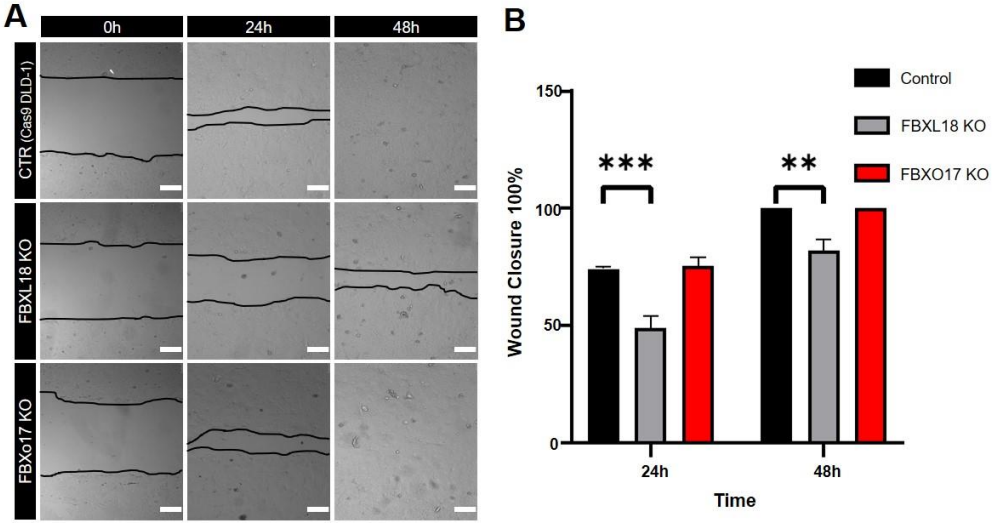


Figure 5-19. FBXL18-KO significantly decreased the migration of the cells in DLD-1 colon cancer cell line. A) Demonstrates the wound healing scratch assay of FBXL18- and FBXO17-KOs vs control (Cas9 DLD-1 parental cells). Scale bar: 75µm. **B)** Wound closure analysis showed that the migration ability and wound closure in FBXL18 cells was markedly reduced as compared with control cells (DLD-1 Cas9). Error bars represent mean ± S.D. **, P ≤ 0.01, ***, P ≤ 0.001.

5.2.6.3 Loss of FBXL18 impeded the proliferation of the DLD-1 colon cancer cells

The proliferation of FBXL18- and FBXO17-KOs cells was evaluated via growth curve analysis over 7 days. This analysis revealed that the cell proliferation was significantly impaired in FBXL18 KO cells in comparison to the parental cells at days 3 to 7 of analysis (Figure 5-20**)**. Furthermore, quantification of the growth curve showed that there were no differences between FBXO17-KO compared with parental cells indicating that loss of FBXO17 may not play a role in modulating the proliferation status of DLD-1 colon cancer cells.

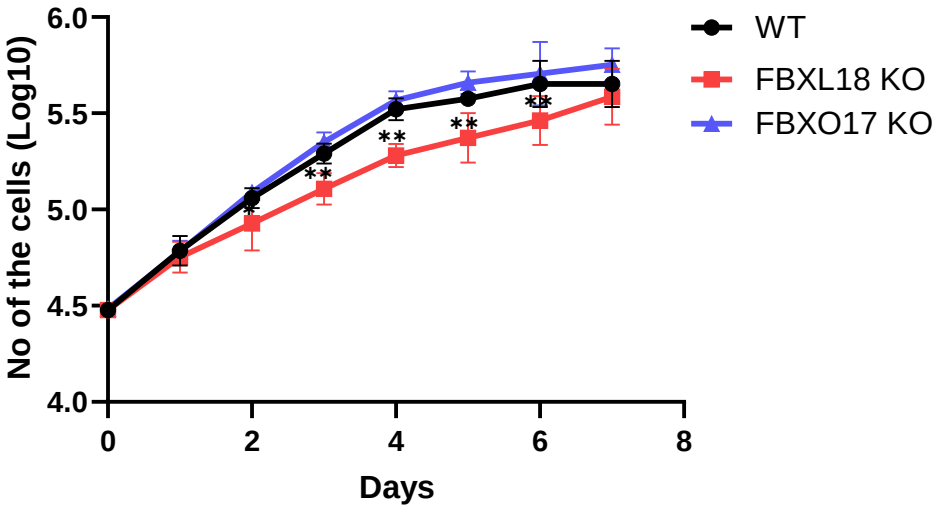


Figure 5-20. Lack of FBXL18 reduced the proliferation of the DLD-1 colon cancer cells in days 3-7. Loss of FBXL18 significantly inhibited the proliferation and growth of DLD-1 colon cancer cells. In addition, further assessment of FBXO17 KO for growth curve showed that the loss of FBXO17 had no effect on proliferation of the DLD-1 colon cancer cells after 7 days. Error bars represent mean ± S.D. Scale bar: 75 μm. ***, P ≤ 0.001, **, P ≤ 0.01.

5.2.6.4 The FBXL18-KO suppressed the colony-forming capacity of DLD-1 colon cancer cells

To investigate the colony formation efficiency of the FBXL18- and FBXO17-KO cells, the cells were seeded for 14 days and the number of the colonies were scored from three independent experiments (Figure 5-21; A, middle panel). Based on our findings the FBXL18-KO significantly hampered the colony-forming efficiency of DLD-1 colon cancer cells compared to control (Cas9 DLD-1 parental cells), (Figure 5-21; B). Furthermore, the FBXL18-KO developed smaller colonies when compared with parental cells.

The assessment of the colony formation showed that despite the formation of the larger colonies in FBXO17-KO cells, there were no significant differences in the number of the colonies compared with control (Cas9 DLD-1 parental cells), (Figure 5-21; A&B).

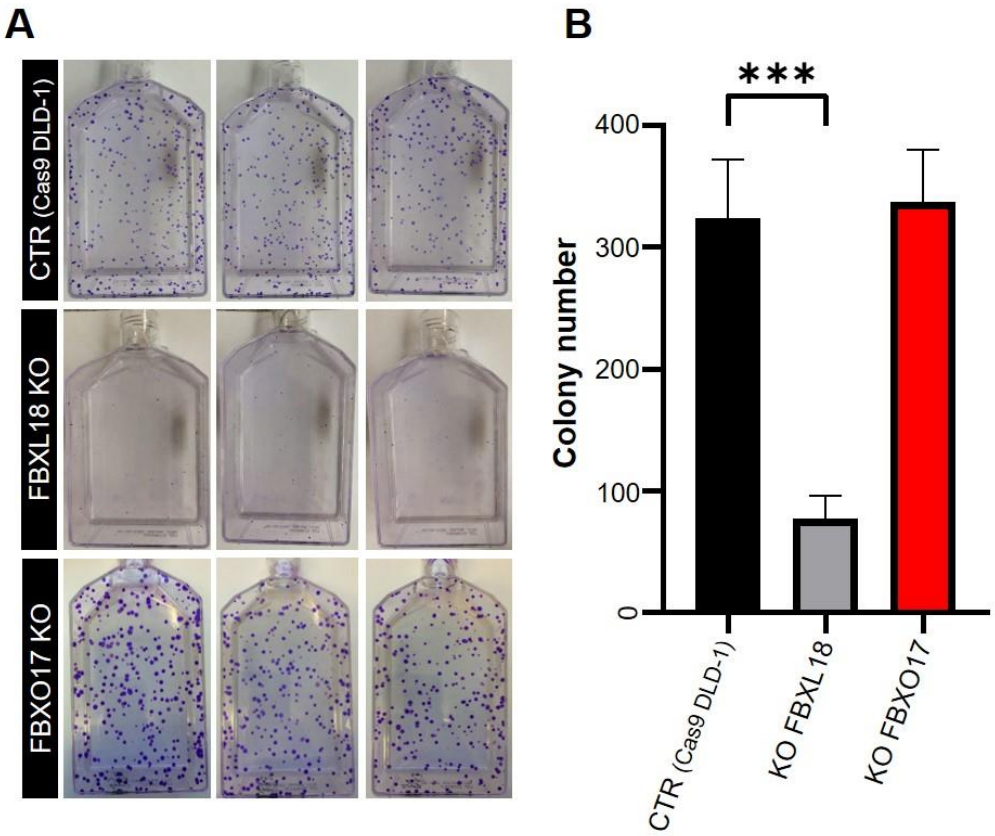


Figure 5-21. The FBXL18-KO inhibited the colony-forming efficiency of colon cancer cells compared to control (Cas9 DLD-1 parental cells). Further evaluation of the FBXL18 and FBXO17 KOs for colony-forming assay for 14 days indicated that the FBXL18 significantly decreased the colony formation of the DLD-1 cancer cells (middle panel). In addition, the result of colony formation assay in FBXO17 showed that the cells developed slightly larger colonies compared to controls. However, there were no significant differences in the number of colonies compared to control condition ($P<0.001$). Error bars represent mean ± S.D. ***, $P \leq 0.001$.

5.2.7 CRISPR/Cas9 mediated deletion of FBXL18 and FBXO17 in patient tumour organoid

Cancer develops through a multistep process of tumourigenesis and CRC as a traditional paradigm is defined by the sequence loss of tumour suppressors such as *APC*, *P53*, *SMAD4* and activation of oncogenes including *KRAS*, *BRAF* and *PIK3CA*. Thus, we aimed to investigate whether the simultaneous loss of candidate F-box expression (FBXL18 or FBXO17) pooled from the screening with CRC driver genes would mediate the progression of the malignant condition or may initiate adverse tumour-promoting events. To address this issue using the organoid-driven model and considering the translational approach in human counterpart, we required a 3D model harbouring a mutation in CRC driver genes to introduce the knockout for F-BOX (FBXL18 and FBXO17). Thus, we adopted the colonic tumour organoids as previously described in chapter 3 to engineer the KO tumour-derived organoids for FBXL18 and FBXO17.

5.2.7.1 Generation of intestinal tumour organoid expressing Cas9

LV transduction was conducted to produce the Cas9 expressing organoids from 2 types of colon tumour organoids (Figure 5-22). The tumour organoids (patients no1 and 2; chapter 3.2.2) underwent the antibiotic selection 48-hour post-transduction with G418 for 6 rounds before the last step of expansion and further validation with the WB. Middle panel illustrates the transduction of tumour organoids with the GFP expressing vectors for the evaluation of transduction

efficiency. The bottom panel shows the selection of the non-transduced tumour organoids with the G418, 200-250µg/ml.

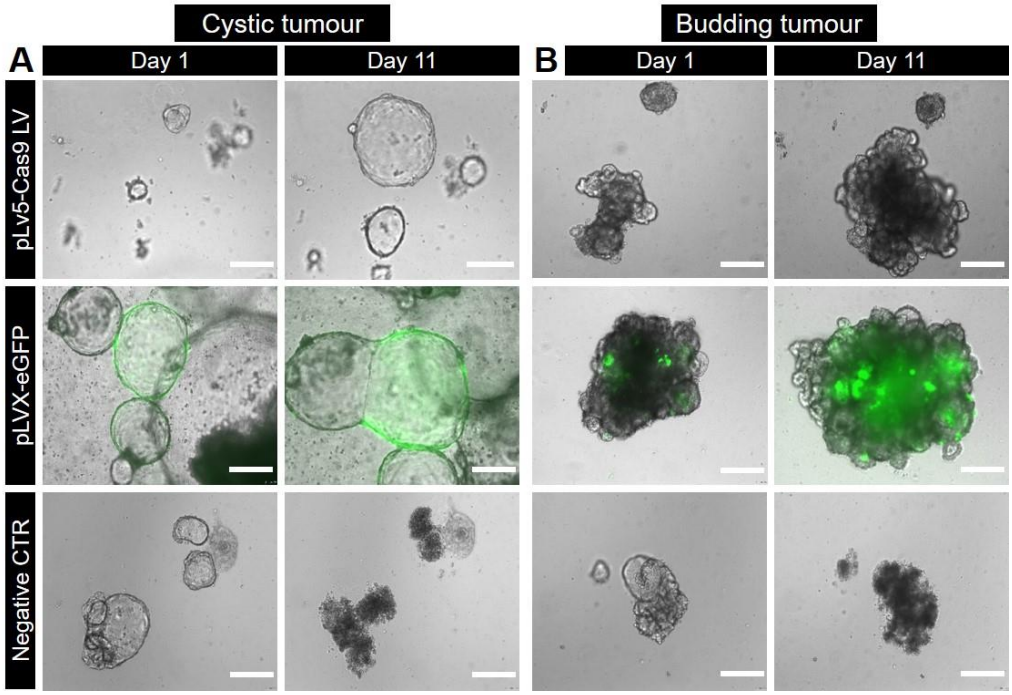


Figure 5-22. Generation of stable Cas9 expressing colon tumour organoid via LV transduction. A & B) Top panel demonstrates the generation of stable Cas9 expressing organoid from cystic and budding colonic tumour organoids after LV transduction. The middle panel shows the GFP transduced organoids (positive control) and the bottom panel is the negative control. As the cystic type of tumour-derived organoid displayed resistance to the antibiotic, 250µg/ml of antibiotic G418 was applied. The selection initiated 48 hours after transduction and lasted for a total of 6 rounds (until all non-transduced controls died). The selected organoids re-cultured again and underwent another 5-6 rounds of antibiotic selection. The organoids then cultured in the antibiotic-free condition and expanded for the validation step via western blot analysis. Scale bar: 75µm.

To further confirm the expression of Cas9 in transduced colon tumour organoids, the selected organoids passaged in free-antibiotic culture medium and expanded

for validation. The WB analysis for Cas9 ab shows the strong expression of Cas9 protein in both tumour-derived organoids (Figure 5-23).

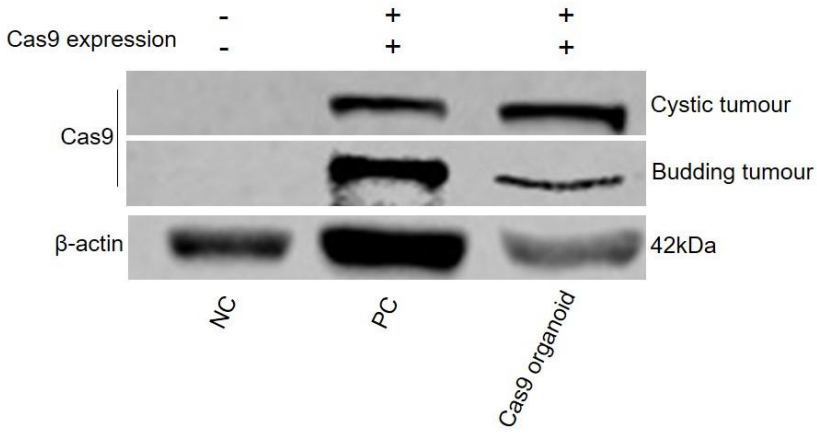
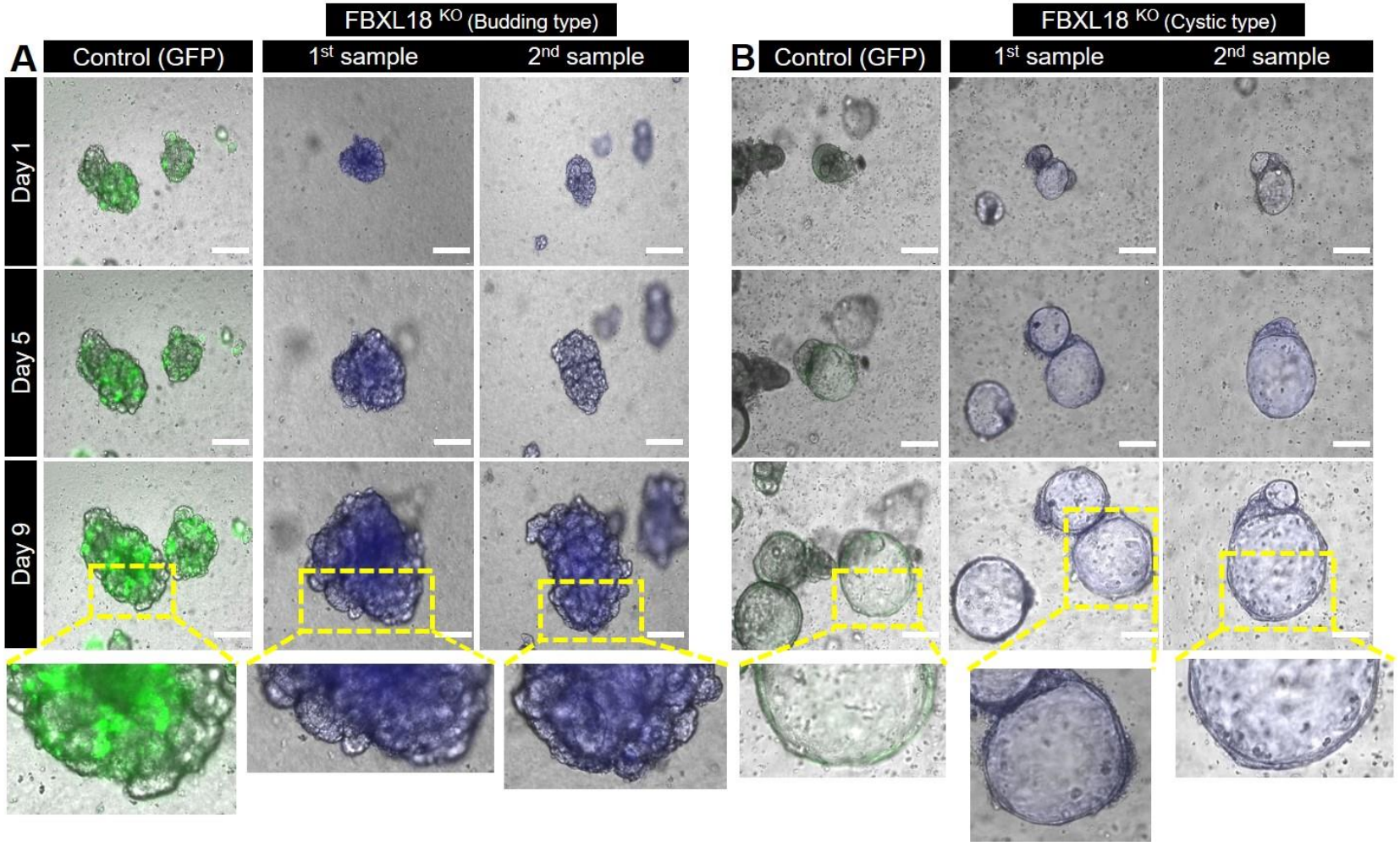


Figure 5-23. Validation of stable tumour organoid expressing Cas9. The WB validation of the tumour-derived organoids (budding and cystic) confirmed a significant expression of Cas9 protein in both conditions.

To evaluate the effect of FBXL18 and FBXO17 loss in tumour organoids and to explore whether the loss of FBXL18 or FBXO17 influence the phenotypical morphology of the tumour-derived organoids, promoting or suppressing the growth pattern as determined in murine counterparts, the Cas9 expressing colon tumour organoids (cystic and budding types) were separately transduced with FBXL18 and FBXO17 gRNA.

5.2.7.2 Lack of FBXL18 expression did not affect colon tumour organoids

Based on our findings, loss of FBXL18 had no effect on phenotypical alteration and growth rates of the colon tumour organoids in neither cystic nor budding type when compared to their GFP transduced controls over a period of 9 days (Figure 5-24; A, B&C). Quantification of the relative mRNA expression determined the significant downregulation of the FBXL18-KO vs control (cystic tumour type), (Figure 5-24; D).


FBXL18 KO (Budding type)
FBXL18 KO (Cystic type)
A
B
Control (GFP)
1st sample
2nd sample
Control (GFP)
1st sample
2nd sample
Day 1
Day 5
Day 9

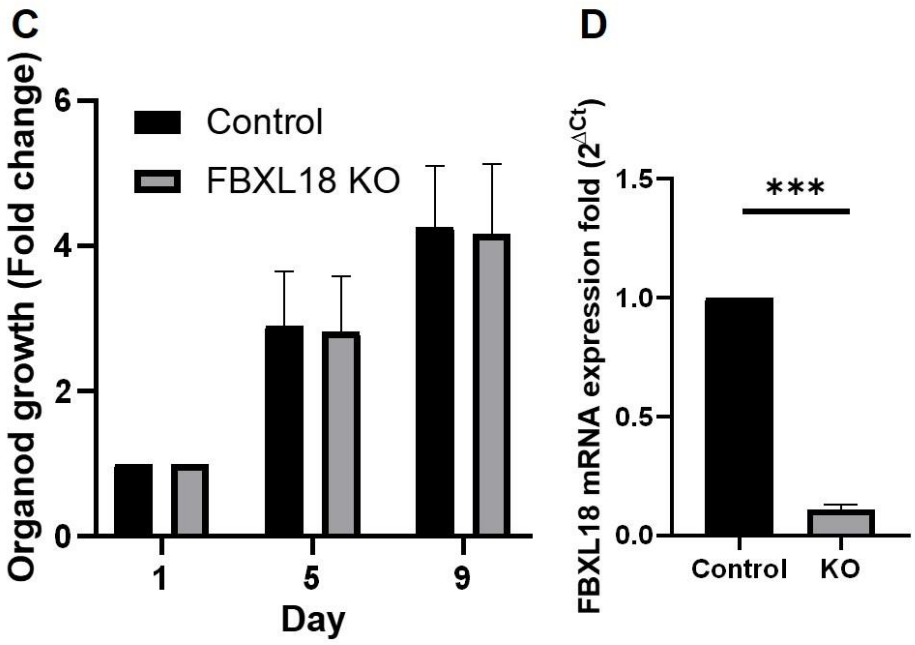
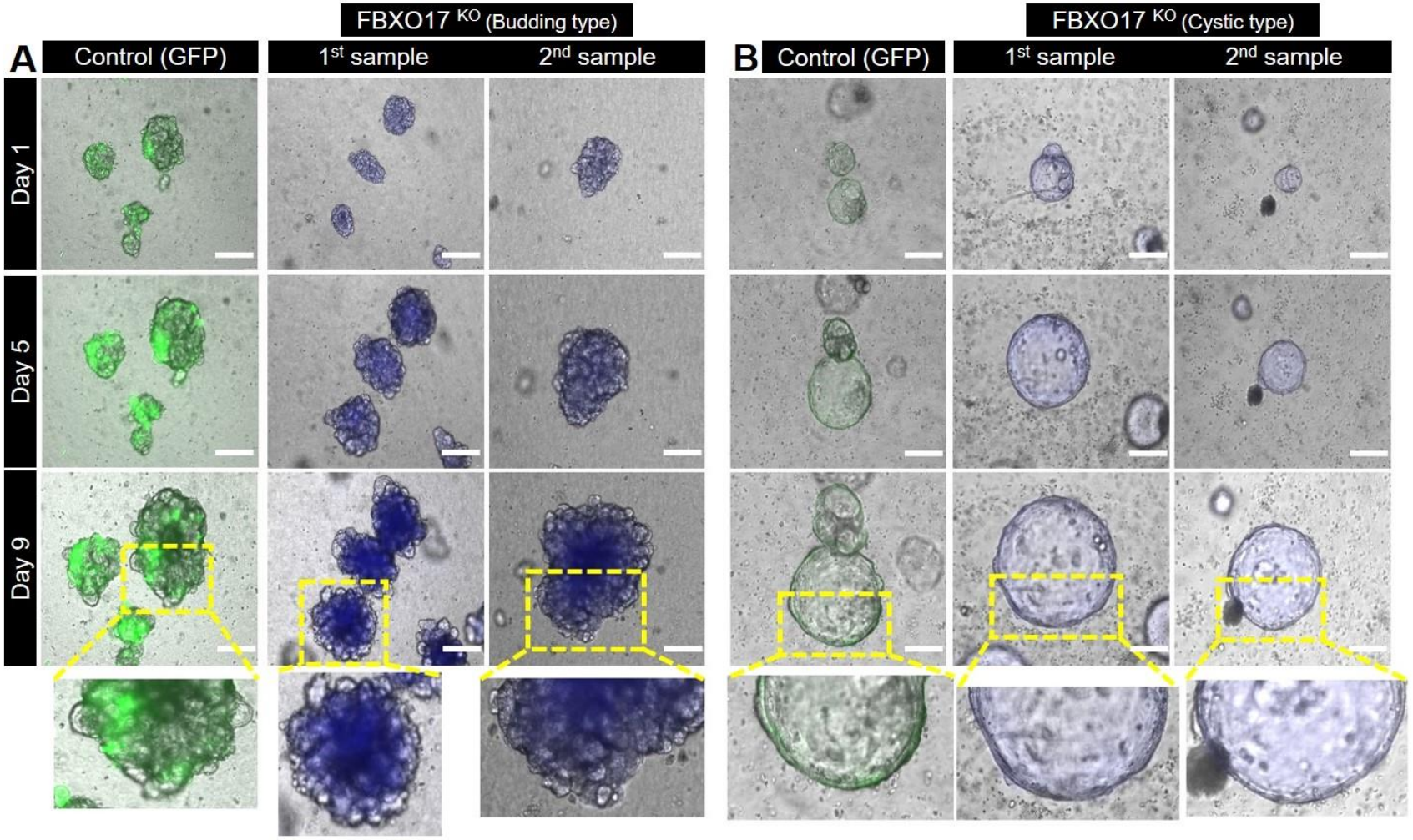


Figure 5-24. Loss of FBXL18 did not alter the key aspect of colonic tumour-derived organoids morphology in culture. A) Demonstrates the generation of FBXL18-KO tumour organoid from budding tumour type. Scale bar: 75µm. **B)** Engineering of the FBXL18-KO from cystic tumour type. The loss of FBXL18 had no effect on size, shape and morphology of neither the cystic nor budding colonic tumour organoid compared to control group. Scale bar: 75µm. **C)** The representative quantification of the growth rate for budding tumour organoids revealed that there were no differences in the growth rate of FBXL18-KO vs control groups. **D)** The mRNA expression level of the FBXL18-KO was significantly reduced (P<0.001) compared to control group (cystic tumour type). Error bars represent mean ± S.D. ***, P ≤ 0.001.

5.2.7.3 Coexistence of loss of FBXO17 and CRC tumour driver genes did not alter the phenotypical features of colonic derived organoids

Further assessment of FBXO17-KO morphology in colon tumour-derived organoids demonstrated in Figure 5-25; A&B. There were no significant differences in shape, size and growth rate between the control and FBXO17-KO after 9 days in both cystic and budding tumour organoid types, (Figure 5-25; C).

Further characterization of the mRNA expression level also revealed that the FBXO17-KO displayed remarkably reduced expression in comparison to control (GFP transduced), (Figure 5-25; D), ($P<0.001$). Error bars represent mean ± S.D. Scale bar: 75μm. ***, $P \leq 0.001$.


FBXO17 KO (Budding type)
FBXO17 KO (Cystic type)
A
B
Control (GFP)
1st sample
2nd sample
Control (GFP)
1st sample
2nd sample
Day 1
Day 5
Day 9

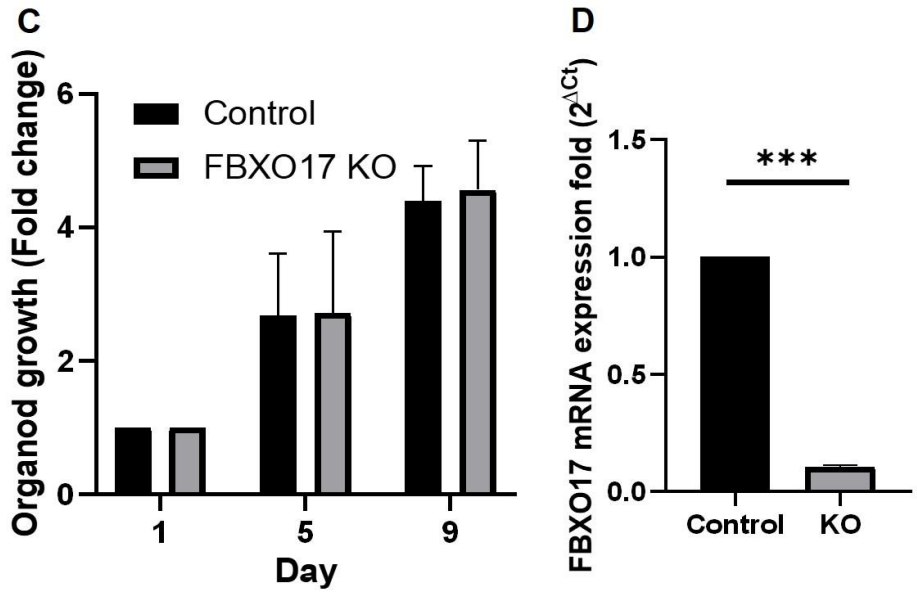


Figure 5-25. Lack of FBXO17 had no effect on phenotype and growth rate of human colon tumour organoids. A) Left panel represents the morphology of the FBXO17-KO cystic tumour colonic organoids vs control. Scale bar: 75µm. **B)** Demonstrates the phenotypical analysis of the FBXO17-KO budding tumour organoids. Scale bar: 75µm. **C)** There were no obvious growth differences between FBXO17-KO tumour organoids in cystic and budding tumour type compared to control. **D)** Reduction of target mRNA expression of FBXO17 was further determined by qRT-PCR, ($P<0.001$), Error bars represent mean ± S.D. ***, $P \leq 0.001$.

Our findings on tumour-derived organoids indicate that the simultaneous combination of loss of FBXO17 or FBXL18 and mutations in driver genes did not inhibit the tumorigenesis in 3D model of colorectal cancer.

5.3 Discussion

The recent advent of organoid culture has allowed the development of an *in-vitro* model that mimics several aspects of original tissue and the malignant condition (51, 65, 426-429). The newly genome-engineering tool, CRISPR/Cas9 endonuclease system support pin-point manipulation of a gene in any biological models. Providing a phenomenal tool for generating genetically modified *in-vitro* models capable of both "knock-in" and "knockout" of selected genes, CRISPR/Cas9 is widely applied for generating *in-vitro* cellular models.

In addition, molecular genetic methods have to be adopted in order to utilize this 3D organoid model in depth. To further develop organoid as a useful model system, new, precise methods to generate loss-of-function mutations have been introduced in organoids (e.g. targeted gene knockout) demonstrating both an ideal platform and tool for assessing the function of individual genes in multiple tissue types without the limitations and ethical implications of generating full *in-vivo* models (340, 424, 430, 431). This study illustrates for the first time, a screening-based method of generating CRISPR/Cas9 mediated knockout organoid lines, representing a significant step forward in reducing and replacing the use of animal models in research. With CRISPR/Cas9 induced-accurate mutations and organoids, faithfully representing their origin tissues, it is now possible to model how individual genes may affect multiple tissue types or explore how a particular tissue type is affected by knockout without the cost and ethical considerations of *in-vivo* alternatives. While organoids will not completely replace animal models in research, they provide both a middle-ground option and triage method for future work. Herein we demonstrated a

screening method, utilized a combination of CRISPR/Cas9 system and mouse intestinal organoid to produce an alternative *in-vitro* model of gene manipulation in comparison to two-dimensional models. CRISPR/Cas9-mediated mutagenesis-based screening method for investigating the phenotypical morphology of large candidate genes with unknown/poorly identified function can provide a promising approach, which facilitates the rapid and accurate identification of new genes involved in development and disease.

The procedure for CRISPR/Cas9 mediated screening of F-box genes in intestinal organoid is outlined in Figure 5-26, A-I. Following the generation of the lentiviral (LV) gRNA library of F-box genes (Figure 5-26; A), the gRNA library was validated through restriction enzyme digestion, sequencing of F-box gRNAs and biological analysis of selected gRNA in human cell lines including HEK293-T cells and DLD-1 colon cancer cells, (Figure 5-26; B). The lentivirus containing CRISPR gRNA were generated for further transduction of intestinal organoids (Figure 5-26; C). In parallel, the transgenic organoids line expressing Cas9 were generated through LV transduction and antibiotic selection (Figure 5-26; D-E). Following transduction of Cas9 organoids with gRNA library of F-box DNA, the phenotypical morphology alterations of the organoid KOs were evaluated for selection and further downstream analysis (Figure 5-26; F-I).

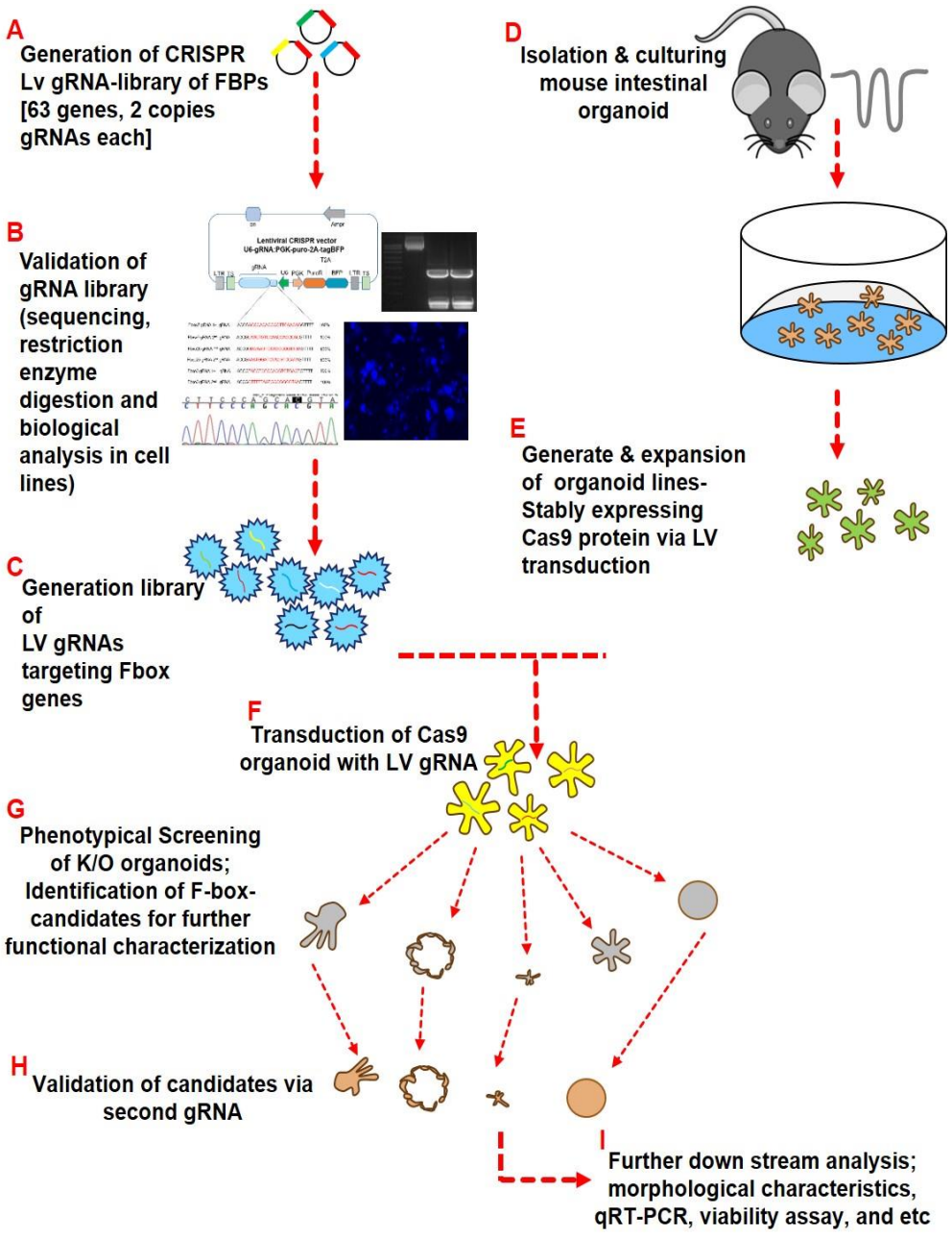


Figure 5-26. The schematic diagram of the CRISPR/Cas9 genetic-based screening of F-box domain E3 ligase in intestinal organoids. A) The generation of the gRNA library targeting the F-box genes (63 pair; 126 total), **B)** gRNA validation via restriction enzyme digestion and sequencing and generation of the KO colon cancer cell lines. **C)** LV production of gRNA library of F-box genes using 2nd generation of packaging plasmids. **D-E)** Isolation of the murine intestinal organoids and generation of the stable organoids

expressing Cas9 endonucleases. **F)** Engineering the knockout organoids for F-box genes via transduction of Cas9 expressing organoids with specific F-box gRNA. **G&H)** phenotypical evaluation of the KO-organoids based on the control (GFP transduced) for identification of the candidates. **I)** downstream analysis of the KO candidates for possible contribution in homeostasis and disease progression.

The biological function of the majority of the F-box proteins in CRC is poorly identified. CRISPR/Cas9 mutagenesis of intestinal organoids linked to the profound phenotypical alterations in several recent studies. Matano et al. introduced a CRISPR/Cas9-mediated sequential mutations in organoids derived from the normal human intestinal epithelium (347). They demonstrated that engineered organoids harbouring mutations at driver genes including *APC*, *SMAD4* and *TP53*, *KRAS* and/or *PIK3CA* grew independent of niche factors similar to the tumour counterparts and developed tumours upon transplantation kidney subcapsule in mice. Inconsistent with the previous study, Drost and colleagues also utilized the CRISPR/Cas9 to engineer intestinal organoids mutated for *APC*, *KRAS*, *TP53* and *SMAD4*. They revealed that simultaneous inactivation of *APC* and *P53* drive the extensive aneuploidy, the main feature of tumour progression (432). In another study, CRISPR/Cas9 mediated engineering of intestinal organoids in cystic fibrosis patients was successfully applied to repair the deletion at position 508 of cystic fibrosis transmembrane conductor receptor (CFTR) (433).

To our knowledge, there have not been reports of CRISPR/Cas9 screens in organoids. The principle for the assessment of organoid KO was monitoring the

engineered organoid growth pattern for varies types of phenotypic traits. This possible differential phenotypic diversity is the indication of an underlying possible loss of F-box gene activity via CRISPR/Cas9 mediated process. In the meantime, one of the main advantages of using organoids derived from normal epithelium for screening-based methodology is that any abnormal phenotypical alterations might be the pure reflection of the loss of related genes which enables the comparison analysis with not only the control un-transduced samples but also other KO organoids. In the meantime, the morphological analysis of the KO-organoids further to transduction of Cas9 organoids with gRNA of the F-box DNA, was performed in the antibiotic-free culture medium. Post phenotypical investigation, the candidate KO-organoid selected for further characterization and downstream analysis via Phalloidin and PI staining, q-RT PCR, proliferation assay and etc. CRISPR/Cas9 mediated screening of F-box genes narrowed our findings to two top candidates with differential phenotypical alterations including Fbxl18 and Fbxo17.

F-box and leucine rich repeat protein 18 (FBXL18) also denote as Fbxl18, located at chromosome 7 (7p22.1) consists of 7 exons and has been reported in different types of cancer via mediating proteasome degradation of several substrates (434-437). The intracellular FBXL18 RNA expression in various types of cancers is illustrated in Figure 5-27; A, (Human Protein Atlas). RNA-seq data analysis also revealed that CRC patients with FBXL18 high expression acquired a poor prognosis compared to patients with lower expression of FBXL18 (Figure 5-27; B) (Human Protein Atlas). In our morphological analysis we observed that the Fbxl18-KO profoundly decreased the growth rate of the

mouse intestinal organoids in culture (Figure 5-10). Further analysis of viability assay also confirmed the reduced proliferation activity in WST-1 assay (Figure 5-12). In addition, DLD-1 cancer cells demonstrated flattened morphology in Phalloidin staining with significantly reduced cell mobility in loss of FBXL18 as confirmed in wound healing scratch assay indicating the low migratory capacity of latter cells (Figure 5-19). Our result on proliferation assay of FBXL18 KODLD-1 cells also affirmed the significantly decreased proliferation activity in days 3-7 compared to controls (Figure 5-20). Assessment of the colony formation assay showed that the cells with loss of FBXL18 tended to develop few numbers of colonies characterized by remarkably small size in comparison to control cells (Figure 5-21).

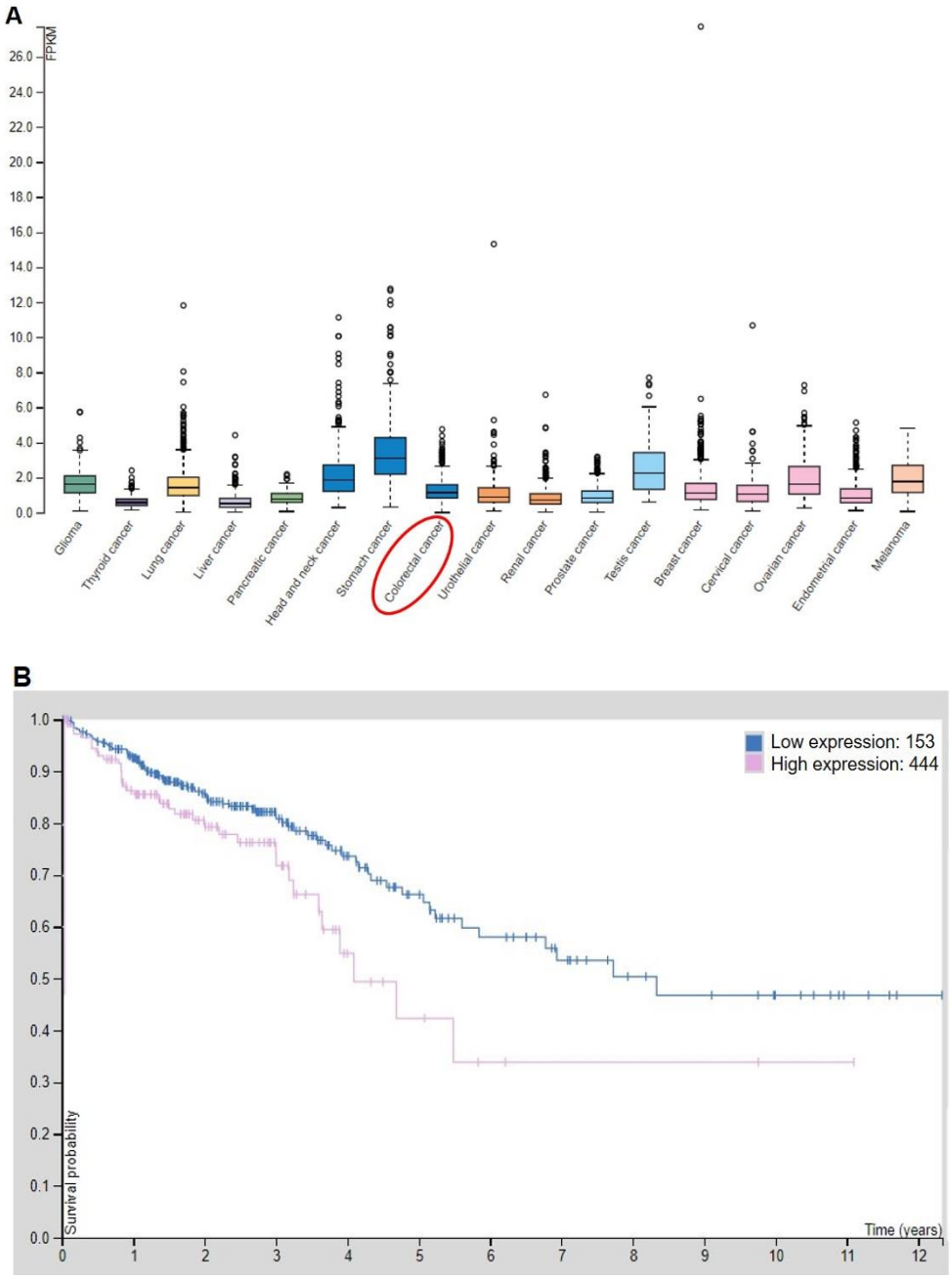


Figure 5-27. The RNA expression profile of FBXL18 in different cancer tissue. A) Demonstrates the RNA expression pattern of FBXL18 in 17 types of tumour tissues. **B)** The FBXL18 high expression is associated with poor survival in patients with CRC (P<0.001). (Adopted from Human Protein Atlas, https://www.proteinatlas.org/ENSG00000155034-BXL18/pathology/colorectal+cancer).

The previous study also revealed that the FBXL18 modulates the polyubiquitylation and following proteasomal degradation of the Fbxl7 (an F-box protein promoting the apoptosis in HELA cells) (434). Liu et al. demonstrated that the apoptotic mediated effects of Fbxl7 were elevated in lack of FBXL18 expression. In addition, expression of FBXL18 reduced the apoptotic activity of overexpressed FBXL7 in HELA cells. This result indicates that the FBXL18 mediates the apoptosis via proteasomal degradation of pro-apoptotic protein Fbxl7 (434). Increasing evidence also revealed that the Fbxl18 regulates leucine-rich repeat kinase 2 (LRRK2) ubiquitination and proteasome degradation in Parkinson's disease (PD). In addition, the Fbxl18 inhibited the cell death induced LRRK2 activity via suppression of caspase 8 in neuroblastoma SH-SY5Y cells (436). Further works indicated that the expression of the FBXL18 has been remarkably elevated in glioma primary tissues. Moreover, FBXL18 reported functioning as an oncogene F-box via inducing K63-mediated ubiquitination of AKT in glioma (437). Jindong Zhang et al. showed that the loss of FBXL18 significantly impeded the AKT activity in glioma cell lines (437). Inconsistent to our result suggesting the apoptotic activity of the KO FBXL18 (Figure 5-28), their findings on U251 and T98 glioma cell lines confirmed that the knockdown of FBXL18 remarkably inhibited the proliferation of the glioma cells while promoting the apoptotic activity.

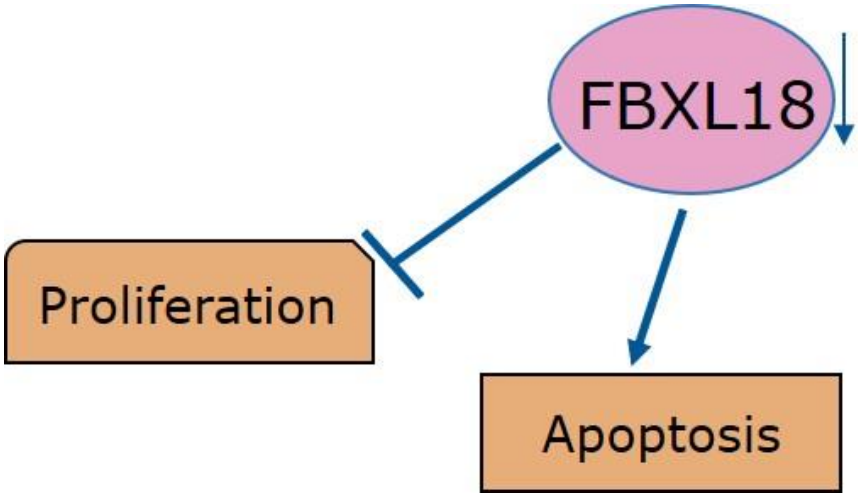


Figure 5-28. The schematic biological activity of the FBXL18 in CRC cell lines and colonic tumour organoids.

Altogether, our results on normal murine derived organoids and DLD-1 colon cancer cells indicated the suppression of proliferation, growth rate and migration in lack of FBXL18 expression on these two different models. Considering the previous data indicated the higher expression of the FBXL18 correlated with poorer survival in CRC tumours, our results suggesting that the loss of FBXL18 might attenuate the tumorigenesis of colon cancer cells via suppressing the proliferation of the cancer cells.

On the other hand, F-box protein 17 (19q13.2) also known as FBG4; FBX26; Fbx17; FBXO26 contains 7 exons. FBXO17 has been reported in modulating several malignancies including glioma and lung adenocarcinoma (438-440). The expression of the FBXO17 in colorectal tumours is relatively low compared to other malignant tissues (Human Protein Atlas). The previous clinical data revealed that CRC patients with high expression of FBXO17 possess lower survival than other individuals, (Figure 5-29, A&B). In the present study,

Fbxo17 KO murine intestinal organoids acquired diverse morphological appearances from partially cystic structure to irregular elongated morphology (Figure 5-13). Further colonogenic assays of KO DLD-1 cells for Fbxo17 also did not show to impact the proliferation and colony formation of the cells in comparison to parental control cells (Figure 5-20;21). Even though the evident morphological differences in Fbxo17 KO murine intestinal organoids compared to control group, our *in-vitro* analysis suggests that the loss of the Fbxo17 may not involve in cancer progression as confirmed in *in-vitro* assays in DLD-1 colon cell lines.

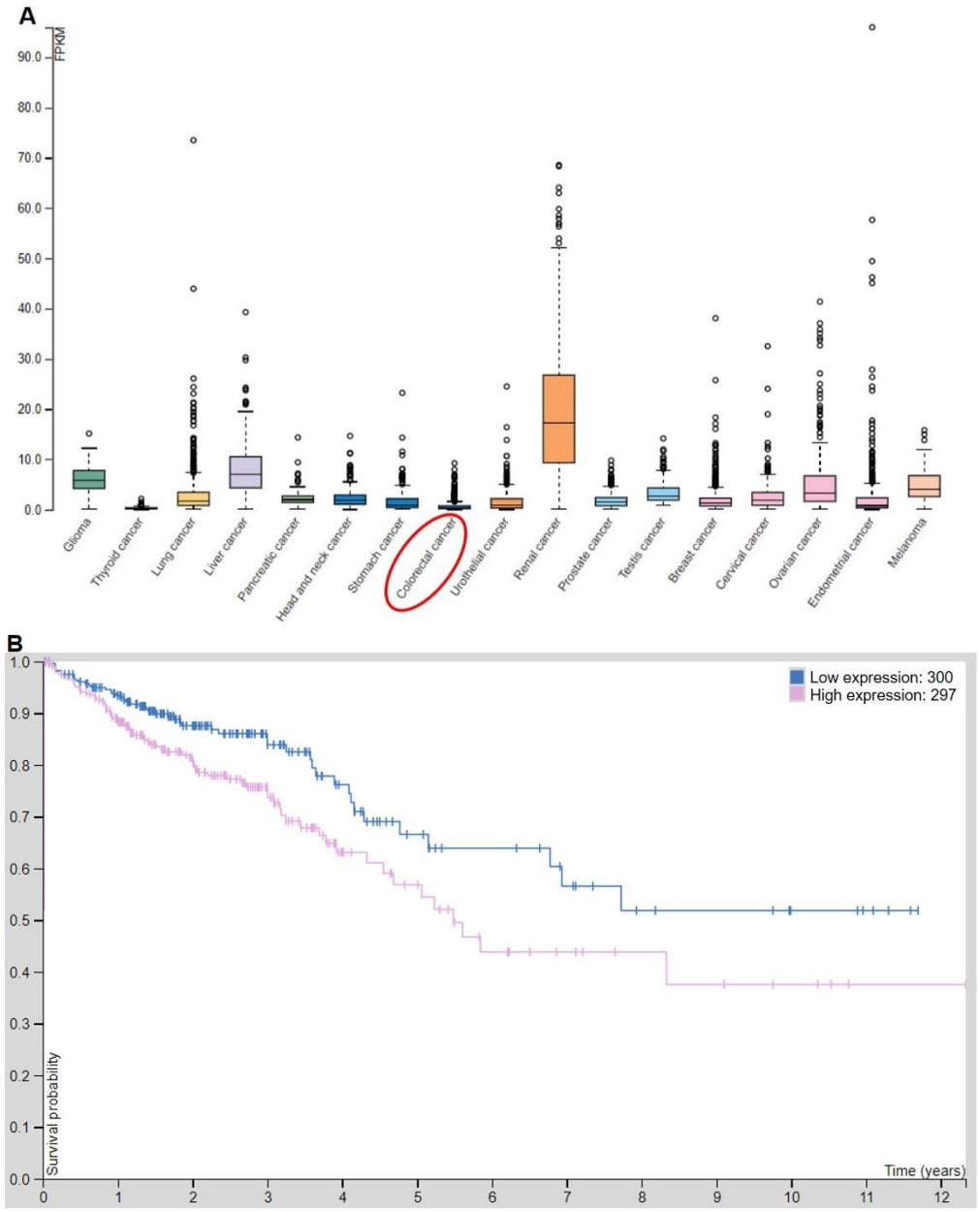


Figure 5-29. FBXO17 mRNA expression pattern in 17 types of malignancies. A) Illustrates the RNA profile of FBXO17 in various tumour samples. **B)** Enhanced FBXO17 expression is a marker of poor survival in CRC individuals (adopted from Human Protein Atlas, https://www.proteinatlas.org/ENSG00000269190-FBXO17/pathology/colorectal+cancer).

Previous work on the clinical value of FBXO17 in high-grade glioma indicated that patient with an enhanced level of FBXO17 expression showed remarkably shorter overall survival than other individuals (438). Further study demonstrated that FBXO17 induced lung adenoma-carcinoma cell proliferation via Akt pathway. Moreover, ERK1/2 phosphorylation was significantly enhanced with FBXO17 overexpression and reduced with FBXO17 knockdown independent of AKT pathway (441). FBXO17 also mediated the polyubiquitination of GSK-3β and negatively regulated the inflammation in murine lung epithelial cells (442).

The recent study also indicated that the FBXO17 negatively modulates the type I IFN signalling via dephosphorylating and following inactivation of IFN regulatory factor 3 (443). Peng D and colleagues interestingly showed that this antagonist activity of FBXO17 is indispensable of conventional functional of F-BOX protein via recruiting by F-box domain. In conclusion and based on our results, KO F-box intestinal organoids demonstrated differential phenotypical alterations that were associated with proliferation and differentiation. CRISPR/Cas9 organoid mutagenesis-based screening method provides a reliable and rapid approach than two-dimensional models for investigating of a large number of genes with unknown/poorly identified biological function and their possible involvement in development, homeostasis, disease progression and tumorigenesis.

CHAPTER 6

GENERAL DISCUSSION

6.1 Overview

One of the most recent and promising modelling systems in disease and cancer research is organoids: a 3D (3-dimentional), multicellular culture that closely mimics the genotype and phenotype of their parental tissue while compatible with many standard laboratory protocols. Stem cells from the organ in question are cultured with appropriate growth factors and stem cell niche factors resulting in a small "organ in a dish" that can be maintained and expanded almost indefinitely. Organoids faithfully reproduce functional genetic or pharmacological changes visible in their originating organ. They have been cultured from the brain (444) retina (445) stomach (446), lung (447) pancreatic and small intestine (448, 449) among others from both human patients and mice. Organoid cultures provided a crucial "middle ground" alternative between immortal cell culture and full *in vivo* animal models for functional genetic analysis, high throughput drug testing (450) bio-banking (342), tumour microenvironment (451), disease modelling (65) and targeted gene editing (452) via CRISPR/Cas9 technology and validating data between experimental models. When generated from both adjacent normal and matched tumour samples of an individual patient, epithelial organoids can provide an excellent tool for researchers to investigate a wide range of cellular and molecular events directly related to an individual patient.

Organoids also represents a paradigm shift in the use of animal models for a wide variety of scientific studies. While animal models in general and mouse models have contributed incalculably to scientific progress, their ethical and practical limitations as well as increasingly limited translatability in genetic and

pharmaceutical studies, requires the adoption of novel systems to replace them. As the method becomes both more widespread and more refined, the potential uses for organoids will increase, further reducing reliance on animal models and allowing research groups lacking animal facilities to utilise these models.

In this thesis, my study focused on the development of the PDOs from CRC samples, *in vitro* culture in our laboratory and further assessing the phenotypical alteration of both tumour and adjacent tissue-derived organoids from 17 patients diagnosed with CRC. My study further evaluated the anticancer therapeutic value of Rifabutin antibiotic using PDO and colon cancer cell lines. Considering the initial promising findings on phenotypical significance application of organoids growth, we then combined the organoid culture with genome editing technology, CRISPR/Cas9 to introduce versatile modelling platforms for rapid and facile screening and identification of genes with unknown biological function in the intestinal epithelium.

6.2 Patient derived organoids reflect the origin tissue in a dish

The phenotypical screening of tumour and normal adjacent organoids may reflect and provide key information on intra genetic signature of their parental tissues. Bio-banking of organoid line from different CRC patients facilitate the rapid analysis of their transcriptome, proteome and epigenome of the tumours in different molecular and pathological stages of disease. In addition, this provides the great opportunity to test different types of therapeutic and assess their genotype-phenotype correlations in a timely manner. In the current study, the normal derived organoids developed multiple branching domains while the

tumour derived organoids showed various phenotypical morphologies in which the cystic trait with rapid growth pattern was the main characteristics. Unlike normal derived organoids, tumour organoids was capable of growing independence of niche signalling factors. Furthermore, a Phalloidin and H&E staining also confirmed the differential morphological phenotypes between tumour and normal derived organoids. Organoids also sustained the growth characteristics of initial culture after excessive passaging and freezing-thawing process. These features make organoid as robust, stable and reliable model for investigating multiple cell and molecular events in both tumour and matched adjacent samples of an individual with cancer which is not feasible in any other traditional models (32). Altogether, based on our findings, monitoring, capturing and further classification of the differential phenotypical alterations of tumour and matched adjacent samples may provide fundamental and basic information which can be of significant value for therapeutic purposes, comparison analysis or gene targeted approaches to pinpoint novel biomarkers in CRC. Therefore, organoids provide a new opportunity and hope for both biomedical researches, in personalised and regenerative medicine approaches, and in particular for the generation and transplant of patient-derived tissue that will prevent rejection and immune responses. While organoids have been demonstrated to self-assemble into ad-hoc structures roughly analogous to their source anatomy (453), they are currently unsuitable to such delicate physical engineering. However, current organoid methodology is still limited by the lack of vasculature. Although several recent studies have started resolving this limitation using different approaches (454).

6.4 CXXC4 as potential targets of Rifabutin anticancer activity in PDO

The application of antibiotics alone or in adjuvant therapy for the treatment of different malignancies has been noted in recent works (247, 248, 400, 455-457). Rifabutin acts as an antibiotic against a majority of bacteria, including mycobacterium tuberculosis and non-tuberculous mycobacteria (NTM) (356). In our study we demonstrated the Rifabutin significantly suppressed the growth capacity of multiple colon cancer cells including SW620, HT29. Rifabutin has also suppressed the motility and invasiveness of the SW620 and HT-29 colon cancer cells in culture. Our initial cytotoxicity determined the IC50 of 26-8µM for SW480, SW620, HCT-116, DLD-1 and IC50 of 29.7µM for the HT-29 in which Rifabutin markedly arrested the growth of CRC cells in culture. However, recent works have also demonstrated a wide range of Rifabutin IC50 values from 5-35.5µM in different cancer cell lines (403, 421, 422).

Further investigation of the Rifabutin effects on PDO showed significant inhibition in growth rate and viability of the organoids in culture (Figures 4-6 & 4-8). Subsequent evaluation of the organoids treated with Rifabutin revealed the dysregulation of multiple Wnt signaling genes. Further validations narrowed the findings to some candidate genes as potential targets for Rifabutin including *CXXC4*, *SOX17*, *FGF4*, *PRICKLE1*, *WIF1*, *SFRP4*, *DVL-1*, *FZD5* (362-369).

The expression level of *CXXC4* enhanced in both colonic tumour organoids, SW620 and SW480 colon cancer cell lines upon treatment with Rifabutin (Figure 4-16). *CXXC4* encodes a CXXC-type zinc finger domain-containing protein that acts as an antagonist of the canonical wingless/integrated signalling pathway. CXXC4 negatively regulating Wnt/β-catenin signalling in colorectal

cancer (412, 413), renal cell carcinoma (414), and gastric (415, 416). CXXC4 conferring its function by directly inhibiting dishevelled (Dvl) in the Dvl/Axin complex. Previous study also revealed that CXXC4 is downregulated in colon cancer, gastric and renal carcinoma tissues (412, 413, 415, 416). Recent study showed that the CXXC4 activated apoptosis in gastric cancer via up-regulating GDF15 (26). The epigenetic down-regulation of CXXC4 also led to the activation of Wnt signalling and mediated the poor outcome in gastric cancer patients (50). In another study, *CXXC4* promoter methylation was detected in head and neck carcinoma as well (49). In conclusion, CXXC4 might be a potential targets of Rifabutin and mediates its anticancer activity by suppressing of proliferation in different cancer cell lines and colonic tumour organoids. However, further *in vivo* and pre-clinical approaches and experiments require to thoroughly verify the clinically Rifabutin/CXXC4 axis for targeted colorectal cancer therapy in future.

6.3 Screening the role of F-box genes with CRISPR-Cas9–modified organoids genome

The CRISPR/Cas9 gene editing system provides a robust tool for generating genetically modified in vitro models. With recent systems capable of both "knock-in" and "knock-out" of chosen genes, CRISPR/Cas9 is used for generating a broad *in vitro* cellular model. Herein, we presented tools and methods for; isolating and culturing mouse intestinal crypts to grow culturing organoids, stably expressing Cas9 protein via lentiviral transduction and subsequent transduction of a lentivirus expressing the gRNA of gene of interest

(Figure 5-26). These knockout organoid lines are suitable for functional and biochemical analysis. We propose that this CRISPR/Cas9-mediated mutagenesis-based screening method can provide a promising approach which facilitates the rapid and reliable identification and selection of new genes play a role in development, and disease.

This model of culturing organoids and genetic screening is straightforward to establish in any laboratory with access to basic cell culture and molecular biology facilities. In studies that have neither a visual reporter gene nor a significant phenotypical change, the genomic DNA sequencing, protein and RNA expression analysis is required for characterising and validating the knockout organoids as outlined previously. To this end, it is recommended that the initial plasmid design may include a visual reporter gene such as GFP to determine transduction efficiency and virus titration. After which, images of experimental samples can be taken using fluorescent and bright field microscopy, and their growth and morphological changes over time compared against control samples. Software such as Image-J, is a user-friendly and accessible software for quantifying organoid size for comparison.

CRISP/Cas9-organoid methodology provides an efficient, reliable, medium-high throughput screening tool which requires significantly fewer animals than comparable *in vivo* studies. In fact, generating a genetically knockout mouse takes approximately 12-18 months on average. To obtain F2 mice that are uniformly homozygous for the intended mutation, breeding about 10 generations of mice is required (458). In each generation, there will be two breeding cages of about 40-50 mice, which results in 400-500 mice other the entire study, and

together with mice needed for blastocyst injection and performing experiments, between 1,000-1,200 mice would be needed for a knockout project per gene (458). While, it currently takes approximately 2 months to go from initial organoid isolation to completed knockout organoid line.

Moreover, similar organoid culture has already been established from multiple different organs (65). These organoids are suitable for *in vitro* phenotype analysis using Lenti and retroviral gain/loss-of-function studies. Using these methods, we pursued a biological objective: studying the regulatory role of the family of F-box domain containing E3 ubiquitin ligases. F-box proteins generally function as negative regulators by promoting degradation of their target proteins. So far genetic studies of this family are still poor, primarily due to the large number of members, ~69 in human (108). In the present study, monitoring the phenotypical alterations of KO-F-box organoids vs control transduced organoids enabled the comparison analysis and selection of candidate F-box genes mediated the abnormal morphology including Fbxl18 and Fbxo17. Of note, not all of the F-box proteins are expressed in intestinal organoids and also some of the genes may not show a profound phenotype due to non-essential functions or functional compensation by their paralogues. Altogether, the method outlined in chapter 5 indicates that organoid culture screens can be used as an effective tool to inform and facilitate future *in vivo* research including, but not limited to, disease progression, tumorigenesis and drug screening studies, which will lead to significant replacement and reduction of mouse modelling.

6.5 Conclusions, experimental limitations and future perspectives

Lack of molecular subtyping of PDOs and their possible correlations with clinical variables

In our study, we have not analysed the molecular profile of the PDOs we have generated in the context of our small biobank. The PDO (tumour and their matched adjacent) and their original tissue can be assessed and compared for their transcriptome (RNA-sequencing), genomics, epigenetics and proteome signatures. These can then be correlated with several clinicopathological characteristics of patients' original tissues and derived organoids including age, tumour grade and staging, tumour location, family history, recurrence and metastasis. In some of the cases, prior medication can further accompany the phenotypical alterations we have obtained through monitoring the morphological evaluation.

Organoid system lacks the mesenchymal, stromal, immune cells that exist in the gut tissue *in vivo*

The fundamental role of microenvironment in homeostasis and tumorigenesis of several tissues highlights the need for the development of modified organoid culture containing the stroma. On the other hand, organoids may also provide a valuable model to study the interaction of stem cells and the progenitors and without confounding factors like the mesenchymal cells. Although several recent studies have focused on resolving the latter limitations in organoid culture using co-culturing system (459, 460).

Lack of an *in vivo* animal study to confirm the effect of Rifabutin on colon cancer progression

Since the foremost objective of any anticancer therapeutics is targeting the human cancer cells, the *in vivo* study would more likely disclose precise and more relevant information on behaviour and mechanism of action of Rifabutin. However, due to time and cost restrictions during this period, we were not able to peruse to *in vivo* animal part of the study.

Further mechanism and validation of anticancer activity of Rifabutin antibiotics

Herein, our finding showed that Rifabutin influenced the expression of various Wnt signalling associated-genes in colonic tumour organoids and colon cancer cells. However, based on the heterogeneous mutation background of cell lines we have not obtained similar results across all colon cancer cells line. Further investigations require to validate and pinpoint the exact mechanism of action of Rifabutin/ CXXC4 in particular in the hallmark of cancer and in various cancer cell lines using different approaches.

Downstream analysis of Fbxo17 and Fbxl18 KO in intestinal stem cell maintenance and tissue homeostasis

The primary purpose of the CRISPR/Cas9 mediated screening on organoids was the establishment of the methodology and further identification of CRISPR/Cas9 engineered organoids with differential phenotypical alterations. However, we did not manage to discover further the mechanism of action of both Fbxo17 and Fbxl18 candidates as E3-ligase in the time frame I had in the laboratory. Further evaluation required to in-depth proteome analyses to characterize the

relationship between these two F-box candidates and their activity on homeostasis, development and disease progression.

Similarly, future studies can be focused on the role of other F-box candidates, i.e., FBXL18, FBXL17, FBXO17, FBOX31 and FBXL5 that we identified in our initial CRISPR-organoid screening system. Dr Nateri's lab has now focused on the function of FBOX31 and FBXL5 in gut homeostasis, disease and CRC malignancy using the above mentioned advanced molecular and genetic approaches.

References

1. Sharma SV, Haber DA, Settleman J. Cell line-based platforms to evaluate the therapeutic efficacy of candidate anticancer agents. Nature reviews Cancer. 2010;10(4):241-53.

2. Cekanova M, Rathore K. Animal models and therapeutic molecular targets of cancer: utility and limitations. Drug design, development and therapy. 2014;8:1911-21.

3. Sharma SV, Haber DA, Settleman J. Cell line-based platforms to evaluate the therapeutic efficacy of candidate anticancer agents. Nature reviews cancer. 2010;10(4):241-53.

4. Barretina J, Caponigro G, Stransky N, Venkatesan K, Margolin AA, Kim S, et al. The Cancer Cell Line Encyclopedia enables predictive modelling of anticancer drug sensitivity. Nature. 2012;483(7391):603-7.

5. Basu A, Bodycombe NE, Cheah JH, Price EV, Liu K, Schaefer GI, et al. An interactive resource to identify cancer genetic and lineage dependencies targeted by small molecules. Cell. 2013;154(5):1151-61.

6. Park ES, Rabinovsky R, Carey M, Hennessy BT, Agarwal R, Liu W, et al. Integrative analysis of proteomic signatures, mutations, and drug responsiveness in the NCI 60 cancer cell line set. Mol Cancer Ther. 2010;9(2):257-67.

7. Scherer WF, Syverton JT, Gey GO. Studies on the propagation in vitro of poliomyelitis viruses IV. Viral multiplication in a stable strain of human malignant epithelial cells (strain HeLa) derived from an epidermoid carcinoma of the cervix. The Journal of experimental medicine. 1953;97(5):695-710.

8. Mattern J, Bak M, Hahn EW, Volm M. Human tumor xenografts as model for drug testing. Cancer and Metastasis Reviews. 1988;7(3):263-84.

9. Nelson-Rees WA. The identification and monitoring of cell line specificity. Progress in clinical and biological research. 1977;26:25-79.

10. Nelson-Rees WA, Flandermeyer RR. Inter-and intraspecies contamination of human breast tumor cell lines HBC and BrCa5 and other cell cultures. Science. 1977;195(4284):1343-4.

11. Nelson-Rees WA, Flandermeyer RR, Hawthorne PK. Banded marker chromosomes as indicators of intraspecies cellular contamination. Science. 1974;184(4141):1093-6.

12. Brown KM, Xue A, Mittal A, Samra JS, Smith R, Hugh TJ. Patient-derived xenograft models of colorectal cancer in pre-clinical research: a systematic review. Oncotarget. 2016;7(40):66212.

13. Pitter KL, Galban CJ, Galban S, Tehrani OS, Li F, Charles N, et al. Perifosine and CCI 779 co-operate to induce cell death and decrease proliferation in PTEN-intact and PTEN-deficient PDGF-driven murine glioblastoma. PLoS One. 2011;6(1):e14545.

14. Singh M, Murriel CL, Johnson L. Genetically engineered mouse models: closing the gap between preclinical data and trial outcomes. Cancer research. 2012;72(11):2695-700.

15. Pollard P, Deheragoda M, Segditsas S, Lewis A, Rowan A, Howarth K, et al. The Apc1322T mouse develops severe polyposis associated with submaximal nuclear β-catenin expression. Gastroenterology. 2009;136(7):2204-13. e13.

16. Sasai H, Masaki M, Wakitani K. Suppression of polypogenesis in a new mouse strain with a truncated ApcΔ474 by a novel COX-2 inhibitor, JTE-522. Carcinogenesis. 2000;21(5):953-8.

17. Curt GA. The use of animal models in cancer drug discovery and development. Stem Cells. 1994;12(1):23-9.

18. Goldin A, Serpick A, Mantel N. Experimental screening procedures and clinical predictability value. Cancer chemotherapy reports Part 1. 1966;50(4):173.

19. Staquet M, Byar D, Green S, Rozencweig M. Clinical predictivity of transplantable tumor systems in the selection of new drugs for solid tumors: rationale for a three-stage strategy. Cancer treatment reports. 1983;67(9):753-65.

20. Monks A, Scudiero D, Skehan P, Shoemaker R, Paull K, Vistica D, et al. Feasibility of a high-flux anticancer drug screen using a diverse panel of cultured human tumor cell lines. Journal of the National Cancer Institute. 1991;83(11):757-66.

21. Tveit K, Pihl A. Do cell lines in vitro reflect the properties of the tumours of origin? A study of lines derived from human melanoma xenografts. British journal of cancer. 1981;44(6):775.

22. Daniel VC, Marchionni L, Hierman JS, Rhodes JT, Devereux WL, Rudin CM, et al. A primary xenograft model of small-cell lung cancer reveals irreversible changes in gene expression imposed by culture in vitro. Cancer research. 2009;69(8):3364-73.

23. Roschke AV, Tonon G, Gehlhaus KS, McTyre N, Bussey KJ, Lababidi S, et al. Karyotypic complexity of the NCI-60 drug-screening panel. Cancer research. 2003;63(24):8634-47.

24. Nelson-Rees W, Owens R, Arnstein P, Kniazeff A. Source, alterations, characteristics and use of a new dog cell line (Cf2Th). In vitro. 1976;12(10):665-9.

25. Young M, Ordonez L, Clarke AR. What are the best routes to effectively model human colorectal cancer? Molecular oncology. 2013;7(2):178-89.

26. Comprehensive molecular characterization of human colon and rectal cancer. Nature. 2012;487(7407):330-7.

27. Roth AD, Delorenzi M, Tejpar S, Yan P, Klingbiel D, Fiocca R, et al. Integrated analysis of molecular and clinical prognostic factors in stage II/III colon cancer. J Natl Cancer Inst. 2012;104(21):1635-46.

28. Smith CG, Fisher D, Claes B, Maughan TS, Idziaszczyk S, Peuteman G, et al. Somatic profiling of the epidermal growth factor receptor pathway in tumors from patients with advanced colorectal cancer treated with chemotherapy +/- cetuximab. Clin Cancer Res. 2013;19(15):4104-13.

29. Grozinsky-Glasberg S, Shimon I, Rubinfeld H. The role of cell lines in the study of neuroendocrine tumors. Neuroendocrinology. 2012;96(3):173-87.

30. Johnson RL, Fleet JC. Animal models of colorectal cancer. Cancer and Metastasis Reviews. 2013;32(1-2):39-61.

31. Jackstadt R, Sansom OJ. Mouse models of intestinal cancer. The Journal of pathology. 2016;238(2):141-51.

32. Ruggeri BA, Camp F, Miknyoczki S. Animal models of disease: pre-clinical animal models of cancer and their applications and utility in drug discovery. Biochemical pharmacology. 2014;87(1):150-61.

33. McIntyre RE, Buczacki SJ, Arends MJ, Adams DJ. Mouse models of colorectal cancer as preclinical models. BioEssays. 2015;37(8):909-20.

34. Francis JC, Melchor L, Campbell J, Kendrick H, Wei W, Armisen-Garrido J, et al. Whole-exome DNA sequence analysis of Brca2-and Trp53-deficient mouse mammary gland tumours. The Journal of pathology. 2015;236(2):186-200.

35. McIntyre RE, van der Weyden L, Adams DJ. Cancer gene discovery in the mouse. Current opinion in genetics & development. 2012;22(1):14-20.

36. Gupta N, Liu JR, Patel B, Solomon DE, Vaidya B, Gupta V. Microfluidics-based 3D cell culture models: Utility in novel drug discovery and delivery research. Bioengineering & translational medicine. 2016;1(1):63-81.

37. Page H, Flood P, Reynaud EG. Three-dimensional tissue cultures: current trends and beyond. Cell Tissue Res. 2013;352(1):123-31.

38. Purpura KA, Bratt-Leal AM, Hammersmith KA, McDevitt TC, Zandstra PW. Systematic engineering of 3D pluripotent stem cell niches to guide blood development. Biomaterials. 2012;33(5):1271-80.

39. Jeanes AI, Maya-Mendoza A, Streuli CH. Cellular microenvironment influences the ability of mammary epithelia to undergo cell cycle. PLoS One. 2011;6(3):e18144.

40. Lu Y, Zhang G, Shen C, Uygun K, Yarmush ML, Meng Q. A novel 3D liver organoid system for elucidation of hepatic glucose metabolism. Biotechnol Bioeng. 2012;109(2):595-604.

41. Cantz T, Martin U. Induced pluripotent stem cells: characteristics and perspectives. Bioreactor systems for tissue engineering II: Springer; 2010. p. 107-26.

42. Nelson CM, Inman JL, Bissell MJ. Three-dimensional lithographically defined organotypic tissue arrays for quantitative analysis of morphogenesis and neoplastic progression. Nature protocols. 2008;3(4):674-8.

43. Roudsari LC, West JL. Studying the influence of angiogenesis in in vitro cancer model systems. Advanced drug delivery reviews. 2016;97:250-9.

44. Grebenyuk S, Ranga A. Engineering organoid vascularization. Frontiers in bioengineering and biotechnology. 2019;7:39.

45. Chen J. The cultivation in fluid medium of organised liver, pancreas and other tissues of foetal rats. Experimental cell research. 1954;7(2):518-29.

46. Li X, Nadauld L, Ootani A, Corney DC, Pai RK, Gevaert O, et al. Oncogenic transformation of diverse gastrointestinal tissues in primary organoid culture. Nature medicine. 2014;20(7):769-77.

47. Sato T, Stange DE, Ferrante M, Vries RG, van Es JH, van den Brink S, et al. Long-term expansion of epithelial organoids from human colon, adenoma, adenocarcinoma, and Barrett's epithelium. Gastroenterology. 2011;141(5):1762-72.

48. Clevers H. The intestinal crypt, a prototype stem cell compartment. Cell. 2013;154(2):274-84.

49. Sasai Y, Eiraku M, Suga H. In vitro organogenesis in three dimensions: self-organising stem cells. Development. 2012;139(22):4111-21.

50. Sasai Y. Next-generation regenerative medicine: organogenesis from stem cells in 3D culture. Cell Stem Cell. 2013;12(5):520-30.

51. Tuveson D, Clevers H. Cancer modeling meets human organoid technology. Science. 2019;364(6444):952-5.

52. Rossi G, Manfrin A, Lutolf MP. Progress and potential in organoid research. Nature Reviews Genetics. 2018;19(11):671-87.

53. Sato T, Vries RG, Snippert HJ, van de Wetering M, Barker N, Stange DE, et al. Single Lgr5 stem cells build crypt villus structures in vitro without a mesenchymal niche. Nature. 2009;459(7244):262-5.

54. Kleinman HK, Martin GR, editors. Matrigel: basement membrane matrix with biological activity. Seminars in cancer biology; 2005: Elsevier.

55. Dye BR, Hill DR, Ferguson MA, Tsai Y-H, Nagy MS, Dyal R, et al. In vitro generation of human pluripotent stem cell derived lung organoids. Elife. 2015;4:e05098.

56. Zumwalde NA, Haag JD, Sharma D, Mirrielees JA, Wilke LG, Gould MN, et al. Analysis of Immune Cells from Human Mammary Ductal Epithelial Organoids Reveals Vδ2+ T Cells That Efficiently Target Breast Carcinoma Cells in the Presence of Bisphosphonate. Cancer Prevention Research. 2016;9(4):305-16.

57. van de Wetering M, Francies HE, Francis JM, Bounova G, Iorio F, Pronk A, et al. Prospective derivation of a living organoid biobank of colorectal cancer patients. Cell. 2015;161(4):933-45.

58. Boj SF, Hwang C-I, Baker LA, Engle DD, Tuveson DA, Clevers H. Model organoids provide new research opportunities for ductal pancreatic cancer. Molecular & Cellular Oncology. 2016;3(1):e1014757.

59. Bertaux-Skeirik N, Centeno J, Feng R, Schumacher MA, Shivdasani RA, Zavros Y. Co-culture of Gastric Organoids and Immortalized Stomach Mesenchymal Cells. Gastrointestinal Physiology and Diseases: Methods and Protocols. 2016:23-31.

60. Ramachandran SD, Schirmer K, Münst B, Heinz S, Ghafoory S, Wölfl S, et al. In vitro generation of functional liver organoid-like structures using adult human cells. PLoS One. 2015;10(10):e0139345.

61. Xu AT, Tong JL, Ran ZH. Organoids derived from digestive tract, liver, and pancreas. Journal of digestive diseases. 2016;17(1):3-10.

62. Takasato M, Pei XE, Chiu HS, Maier B, Baillie GJ, Ferguson C, et al. Kidney organoids from human iPS cells contain multiple lineages and model human nephrogenesis. Nature. 2015;526(7574):564-8.

63. Nadkarni RR, Abed S, Draper JS. Organoids as a model system for studying human lung development and disease. Biochemical and biophysical research communications. 2016;473(3):675-82.

64. Morizane R, Bonventre JV. Generation of nephron progenitor cells and kidney organoids from human pluripotent stem cells. Nature Protocols. 2017;12(1):195-207.

65. Dutta D, Heo I, Clevers H. Disease modeling in stem cell-derived 3D organoid systems. Trends in molecular medicine. 2017;23(5):393-410.

66. Kwong J, Chan FL, Wong K-k, Birrer MJ, Archibald KM, Balkwill FR, et al. Inflammatory cytokine tumor necrosis factor α confers precancerous phenotype in an organoid model of normal human ovarian surface epithelial cells. Neoplasia. 2009;11(6):529-41.

67. Ciancanelli MJ, Huang SX, Luthra P, Garner H, Itan Y, Volpi S, et al. Life-threatening influenza and impaired interferon amplification in human IRF7 deficiency. Science. 2015;348(6233):448-53.

68. Bartfeld S, Bayram T, van de Wetering M, Huch M, Begthel H, Kujala P, et al. In vitro expansion of human gastric epithelial stem cells and their responses to bacterial infection. Gastroenterology. 2015;148(1):126-36 e6.

69. Farin HF, Karthaus WR, Kujala P, Rakhshandehroo M, Schwank G, Vries RG, et al. Paneth cell extrusion and release of antimicrobial products is directly controlled by immune cell-derived IFN-gamma. J Exp Med. 2014;211(7):1393-405.

70. Zhang YG, Wu S, Xia Y, Sun J. Salmonella-infected crypt-derived intestinal organoid culture system for host–bacterial interactions. Physiological reports. 2014;2(9):e12147.

71. Klotz C, Aebischer T, Seeber F. Stem cell-derived cell cultures and organoids for protozoan parasite propagation and studying host–parasite interaction. International Journal of Medical Microbiology. 2012;302(4):203-9.

72. Finkbeiner SR, Zeng X-L, Utama B, Atmar RL, Shroyer NF, Estes MK. Stem cell-derived human intestinal organoids as an infection model for rotaviruses. MBio. 2012;3(4):e00159-12.

73. Matano M, Date S, Shimokawa M, Takano A, Fujii M, Ohta Y, et al. Modeling colorectal cancer using CRISPR-Cas9-mediated engineering of human intestinal organoids. Nature medicine. 2015;21(3):256-62.

74. Schwank G, Koo B-K, Sasselli V, Dekkers JF, Heo I, Demircan T, et al. Functional repair of CFTR by CRISPR/Cas9 in intestinal stem cell organoids of cystic fibrosis patients. Cell stem cell. 2013;13(6):653-8.

75. Fouad YA, Aanei C. Revisiting the hallmarks of cancer. American journal of cancer research. 2017;7(5):1016.

76. Takahashi T. Organoids for drug discovery and personalized medicine. Annual review of pharmacology and toxicology. 2019;59:447-62.

77. van de Wetering M, Francies HE, Francis JM, Bounova G, Iorio F, Pronk A, et al. Prospective derivation of a living organoid biobank of colorectal cancer patients. Cell. 2015;161(4):933-45.

78. Ishino Y, Shinagawa H, Makino K, Amemura M, Nakata A. Nucleotide sequence of the iap gene, responsible for alkaline phosphatase isozyme conversion in Escherichia coli, and identification of the gene product. Journal of bacteriology. 1987;169(12):5429-33.

79. Kampmann M. CRISPRi and CRISPRa Screens in Mammalian Cells for Precision Biology and Medicine. ACS chemical biology. 2018;13(2):406-16.

80. Pourcel C, Salvignol G, Vergnaud G. CRISPR elements in Yersinia pestis acquire new repeats by preferential uptake of bacteriophage DNA, and provide additional tools for evolutionary studies. Microbiology. 2005;151(3):653-63.

81. Mojica FJ, Diez-Villasenor C, Garcia-Martinez J, Soria E. Intervening sequences of regularly spaced prokaryotic repeats derive from foreign genetic elements. Journal of molecular evolution. 2005;60(2):174-82.

82. Barrangou R, Fremaux C, Deveau H, Richards M, Boyaval P, Moineau S, et al. CRISPR provides acquired resistance against viruses in prokaryotes. Science. 2007;315(5819):1709-12.

83. Gasiunas G, Barrangou R, Horvath P, Siksnys V. Cas9–crRNA ribonucleoprotein complex mediates specific DNA cleavage for adaptive immunity in bacteria. Proceedings of the National Academy of Sciences. 2012;109(39):E2579-E86.

84. Jinek M, Chylinski K, Fonfara I, Hauer M, Doudna JA, Charpentier E. A programmable dual-RNA–guided DNA endonuclease in adaptive bacterial immunity. science. 2012;337(6096):816-21.

85. Jiang F, Doudna JA. CRISPR–Cas9 structures and mechanisms. Annual review of biophysics. 2017;46:505-29.

86. Jinek M, Chylinski K, Fonfara I, Hauer M, Doudna JA, Charpentier E. A programmable dual-RNA-guided DNA endonuclease in adaptive bacterial immunity. Science (New York, NY). 2012;337(6096):816-21.

87. Behan FM, Iorio F, Picco G, Goncalves E, Beaver CM, Migliardi G, et al. Prioritization of cancer therapeutic targets using CRISPR-Cas9 screens. Nature. 2019;568(7753):511-6.

88. Cong L, Ran FA, Cox D, Lin S, Barretto R, Habib N, et al. Multiplex genome engineering using CRISPR/Cas systems. Science. 2013;339(6121):819-23.

89. Mali P, Yang L, Esvelt KM, Aach J, Guell M, DiCarlo JE, et al. RNA-guided human genome engineering via Cas9. Science. 2013;339(6121):823-6.

90. Hu JH, Miller SM, Geurts MH, Tang W, Chen L, Sun N, et al. Evolved Cas9 variants with broad PAM compatibility and high DNA specificity. Nature. 2018;556(7699):57-63.

91. Jiang F, Doudna JA. The structural biology of CRISPR-Cas systems. Current opinion in structural biology. 2015;30:100-11.

92. Ran FA, Hsu PD, Wright J, Agarwala V, Scott DA, Zhang F. Genome engineering using the CRISPR-Cas9 system. Nature protocols. 2013;8(11):2281.

93. Gaj T, Gersbach CA, Barbas III CF. ZFN, TALEN, and CRISPR/Cas-based methods for genome engineering. Trends in biotechnology. 2013;31(7):397-405.

94. Wei C, Liu J, Yu Z, Zhang B, Gao G, Jiao R. TALEN or Cas9–rapid, efficient and specific choices for genome modifications. Journal of genetics and genomics. 2013;40(6):281-9.

95. Zhen S, Hua L, Takahashi Y, Narita S, Liu Y-H, Li Y. In vitro and in vivo growth suppression of human papillomavirus 16-positive cervical cancer cells by CRISPR/Cas9. Biochemical and biophysical research communications. 2014;450(4):1422-6.

96. Xiao-Jie L, Hui-Ying X, Zun-Ping K, Jin-Lian C, Li-Juan J. CRISPR-Cas9: a new and promising player in gene therapy. Journal of medical genetics. 2015;52(5):289-96.

97. Hershko A, Ciechanover A. The ubiquitin system. Annual review of biochemistry. 1998;67:425-79.

98. Christianson JC, Ye Y. Cleaning up in the endoplasmic reticulum: ubiquitin in charge. Nature structural & molecular biology. 2014;21(4):325-35.

99. Ciechanover A. Intracellular protein degradation: from a vague idea through the lysosome and the ubiquitin-proteasome system and onto human diseases and drug targeting. Bioorganic & medicinal chemistry. 2013;21(12):3400-10.

100. Varshavsky A. The ubiquitin system, an immense realm. Annual review of biochemistry. 2012;81:167-76.

101. Ravid T, Hochstrasser M. Diversity of degradation signals in the ubiquitin-proteasome system. Nature reviews Molecular cell biology. 2008;9(9):679-90.

102. Budenholzer L, Cheng CL, Li Y, Hochstrasser M. Proteasome Structure and Assembly. Journal of molecular biology. 2017;429(22):3500-24.

103. Skaar JR, Pagan JK, Pagano M. Mechanisms and function of substrate recruitment by F-box proteins. Nature reviews Molecular cell biology. 2013;14(6):369-81.

104. Bai C, Sen P, Hofmann K, Ma L, Goebl M, Harper JW, et al. SKP1 connects cell cycle regulators to the ubiquitin proteolysis machinery through a novel motif, the F-box. Cell. 1996;86(2):263-74.

105. Liu J, Peng Y, Zhang J, Long J, Liu J, Wei W. Targeting SCF E3 Ligases for Cancer Therapies. Advances in experimental medicine and biology. 2020;1217:123-46.

106. Yan L, Lin M, Pan S, Assaraf YG, Wang ZW, Zhu X. Emerging roles of F-box proteins in cancer drug resistance. Drug resistance updates : reviews and commentaries in antimicrobial and anticancer chemotherapy. 2019;49:100673.

107. Nguyen KM, Busino L. The Biology of F-box Proteins: The SCF Family of E3 Ubiquitin Ligases. Advances in experimental medicine and biology. 2020;1217:111-22.

108. Wang Z, Liu P, Inuzuka H, Wei W. Roles of F-box proteins in cancer. Nature reviews Cancer. 2014;14(4):233-47.

109. Skowyra D, Craig KL, Tyers M, Elledge SJ, Harper JW. F-box proteins are receptors that recruit phosphorylated substrates to the SCF ubiquitin-ligase complex. Cell. 1997;91(2):209-19.

110. Shen J, Spruck C. F-box proteins in epigenetic regulation of cancer. Oncotarget. 2017;8(66):110650.

111. Babaei-Jadidi R, Li N, Saadeddin A, Spencer-Dene B, Jandke A, Muhammad B, et al. FBXW7 influences murine intestinal homeostasis and cancer, targeting Notch, Jun, and DEK for degradation. The Journal of experimental medicine. 2011;208(2):295-312.

112. Li N, Lorenzi F, Kalakouti E, Normatova M, Babaei-Jadidi R, Tomlinson I, et al. FBXW7-mutated colorectal cancer cells exhibit aberrant expression of phosphorylated-p53 at Serine-15. Oncotarget. 2015;6(11):9240-56.

113. Takeishi S, Nakayama K. Role of Fbxw7 in the maintenance of normal stem cells and cancer-initiating cells. British journal of cancer. 2014;111(6):1054-9.

114. Yumimoto K, Nakayama KI, editors. Recent insight into the role of FBXW7 as a tumor suppressor. Seminars in cancer biology; 2020: Elsevier.

115. Sailo BL, Banik K, Girisa S, Bordoloi D, Fan L, Halim CE, et al. FBXW7 in cancer: What has been unraveled thus far? Cancers. 2019;11(2):246.

116. Sancho R, Blake SM, Tendeng C, Clurman BE, Lewis J, Behrens A. Fbw7 repression by hes5 creates a feedback loop that modulates Notch-mediated intestinal and neural stem cell fate decisions. PLoS biology. 2013;11(6).

117. Forbes SA, Beare D, Boutselakis H, Bamford S, Bindal N, Tate J, et al. COSMIC: somatic cancer genetics at high-resolution. Nucleic acids research. 2017;45(D1):D777-D83.

118. Yeh CH, Bellon M, Nicot C. FBXW7: a critical tumor suppressor of human cancers. Mol Cancer. 2018;17(1):115.

119. Babaei-Jadidi R, Li N, Saadeddin A, Spencer-Dene B, Jandke A, Muhammad B, et al. FBXW7 influences murine intestinal homeostasis and cancer, targeting Notch, Jun, and DEK for degradation. Journal of Experimental Medicine. 2011;208(2):295-312.

120. Grim JE, Knoblaugh SE, Guthrie KA, Hagar A, Swanger J, Hespelt J, et al. Fbw7 and p53 cooperatively suppress advanced and chromosomally unstable intestinal cancer. Molecular and cellular biology. 2012;32(11):2160-7.

121. Liu H, Wang K, Fu H, Song J. Low expression of the ubiquitin ligase FBXW7 correlates with poor prognosis of patients with colorectal cancer. International Journal of Clinical and Experimental Pathology. 2018;11(1):413.

122. Li N, Babaei-Jadidi R, Lorenzi F, Spencer-Dene B, Clarke P, Domingo E, et al. An FBXW7-ZEB2 axis links EMT and tumour microenvironment to promote colorectal cancer stem cells and chemoresistance. Oncogenesis. 2019;8(3):1-17.

123. Cai L, Li J, Zhao J, Guo Y, Xie M, Zhang X, et al. Fbxo6 confers drug-sensitization to cisplatin via inhibiting the activation of Chk1 in non-small cell lung cancer. FEBS letters. 2019;593(14):1827-36.

124. Cui D, Xiong X, Shu J, Dai X, Sun Y, Zhao Y. FBXW7 Confers Radiation Survival by Targeting p53 for Degradation. Cell Reports. 2020;30(2):497-509. e4.

125. Mao JH, Perez-Losada J, Wu D, Delrosario R, Tsunematsu R, Nakayama KI, et al. Fbxw7/Cdc4 is a p53-dependent, haploinsufficient tumour suppressor gene. Nature. 2004;432(7018):775-9.

126. Yokobori T, Mimori K, Iwatsuki M, Ishii H, Onoyama I, Fukagawa T, et al. p53-Altered FBXW7 expression determines poor prognosis in gastric cancer cases. Cancer research. 2009;69(9):3788-94.

127. Hao S, Cong L, Qu R, Liu R, Zhang G, Li Y. Emerging roles of circular RNAs in colorectal cancer. OncoTargets and therapy. 2019;12:4765.

128. Li J, Guo Y, Liang X, Sun M, Wang G, De W, et al. MicroRNA-223 functions as an oncogene in human gastric cancer by targeting FBXW7/hCdc4. Journal of cancer research and clinical oncology. 2012;138(5):763-74.

129. Wu Z-H, Pfeffer LM, editors. MicroRNA regulation of F-box proteins and its role in cancer. Seminars in cancer biology; 2016: Elsevier.

130. Tamimi Y, Al Hinai M, Gupta I, Lakhtakia R, Al Kalbani M, Okamoto A, et al. EP994 Epigenetic silencing of FBXW7 through promotor hypermethylation in ovarian cancer. BMJ Specialist Journals; 2019.

131. Yeh C-H, Bellon M, Nicot C. FBXW7: a critical tumor suppressor of human cancers. Molecular cancer. 2018;17(1):115.

132. Akhoondi S, Lindstrom L, Widschwendter M, Corcoran M, Bergh J, Spruck C, et al. Inactivation of FBXW7/hCDC4-beta expression by promoter hypermethylation is associated with favorable prognosis in primary breast cancer. Breast cancer research : BCR. 2010;12(6):R105.

133. Tang W, Li Y, Yu D, Thomas-Tikhonenko A, Spiegelman VS, Fuchs SY. Targeting β-transducin repeat–containing protein E3 ubiquitin ligase augments the effects of antitumor drugs on breast cancer cells. Cancer research. 2005;65(5):1904-8.

134. Müerköster S, Arlt A, Sipos B, Witt M, Großmann M, Klöppel G, et al. Increased expression of the E3-ubiquitin ligase receptor subunit βTRCP1 relates to constitutive nuclear factor-κB activation and chemoresistance in pancreatic carcinoma cells. Cancer research. 2005;65(4):1316-24.

135. Koch A, Waha A, Hartmann W, Hrychyk A, Schüller U, Waha A, et al. Elevated expression of Wnt antagonists is a common event in hepatoblastomas. Clinical cancer research. 2005;11(12):4295-304.

136. Randle SJ, Laman H, editors. F-box protein interactions with the hallmark pathways in cancer. Seminars in cancer biology; 2016: Elsevier.

137. Muto Y, Nishiyama M, Nita A, Moroishi T, Nakayama KI. Essential role of FBXL5-mediated cellular iron homeostasis in maintenance of hematopoietic stem cells. Nature communications. 2017;8:16114.

138. Ahmed M, Jinks N, Babaei-Jadidi R, Kashfi H, Castellanos-Uribe M, May ST, et al. Repurposing Antibacterial AM404 as a Potential Anticancer Drug for Targeting Colorectal Cancer Stem-Like Cells. Cancers. 2019;12(1).

139. Vinas-Castells R, Frias A, Robles-Lanuza E, Zhang K, Longmore GD, Garcia de Herreros A, et al. Nuclear ubiquitination by FBXL5 modulates Snail1 DNA binding and stability. Nucleic acids research. 2014;42(2):1079-94.

140. Yao H, Su S, Xia D, Wang M, Li Z, Chen W, et al. F-box and leucine-rich repeat protein 5 promotes colon cancer progression by modulating PTEN/PI3K/AKT signaling pathway. Biomedicine & pharmacotherapy = Biomedecine & pharmacotherapie. 2018;107:1712-9.

141. Wu W, Ding H, Cao J, Zhang W. FBXL5 inhibits metastasis of gastric cancer through suppressing Snail1. Cellular physiology and biochemistry : international journal of experimental cellular physiology, biochemistry, and pharmacology. 2015;35(5):1764-72.

142. Wu WD, Wang M, Ding HH, Qiu ZJ. FBXL5 attenuates RhoGDI2-induced cisplatin resistance in gastric cancer cells. European review for medical and pharmacological sciences. 2016;20(12):2551-7.

143. Wang Z, Chen X, Zhao Y, Jin Y, Zheng J. G-protein-coupled estrogen receptor suppresses the migration of osteosarcoma cells via post-translational regulation of Snail. J Cancer Res Clin Oncol. 2019;145(1):87-96.

144. Wang Z, Chen X, Zhao Y, Jin Y, Zheng J. G-protein-coupled estrogen receptor suppresses the migration of osteosarcoma cells via post-translational regulation of Snail. Journal of cancer research and clinical oncology. 2019;145(1):87-96.

145. Kogo R, Mimori K, Tanaka F, Komune S, Mori M. FBXO31 determines poor prognosis in esophageal squamous cell carcinoma. International journal of oncology. 2011;39(1):155-9.

146. Zou S, Ma C, Yang F, Xu X, Jia J, Liu Z. FBXO31 Suppresses Gastric Cancer EMT by Targeting Snail1 for Proteasomal Degradation. Molecular cancer research : MCR. 2018;16(2):286-95.

147. D'Angiolella V, Donato V, Vijayakumar S, Saraf A, Florens L, Washburn MP, et al. SCF Cyclin F controls centrosome homeostasis and mitotic fidelity through CP110 degradation. Nature. 2010;466(7302):138-42.

148. Santra MK, Wajapeyee N, Green MR. F-box protein FBXO31 mediates cyclin D1 degradation to induce G1 arrest after DNA damage. Nature. 2009;459(7247):722-5.

149. Johansson P, Jeffery J, Al-Ejeh F, Schulz RB, Callen DF, Kumar R, et al. SCF-FBXO31 E3 ligase targets DNA replication factor Cdt1 for proteolysis in the G2 phase of cell cycle to prevent re-replication. The Journal of biological chemistry. 2014;289(26):18514-25.

150. Huang HL, Jiang Y, Wang YH, Chen T, He HJ, Liu T, et al. FBXO31 promotes cell proliferation, metastasis and invasion in lung cancer. American journal of cancer research. 2015;5(5):1814-22.

151. Dutta P, Islam S, Choppara S, Sengupta P, Kumar A, Kumar A, et al. The tumor suppressor FBXO31 preserves genomic integrity by regulating DNA replication and segregation through precise control of cyclin A levels. The Journal of biological chemistry. 2019;294(41):14879-95.

152. Huang HL, Zheng WL, Zhao R, Zhang B, Ma WL. FBXO31 is down-regulated and may function as a tumor suppressor in hepatocellular carcinoma. Oncology reports. 2010;24(3):715-20.

153. Kumar R, Neilsen PM, Crawford J, McKirdy R, Lee J, Powell JA, et al. FBXO31 is the chromosome 16q24.3 senescence gene, a candidate breast tumor suppressor, and a component of an SCF complex. Cancer research. 2005;65(24):11304-13.

154. Zhang X, Kong Y, Xu X, Xing H, Zhang Y, Han F, et al. F-box protein FBXO31 is down-regulated in gastric cancer and negatively regulated by miR-17 and miR-20a. Oncotarget. 2014;5(15):6178-90.

155. Said HM. Physiology of the Gastrointestinal Tract, Two Volume Set: Elsevier Science; 2012.

156. Board WCTE. Digestive System Tumours: International Agency for Research on Cancer; 2019.

157. Gazouli M, Theodoropoulos GE. Digestive System Diseases: Stem Cell Mechanisms and Therapies: Springer International Publishing; 2019.

158. Peterson LW, Artis D. Intestinal epithelial cells: regulators of barrier function and immune homeostasis. Nat Rev Immunol. 2014;14(3):141-53.

159. Umar S. Intestinal stem cells. Curr Gastroenterol Rep. 2010;12(5):340-8.

160. Vermeulen L, Snippert HJ. Stem cell dynamics in homeostasis and cancer of the intestine. Nat Rev Cancer. 2014;14(7):468-80.

161. Sato T, van Es JH, Snippert HJ, Stange DE, Vries RG, van den Born M, et al. Paneth cells constitute the niche for Lgr5 stem cells in intestinal crypts. Nature. 2011;469(7330):415-8.

162. Davies EJ, Marsh V, Clarke AR. Origin and maintenance of the intestinal cancer stem cell. Molecular carcinogenesis. 2011;50(4):254-63.

163. Brittan M, Wright N. Stem cell in gastrointestinal structure and neoplastic development. Gut. 2004;53(6):899-910.

164. Regad T, Sayers T, Rees R. Principles of Stem Cell Biology and Cancer: Future Applications and Therapeutics: Wiley; 2015.

165. Potten CS, Hume WJ, Reid P, Cairns J. The segregation of DNA in epithelial stem cells. Cell. 1978;15(3):899-906.

166. Potten CS, Owen G, Booth D. Intestinal stem cells protect their genome by selective segregation of template DNA strands. J Cell Sci. 2002;115(11):2381-8.

167. Sangiorgi E, Capecchi MR. Bmi1 is expressed in vivo in intestinal stem cells. Nat Genet. 2008;40(7):915-20.

168. Montgomery RK, Carlone DL, Richmond CA, Farilla L, Kranendonk ME, Henderson DE, et al. Mouse telomerase reverse transcriptase (mTert) expression marks slowly cycling intestinal stem cells. Proceedings of the National Academy of Sciences. 2011;108(1):179-84.

169. Takeda N, Jain R, LeBoeuf MR, Wang Q, Lu MM, Epstein JA. Interconversion between intestinal stem cell populations in distinct niches. Science. 2011;334(6061):1420-4.

170. Powell AE, Wang Y, Li Y, Poulin EJ, Means AL, Washington MK, et al. The pan-ErbB negative regulator Lrig1 is an intestinal stem cell marker that functions as a tumor suppressor. Cell. 2012;149(1):146-58.

171. Itzkovitz S, Lyubimova A, Blat IC, Maynard M, van Es J, Lees J, et al. Single-molecule transcript counting of stem-cell markers in the mouse intestine. Nature cell biology. 2012;14(1):106-14.

172. Muñoz J, Stange DE, Schepers AG, van de Wetering M, Koo BK, Itzkovitz S, et al. The Lgr5 intestinal stem cell signature: robust expression of proposed quiescent '+ 4'cell markers. The EMBO journal. 2012;31(14):3079-91.

173. Buczacki SJ, Zecchini HI, Nicholson AM, Russell R, Vermeulen L, Kemp R, et al. Intestinal label-retaining cells are secretory precursors expressing Lgr5. Nature. 2013;495(7439):65-9.

174. Potten CS, Owen G, Booth D. Intestinal stem cells protect their genome by selective segregation of template DNA strands. J Cell Sci. 2002;115(Pt 11):2381-8.

175. Takeda N, Jain R, LeBoeuf MR, Wang Q, Lu MM, Epstein JA. Interconversion between intestinal stem cell populations in distinct niches. Science. 2011;334(6061):1420-4.

176. Li L, Clevers H. Coexistence of quiescent and active adult stem cells in mammals. Science. 2010;327(5965):542-5.

177. Roth S, Franken P, Sacchetti A, Kremer A, Anderson K, Sansom O, et al. Paneth cells in intestinal homeostasis and tissue injury. PLoS One. 2012;7(6):e38965.

178. Clevers H. Stem Cells: A unifying theory for the crypt. Nature. 2013;495(7439):53-4.

179. Potten CS, Kovacs L, Hamilton E. Continuous labelling studies on mouse skin and intestine. Cell Tissue Kinet. 1974;7(3):271-83.

180. Korinek V, Barker N, Moerer P, van Donselaar E, Huls G, Peters PJ, et al. Depletion of epithelial stem-cell compartments in the small intestine of mice lacking Tcf-4. Nature genetics. 1998;19(4):379-83.

181. Flanagan DJ, Austin CR, Vincan E, Phesse TJ. Wnt signalling in gastrointestinal epithelial stem cells. Genes. 2018;9(4):178.

182. Kretzschmar K, Clevers H. Wnt/β-catenin signaling in adult mammalian epithelial stem cells. Developmental biology. 2017;428(2):273-82.

183. Fevr T, Robine S, Louvard D, Huelsken J. Wnt/β-catenin is essential for intestinal homeostasis and maintenance of intestinal stem cells. Molecular and cellular biology. 2007;27(21):7551-9.

184. Siegfried E, Wilder EL, Perrimon N. Components of wingless signalling in Drosophila. Nature. 1994;367(6458):76-80.

185. Logan CY, Nusse R. The Wnt signaling pathway in development and disease. Annu Rev Cell Dev Biol. 2004;20:781-810.

186. Zhan T, Rindtorff N, Boutros M. Wnt signaling in cancer. Oncogene. 2016.

187. Roose J, Clevers H. TCF transcription factors: molecular switches in carcinogenesis. Biochimica et Biophysica Acta (BBA)-Reviews on Cancer. 1999;1424(2):M23-M37.

188. Aberle H, Bauer A, Stappert J, Kispert A, Kemler R. β-catenin is a target for the ubiquitin–proteasome pathway. The EMBO journal. 1997;16(13):3797-804.

189. Niehrs C. The complex world of WNT receptor signalling. Nature reviews Molecular cell biology. 2012;13(12):767-79.

190. MacDonald BT, Tamai K, He X. Wnt/β-catenin signaling: components, mechanisms, and diseases. Developmental cell. 2009;17(1):9-26.

191. Fevr T, Robine S, Louvard D, Huelsken J. Wnt/beta-catenin is essential for intestinal homeostasis and maintenance of intestinal stem cells. Mol Cell Biol. 2007;27(21):7551-9.

192. Korinek V, Barker N, Moerer P, van Donselaar E, Huls G, Peters PJ, et al. Depletion of epithelial stem-cell compartments in the small intestine of mice lacking Tcf-4. Nat Genet. 1998;19(4):379-83.

193. Axelrod JD, editor Progress and challenges in understanding planar cell polarity signaling. Seminars in cell & developmental biology; 2009: Elsevier.

194. De A. Wnt/Ca2+ signaling pathway: a brief overview. Acta biochimica et biophysica Sinica. 2011:gmr079.

195. de Lau W, Barker N, Low TY, Koo B-K, Li VS, Teunissen H, et al. Lgr5 homologues associate with Wnt receptors and mediate R-spondin signalling. Nature. 2011;476(7360):293-7.

196. Barker N, van Es JH, Kuipers J, Kujala P, van den Born M, Cozijnsen M, et al. Identification of stem cells in small intestine and colon by marker gene Lgr5. Nature. 2007;449(7165):1003-7.

197. Barker N, Huch M, Kujala P, van de Wetering M, Snippert HJ, van Es JH, et al. Lgr5+ ve stem cells drive self-renewal in the stomach and build long-lived gastric units in vitro. Cell stem cell. 2010;6(1):25-36.

198. Jaks V, Barker N, Kasper M, Van Es JH, Snippert HJ, Clevers H, et al. Lgr5 marks cycling, yet long-lived, hair follicle stem cells. Nature genetics. 2008;40(11):1291-9.

199. Sato T, van Es JH, Snippert HJ, Stange DE, Vries RG, van den Born M, et al. Paneth cells constitute the niche for Lgr5 stem cells in intestinal crypts. Nature. 2011;469(7330):415-8.

200. Ohkawara B, Glinka A, Niehrs C. Rspo3 binds syndecan 4 and induces Wnt/PCP signaling via clathrin-mediated endocytosis to promote morphogenesis. Developmental cell. 2011;20(3):303-14.

201. Jin Y-R, Yoon JK. The R-spondin family of proteins: emerging regulators of WNT signaling. The international journal of biochemistry & cell biology. 2012;44(12):2278-87.

202. Glinka A, Dolde C, Kirsch N, Huang YL, Kazanskaya O, Ingelfinger D, et al. LGR4 and LGR5 are R-spondin receptors mediating Wnt/β-catenin and Wnt/PCP signalling. EMBO reports. 2011;12(10):1055-61.

203. Kim K-A, Wagle M, Tran K, Zhan X, Dixon MA, Liu S, et al. R-Spondin family members regulate the Wnt pathway by a common mechanism. Molecular biology of the cell. 2008;19(6):2588-96.

204. Nam J-S, Turcotte TJ, Smith PF, Choi S, Yoon JK. Mouse cristin/R-spondin family proteins are novel ligands for the Frizzled 8 and LRP6 receptors and activate β-catenin-dependent gene expression. Journal of Biological Chemistry. 2006;281(19):13247-57.

205. Koo BK, Spit M, Jordens I, Low TY, Stange DE, van de Wetering M, et al. Tumour suppressor RNF43 is a stem-cell E3 ligase that induces endocytosis of Wnt receptors. Nature. 2012;488(7413):665-9.

206. de Lau W, Peng WC, Gros P, Clevers H. The R-spondin/Lgr5/Rnf43 module: regulator of Wnt signal strength. Genes & development. 2014;28(4):305-16.

207. Hao H-X, Xie Y, Zhang Y, Charlat O, Oster E, Avello M, et al. ZNRF3 promotes Wnt receptor turnover in an R-spondin-sensitive manner. Nature. 2012;485(7397):195-200.

208. Snippert HJ, Van Der Flier LG, Sato T, Van Es JH, Van Den Born M, Kroon-Veenboer C, et al. Intestinal crypt homeostasis results from neutral competition between symmetrically dividing Lgr5 stem cells. Cell. 2010;143(1):134-44.

209. Kim TH, Escudero S, Shivdasani RA. Intact function of Lgr5 receptor-expressing intestinal stem cells in the absence of Paneth cells. Proc Natl Acad Sci U S A. 2012;109(10):3932-7.

210. Durand A, Donahue B, Peignon G, Letourneur F, Cagnard N, Slomianny C, et al. Functional intestinal stem cells after Paneth cell ablation induced by the loss of transcription factor Math1 (Atoh1). Proc Natl Acad Sci U S A. 2012;109(23):8965-70.

211. Kang MH, Kim JS, Seo JE, Oh SC, Yoo YA. BMP2 accelerates the motility and invasiveness of gastric cancer cells via activation of the phosphatidylinositol 3-kinase (PI3K)/Akt pathway. Exp Cell Res. 2010;316(1):24-37.

212. Kang HW, Gupta S, Bogdanov A, Jr. Orthotopic expression of noggin protein in cancer cells inhibits human lung carcinoma growth in vivo. Molecular imaging and biology : MIB : the official publication of the Academy of Molecular Imaging. 2012;14(4):480-8.

213. Sharov AA, Mardaryev AN, Sharova TY, Grachtchouk M, Atoyan R, Byers HR, et al. Bone morphogenetic protein antagonist noggin promotes skin tumorigenesis via stimulation of the Wnt and Shh signaling pathways. Am J Pathol. 2009;175(3):1303-14.

214. Yokoyama Y, Watanabe T, Tamura Y, Hashizume Y, Miyazono K, Ehata S. Autocrine BMP-4 Signaling Is a Therapeutic Target in Colorectal Cancer. Cancer Res. 2017;77(15):4026-38.

215. Krause C, Guzman A, Knaus P. Noggin. The international journal of biochemistry & cell biology. 2011;43(4):478-81.

216. Smith WC, Harland RM. Expression cloning of noggin, a new dorsalizing factor localized to the Spemann organizer in Xenopus embryos. Cell. 1992;70(5):829-40.

217. Zimmerman LB, De Jesus-Escobar JM, Harland RM. The Spemann organizer signal noggin binds and inactivates bone morphogenetic protein 4. Cell. 1996;86(4):599-606.

218. Piccolo S, Sasai Y, Lu B, De Robertis EM. Dorsoventral patterning in Xenopus: inhibition of ventral signals by direct binding of chordin to BMP-4. Cell. 1996;86(4):589-98.

219. Sukhotnik I, Berkowitz D, Dorfman T, Halabi S, Pollak Y, Bejar J, et al. The role of the BMP signaling cascade in regulation of stem cell activity following massive small bowel resection in a rat. Pediatric surgery international. 2016;32(2):169-74.

220. Hardwick JC, Van Den Brink GR, Bleuming SA, Ballester I, Van Den Brande JM, Keller JJ, et al. Bone morphogenetic protein 2 is expressed by, and acts upon, mature epithelial cells in the colon. Gastroenterology. 2004;126(1):111-21.

221. Kuroda K, Kuang S, Taketo MM, Rudnicki MA. Canonical Wnt signaling induces BMP-4 to specify slow myofibrogenesis of fetal myoblasts. Skeletal muscle. 2013;3(1):5.

222. Davis H, Irshad S, Bansal M, Rafferty H, Boitsova T, Bardella C, et al. Aberrant epithelial GREM1 expression initiates colonic tumorigenesis from cells outside the stem cell niche. Nature medicine. 2015;21(1):62-70.

223. Haramis A-PG, Begthel H, Van Den Born M, Van Es J, Jonkheer S, Offerhaus GJA, et al. De novo crypt formation and juvenile polyposis on BMP inhibition in mouse intestine. Science. 2004;303(5664):1684-6.

224. He XC, Zhang J, Tong W-G, Tawfik O, Ross J, Scoville DH, et al. BMP signaling inhibits intestinal stem cell self-renewal through suppression of Wnt–β-catenin signaling. Nature genetics. 2004;36(10):1117-21.

225. Tarragona M, Pavlovic M, Arnal-Estapé A, Urosevic J, Morales M, Guiu M, et al. Identification of NOG as a specific breast cancer bone metastasis-supporting gene. Journal of Biological Chemistry. 2012;287(25):21346-55.

226. Virk MS, Petrigliano FA, Liu NQ, Chatziioannou AF, Stout D, Kang CO, et al. Influence of simultaneous targeting of the bone morphogenetic protein pathway and RANK/RANKL axis in osteolytic prostate cancer lesion in bone. Bone. 2009;44(1):160-7.

227. Sato T, Stange DE, Ferrante M, Vries RG, Van Es JH, Van den Brink S, et al. Long-term expansion of epithelial organoids from human colon, adenoma, adenocarcinoma, and Barrett's epithelium. Gastroenterology. 2011;141(5):1762-72.

228. Sato T, Vries RG, Snippert HJ, van de Wetering M, Barker N, Stange DE, et al. Single Lgr5 stem cells build crypt-villus structures in vitro without a mesenchymal niche. Nature. 2009;459(7244):262-5.

229. Sugimoto S, Sato T. Establishment of 3D intestinal organoid cultures from intestinal stem cells. 3D Cell Culture: Springer; 2017. p. 97-105.

230. Ferlay J, Soerjomataram I, Ervik M, Eser S, Mathers C, Rebelo M. GLOBOCAN 2012 v1. 0, Cancer Incidence and Mortality Worldwide: IARC Cancer Base No. 11 2013. Lyon, France: International Agency for Research on Cancer. 2014.

231. Gini A, Jansen EE, Zielonke N, Meester RG, Senore C, Anttila A, et al. Impact of colorectal cancer screening on cancer-specific mortality in Europe: A systematic review. European Journal of Cancer. 2020.

232. Vogelstein B, Fearon ER, Hamilton SR, Kern SE, Preisinger AC, Leppert M, et al. Genetic alterations during colorectal-tumor development. N Engl J Med. 1988;319(9):525-32.

233. Vries RG, Huch M, Clevers H. Stem cells and cancer of the stomach and intestine. Molecular oncology. 2010;4(5):373-84.

234. Markowitz SD, Bertagnolli MM. Molecular basis of colorectal cancer. New England Journal of Medicine. 2009;361(25):2449-60.

235. Tariq K, Ghias K. Colorectal cancer carcinogenesis: a review of mechanisms. Cancer biology & medicine. 2016;13(1):120.

236. Nazemalhosseini Mojarad E, Kuppen PJ, Aghdaei HA, Zali MR. The CpG island methylator phenotype (CIMP) in colorectal cancer. Gastroenterol Hepatol Bed Bench. 2013;6(3):120-8.

237. Tijhuis AE, Johnson SC, McClelland SE. The emerging links between chromosomal instability (CIN), metastasis, inflammation and tumour immunity. Molecular cytogenetics. 2019;12:17.

238. Colussi D, Brandi G, Bazzoli F, Ricciardiello L. Molecular pathways involved in colorectal cancer: implications for disease behavior and prevention. Int J Mol Sci. 2013;14(8):16365-85.

239. Guinney J, Dienstmann R, Wang X, De Reyniès A, Schlicker A, Soneson C, et al. The consensus molecular subtypes of colorectal cancer. Nature medicine. 2015;21(11):1350-6.

240. Engstrom PF, Arnoletti JP, Benson AB, Chen Y-J, Choti MA, Cooper HS, et al. Colon cancer. Journal of the National Comprehensive Cancer Network. 2009;7(8):778-831.

241. Rutman RJ, Cantarow A, Paschkis KE. Studies in 2-acetylaminofluorene carcinogenesis. III. The utilization of uracil-2-C14 by preneoplastic rat liver and rat hepatoma. Cancer Res. 1954;14(2):119-23.

242. Noordhuis P, Holwerda U, Van der Wilt CL, Van Groeningen CJ, Smid K, Meijer S, et al. 5-Fluorouracil incorporation into RNA and DNA in relation to thymidylate synthase inhibition of human colorectal cancers. Annals of oncology : official journal of the European Society for Medical Oncology. 2004;15(7):1025-32.

243. Zhang N, Yin Y, Xu SJ, Chen WS. 5-Fluorouracil: mechanisms of resistance and reversal strategies. Molecules (Basel, Switzerland). 2008;13(8):1551-69.

244. Carethers JM. Systemic treatment of advanced colorectal cancer: tailoring therapy to the tumor. Therapeutic advances in gastroenterology. 2008;1(1):33-42.

245. Evrard A, Cuq P, Ciccolini J, Vian L, Cano JP. Increased cytotoxicity and bystander effect of 5-fluorouracil and 5-deoxy-5-fluorouridine in human colorectal cancer cells transfected with thymidine phosphorylase. British journal of cancer. 1999;80(11):1726-33.

246. Van der Jeught K, Xu H-C, Li Y-J, Lu X-B, Ji G. Drug resistance and new therapies in colorectal cancer. World journal of gastroenterology. 2018;24(34):3834-48.

247. Alibek K, Bekmurzayeva A, Mussabekova A, Sultankulov B. Using antimicrobial adjuvant therapy in cancer treatment: a review. Infectious agents and cancer. 2012;7(1):33.

248. Herold C, Ocker M, Ganslmayer M, Gerauer H, Hahn EG, Schuppan D. Ciprofloxacin induces apoptosis and inhibits proliferation of human colorectal carcinoma cells. British journal of cancer. 2002;86(3):443-8.

249. Dong Z, Abbas MN, Kausar S, Yang J, Li L, Tan L, et al. Biological Functions and Molecular Mechanisms of Antibiotic Tigecycline in the Treatment of Cancers. Int J Mol Sci. 2019;20(14).

250. Kan JY, Hsu YL, Chen YH, Chen TC, Wang JY, Kuo PL. Gemifloxacin, a fluoroquinolone antimicrobial drug, inhibits migration and invasion of human colon cancer cells. BioMed research international. 2013;2013:159786.

251. Relier S, Yazdani L, Ayad O, Choquet A, Bourgaux JF, Prudhomme M, et al. Antibiotics inhibit sphere-forming ability in suspension culture. Cancer cell international. 2016;16:6.

252. Ahmed M, Jinks N, Babaei-Jadidi R, Kashfi H, Castellanos-Uribe M, May ST, et al. Repurposing Antibacterial AM404 as a Potential Anticancer Drug for Targeting Colorectal Cancer Stem-Like Cells. Cancers. 2019;12(1):106.

253. Lindmark G, Gerdin B, Påhlman L, Bergström R, Glimelius B. Prognostic predictors in colorectal cancer. Diseases of the colon & rectum. 1994;37(12):1219-27.

254. Van Cutsem E, Cervantes A, Nordlinger B, Arnold D. Metastatic colorectal cancer: ESMO Clinical Practice Guidelines for diagnosis, treatment and follow-up. Annals of oncology. 2014:mdu260.

255. Andres A, Mentha G, Adam R, Gerstel E, Skipenko O, Barroso E, et al. Surgical management of patients with colorectal cancer and simultaneous liver and lung metastases. British Journal of Surgery. 2015;102(6):691-9.

256. Baumann M. Oxford Textbook of Oncology: Oxford University Press; 2016.

257. Brabletz T. EMT and MET in metastasis: where are the cancer stem cells? Cancer cell. 2012;22(6):699-701.

258. Vermeulen L, Todaro M, de Sousa Mello F, Sprick MR, Kemper K, Perez Alea M, et al. Single-cell cloning of colon cancer stem cells reveals a multi-lineage differentiation capacity. Proc Natl Acad Sci U S A. 2008;105(36):13427-32.

259. Puglisi MA, Tesori V, Lattanzi W, Gasbarrini GB, Gasbarrini A. Colon cancer stem cells: controversies and perspectives. World J Gastroenterol. 2013;19(20):2997-3006.

260. O'Brien CA, Pollett A, Gallinger S, Dick JE. A human colon cancer cell capable of initiating tumour growth in immunodeficient mice. Nature. 2007;445(7123):106-10.

261. Ricci-Vitiani L, Lombardi D, Signore M, Biffoni M, Pallini R, Parati E, et al. Human neural progenitor cells display limited cytotoxicity and increased oligodendrogenesis during inflammation. Cell Death & Differentiation. 2007;14(4):876-8.

262. Barker N, Ridgway RA, Van Es JH, Van De Wetering M, Begthel H, Van Den Born M, et al. Crypt stem cells as the cells-of-origin of intestinal cancer. Nature. 2009;457(7229):608-11.

263. Kemper K, Prasetyanti PR, De Lau W, Rodermond H, Clevers H, Medema JP. Monoclonal antibodies against Lgr5 identify human colorectal cancer stem cells. Stem Cells. 2012;30(11):2378-86.

264. Dalerba P, Dylla SJ, Park I-K, Liu R, Wang X, Cho RW, et al. Phenotypic characterization of human colorectal cancer stem cells. Proceedings of the National Academy of Sciences. 2007;104(24):10158-63.

265. Huang EH, Hynes MJ, Zhang T, Ginestier C, Dontu G, Appelman H, et al. Aldehyde dehydrogenase 1 is a marker for normal and malignant human colonic stem cells (SC) and tracks SC overpopulation during colon tumorigenesis. Cancer research. 2009;69(8):3382-9.

266. Vermeulen L, Felipe De Sousa EM, van der Heijden M, Cameron K, de Jong JH, Borovski T, et al. Wnt activity defines colon cancer stem cells and is regulated by the microenvironment. Nature cell biology. 2010;12(5):468-76.

267. Schepers AG, Snippert HJ, Stange DE, van den Born M, van Es JH, van de Wetering M, et al. Lineage tracing reveals Lgr5+ stem cell activity in mouse intestinal adenomas. Science. 2012;337(6095):730-5.

268. Ricci-Vitiani L, Lombardi DG, Pilozzi E, Biffoni M, Todaro M, Peschle C, et al. Identification and expansion of human colon-cancer-initiating cells. Nature. 2007;445(7123):111-5.

269. Dick D. Human acute myeloid leukemia is organized as a hierarchy that originates from a primitive hematopoietic cell. Nature Med. 1997;3:730-7.

270. Singh SK, Clarke ID, Terasaki M, Bonn VE, Hawkins C, Squire J, et al. Identification of a cancer stem cell in human brain tumors. Cancer research. 2003;63(18):5821-8.

271. Al-Hajj M, Wicha MS, Benito-Hernandez A, Morrison SJ, Clarke MF. Prospective identification of tumorigenic breast cancer cells. Proceedings of the National Academy of Sciences. 2003;100(7):3983-8.

272. Li C, Heidt DG, Dalerba P, Burant CF, Zhang L, Adsay V, et al. Identification of pancreatic cancer stem cells. Cancer research. 2007;67(3):1030-7.

273. Eramo A, Lotti F, Sette G, Pilozzi E, Biffoni M, Di Virgilio A, et al. Identification and expansion of the tumorigenic lung cancer stem cell population. Cell Death & Differentiation. 2008;15(3):504-14.

274. Patrawala L, Calhoun T, Schneider-Broussard R, Li H, Bhatia B, Tang S, et al. Highly purified CD44+ prostate cancer cells from xenograft human tumors are enriched in tumorigenic and metastatic progenitor cells. Oncogene. 2006;25(12):1696-708.

275. Tata PR, Mou H, Pardo-Saganta A, Zhao R, Prabhu M, Law BM, et al. Dedifferentiation of committed epithelial cells into stem cells in vivo. Nature. 2013;503(7475):218-23.

276. Maitland NJ, Collins AT. Prostate cancer stem cells: a new target for therapy. J Clin Oncol. 2008;26(17):2862-70.

277. Zhang M, Behbod F, Atkinson RL, Landis MD, Kittrell F, Edwards D, et al. Identification of tumor-initiating cells in a p53-null mouse model of breast cancer. Cancer Res. 2008;68(12):4674-82.

278. Visvader JE. Keeping abreast of the mammary epithelial hierarchy and breast tumorigenesis. Genes Dev. 2009;23(22):2563-77.

279. Owens TW, Naylor MJ. Breast cancer stem cells. Front Physiol. 2013;4:225.

280. Croker AK, Goodale D, Chu J, Postenka C, Hedley BD, Hess DA, et al. High aldehyde dehydrogenase and expression of cancer stem cell markers selects for breast cancer cells with enhanced malignant and metastatic ability. J Cell Mol Med. 2009;13(8B):2236-52.

281. Brabletz T, Jung A, Spaderna S, Hlubek F, Kirchner T. Opinion: migrating cancer stem cells - an integrated concept of malignant tumour progression. Nat Rev Cancer. 2005;5(9):744-9.

282. Aref A, Huang R, Kang W, Jing S, Thiery J, Kamm R. Transitions Between Epithelial and Mesenchymal States in Microfluidic Platform: Acquisition of Malignant and Stem Cell Traits. une. 2016;13:15.

283. Michl M, Heinemann V, Jung A, Engel J, Kirchner T, Neumann J. Expression of cancer stem cell markers in metastatic colorectal cancer correlates with liver metastasis, but not with metastasis to the central nervous system. Pathol Res Pract. 2015;211(8):601-9.

284. Michl M, Heinemann V, Jung A, Engel J, Kirchner T, Neumann J. Expression of cancer stem cell markers in metastatic colorectal cancer correlates with liver metastasis, but not with metastasis to the central nervous system. Pathology-Research and Practice. 2015;211(8):601-9.

285. Pang R, Law WL, Chu AC, Poon JT, Lam CS, Chow AK, et al. A subpopulation of CD26+ cancer stem cells with metastatic capacity in human colorectal cancer. Cell stem cell. 2010;6(6):603-15.

286. Frank NY, Margaryan A, Huang Y, Schatton T, Waaga-Gasser AM, Gasser M, et al. ABCB5-mediated doxorubicin transport and chemoresistance in human malignant melanoma. Cancer research. 2005;65(10):4320-33.

287. Zhang HL, Wang P, Lu MZ, Zhang SD. [c-Myc regulation of ATP-binding cassette transporter reverses chemoresistance in CD133(+) colon cancer stem cells]. Sheng Li Xue Bao. 2016;68(2):171-8.

288. Cojoc M, Mäbert K, Muders MH, Dubrovska A, editors. A role for cancer stem cells in therapy resistance: cellular and molecular mechanisms. Seminars in cancer biology; 2015: Elsevier.

289. Fletcher JI, Williams RT, Henderson MJ, Norris MD, Haber M. ABC transporters as mediators of drug resistance and contributors to cancer cell biology. Drug Resistance Updates. 2016;26:1-9.

290. Zheng W, Yin T, Chen Q, Qin X, Huang X, Zhao S, et al. Co-delivery of Se nanoparticles and pooled SiRNAs for overcoming drug resistance mediated by P-glycoprotein and class III β-tubulin in drug-resistant breast cancers. Acta biomaterialia. 2016;31:197-210.

291. Macalou S, Robey R, Gozzi GJ, Shukla S, Grosjean I, Hegedus T, et al. The linker region of breast cancer resistance protein ABCG2 is critical for coupling of ATP-dependent drug transport. Cellular and Molecular Life Sciences. 2016;73(9):1927-37.

292. Bleau A-M, Hambardzumyan D, Ozawa T, Fomchenko EI, Huse JT, Brennan CW, et al. PTEN/PI3K/Akt pathway regulates the side population phenotype and ABCG2 activity in glioma tumor stem-like cells. Cell stem cell. 2009;4(3):226-35.

293. Huang W-C, Hsieh Y-L, Hung C-M, Chien P-H, Chien Y-F, Chen L-C, et al. BCRP/ABCG2 inhibition sensitizes hepatocellular carcinoma cells to sorafenib. PLoS One. 2013;8(12):e83627.

294. Zhang H, Wang P, Lu M, Zhang S. [c-Myc regulation of ATP-binding cassette transporter reverses chemoresistance in CD133 (+) colon cancer stem cells]. Sheng li xue bao:[Acta physiologica Sinica]. 2016;68(2):171-8.

295. Candeil L, Gourdier I, Peyron D, Vezzio N, Copois V, Bibeau F, et al. ABCG2 overexpression in colon cancer cells resistant to SN38 and in irinotecan-treated metastases. International Journal of Cancer. 2004;109(6):848-54.

296. Huang F-F, Wu D-S, Zhang L, Yu Y-H, Yuan X-Y, Li W-J, et al. Inactivation of PTEN increases ABCG2 expression and the side population through the PI3K/Akt pathway in adult acute leukemia. Cancer letters. 2013;336(1):96-105.

297. Uchida N, Buck DW, He D, Reitsma MJ, Masek M, Phan TV, et al. Direct isolation of human central nervous system stem cells. Proc Natl Acad Sci U S A. 2000;97(26):14720-5.

298. Belicchi M, Pisati F, Lopa R, Porretti L, Fortunato F, Sironi M, et al. Human skin-derived stem cells migrate throughout forebrain and differentiate into astrocytes after injection into adult mouse brain. J Neurosci Res. 2004;77(4):475-86.

299. Abdullah LN, Chow EK-H. Mechanisms of chemoresistance in cancer stem cells. Clinical and translational medicine. 2013;2(1):1.

300. Hlavata I, Mohelnikova-Duchonova B, Vaclavikova R, Liska V, Pitule P, Novak P, et al. The role of ABC transporters in progression and clinical outcome of colorectal cancer. Mutagenesis. 2012;27(2):187-96.

301. Higgins CF. ABC transporters: from microorganisms to man. Annual review of cell biology. 1992;8(1):67-113.

302. Emmink BL, Van Houdt WJ, Vries RG, Hoogwater FJ, Govaert KM, Verheem A, et al. Differentiated human colorectal cancer cells protect tumor-initiating cells from irinotecan. Gastroenterology. 2011;141(1):269-78.

303. Hostettler L, Zlobec I, Terracciano L, Lugli A. ABCG5-positivity in tumor buds is an indicator of poor prognosis in node-negative colorectal cancer patients. World J Gastroenterol. 2010;16(6):732-9.

304. O'Brien CA, Pollett A, Gallinger S, Dick JE. A human colon cancer cell capable of initiating tumour growth in immunodeficient mice. Nature. 2007;445(7123):106-10.

305. Ricci-Vitiani L, Lombardi DG, Pilozzi E, Biffoni M, Todaro M, Peschle C, et al. Identification and expansion of human colon-cancer-initiating cells. Nature. 2007;445(7123):111-5.

306. Dalerba P, Dylla SJ, Park IK, Liu R, Wang X, Cho RW, et al. Phenotypic characterization of human colorectal cancer stem cells. Proc Natl Acad Sci U S A. 2007;104(24):10158-63.

307. Todaro M, Alea MP, Di Stefano AB, Cammareri P, Vermeulen L, Iovino F, et al. Colon cancer stem cells dictate tumor growth and resist cell death by production of interleukin-4. Cell Stem Cell. 2007;1(4):389-402.

308. Pang R, Law WL, Chu AC, Poon JT, Lam CS, Chow AK, et al. A subpopulation of CD26+ cancer stem cells with metastatic capacity in human colorectal cancer. Cell Stem Cell. 2010;6(6):603-15.

309. Ren F, Sheng W-Q, Du X. CD133: a cancer stem cells marker, is used in colorectal cancers. World J Gastroenterol. 2013;19(17):2603-11.

310. Moncharmont C, Levy A, Gilormini M, Bertrand G, Chargari C, Alphonse G, et al. Targeting a cornerstone of radiation resistance: cancer stem cell. Cancer Lett. 2012;322(2):139-47.

311. Peitzsch C, Kurth I, Kunz-Schughart L, Baumann M, Dubrovska A. Discovery of the cancer stem cell related determinants of radioresistance. Radiother Oncol. 2013;108(3):378-87.

312. Pawlik TM, Keyomarsi K. Role of cell cycle in mediating sensitivity to radiotherapy. Int J Radiat Oncol Biol Phys. 2004;59(4):928-42.

313. Horsman MR, Wouters BG, Joiner MC, Overgaard J. The oxygen effect and fractionated radiotherapy. Basic clinical radiobiology: Edward Arnold, London; 2009. p. 207-16.

314. Bussink J, Kaanders JHA, Rijken PFJ, Raleigh JA, Van der Kogel AJ. Changes in blood perfusion and hypoxia after irradiation of a human squamous cell carcinoma xenograft tumor line. Radiation research. 2000;153(4):398-404.

315. Park SE, Georgescu A, Huh D. Organoids-on-a-chip. Science. 2019;364(6444):960-5.

316. Ahmed M, Jinks N, Babaei-Jadidi R, Kashfi H, Castellanos-Uribe M, May ST, et al. Repurposing Antibacterial AM404 as a Potential Anticancer Drug for Targeting Colorectal Cancer Stem-Like Cells. Cancers. 2020;12(1):106.

317. Mao JH, Kim IJ, Wu D, Climent J, Kang HC, DelRosario R, et al. FBXW7 targets mTOR for degradation and cooperates with PTEN in tumor suppression. Science. 2008;321(5895):1499-502.

318. Rajagopalan H, Jallepalli PV, Rago C, Velculescu VE, Kinzler KW, Vogelstein B, et al. Inactivation of hCDC4 can cause chromosomal instability. Nature. 2004;428(6978):77-81.

319. Lorenzi F, Babaei-Jadidi R, Sheard J, Spencer-Dene B, Nateri AS. Fbxw7-associated drug resistance is reversed by induction of terminal differentiation in murine intestinal organoid culture. Molecular therapy Methods & clinical development. 2016;3:16024.

320. Ibrahim EE, Babaei-Jadidi R, Saadeddin A, Spencer-Dene B, Hossaini S, Abuzinadah M, et al. Embryonic NANOG Activity Defines Colorectal Cancer Stem Cells and Modulates through AP1- and TCF-dependent Mechanisms. STEM CELLS. 2012;30(10):2076-87.

321. Vichai V, Kirtikara K. Sulforhodamine B colorimetric assay for cytotoxicity screening. Nature Protocols. 2006;1(3):1112-6.

322. Li NN, Lorenzi F, Kalakouti E, Normatova M, Babaei-Jadidi R, Tomlinson I, et al. FBXW7-mutated colorectal cancer cells exhibit aberrant expression of phosphorylated-p53 at Serine-15. Oncotarget. 2015;6(11):9240-56.

323. Lorenzi F, Babaei-Jadidi R, Sheard J, Spencer-Dene B, Nateri AS. Fbxw7-associated drug resistance is reversed by induction of terminal differentiation in murine intestinal organoid culture. Molecular Therapy — Methods & Clinical Development. 2016;3:16024.

324. Rodriguez LG, Wu X, Guan J-L. Wound-healing assay. Cell Migration: Springer; 2005. p. 23-9.

325. Weiswald L-B, Bellet D, Dangles-Marie V. Spherical Cancer Models in Tumor Biology. Neoplasia. 2015;17(1):1-15.

326. Shaheen S, Ahmed M, Lorenzi F, Nateri AS. Spheroid-Formation (Colonosphere) Assay for in Vitro Assessment and Expansion of Stem Cells in Colon Cancer. Stem cell reviews. 2016;12(4):492-9.

327. Rossi G, Manfrin A, Lutolf MP. Progress and potential in organoid research. Nature reviews Genetics. 2018;19(11):671-87.

328. Drost J, Clevers H. Organoids in cancer research. Nature Reviews Cancer. 2018;18(7):407.

329. Roper J, Tammela T, Akkad A, Almeqdadi M, Santos SB, Jacks T, et al. Colonoscopy-based colorectal cancer modeling in mice with CRISPR–Cas9 genome editing and organoid transplantation. Nature protocols. 2018;13(2):217.

330. Kashfi SMH, Almozyan S, Jinks N, Koo BK, Nateri AS. Morphological alterations of cultured human colorectal matched tumour and normal organoids. Oncotarget. 2018;9(12):10572-84.

331. Matsui M. Multiple Roles of Noggin, a BMP Antagonist, in Development of Craniofacial Skeletal: Duke University; 2014.

332. Marcelino J, Sciortino CM, Romero MF, Ulatowski LM, Ballock RT, Economides AN, et al. Human disease-causing NOG missense mutations: effects on noggin secretion, dimer formation, and bone morphogenetic protein binding. Proceedings of the National Academy of Sciences of the United States of America. 2001;98(20):11353-8.

333. Dedhia PH, Bertaux-Skeirik N, Zavros Y, Spence JR. Organoid models of human gastrointestinal development and disease. Gastroenterology. 2016;150(5):1098-112.

334. Punt CJ, Koopman M, Vermeulen L. From tumour heterogeneity to advances in precision treatment of colorectal cancer. Nature reviews Clinical oncology. 2017;14(4):235-46.

335. Prasetyanti PR, Medema JP. Intra-tumor heterogeneity from a cancer stem cell perspective. Molecular cancer. 2017;16(1):41.

336. Drost J, Van Jaarsveld RH, Ponsioen B, Zimberlin C, Van Boxtel R, Buijs A, et al. Sequential cancer mutations in cultured human intestinal stem cells. Nature. 2015;521(7550):43.

337. Verissimo CS, Overmeer RM, Ponsioen B, Drost J, Mertens S, Verlaan-Klink I, et al. Targeting mutant RAS in patient-derived colorectal cancer organoids by combinatorial drug screening. Elife. 2016;5:e18489.

338. Riccardi C, Nicoletti I. Analysis of apoptosis by propidium iodide staining and flow cytometry. Nature protocols. 2006;1(3):1458.

339. Bartfeld S, Clevers H. Stem cell-derived organoids and their application for medical research and patient treatment. Journal of molecular medicine (Berlin, Germany). 2017;95(7):729-38.

340. Drost J, Van Boxtel R, Blokzijl F, Mizutani T, Sasaki N, Sasselli V, et al. Use of CRISPR-modified human stem cell organoids to study the origin of mutational signatures in cancer. Science. 2017;358(6360):234-8.

341. Fujii M, Shimokawa M, Date S, Takano A, Matano M, Nanki K, et al. A colorectal tumor organoid library demonstrates progressive loss of niche factor requirements during tumorigenesis. Cell stem cell. 2016;18(6):827-38.

342. Kashfi SMH, Almozyan S, Jinks N, Koo B-K, Nateri AS. Morphological alterations of cultured human colorectal matched tumour and normal organoids. Oncotarget. 2018;9(12):10572.

343. Cai T, Qi Y, Jergens A, Wannemuehler M, Barrett TA, Wang Q. Effects of six common dietary nutrients on murine intestinal organoid growth. PloS one. 2018;13(2):e0191517.

344. Nam MO, Hahn S, Jee JH, Hwang TS, Yoon H, Lee DH, et al. Effects of a small molecule R-spondin-1 substitute RS-246204 on a mouse intestinal organoid culture. Oncotarget. 2018;9(5):6356-68.

345. Pastula A, Middelhoff M, Brandtner A, Tobiasch M, Hohl B, Nuber AH, et al. Three-Dimensional Gastrointestinal Organoid Culture in Combination with Nerves or Fibroblasts: A Method to Characterize the Gastrointestinal Stem Cell Niche. Stem cells international. 2016;2016:3710836.

346. Fujii M, Clevers H, Sato T. Modeling Human Digestive Diseases With CRISPR-Cas9–Modified Organoids. Gastroenterology. 2019;156(3):562-76.

347. Matano M, Date S, Shimokawa M, Takano A, Fujii M, Ohta Y, et al. Modeling colorectal cancer using CRISPR-Cas9-mediated engineering of human intestinal organoids. Nature medicine. 2015;21(3):256-62.

348. Takeda H, Kataoka S, Nakayama M, Ali MAE, Oshima H, Yamamoto D, et al. CRISPR-Cas9-mediated gene knockout in intestinal tumor organoids provides functional validation for colorectal cancer driver genes. Proceedings of the National Academy of Sciences of the United States of America. 2019;116(31):15635-44.

349. Schwank G, Clevers H. CRISPR/Cas9-Mediated Genome Editing of Mouse Small Intestinal Organoids. Methods in molecular biology (Clifton, NJ). 2016;1422:3-11.

350. Fujii M, Shimokawa M, Date S, Takano A, Matano M, Nanki K, et al. A Colorectal Tumor Organoid Library Demonstrates Progressive Loss of Niche Factor Requirements during Tumorigenesis. Cell stem cell. 2016;18(6):827-38.

351. Cristobal A, van den Toorn HWP, van de Wetering M, Clevers H, Heck AJR, Mohammed S. Personalized Proteome Profiles of Normal and Tumor Human Colon Organoids Reveal Both Individual Diversity and Basic Features of Colorectal Cancer. Cell reports. 2017;18(1):263-74.

352. Gjorevski N, Sachs N, Manfrin A, Giger S, Bragina ME, Ordonez-Moran P, et al. Designer matrices for intestinal stem cell and organoid culture. Nature. 2016;539(7630):560-4.

353. Yin X, Farin HF, van Es JH, Clevers H, Langer R, Karp JM. Niche-independent high-purity cultures of Lgr5+ intestinal stem cells and their progeny. Nature methods. 2014;11(1):106-12.

354. AlShaibi HF, Ahmed F, Buckle C, Fowles ACM, Awlia J, Cecchini MG, et al. The BMP antagonist Noggin is produced by osteoblasts in response to the presence of prostate cancer cells. Biotechnol Appl Biochem. 2018;65(3):407-18.

355. Lombardo Y, Scopelliti A, Cammareri P, Todaro M, Iovino F, Ricci–Vitiani L, et al. Bone morphogenetic protein 4 induces differentiation of colorectal cancer stem cells and increases their response to chemotherapy in mice. Gastroenterology. 2011;140(1):297-309. e6.

356. Crabol Y, Catherinot E, Veziris N, Jullien V, Lortholary O. Rifabutin: where do we stand in 2016? Journal of Antimicrobial Chemotherapy. 2016;71(7):1759-71.

357. Ma Z, Ginsberg AM, Spigelman M. 7.24 - Antimycobacterium Agents. In: Taylor JB, Triggle DJ, editors. Comprehensive Medicinal Chemistry II. Oxford: Elsevier; 2007. p. 699-730.

358. Das B, Patra S. Antimicrobials: Meeting the Challenges of Antibiotic Resistance Through Nanotechnology. Nanostructures for Antimicrobial Therapy: Elsevier; 2017. p. 1-22.

359. Jenks JD, Kumarasamy N, Ezhilarasi C, Poongulali S, Ambrose P, Yepthomi T, et al. Improved tuberculosis outcomes with daily vs. intermittent rifabutin in HIV-TB coinfected patients in India. The international journal of tuberculosis and lung disease : the official journal of the International Union against Tuberculosis and Lung Disease. 2016;20(9):1181-4.

360. Kast RE, Skuli N, Cos S, Karpel-Massler G, Shiozawa Y, Goshen R, et al. The ABC7 regimen: a new approach to metastatic breast cancer using seven common drugs to inhibit epithelial-to-mesenchymal transition and augment capecitabine efficacy. Breast Cancer (Dove Med Press). 2017;9:495-514.

361. Li N, Babaei-Jadidi R, Lorenzi F, Spencer-Dene B, Clarke P, Domingo E, et al. An FBXW7-ZEB2 axis links EMT and tumour microenvironment to promote colorectal cancer stem cells and chemoresistance. Oncogenesis. 2019;8(3):13.

362. Han M, Dai D, Yousafzai NA, Wang F, Wang H, Zhou Q, et al. CXXC4 activates apoptosis through up-regulating GDF15 in gastric cancer. Oncotarget. 2017;8(61):103557.

363. Kuo IY, Wu CC, Chang JM, Huang YL, Lin CH, Yan JJ, et al. Low SOX17 expression is a prognostic factor and drives transcriptional dysregulation and esophageal cancer progression. International journal of cancer. 2014;135(3):563-73.

364. Abdalkareem EA, Ong CY, Lim BH, Khoo BY. Neutralizing FGF4 protein in conditioned medium of IL-21-silenced HCT116 cells restores the migratory activity of the colorectal cancer cells. Cytotechnology. 2018;70(5):1363-74.

365. Daulat AM, Bertucci F, Audebert S, Sergé A, Finetti P, Josselin E, et al. PRICKLE1 contributes to cancer cell dissemination through its interaction with mTORC2. Developmental cell. 2016;37(4):311-25.

366. Hu H, Li B, Zhou C, Ying X, Chen M, Huang T, et al. Diagnostic value of WIF1 methylation for colorectal cancer: a meta-analysis. Oncotarget. 2018;9(4):5378.

367. Sandsmark E, Andersen MK, Bofin AM, Bertilsson H, Drabløs F, Bathen TF, et al. SFRP4 gene expression is increased in aggressive prostate cancer. Scientific reports. 2017;7(1):1-10.

368. Castro-Piedras I, Sharma M, den Bakker M, Molehin D, Martinez EG, Vartak D, et al. DVL1 and DVL3 differentially localize to CYP19A1 promoters and regulate aromatase mRNA in breast cancer cells. Oncotarget. 2018;9(86):35639.

369. Thiele S, Zimmer A, Göbel A, Rachner TD, Rother S, Fuessel S, et al. Role of WNT5A receptors FZD5 and RYK in prostate cancer cells. Oncotarget. 2018;9(43):27293.

370. Lee SY, Kim KA, Kim CH, Kim YJ, Lee JH, Kim HR. CD44-shRNA recombinant adenovirus inhibits cell proliferation, invasion, and migration, and promotes apoptosis in HCT116 colon cancer cells. International journal of oncology. 2017;50(1):329-36.

371. Park YS, Huh JW, Lee JH, Kim HR. shRNA against CD44 inhibits cell proliferation, invasion and migration, and promotes apoptosis of colon carcinoma cells. Oncology reports. 2012;27(2):339-46.

372. Xia P, Xu XY. Prognostic significance of CD44 in human colon cancer and gastric cancer: Evidence from bioinformatic analyses. Oncotarget. 2016;7(29):45538-46.

373. Bobbs A, Gellerman K, Hallas WM, Joseph S, Yang C, Kurkewich J, et al. ARID3B Directly Regulates Ovarian Cancer Promoting Genes. PloS one. 2015;10(6):e0131961.

374. Long QZ, Du YF, Liu XG, Li X, He DL. miR-124 represses FZD5 to attenuate P-glycoprotein-mediated chemo-resistance in renal cell carcinoma. Tumour biology : the journal of the International Society for Oncodevelopmental Biology and Medicine. 2015;36(9):7017-26.

375. Liu F, Liu Y, Shen J, Zhang G, Han J. MicroRNA-224 inhibits proliferation and migration of breast cancer cells by down-regulating Fizzled 5 expression. Oncotarget. 2016;7(31):49130-42.

376. Burns CJ, Zhang J, Brown EC, Van Bibber AM, Van Es J, Clevers H, et al. Investigation of Frizzled-5 during embryonic neural development in mouse. Developmental dynamics : an official publication of the American Association of Anatomists. 2008;237(6):1614-26.

377. Thiele S, Zimmer A, Gobel A, Rachner TD, Rother S, Fuessel S, et al. Role of WNT5A receptors FZD5 and RYK in prostate cancer cells. Oncotarget. 2018;9(43):27293-304.

378. Steinhart Z, Pavlovic Z, Chandrashekhar M, Hart T, Wang X, Zhang X, et al. Genome-wide CRISPR screens reveal a Wnt-FZD5 signaling circuit as a druggable vulnerability of RNF43-mutant pancreatic tumors. Nature medicine. 2017;23(1):60-8.

379. Zeng CM, Chen Z, Fu L. Frizzled Receptors as Potential Therapeutic Targets in Human Cancers. International journal of molecular sciences. 2018;19(5).

380. Liu Z, Dai W, Jiang L, Cheng Y. Over-expression of LGR5 correlates with poor survival of colon cancer in mice as well as in patients. Neoplasma. 2014;61(2):177-85.

381. Hsu HC, Liu YS, Tseng KC, Tan BC, Chen SJ, Chen HC. LGR5 regulates survival through mitochondria-mediated apoptosis and by targeting the Wnt/beta-catenin signaling pathway in colorectal cancer cells. Cellular signalling. 2014;26(11):2333-42.

382. Maurer U, Preiss F, Brauns-Schubert P, Schlicher L, Charvet C. GSK-3 - at the crossroads of cell death and survival. Journal of cell science. 2014;127(Pt 7):1369-78.

383. Montori-Grau M, Tarrats N, Osorio-Conles O, Orozco A, Serrano-Marco L, Vazquez-Carrera M, et al. Glucose dependence of glycogen synthase activity regulation by GSK3 and MEK/ERK inhibitors and angiotensin-(1-7) action on these pathways in cultured human myotubes. Cellular signalling. 2013;25(5):1318-27.

384. Pandey MK, DeGrado TR. Glycogen Synthase Kinase-3 (GSK-3)-Targeted Therapy and Imaging. Theranostics. 2016;6(4):571-93.

385. Tejeda-Munoz N, Robles-Flores M. Glycogen synthase kinase 3 in Wnt signaling pathway and cancer. IUBMB life. 2015;67(12):914-22.

386. Goto H, Kawano K, Kobayashi I, Sakai H, Yanagisawa S. Expression of cyclin D1 and GSK-3beta and their predictive value of prognosis in squamous cell carcinomas of the tongue. Oral oncology. 2002;38(6):549-56.

387. Ban KC, Singh H, Krishnan R, Seow HF. GSK-3beta phosphorylation and alteration of beta-catenin in hepatocellular carcinoma. Cancer letters. 2003;199(2):201-8.

388. McCubrey JA, Steelman LS, Bertrand FE, Davis NM, Sokolosky M, Abrams SL, et al. GSK-3 as potential target for therapeutic intervention in cancer. Oncotarget. 2014;5(10):2881-911.

389. Bilim V, Ougolkov A, Yuuki K, Naito S, Kawazoe H, Muto A, et al. Glycogen synthase kinase-3: a new therapeutic target in renal cell carcinoma. British journal of cancer. 2009;101(12):2005-14.

390. O'Flaherty L, Shnyder SD, Cooper PA, Cross SJ, Wakefield JG, Pardo OE, et al. Tumor growth suppression using a combination of taxol-based therapy and GSK3 inhibition in non-small cell lung cancer. PloS one. 2019;14(4):e0214610.

391. Ding L, Madamsetty VS, Kiers S, Alekhina O, Ugolkov A, Dube J, et al. Glycogen Synthase Kinase-3 Inhibition Sensitizes Pancreatic Cancer Cells to Chemotherapy by Abrogating the TopBP1/ATR-Mediated DNA Damage Response. Clinical Cancer Research. 2019;25(21):6452-62.

392. White BD, Chien AJ, Dawson DW. Dysregulation of Wnt/β-catenin signaling in gastrointestinal cancers. Gastroenterology. 2012;142(2):219-32.

393. Tang Y, Huang A, Wang K, Zong S. The Prognostic and Clinical Value of CD44 in Colorectal Cancer: A Meta-Analysis. Frontiers in oncology. 2019;9:309.

394. White BD, Chien AJ, Dawson DW. Dysregulation of Wnt/beta-catenin signaling in gastrointestinal cancers. Gastroenterology. 2012;142(2):219-32.

395. Wu XS, Xi HQ, Chen L. Lgr5 is a potential marker of colorectal carcinoma stem cells that correlates with patient survival. World journal of surgical oncology. 2012;10:244.

396. Han Y, Xue X, Jiang M, Guo X, Li P, Liu F, et al. LGR5, a relevant marker of cancer stem cells, indicates a poor prognosis in colorectal cancer patients: a meta-analysis. Clinics and research in hepatology and gastroenterology. 2015;39(2):267-73.

397. Walker F, Zhang HH, Odorizzi A, Burgess AW. LGR5 is a negative regulator of tumourigenicity, antagonizes Wnt signalling and regulates cell adhesion in colorectal cancer cell lines. PloS one. 2011;6(7):e22733.

398. Morgan RG, Mortensson E, Williams AC. Targeting LGR5 in Colorectal Cancer: therapeutic gold or too plastic? British journal of cancer. 2018;118(11):1410-8.

399. Gulla A, Liang H, Kazlauskas E, Matulis D, Strupas K, Eshleman JR. AB035. P006. Activity of heat shock protein-90 (HSP90) inhibitors against pancreatic cancers grown in 3 dimensions. Annals of Pancreatic Cancer. 2018;1.

400. Li J, Huang Y, Gao Y, Wu H, Dong W, Liu L. Antibiotic drug rifabutin is effective against lung cancer cells by targeting the eIF4E-beta-catenin axis. Biochemical and biophysical research communications. 2016;472(2):299-305.

401. Lim S, Saw TY, Zhang M, Janes MR, Nacro K, Hill J, et al. Targeting of the MNK–eIF4E axis in blast crisis chronic myeloid leukemia inhibits leukemia stem cell function. 2013;110(25):E2298-E307.

402. Siddiqui N, Sonenberg N. Signalling to eIF4E in cancer. Biochem Soc Trans. 2015;43(5):763-72.

403. Li J, Huang Y, Gao Y, Wu H, Dong W, Liu L. Antibiotic drug rifabutin is effective against lung cancer cells by targeting the eIF4E-β-catenin axis. Biochemical and biophysical research communications. 2016;472(2):299-305.

404. Zhang X, Dong S, Xu F. Structural and druggability landscape of Frizzled G protein-coupled receptors. Trends in biochemical sciences. 2018;43(12):1033-46.

405. Zhang X, Dong S, Xu F. Structural and Druggability Landscape of Frizzled G Protein-Coupled Receptors. Trends Biochem Sci. 2018;43(12):1033-46.

406. Undi RB, Gutti U, Sahu I, Sarvothaman S, Pasupuleti SR, Kandi R, et al. Wnt signaling: role in regulation of haematopoiesis. Indian Journal of Hematology and Blood Transfusion. 2016;32(2):123-34.

407. Grainger S, Willert K. Mechanisms of Wnt signaling and control. Wiley Interdisciplinary Reviews: Systems Biology and Medicine. 2018;10(5):e1422.

408. Aschenbach WG, Ho RC, Sakamoto K, Fujii N, Li Y, Kim Y-B, et al. Regulation of Dishevelled and β-catenin in rat skeletal muscle: an alternative exercise-induced GSK-3β signaling pathway. American Journal of Physiology-Endocrinology and Metabolism. 2006;291(1):E152-E8.

409. Zhang K, Song H, Yang P, Dai X, Li Y, Wang L, et al. Silencing dishevelled-1 sensitizes paclitaxel-resistant human ovarian cancer cells via AKT/GSK-3β/β-catenin signalling. Cell proliferation. 2015;48(2):249-58.

410. Cook D, Fry MJ, Hughes K, Sumathipala R, Woodgett JR, Dale TC. Wingless inactivates glycogen synthase kinase-3 via an intracellular signalling pathway which involves a protein kinase C. The EMBO journal. 1996;15(17):4526-36.

411. Arend RC, Londoño-Joshi AI, Straughn Jr JM, Buchsbaum DJ. The Wnt/β-catenin pathway in ovarian cancer: A review. Gynecologic oncology. 2013;131(3):772-9.

412. Lu J, Lu S, Li J, Yu Q, Liu L, Li Q. MiR-629-5p promotes colorectal cancer progression through targetting CXXC finger protein 4. Bioscience reports. 2018;38(4).

413. Yu F, Zhou C, Zeng H, Liu Y, Li S. BMI1 activates WNT signaling in colon cancer by negatively regulating the WNT antagonist IDAX. Biochemical and biophysical research communications. 2018;496(2):468-74.

414. Kojima T, Shimazui T, Hinotsu S, Joraku A, Oikawa T, Kawai K, et al. Decreased expression of CXXC4 promotes a malignant phenotype in renal cell carcinoma by activating Wnt signaling. Oncogene. 2009;28(2):297-305.

415. Han M, Dai D, Yousafzai NA, Wang F, Wang H, Zhou Q, et al. CXXC4 activates apoptosis through up-regulating GDF15 in gastric cancer. Oncotarget. 2017;8(61):103557-67.

416. Lu H, Sun J, Wang F, Feng L, Ma Y, Shen Q, et al. Enhancer of zeste homolog 2 activates wnt signaling through downregulating CXXC finger protein 4. Cell death & disease. 2013;4(8):e776-e.

417. Fu Y, Wang Z, Luo C, Wang Y, Wang Y, Zhong X, et al. Downregulation of CXXC Finger Protein 4 Leads to a Tamoxifen-resistant Phenotype in Breast Cancer Cells Through Activation of the Wnt/β-catenin Pathway. Translational Oncology. 2020;13(2):423-40.

418. Tang Q, Zhao H, Yang B, Li L, Shi Q, Jiang C, et al. WIF-1 gene inhibition and Wnt signal transduction pathway activation in NSCLC tumorigenesis. Oncology letters. 2017;13(3):1183-8.

419. Lin Y-C, You L, Xu Z, He B, Yang C-T, Chen J-K, et al. Wnt inhibitory factor-1 gene transfer inhibits melanoma cell growth. Human gene therapy. 2007;18(4):379-86.

420. Sailo BL, Banik K, Girisa S, Bordoloi D, Fan L, Halim CE, et al. FBXW7 in Cancer: What Has Been Unraveled Thus Far? Cancers (Basel). 2019;11(2).

421. Patil SP, Yoon SC, Aradhya AG, Hofer J, Fink MA, Enley ES, et al. Macrocyclic Compounds from Ansamycin Antibiotic Class as Inhibitors of PD1-PDL1 Protein-Protein Interaction. Chemical & pharmaceutical bulletin. 2018;66(8):773-8.

422. Parvez MM, Jung JA, Shin HJ, Kim DH, Shin JG. Characterization of 22 Antituberculosis Drugs for Inhibitory Interaction Potential on Organic Anionic

Transporter Polypeptide (OATP)-Mediated Uptake. Antimicrobial agents and chemotherapy. 2016;60(5):3096-105.

423. Chen S, Yao Y, Zhang Y, Fan G. CRISPR system: Discovery, development and off-target detection. Cellular signalling. 2020:109577.

424. Matano M, Date S, Shimokawa M, Takano A, Fujii M, Ohta Y, et al. Modeling colorectal cancer using CRISPR-Cas9–mediated engineering of human intestinal organoids. Nature medicine. 2015;21(3):256.

425. Gong J, Zhou Y, Liu D, Huo J. F-box proteins involved in cancer-associated drug resistance. Oncology letters. 2018;15(6):8891-900.

426. Kondo J, Inoue M. Application of Cancer Organoid Model for Drug Screening and Personalized Therapy. Cells. 2019;8(5):470.

427. Clevers H, Tuveson DA. Organoid Models for Cancer Research. Annual Review of Cancer Biology. 2019;3:223-34.

428. Kuo CJ, Curtis C. Organoids reveal cancer dynamics. Nature Publishing Group; 2018.

429. Huch M, Koo B-K. Modeling mouse and human development using organoid cultures. Development. 2015;142(18):3113-25.

430. Fujii M, Clevers H, Sato T. Modeling human digestive diseases with CRISPR-Cas9-modified organoids. Gastroenterology. 2018.

431. Wang P, Mokhtari R, Pedrosa E, Kirschenbaum M, Bayrak C, Zheng D, et al. CRISPR/Cas9-mediated heterozygous knockout of the autism gene CHD8 and characterization of its transcriptional networks in cerebral organoids derived from iPS cells. Molecular autism. 2017;8(1):11.

432. Drost J, van Jaarsveld RH, Ponsioen B, Zimberlin C, van Boxtel R, Buijs A, et al. Sequential cancer mutations in cultured human intestinal stem cells. Nature. 2015;521(7550):43-7.

433. Schwank G, Koo BK, Sasselli V, Dekkers JF, Heo I, Demircan T, et al. Functional repair of CFTR by CRISPR/Cas9 in intestinal stem cell organoids of cystic fibrosis patients. Cell stem cell. 2013;13(6):653-8.

434. Liu Y, Lear T, Zhao Y, Zhao J, Zou C, Chen BB, et al. F-box protein Fbxl18 mediates polyubiquitylation and proteasomal degradation of the pro-apoptotic SCF subunit Fbxl7. Cell death & disease. 2015;6:e1630.

435. Ueda M, Matsuura K, Kawai H, Wakasugi M, Matsunaga T. Spironolactone-induced XPB degradation depends on CDK7 kinase and SCFFBXL18 E3 ligase. Genes to Cells. 2019;24(4):284-96.

436. Ding X, Barodia SK, Ma L, Goldberg MS. Fbxl18 targets LRRK2 for proteasomal degradation and attenuates cell toxicity. Neurobiology of disease. 2017;98:122-36.

437. Zhang J, Yang Z, Ou J, Xia X, Zhi F, Cui J. The F-box protein FBXL18 promotes glioma progression by promoting K63-linked ubiquitination of Akt. FEBS letters. 2017;591(1):145-54.

438. Du D, Yuan J, Ma W, Ning J, Weinstein JN, Yuan X, et al. Clinical significance of FBXO17 gene expression in high-grade glioma. BMC cancer. 2018;18(1):773.

439. Suber T, Wei J, Jacko AM, Nikolli I, Zhao Y, Zhao J, et al. SCFFBXO17 E3 ligase modulates inflammation by regulating proteasomal degradation of glycogen synthase kinase-3β in lung epithelia. Journal of Biological Chemistry. 2017;292(18):7452-61.

440. Suber TL, Nikolli I, O'Brien ME, Londino J, Zhao J, Chen K, et al. FBXO17 promotes cell proliferation through activation of Akt in lung adenocarcinoma cells. Respiratory research. 2018;19(1):206.

441. Suber TL, Nikolli I, O'Brien ME, Londino J, Zhao J, Chen K, et al. FBXO17 promotes cell proliferation through activation of Akt in lung adenocarcinoma cells. Respiratory research. 2018;19(1):206.

442. Suber T, Wei J, Jacko AM, Nikolli I, Zhao Y, Zhao J, et al. SCF(FBXO17) E3 ligase modulates inflammation by regulating proteasomal degradation of glycogen synthase kinase-3beta in lung epithelia. The Journal of biological chemistry. 2017;292(18):7452-61.

443. Peng D, Wang Z, Huang A, Zhao Y, Qin FX. A Novel Function of F-Box Protein FBXO17 in Negative Regulation of Type I IFN Signaling by Recruiting PP2A for IFN Regulatory Factor 3 Deactivation. Journal of immunology (Baltimore, Md : 1950). 2017;198(2):808-19.

444. Wang Y, Wang L, Zhu Y, Qin J. Human brain organoid-on-a-chip to model prenatal nicotine exposure. Lab on a Chip. 2018;18(6):851-60.

445. Mazerik JN, Becker S, Sieving PA. 3-D retina organoids: Building platforms for therapies of the future. Cell medicine. 2018;10:2155179018773758.

446. Jones B, Giobbe G, Sgualdino F, De Coppi P. 127 Modelling human stomach development in vitro with the use of gastric organoids. BMJ Publishing Group Ltd; 2019.

447. Barkauskas CE, Chung M-I, Fioret B, Gao X, Katsura H, Hogan BL. Lung organoids: current uses and future promise. Development. 2017;144(6):986-97.

448. Baker LA, Tiriac H, Clevers H, Tuveson DA. Modeling pancreatic cancer with organoids. Trends in cancer. 2016;2(4):176-90.

449. Kasendra M, Tovaglieri A, Sontheimer-Phelps A, Jalili-Firoozinezhad S, Bein A, Chalkiadaki A, et al. Development of a primary human Small Intestine-on-a-Chip using biopsy-derived organoids. Scientific reports. 2018;8(1):1-14.

450. Crespo M, Vilar E, Tsai S-Y, Chang K, Amin S, Srinivasan T, et al. Colonic organoids derived from human induced pluripotent stem cells for modeling colorectal cancer and drug testing. Nature medicine. 2017;23(7):878.

451. Neal JT, Li X, Zhu J, Giangarra V, Grzeskowiak CL, Ju J, et al. Organoid modeling of the tumor immune microenvironment. Cell. 2018;175(7):1972-88. e16.

452. Driehuis E, Clevers H. CRISPR/Cas 9 genome editing and its applications in organoids. American Journal of Physiology-Gastrointestinal and Liver Physiology. 2017;312(3):G257-G65.

453. Sachs N, Tsukamoto Y, Kujala P, Peters PJ, Clevers H. Intestinal epithelial organoids fuse to form self-organizing tubes in floating collagen gels. Development. 2017;144(6):1107-12.

454. Ranga A, Grebenyuk S. Engineering organoid vascularization. Frontiers in bioengineering and biotechnology. 2019;7:39.

455. Ding Z-H, Qi J, Shang A-Q, Zhang Y-J, Wei J, Hu L-Q, et al. Docking of CDK1 with antibiotic drugs revealed novel therapeutic value in breast ductal cancer in situ. Oncotarget. 2017;8(37):61998.

456. Tinsley N, Zhou C, Tan G, Rack S, Lorigan P, Blackhall F, et al. Cumulative antibiotic use significantly decreases efficacy of checkpoint inhibitors in patients with advanced cancer. The oncologist. 2019:theoncologist. 2019-0160.

457. Munster PN, Basso A, Solit D, Norton L, Rosen N. Modulation of Hsp90 function by ansamycins sensitizes breast cancer cells to chemotherapy-induced apoptosis in an RB- and schedule-dependent manner. See: E. A. Sausville, Combining cytotoxics and 17-allylamino, 17-demethoxygeldanamycin: sequence and tumor biology matters, Clin. Cancer Res., 7: 2155-2158, 2001. Clinical cancer research : an official journal of the American Association for Cancer Research. 2001;7(8):2228-36.

458. Austin CP, Battey JF, Bradley A, Bucan M, Capecchi M, Collins FS, et al. The knockout mouse project. Nature genetics. 2004;36(9):921.

459. Fatehullah A, Tan SH, Barker N. Organoids as an in vitro model of human development and disease. Nature cell biology. 2016;18(3):246-54.

460. Takebe T, Wells JM. Organoids by design. Science. 2019;364(6444):956-9.

Appendix

Appendix 1

Gene table for RT^2 Profiler^{TM} PCR Array Human WNT Signalling Pathway Plus.

Unigene	RefSeq number	Symbol	Description
Hs.158932	NM_000038	APC	Adenomatous polyposis coli
Hs.592082	NM_003502	AXIN1	Axin 1
Hs.156527	NM_004655	AXIN2	Axin 2
Hs.643802	NM_033637	BTRC	Beta-transducin repeat containing
Hs.529862	NM_001892	CSNK1A1	Casein kinase 1, alpha 1
Hs.208597	NM_001328	CTBP1	C-terminal binding protein 1
Hs.712929	NM_001904	CTNNB1	Catenin (cadherin-associated protein), beta 1, 88kDa
Hs.685322	NM_020248	CTNNBIP1	Catenin, beta interacting protein 1
Hs.654934	NM_014992	DAAM1	Dishevelled associated activator of morphogenesis 1
Hs.696631	NM_001343	DAB2	Disabled homolog 2, mitogen-responsive phosphoprotein (Drosophila)
Hs.40499	NM_012242	DKK1	Dickkopf homolog 1 (Xenopus laevis)
Hs.292156	NM_015881	DKK3	Dickkopf homolog 3 (Xenopus laevis)
Hs.731450	NM_004421	DVL1	Dishevelled, dsh homolog 1 (Drosophila)
Hs.118640	NM_004422	DVL2	Dishevelled, dsh homolog 2 (Drosophila)
Hs.12248	NM_025212	CXXC4	CXXC Finger Protein 4
Hs.517517	NM_001429	EP300	E1A binding protein p300
Hs.484138	NM_012300	FBXW11	F-box and WD repeat domain containing 11
Hs.1755	NM_002007	FGF4	Fibroblast growth factor 4
Hs.283565	NM_005438	FOSL1	FOS-like antigen 1
Hs.126057	NM_005479	FRAT1	Frequently rearranged in advanced T-cell lymphomas
Hs.128453	NM_001463	FRZB	Frizzled-related protein
Hs.94234	NM_003505	FZD1	Frizzled family receptor 1
Hs.142912	NM_001466	FZD2	Frizzled family receptor 2
Hs.40735	NM_017412	FZD3	Frizzled family receptor 3
Hs.591968	NM_012193	FZD4	Frizzled family receptor 4
Hs.17631	NM_003468	FZD5	Frizzled family receptor 5
Hs.591863	NM_003506	FZD6	Frizzled family receptor 6
Hs.173859	NM_003507	FZD7	Frizzled family receptor 7
Hs.302634	NM_031866	FZD8	Frizzled family receptor 8

Hs.647029	NM_003508	FZD9	Frizzled family receptor 9
Hs.445733	NM_002093	GSK3B	Glycogen synthase kinase 3 beta
Hs.696684	NM_002228	JUN	Jun proto-oncogene
Hs.229335	NM_001039570	KREMEN1	Kringle containing transmembrane protein 1
Hs.6347	NM_002335	LRP5	Low density lipoprotein receptor-related protein 5
Hs.584775	NM_002336	LRP6	Low density lipoprotein receptor-related protein 6
Hs.138211	NM_002750	MAPK8	Mitogen-activated protein kinase 8
Hs.2256	NM_002423	MMP7	Matrix metallopeptidase 7 (matrilysin, uterine)
Hs.534074	NM_172390	NFATC1	Nuclear factor of activated T-cells, cytoplasmic, calcineurin-dependent 1
Hs.187578	NM_033119	NKD1	Naked cuticle homolog 1 (Drosophila)
Hs.208759	NM_016231	NLK	Nemo-like kinase
Hs.643588	NM_000325	PITX2	Paired-like homeodomain 2
Hs.386453	NM_022825	PORCN	Porcupine homolog (Drosophila)
Hs.696032	NM_006238	PPARD	Peroxisome proliferator-activated receptor delta
Hs.524348	NM_153026	PRICKLE1	Prickle homolog 1 (Drosophila)
Hs.247077	NM_001664	RHOA	Ras homolog gene family, member A
Hs.710868	NM_003707	RUVBL1	RuvB-like 1 (E. coli)
Hs.213424	NM_003012	SFRP1	Secreted frizzled-related protein 1
Hs.658169	NM_003014	SFRP4	Secreted frizzled-related protein 4
Hs.98367	NM_022454	SOX17	SRY (sex determining region Y)-box 17
Hs.573153	NM_003202	TCF7	Transcription factor 7 (T-cell specific, HMG-box)
Hs.516297	NM_031283	TCF7L1	Transcription factor 7-like 1 (T-cell specific, HMG-box)
Hs.99477	NM_020335	VANGL2	Vang-like 2 (van gogh, Drosophila)
Hs.284122	NM_007191	WIF1	WNT inhibitory factor 1
Hs.492974	NM_003882	WISP1	WNT1 inducible signaling pathway protein 1
Hs.248164	NM_005430	WNT1	Wingless-type MMTV integration site family, member 1
Hs.121540	NM_025216	WNT10A	Wingless-type MMTV integration site family, member 10A
Hs.108219	NM_004626	WNT11	Wingless-type MMTV integration site family, member 11

Hs.567356	NM_003391	WNT2	Wingless-type MMTV integration site family member 2
Hs.258575	NM_004185	WNT2B	Wingless-type MMTV integration site family, member 2B
Hs.445884	NM_030753	WNT3	Wingless-type MMTV integration site family, member 3
Hs.336930	NM_033131	WNT3A	Wingless-type MMTV integration site family, member 3A
Hs.25766	NM_030761	WNT4	Wingless-type MMTV integration site family, member 4
Hs.643085	NM_003392	WNT5A	Wingless-type MMTV integration site family, member 5A
Hs.306051	NM_032642	WNT5B	Wingless-type MMTV integration site family, member 5B
Hs.29764	NM_006522	WNT6	Wingless-type MMTV integration site family, member 6
Hs.72290	NM_004625	WNT7A	Wingless-type MMTV integration site family, member 7A
Hs.512714	NM_058238	WNT7B	Wingless-type MMTV integration site family, member 7B
Hs.591274	NM_058244	WNT8A	Wingless-type MMTV integration site family, member 8A
Hs.149504	NM_003395	WNT9A	Wingless-type MMTV integration site family, member 9A
Hs.272375	NM_016087.2	WNT16	Wingless-type MMTV integration site family, member 16
Hs.197320	NM_001303103	TLE1	TLE Family Member 1, Transcriptional Corepressor
Hs.425091	NM_138369	BOD1	Biorientation of chromosomes in cell division 1
Hs.282410	NM_006888	CALM1	Calmodulin 1 (phosphorylase kinase, delta)
Hs.523852	NM_053056	CCND1	Cyclin D1
Hs.376071	NM_001759	CCND2	Cyclin D2
Hs.256587	NM_001330326	PYGO1	Pygopus Family PHD Finger 1
Hs.647774	NM_021205.6	RHOU	Ras Homolog Family Member U
Hs.663679	NM_001369369.1	FOXN1	Forkhead Box N1
Hs.500822	NM_001323541.1	FBXW4	F-Box And WD Repeat Domain Containing 4
Hs.743478	NM_016269	LEF1	Lymphoid enhancer-binding factor 1
Hs.655199	NM_005946	MT1A	Metallothionein 1A
Hs.713636	NM_016498	MTFP1	Mitochondrial fission process 1
Hs.700429	NM_014751	MTSS1	Metastasis suppressor 1
Hs.202453	NM_002467	MYC	V-myc myelocytomatosis viral oncogene homolog (avian)

Hs.26006	NM_018137	PRMT6	Protein arginine methyltransferase 6
Hs.520640	NM_001101	ACTB	Actin, beta
Hs.534255	NM_004048	B2M	Beta-2-microglobulin
Hs.592355	NM_002046	GAPDH	Glyceraldehyde-3-phosphate dehydrogenase
Hs.412707	NM_000194	HPRT1	Hypoxanthine phosphoribosyltransferase 1
Hs.546285	NM_001002	RPLP0	Ribosomal protein, large, P0

Appendix 2		**F-box gRNA data sheets**					
Approved Symbol	**Approved Name**	**Previous Symbols**	**Synonyms**	**Chromosome**	**Approved Symbol**	**gRNA pair**	**LV gRNA Sequence**
mFBXL2	F-box and leucine rich repeat protein 2		FBL2, FBL3	3p22.3	FBXL2	1st gRNA	TCCAGGGCTAAGATGTTCCAGG
						2nd gRNA	GGCAGCAACTGGCAACGGGTGG
mFBXL3	F-box and leucine rich repeat protein 3	FBXL3A	FBL3, FBL3A	13q22.3	FBXL3	1st gRNA	CGGACTTATCTCGACTGCCCGG
						2nd gRNA	AGATCCATAAAGCTTGGCCGGG
mFBXL4	F-box and leucine rich repeat protein 4		FBL4, FBL5	6q16.1-q16.2	FBXL4	1st gRNA	GTTGTGCTGCATGGTACGAAGG
						2nd gRNA	ATTGACTTCCAGTCGTATGAGG
mFBXL5	F-box and leucine rich repeat protein 5		FBL4, FBL5, FLR1	4p15.32	FBXL5	1st gRNA	ATATCTTTAAGCTCCTCGTAGG
						2nd gRNA	AAATGGACAGCATTACCTCAGG
mFBXL6	F-box and leucine rich repeat protein 6		FBL6	8q24.3	FBXL6	1st gRNA	GCTGGCAAGGGCAACCTTAAGG
						2nd gRNA	CAGCCACAGTTTACGCATTCGGG
mFBXL7	F-box and leucine rich repeat protein 7		FBL7, FBL6	5p15.1	FBXL7	1st gRNA	TCTGTGCTTGAACTCACGTCGG
						2nd gRNA	CCTGAAAGTACTGACCCGCAGG

Approved Symbol	Approved Name	Previous Symbols	Synonyms	Chromosome	Approved Symbol	gRNA pair	LV gRNA Sequence
mFBXL8	F-box and leucine rich repeat protein 8		Fbl8	16q22.1	FBXL8	1st gRNA	GGAAGCACGAGCATCTTCGGGG
						2nd gRNA	CTTGAGCGTATAGCTGCGCAGG
mFBXL13	F-box and leucine rich repeat protein 13		MGC21636, Fbl13, DRC6	7q22.1	FBXL13	1st gRNA	GCTATCATTAAAAGAGGTCTGG
						2nd gRNA	ATGCTTTTATCATCAACTCTGG
mFBXL14	F-box and leucine rich repeat protein 14		MGC40195, Fbl14	12p13.33	FBXL14	1st gRNA	CTTCTGCACCTGTCGCACATGG
						2nd gRNA	GGGAACAGGCACGAGATGTGGG
mFBXL15	F-box and leucine rich repeat protein 15	FBXO37	MGC11279, Fbl15	10q24.32	FBXL15	1st gRNA	GCGCGTCAGTCGCGCCTTCCGG
						2nd gRNA	AGCTGAACGAGCGCCCGGAAGG
mFBXL16	F-box and leucine rich repeat protein 16	C16orf22	MGC33974, Fbl16	16p13.3	FBXL16	1st gRNA	TGCCCTCGGATCACCGATATGG
						2nd gRNA	TGCCATATCGGTGATCCGAGGG
mFBXL17	F-box and leucine rich repeat protein 17	FBXO13	DKFZP434C1715, Fbx13, Fbl17	5q21.3	FBXL17	1st gRNA	ACCCATGAAGCCAACATACTGG
						2nd gRNA	GTTGTTCAGTTACTTCCAAAGG

Approved Symbol	Approved Name	Previous Symbols	Synonyms	Chromosome	Approved Symbol	gRNA pair	LV gRNA Sequence
mFBXL18	F-box and leucine rich repeat protein 18		FLJ11467, Fbl18	7p22.1	FBXL18	1st gRNA	CACTCTTCACGCCGTCCTACGG
						2nd gRNA	TTGGCAAGAAGGTGCGCATTGG
mFBXL19	F-box and leucine rich repeat protein 19		DKFZp434K0410, Fbl19, JHDM1C, CXXC11	16p11.2	FBXL19	1st gRNA	GGGCTGACAATGGTGAGGAAGG
						2nd gRNA	GTGAGGAAGGCGCTAACCTAGG
mFBXL20	F-box and leucine rich repeat protein 20		MGC15482, Fbl2, Fbl20	17q12	FBXL20	1st gRNA	ACCCTGTGTCGCTGTGCTCAGG
						2nd gRNA	AGCTCTGGATGGCAGTAACTGG
mFBXL22	F-box and leucine rich repeat protein 22		Fbl22, FLJ39626	15q22.31	FBXL22	1st gRNA	TCAGCTTTCTCGGCTGCACCGG
						2nd gRNA	AGCGTGACGGACGTCAGGTTGG
mKDM2A	lysine demethylase 2A	FBXL11	KIAA1004, FBL11, LILINA, DKFZP434M1735,	11q13.2	KDM2A	1st gRNA	TCTTCATAGCGACGACGCATGG
						2nd gRNA	ATGTAGAGTATATCCAGCGGGG

Approved Symbol	Approved Name	Previous Symbols	Synonyms	Chromosome	Approved Symbol	gRNA pair	LV gRNA Sequence
mKDM2B	lysine demethylase 2B	FBXL10	PCCX2, CXXC2, Fbl10, JHDM1B	12q24.31	KDM2B	1st gRNA	GCTCCTGCTGTTGTTCGGTTGG
						2nd gRNA	CTCTCCACACTCCGTCCGCAGG
mSKP2	S-phase kinase associated protein 2		FBXL1, FBL1, p45	5p13.2	SKP2	1st gRNA	CTGGTCCGGAATCTCCTGAAGG
						2nd gRNA	TGACGTTGCCACTCTGGTCCGG
mBTRC	beta-transducin repeat containing E3 ligase		bTrCP, betaTrCP, FBXW1A, Fwd1, bTrCP1	10q24.32	BTRC	1st gRNA	CTGAGAGTTTCCGCTGCTTGGG
						2nd gRNA	CATGATTGTGCCCAAGCAGCGG
mFBXW2	F-box and WD repeat domain containing 2		FBW2, Md6, Fwd2	9q33.2	FBXW2	1st gRNA	ATGCCCAGTGAGTGTATTCAGG
						2nd gRNA	ACTCACTGGGCATACTGAATGG
mFBXW5	F-box and WD repeat domain containing 5		DKFZP434B205, MGC20962, Fbw5	9q34.3	FBXW5	1st gRNA	GCAAACTGGTACCCCGAGTGGG
						2nd gRNA	CCTCAGCTTCTCCCACTCGGGG
mFBXW7	F-box and WD repeat domain containing 7		AGO, FLJ11071, SEL-10, FBX30, CDC4, FBXW6	4q31.3	FBXW7	1st gRNA	ACCCACAGGCCTTCAAGAGTGG
						2nd gRNA	CATCTGTCCAACCACCCACAGG

Approved Symbol	Approved Name	Previous Symbols	Synonyms	Chromosome	Approved Symbol	gRNA pair	LV gRNA Sequence
mFBXW8	F-box and WD repeat domain containing 8	FBXO29	FBX29, FBW6, FBW8	12q24.22	FBXW8	1st gRNA	GTCCGTCTGCCTTACGAACTGG
mFBXW9	F-box and WD repeat domain containing 9		MGC10870, Fbw9	19p13.13	FBXW9	1st gRNA	AGCAGCAACACCGCATCAATGG
						2nd gRNA	CCAGCCGCCTGCATTGAGCTGG
mFBXW10	F-box and WD repeat domain containing 10	C17orf1, C17orf1A	SM2SH2, HREP, Fbw10	17p11.2	FBXW10	1st gRNA	AAAAAGTACAGCGGTACACAGG
						2nd gRNA	TCCCAATGTCCAAACATTTAGG
mFBXW11	F-box and WD repeat domain containing 11	FBXW1B	KIAA0696, Fbw1b, BTRCP2, BTRC2, Hos, Fbw11	5q35.1	FBXW11	1st gRNA	AGTTGGGAGGGCCATCTGTAGG
						2nd gRNA	TTAAAAACAGACCTACAGATGG
mCCNF	cyclin F		FBX1, FBXO1	16p13.3	CCNF	1st gRNA	TTTTGATTCTTCGTTTAGTAGG
						2nd gRNA	TCAAGATGGTTAAGTTTCTGGG

Approved Symbol	Approved Name	Previous Symbols	Synonyms	Chromosome	Approved Symbol	gRNA pair	LV gRNA Sequence
mECT2L	epithelial cell transforming 2 like	C6orf91	ARHGEF32, FBXO49, LFDH	6q24.1	ECT2L	1st gRNA	AATTCCCGCCGTTGCTTGTTGG
						2nd gRNA	CTGGACCAACAAGCAACGGCGG
mFBXO2	F-box protein 2	OCP1	FBX2, Nfb42, Fbs1, Fbg1	1p36.22	FBXO2	1st gRNA	TCCTCTGGGCTCGCTTCTTCGG
				1p36.22	FBXO2	2nd gRNA	CACTTGAGCAGCCACAGTGGGG
mFBXO3	F-box protein 3		FBX3, FBA	11p13	FBXO3	1st gRNA	TACCTCCCCACGTCTGAGTAGG
						2nd gRNA	CTTTTTAATGGCGGCGTAATGG
mFBXO4	F-box protein 4		FBX4	5p13.1	FBXO4	1st gRNA	CCAGCTGGCACAGATCGTGGGG
						2nd gRNA	TTCTTGGTCTTCGGTTGATTGG
mFBXO5	F-box protein 5		FBX5, Fbxo31, EMI1	6q25.2	FBXO5	1st gRNA	TGCAGTCTAAAGTTCCCGCTGG
						2nd gRNA	GGCTTCACCACTTCAAGCTCGG
mFBXO6	F-box protein 6		FBX6, FBG2, FBS2, Fbx6b	1p36.22	FBXO6	1st gRNA	CGGATAGACTCCAACGGAGGGG
						2nd gRNA	GGCGGATAGACTCCAACGGAGG

Approved Symbol	Approved Name	Previous Symbols	Synonyms	Chromosome	Approved Symbol	gRNA pair	LV gRNA Sequence
mFBXO7	F-box protein 7		FBX7, Fbx, PARK15	22q12.3	FBXO7	1st gRNA	ATTCAGGATGCCATGAGTATGG
						2nd gRNA	AGTGATGCCTTGATAGTGCTGG
mFBXO8	F-box protein 8		FBX8, FBS	4q34.1	FBXO8	1st gRNA	AAAAGAAAATCCTAAAGGTGGG
						2nd gRNA	TCCTCTGGGTTGGCATTAAAGG
mFBXO9	F-box protein 9		FBX9, NY-REN-57	6p12.1	FBXO9	1st gRNA	CTGACAGAGTAGGCGATGAAGG
						2nd gRNA	GCCAGTTCCTGTCGTCCTTTGG
mFBXO10	F-box protein 10		FBX10	9p13.2	FBXO10	1st gRNA	CCAGTTCTTATCCGCCGACGGG
						2nd gRNA	GAAGAGGCACTTGCGGATAAGG
mFBXO11	F-box protein 11		FBX11, UBR6	2p16.3	FBXO11	1st gRNA	TTTTTCTGCGAAGTTGGTATGG
						2nd gRNA	TAGGACACGCTGTTCTTTTTGG
mFBXO15	F-box protein 15		MGC39671, FBX15	18q22.3	FBXO15	1st gRNA	TCGCTGTGCTGGTTTCGCCAGG
						2nd gRNA	TCCATCAGTTCTATATCCCTGG

Approved Symbol	Approved Name	Previous Symbols	Synonyms	Chromosome	Approved symbol	gRNA Pair	LV gRNA Sequence
mFBXO16	F-box protein 16		FBX16	8p21.1	FBXO16	1st gRNA	TGCACAACGGCAAAGACTCCGG
						2nd gRNA	CAGGGAACAGCGCTCTAGTAGG
mFBXO17	F-box protein 17	FBXO26	FBG4, FLJ25205, MGC9379, FLJ11798, Fbx17	19q13.2	FBXO17	1st gRNA	AAGTGGAGCACGGCGGAAATGG
						2nd gRNA	GTGGAAAAGAATTTGACGCTGG
mFBXO18	F-box protein, helicase, 18		FBH1, FLJ14590, Fbx18	10p15.1	FBXO18	1st gRNA	CTCTCAGGGTCAACACTTGGGG
						2nd gRNA	GGAGGCTGAGGCGTGCATGCGG
mFBXO21	F-box protein 21		FBX21, KIAA0875	12q24.22	FBXO21	1st gRNA	CCCCACCGACTACGTCAATTGG
						2nd gRNA	CCAATTGACGTAGTCGGTGGGG
mFBXO22	F-box protein 22		FBX22, FISTC1	15q24.2	FBXO22	1st gRNA	GATTGCTACCTGATCCCATTGG
						2nd gRNA	AGTGCTGACTACCCGATGCAGG
mFBXO24	F-box protein 24		FBX24	7q22.1	FBXO24	1st gRNA	AGGAGCAGTAGGGCCCGCTGGG
						2nd gRNA	TCACAGGCGCGGCTACCGGTGG

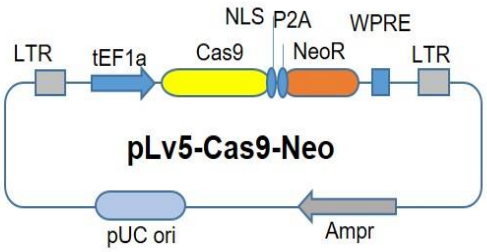
Approved Symbol	Approved Name	Previous Symbols	Synonyms	Chromosome	Approved symbol	gRNA Pair	LV gRNA Sequence
mFBXO25	F-box protein 25		FBX25	8p23.3	FBXO25	1st gRNA	AAATGGATCTACGTCCATAAGG
						2nd gRNA	GAGAAGTCTAGCCGGTTGAAGG
mFBXO27	F-box protein 27		Fbg5, Fbx27	19q13.2	FBXO27	1st gRNA	GCCAGATCCCATTGAACAGTGG
						2nd gRNA	GAACTTATCTATGACGTTCTGG
mFBXO28	F-box protein 28		FLJ10766, KIAA0483, Fbx28,	1q42.11	FBXO28	1st gRNA	TCAGAGAATGTTGAATCAGGGG
						2nd gRNA	TGTCAGAGAATGTTGAATCAGG
mFBXO30	F-box protein 30		MGC21674, Fbx30	6q24.3	FBXO30	1st gRNA	GGCTAATGAGGGACGTTTGTGG
						2nd gRNA	GACCAGGACCACCTTGATGAGG
mFBXO31	F-box protein 31		FBX14, FBXO14, Fbx31, MGC15419	16q24.2	FBXO31	1st gRNA	TGTGAGAACCTGCGGAAGCTGG
						2nd gRNA	TGTGATCTCCAGCTTCCGCAGG
mFBXO32	F-box protein 32		MAFbx, ATROGIN1, Fbx32	8q24.13	FBXO32	1st gRNA	GGCTGCGACGTCGTAGTTCAGG
						2nd gRNA	GTTCACAAAGGAAGTACGAAGG

Approved Symbol	Approved Name	Previous Symbols	Synonyms	Chromosome	Approved symbol	gRNA Pair	LV gRNA Sequence
mFBXO33	F-box protein 33		Fbx33	14q21.1	FBXO33	1st gRNA	GCTGGACAAACTTCCTTGCTGG
						2nd gRNA	GTCCAGCACGTACCTCAGCAGG
mFBXO36	F-box protein 36		Fbx36, FLJ37592	2q36.3	FBXO36	1st gRNA	ATGTCTTCAACCTGTGCGAAGG
						2nd gRNA	GTCAAATTTACCTTCGCACAGG
mFBXO38	F-box protein 38		MOKA, SP329, FLJ13962, Fbx38	5q32	FBXO38	1st gRNA	TGCCTCTCTCGGAAGCTAAAGG
						2nd gRNA	TCGCCTCTCGAGGTATCTAGGG
mFBXO39	F-box protein 39		MGC35179, Fbx39, CT144	17p13.1	FBXO39	1st gRNA	CTCCACAAACTTAACGTCCAGG
						2nd gRNA	TTCCTGGACGTTAAGTTTGTGG
mFBXO40	F-box protein 40		KIAA1195, Fbx40	3q13.33	FBXO40	1st gRNA	TCTCCTTGGGCGTACAAGCAGG
						2nd gRNA	TTGTTTGCCGGCAACCAGTAGG
mFBXO41	F-box protein 41		KIAA1940, Fbx41	2p13.2	FBXO41	1st gRNA	CCGAGCTGCCGTCTCCTTCAGG
						2nd gRNA	AGGTGGGGGCAGTGCCTCGGGG

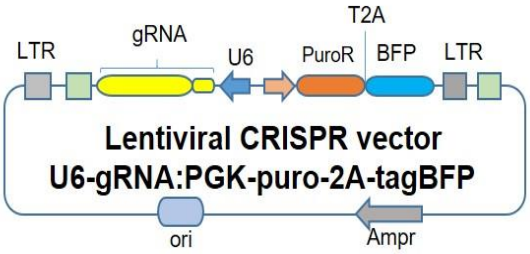
Approved Symbol	Approved Name	Previous Symbols	Synonyms	Chromosome	Approved symbol	gRNA Pair	LV gRNA Sequence
FBXO42	F-box protein 42		KIAA1332, Fbx42	1p36.13	FBXO42	1st gRNA	GATAGGGGTTCCCGGATAAGGG
						2nd gRNA	GCTGAGTGATAGGGGTTCCCGG
FBXO43	F-box protein 43		Fbx43	8q22.2	FBXO43	1st gRNA	TAAGGCCAAGCGACTCAGAAGG
						2nd gRNA	GTCAGAACATCCCCCCAAGGGG
FBXO44	F-box protein 44		FBX30, FBG3, MGC14140, Fbxo6a, Fbx44	1p36.22	FBXO44	1st gRNA	AGCACAAGGGTTGTGAAGGAGG
						2nd gRNA	CTGCTGCTGCGCTGCCGACCGG
FBXO45	F-box protein 45		Fbx45	3q29	FBXO45	1st gRNA	GAAGTGACGACCAGAGCTGGGG
						2nd gRNA	CCATCAGTGCTCTGAGCGATGG
FBXO47	F-box protein 47			17q12	FBXO47	1st gRNA	GATATTGGCATGTTAAGTATGG
						2nd gRNA	ATTATATCTCAACATCATCTGG
hFBXL18	F-box and leucine rich repeat protein 18		FLJ11467, Fbl18	7p22.1	FBXL18	gRNA	CGGATGGCGGGCTCGTTGCGGGG
hFBXO17	F-box protein 17		FBG4, FBXO26, FLJ11798, Fbx17	19	FBXO17	gRNA	AAGATGAGATTGCGGCCGAAGGG

Appendix 3. Plasmid and LV construct used in the current study (Cas9 neo-CRISPR gRNA F-box vector and PLVX GFP)

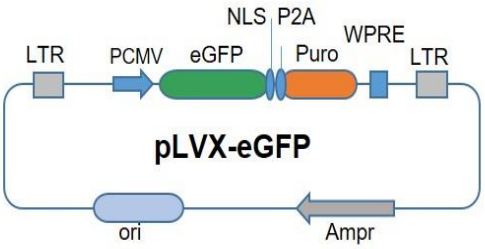
pLv5-Cas9-Neo



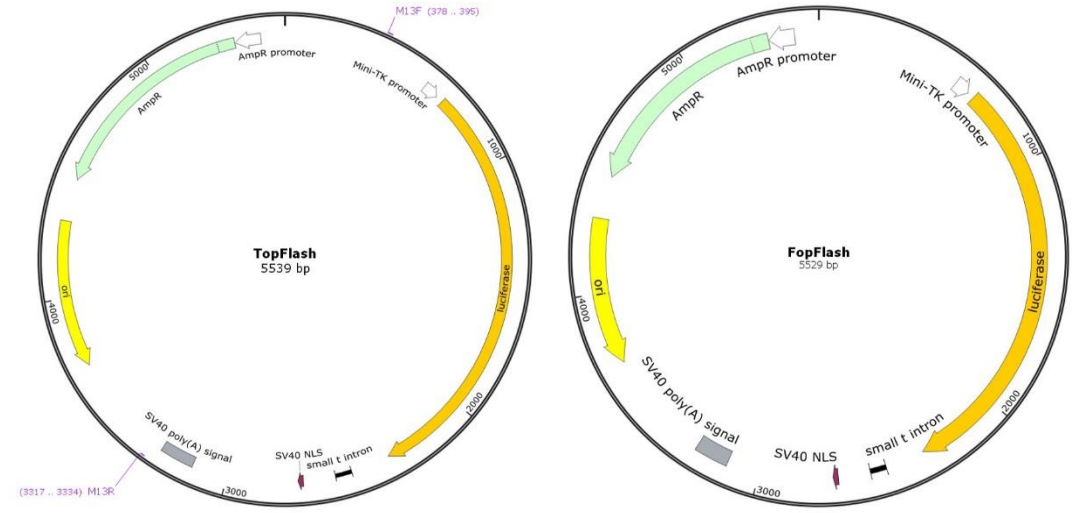
LV CRISPR gRNA F-box



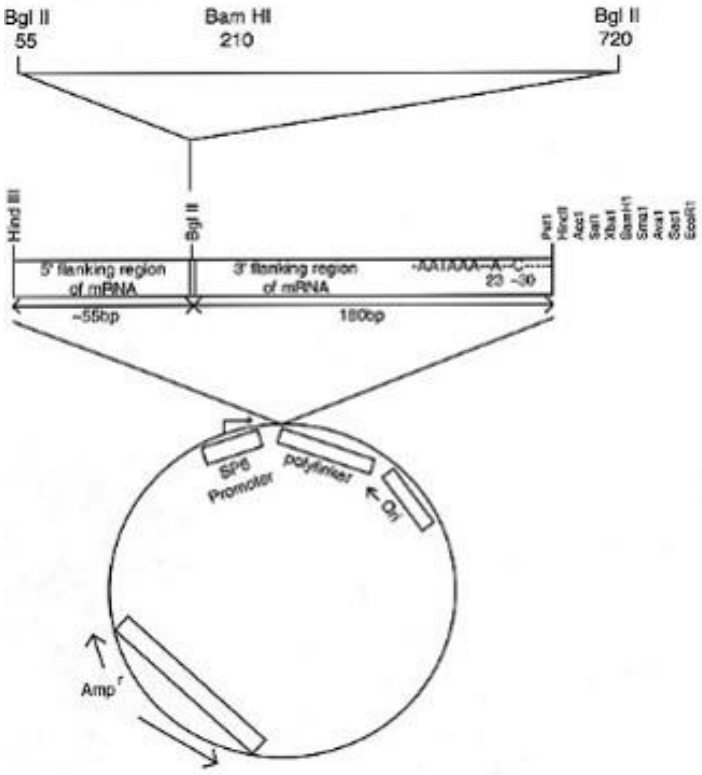
pLVX-eGFP



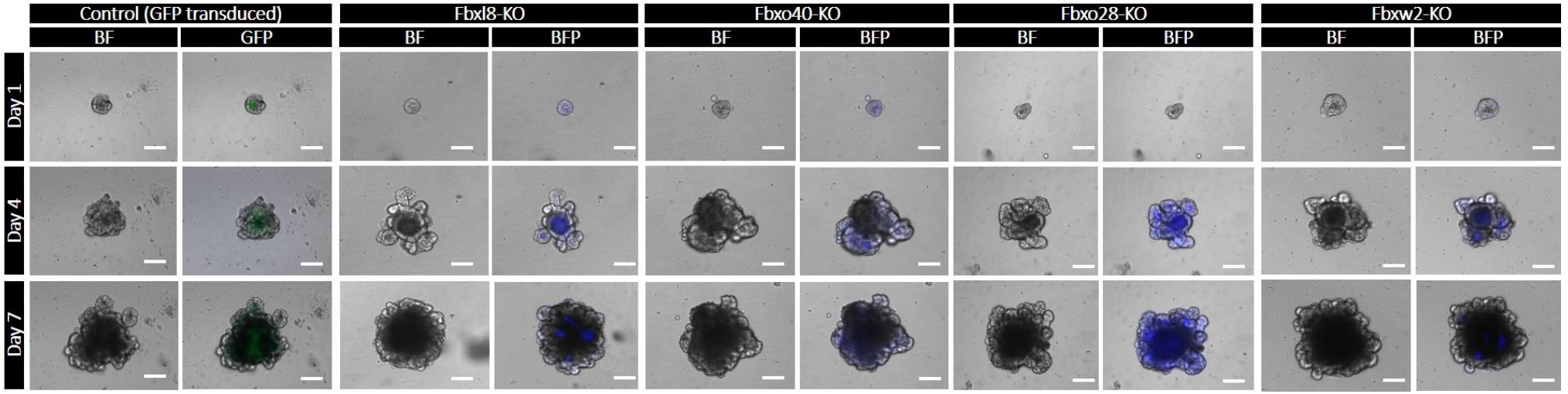
Appendix 3. DNA Plasmid used in the current study (Top/Fop flash luciferase and Noggin)

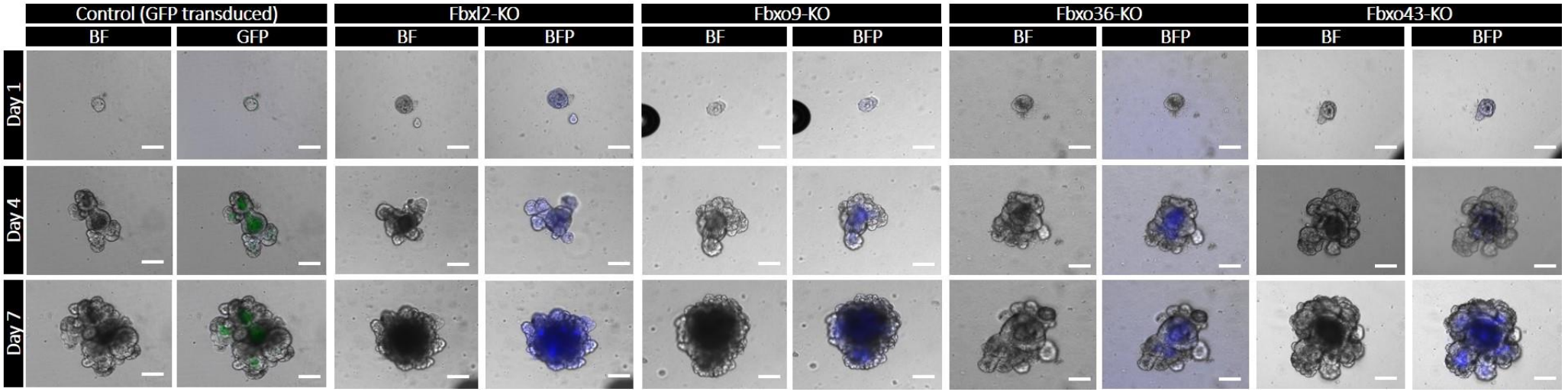


Noggin



Appendix 4. Representative F-box KO-organoid without any morphological differences in comparison to control.




Control (GFP transduced)
Fbxl2-KO
Fbxo9-KO
Fbxo36-KO
Fbxo43-KO
BF
GFP
BF
BFP
BF
BFP
BF
BFP
BF
BFP
Day 1
Day 4
Day 7